

Universiteit
Leiden
The Netherlands

Extending the self-assembly of coiled-coil hybrids

Robson, M.H.

Citation
Robson, M. H. (2009, December 9). *Extending the self-assembly of coiled-coil hybrids*. Retrieved from https://hdl.handle.net/1887/14498

Version:	Corrected Publisher's Version
License:	Licence agreement concerning inclusion of doctoral thesis in the Institutional Repository of the University of Leiden
Downloaded from:	https://hdl.handle.net/1887/14498

Note: To cite this publication please use the final published version (if applicable).

EXTENDING **THE SELF-ASSEMBLY OF COILED-COIL HYBRIDS** · *HANA ROBSON MARSDEN*

EXTENDING THE SELF-ASSEMBLY OF COILED-COIL HYBRIDS

PROEFSCRIFT

ter verkrijging van
de graad van Doctor aan de Universiteit Leiden,
op gezag van Rector Magnificus prof. mr. P. F. van der Heijden,
volgens besluit van het College voor Promoties
te verdedigen op 9 december 2009
klokke 16.15 uur

door

HANA ROBSON MARSDEN

geboren te Wellington, Nieuw Zeeland in 1980

PROMOTIECOMMISSIE:

Commissie chair:	Prof. dr. J. Brouwer
Promotor:	Prof. dr. ir. J. G. E. M. Fraaije
Copromotor:	Dr. A. Kros
Thesis Commissie:	Prof. dr. J. J. L. M. Cornelissen (Universiteit Twente) Prof. dr. R. M. J. Liskamp (Universiteit Utrecht) Prof. dr. B. J. Ravoo (Universiteit Münster, Duitsland) Dr. J. Raap

Robson Marsden, H.
Extending the self-assembly of coiled-coil hybrids
Leiden Institute of Chemistry, Leiden University, the Netherlands
December 2009
ISBN: 978-90-9024896-7
Printing: Ipskamp Drukkers B.V., Enschede, the Netherlands.

CONTENTS

1.	Coiled-coil self-assembly in synthetic biology: inspiration and progress	*1*
2.	Understanding the binding of the E/K peptide dimer in aqueous solution, a combined experimental and computational study	*35*
3.	Noncovalent triblock copolymers based on a coiled-coil peptide motif	*59*
4.	Uniting polypeptides with sequence-designed peptides: synthesis and assembly of poly(γ-benzyl L-glutamate)-*b*-coiled-coil peptide copolymers	*89*
5.	Detergent aided polymersome formation	*113*
6.	Rapid preparation of polymersomes by a water addition – solvent evaporation method	*125*
7.	A reduced SNARE model for membrane fusion	*145*
8.	Peptide-polymer block copolymers – an overview and assessment of synthesis methods	*165*
9.	Summary	*187*
	Samenvatting	*191*
	Abbreviations	*196*
	Curriculum vitae	*198*
	Acknowledgements	*200*

COILED-COIL SELF-ASSEMBLY IN SYNTHETIC BIOLOGY: INSPIRATION AND PROGRESS

Biological self-assembly is very complex, and results in highly functional materials. In effect it uses a bottom-up approach using well-defined biomolecular building blocks of precisely-defined shapes, sizes, hydrophobicity, and spatial distribution of functionality. Inspired by and drawing lessons from the self-assembly processes in nature, scientists are learning how to control the balance of many small forces to increase the complexity and functionality of self-assembled nanomaterials. This thesis takes the coiled-coil peptide motif, which plays a variety of roles in natural self-assembly, and connects it to other molecules to push the boundaries of synthetic self-assembly using this motif.

INTRODUCTION

Synthetic biology aims to understand and harness the emergent properties of complex biological systems. As discussed here, one approach towards this is the use of biological, or biologically inspired modules, for the prescriptive self-assembly of functional synthetic systems. This Chapter draws attention to the versatility in nature of one of these biological modules, the simple coiled-coil peptide structure, and then highlights recent efforts towards meeting the synthetic-biological challenge this presents: attempts to use coiled-coil forming peptides to assemble functional units, assemblies, and systems of increasing complexity (Figure 1).

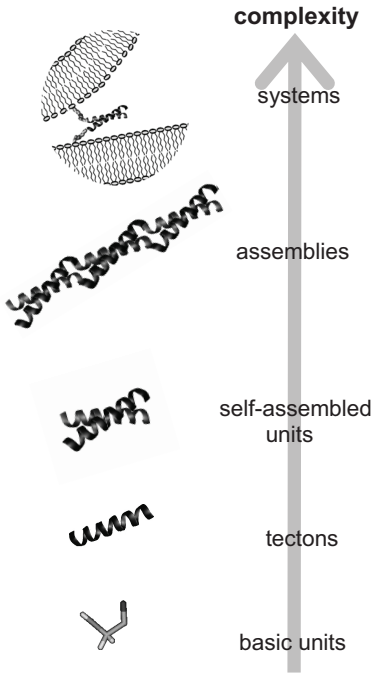


Figure 1. An overview of the use of the coiled-coil peptide motif in prescriptive self-assembly. In synthetic biology there are a range of natural and synthetic basic units, and for each there is a progression from basic units, to tectons, to self-assembled units, to assemblies. As a final goal multiple assemblies combine to yield functional systems.[1]

Both in nature and in the laboratory, α-helical coiled coils are formed by the binding of two or more α-helical peptides in a specific manner producing a stable complex in aqueous solution. The specificity of binding results from the amino acid sequences: the majority of coiled-coil forming peptides are characterized by a heptad repeat, denoted abcdefg, with apolar amino acids at most of the a and d positions, resulting in an amphipathic helix (figure 2). The packing of the hydrophobic a,d face against that of another coiled-coil forming peptide produces the majority of the binding energy. The apolar face of the helix is not parallel to the helical axis, but winds around the helix once every ~ 15 nm, such that the packing of the hydrophobic strips against one another leads to the coiling of individual α-helical 'coils'. Amino acids with charged side chains are often located at positions e and g, which border the hydrophobic core when the peptides are in the coiled-coil conformation, and contribute to the specificity of binding. Coiled coils have a rope-like structure, with each heptad extending the length of the complex by ~ 1 nm. Many aspects of coiled-coil binding are determined by the amino acid sequence: the oligomerization state (two or more peptides), size (~ 2 nm – 200 nm long), direction of binding (parallel or antiparallel), homo- or heterobinding, stability, and rigidity. The non-covalent association of these peptides is sensitive to changes in the environment, for example pH, temperature, ionic strength and metal ions, which affect the electrostatic or hydrophobic interactions. This versatility arising from a simple helix has resulted in many functions of coiled coils in nature, and has inspired many advances in synthetic biology.[2]

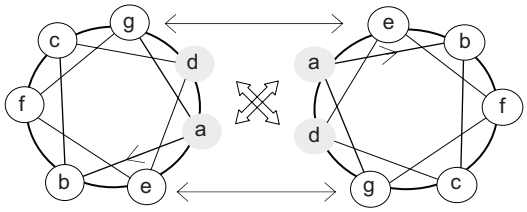


Figure 2. Helical wheel representation of a parallel dimer with a heptad repeat of amino acids. The heptad repeat positions are labeled from a to g and the α-helices propagate into the page. The a,d surface (shaded grey) is predominantly hydrophobic, and residues at positions e and g are often charged.

COILED COILS IN NATURE

Predictions based on analyses of primary sequences suggest that the α-helical coiled-coil motif makes up approximately 2.5% of all protein residues.[3] An analysis of a yeast proteome using two coiled-coil predicting programs identified 1,316 proteins that are thought to contain at least one potential coiled-coil domain, which corresponds to approximately 20% of the proteome of S. cerevisiae.[4]

α-Helical coiled coils are remarkable not only for their quantity, but for the range of functions that they exhibit in vivo. The very definition of coiled coils – two or more α-helices binding together in a specific manner – means that wherever they are found – in every compartment of plant cells, in every eukaryote and prokaryote cell, they all have one role in common: the molecular recognition between two or more α-helices causes the peptide segments to function as 'cellular velcro' – holding together the molecules and sub-cellular structures to which they are covalently attached.[5] The specific amino acid sequences modulate the velcro binding properties, and can also give rise to the other, more specific functions of coiled coils. Shorter coiled coils function primarily as highly specific cellular velcro, whereas longer coiled coils act as binding domains and simultaneously take on a wider variety of tasks in the cell.[6] In vivo many coiled-coils domains are long, containing several hundred amino acids, and the proteins are often composed of a long coiled-coil domain flanked at one or both ends by a globular domain. In contrast to short coiled-coil domains, where binding leads to lateral positioning of protein segments, the binding of long coiled-coil domains results in rod-like supramolecular structures. Only few long coiled-coil proteins have been characterized in prokaryotes (organisms without a cell nucleus, usually single-celled). In contrast eukaryotic organisms (containing a nucleus, multiple cells) contain more types of long coiled-coil proteins, such as motor proteins, membrane tethering and vesicle transport proteins, many of which are eukaryote-specific, suggesting that coiled-coil proteins have gained functions in the increasingly complex processes of the eukaryotic cell.[5] Although thousands of proteins have been acknowledged to contain coiled-coil domains, in the majority of cases the function of these coiled coils is not known. The functions of coiled-coil domains that have been elucidated to date have predominantly been binding, structural and dynamic. All of the

identified functions are summarized in the following sections, with one or two proteins that fulfill each role chosen as illustrative examples.

Protein binding

Short coiled-coil domains are most commonly found as oligomerization segments, where by means of molecular recognition they bring together proteins or protein segments, mediating a large number of specific protein interactions.[6] These coiled-coil domains can contain as little as two heptad repeats (~ 2 nm long),[7] but often have six or seven heptad repeats (~ 6 – 7 nm long). The folding of these domains into a stable complex can result in intramolecular binding, such as contributing to the assembly of the hydrophobic core of globular proteins,[8] or intermolecular binding, examples being in the assembly of ion channel signaling complexes and transcription factors (proteins that bind to specific sequences of DNA to either activate or repress gene transcription).[6, 9] The most widely studied coiled-coil containing proteins are the bZIP transcription factors. Proteins in this family consist of a 'basic region leucine zipper' (bZIP) domain, and an activation domain, which modifies the gene transcription. The protein complexes are formed by coiled-coil dimerization of the leucine zipper, and are anchored in position by a basic DNA-binding sequence (Figure 3). Homo- or hetero-dimerization of coiled-coil forming domains on different bZIP containing proteins determines which activation domains are in the protein complex, and hence precisely modulates the transcription of genes. An example of how sensitive the coiled-coil function is to amino acid sequence is the large extent to which a single amino acid modification can modulate the level of transcription. A serine in the e position of a 31 residue coiled-coil domain of a bZIP transcription factor was phosphorylated, leading to additional intra- and interhelical electrostatic interactions. This resulted in the protein dimer becoming more stable, and as a consequence the phosphorylated protein bound to DNA with a 15-fold higher affinity.[10] Although the binding even of short coiled coils is specific it is not necessarily exclusive, and it is thought that the coiled-coil sequence of some signaling complexes allows for different coiled-coil partners at different stages of the signaling process.[11]

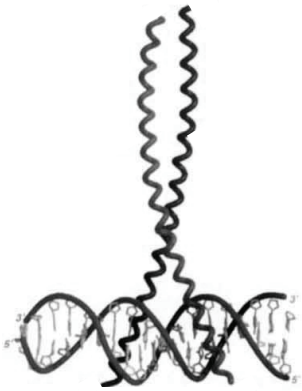


Figure 3. Crystal structure of the heterodimeric bZIP domain of the transcription factor c-Fos–c-Jun. The upper eleven helix turns constitute the coiled coil, and pincer the proteins onto the DNA strand. The activation domains are not shown.[12]

Structural functions

As coiled coils have a rod-like morphology an unsurprising role is as a structural component of the cell.

In some proteins the function of the long coiled-coil domain is to serve as a rod, which connects, spaces, and positions functional head and tail domains,[6] leading to the assembly of multi-unit complexes, bringing together bioactive components with defined stoichiometries and orientations at set distances with nanometer precision.[1] Examples of long coiled-coil spacer rods are the 8.3 nm long parallel homotrimer that separates the outer membrane from the bacterial cell wall in *Escherichia coli*,[13] and in the yeast spindle pole body where the distance between the plaques is determined by the length of a parallel homodimer in the connecting proteins.[5, 14] The amino acid sequence of spacer rods varies considerably between species, with positions a and d showing the least variation.[15] The sequence divergence is constrained only by the need to maintain the coiled-coil structure, which is predominantly driven by positions a and d. Coiled-coil rods are often homooligomers, with maximal apolar and/or ionic interactions[16] accounting for their rigidity.

A remarkably stable coiled-coil stalk forms a structural edifice at the cell surface of the bacterium Staphylothermus marinus, which inhabits geothermally heated marine environments, and has an optimum growth temperature of 92 °C.[17] The bacterium is coated by umbrella-like tetrabrachion proteins consisting of four identical subunits that form a 70 nm long coiled-coil stalk that is anchored to the cell membrane at its C-terminus and branches into four β-sheet arms each 24 nm long at its N-terminus (Figure 4).[18] The arms form a canopy-like meshwork by end-to-end contacts that creates a semi-isolated sheath around the bacterium.[19] The coiled-coil domain sequence is such that the tetramer is remarkably stable, remaining folded at temperatures of 130 °C and in the presence of strong denaturants such as 6 M guanidinium hydrochloride.[18] The core positions contain an almost flawless pattern of aliphatic residues, mainly leucine and isoleucine, which contributes to its extreme stability.[20] This surface meshwork presumably has a cytoskeleton-like structural function,[21] and acts as a stabilization structure for the lipids and proteins of the cytoplasmic membrane.[22]

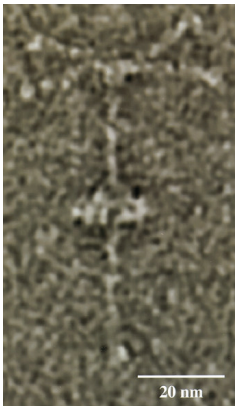


Figure 4. Negative stained TEM image of the tetrabrachion protein.[17] The 70 nm long coiled-coil stalk is stable to 130 °C and 6 M guanidine hydrochloride.[18] There are four β-sheet arms at the top of the coiled coil and two proteases noncovalently bound around the center of the stalk.[19]

The protein family of intermediate filaments has high sequence divergence, but all contain a ~ 45 nm coiled-coil rod.[23] Intermediate filaments dimerize via homo or hetero coiled-coil formation. These parallel coiled-coil dimers pack together into filaments that are ~ 10 nm wide and micrometers long.[24] The filaments have a persistence length of ~ 1 μm, and can be stretched to 350% of their original length. Both the properties of the coiled-coil dimers[23] and axial slipping between dimers[25] lead to the flexibility of intermediate filaments, and they are thought to function as stress absorbers in animal cells, which lack a cell wall.[23]

Many coiled-coil proteins utilize long coiled coils to create ordered two-dimensional networks and three-dimensional scaffolds that support the cell.[26] Like the intermediate filaments, these two and three dimensional structures can span microns. One such protein is spectrin, a cytoskeletal protein that forms a planar layer on the inner surface of the cell membrane of all animal cells (Figure 5a).[27] Spectrin is a fibrous protein largely made up of multiple 106-residue coiled-coil domains that fold into repeats of intramolecular coiled-coil trimers (Figure 5b). Four folded spectrin proteins self-associate end-on-end and side-to-side in a manner that is not fully elucidated but does not seem to be through coiled-coil interactions.[28] Multiple spectrin tetramers bind at actin junctions such that a membrane skeleton composed of ordered mosaics is formed (Figure 5a). These mosaics link to both membrane proteins, and to proteins in the cytoplasm.[29] The coiled-coil binding is dynamic, and coiled-coil rearrangements (the switching of one section of the protein between a loop and an α-helix, Figure 5b) and variations in binding between two spectrin chains can rapidly vary the length and flexibility of the molecule, which controls the organization of proteins that are bound to each mosaic, and the membrane shape and mechanical resilience.[29, 30] An equivalent coiled-coil protein has also been found in a bacterial cell, and was found to be essential for the shape of the cell.[31]

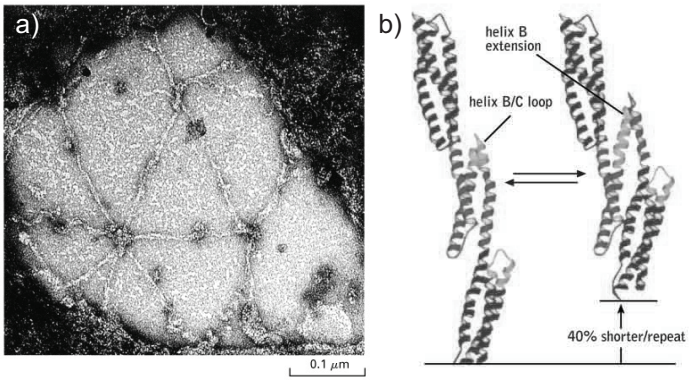


Figure 5. a) TEM image of a membrane skeletal network showing the actin hubs and linking spectrin network. The darker spots along the spectrin spokes are where spectrin is cross-linked to membrane proteins.[32] b) Spectrin mosaics are largely composed of intramolecular antiparallel heterotrimers. The coiled-coil trimer repeats are depicted in dark grey, and the section that switches between loop and α-helical conformations is depicted in light grey.[29]

The protein NuMa contains the longest known coiled-coil domain, (1485 residues, 207 nm long) which forms the major component of this fibrous nucleoskeletal protein. In vitro it self-assembles into multi-arm oligomers, and when overexpressed in vivo it induces a three-dimensional nuclear scaffold with a quasi-hexagonal organization that can fill the nuclei (Figure 6), indicating that its function is related to building up the architecture of the nuclear matrix.[33]

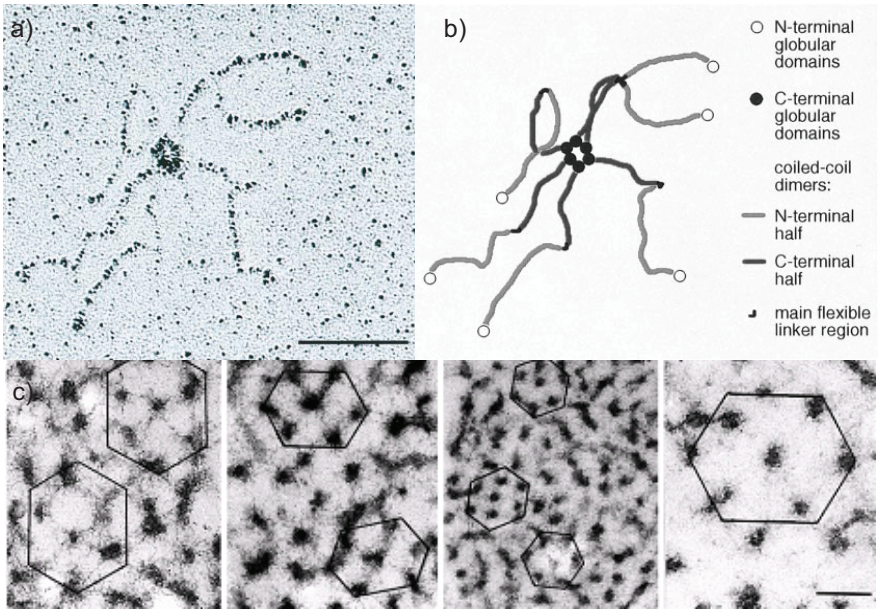


Figure 6. a) TEM image and b) schematic of NuMa multi-armed oligomers in vitro in which each arm is a homodimeric coiled coil. Scale bar 100 nm. The globular N-terminus domains (rings) can bind to the centers of neighboring oligomers resulting in a coiled-coil scaffold. c) When NuMa is overexpressed in vivo it forms a 3D scaffold with the mesh size determined by the engineered coiled-coil domain length. TEM images, scale bar 200 nm.

Dynamic functions

Directly interacting with the cytoskeleton are the cytoskeletal motor proteins. Three classes of cytoskeletal motor proteins have been identified – myosins, kinesins and dyneins, all of which contain coiled-coil domains.[6] These 'movement' proteins undergo large conformational changes in which the dynamic nature of the coiled-coil domains plays a key role. During each movement cycle of the proteins, which lasts tens of milliseconds,[34-37] the coiled-coil packing changes in response to applied force.

In muscle cells, myosin II is responsible for producing the contractile force by pulling along actin filaments. Myosin has a globular head domain and a ~150 nm long coiled-coil forming tail.[38] Parallel homodimers lead to two globular head domains, the motor units, being positioned adjacent to one another. Multiple coiled-coil tail domains associate laterally and longitudinally, in a very precise manner, forming thick filaments The force-producing head domains protrude from the side of the thick filament, arranged helically around the filament with a repeat distance of 43.0 Å (Figure 7a). The packing of many

coiled-coil domains together means that not only the a d interface directs the packing, but the outer residues as well, and in fact in myosin the positions b, c, e, f, and g are more constrained between species than are residues in positions a and d.[15] The amino acid sequences of myosin coiled-coil domains are such that the N-terminus of the coiled-coil dimers extend out from the filament (Figure 7b). Thus, the packing of the coiled-coil domains keeps the myosin heads in the required orientation and spacing along the thick filament,[21] and the flexibility of coiled-coil domain allows movement of the head groups along the adjacent actin filaments, creating tension.[6] In vitro the myosin thick filaments have been shown to bend and to reversibly and quickly extend to more than 350% of their original length (Figure 7c).[38, 39] Bending is dominated by shearing between the coiled-coil dimers within the thick filament, whereas the stretching behavior is explained by shearing between coiled-coil dimers and coiled coil and α-helix unfolding.[39] Elastic energy storage has been proposed as an important mechanism for minimizing the energetic cost of insect flight, and these elastic properties of myosin thick filaments in muscle may constitute part of this mechanism.[39]

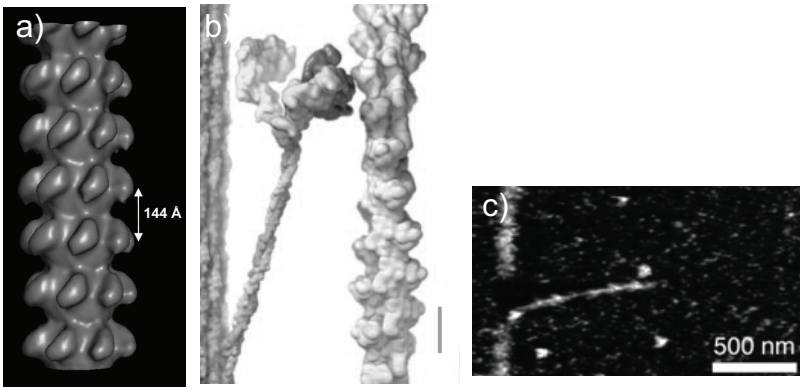


Figure 7. a) 3D reconstruction from single particle EM analysis of relaxed muscle myosin thick filament illustrating the regular configuration of the myosin headgroups brought about by the packing of coiled-coil dimers.[40] b) Model of myosin dimer flexing out from the thick filament and binding to an actin filament on the right of the image. The elasticity of the coiled-coil domain allows the motor head group to 'walk' along actin filaments. Scale bar 60 nm.[41] c) AFM image of a myosin thick filament that has been stretched and broken by lateral pushing by the AFM tip.[39]

In myosin the coiled-coil dimer must be flexible in order to bend out from the thick filament to allow the head domains to 'walk' along actin filaments. In another motor protein, kinesin, the coiled coil plays a more direct mechanical role in the 'foot over foot' movement of the molecular motor along microtubules. Kinesin contains a central coiled coil with a motor domain at one end and a cargo binding domain at the other, and forms a dimer via the coiled-coil domain (Figure 8a). A small conformational change at the forward most 'foot' is conveyed and amplified by the coiled-coil 'lever' to the trailing motor domain, thrusting it forward, and pulling the cargo 8 nm along the microtubule.[41] The length of the coiled-coil 'lever' determines the velocity of the gliding motion (Figure 8b).[42] In order for the motor domains to walk along the microtubules it is essential that the

strands of the coiled-coil dimer adjacent to the motor domains can unwind. To demonstrate this the dynamic native domain was replaced with a more stable coiled coil, and the motility of the protein was effectively eliminated.[43]

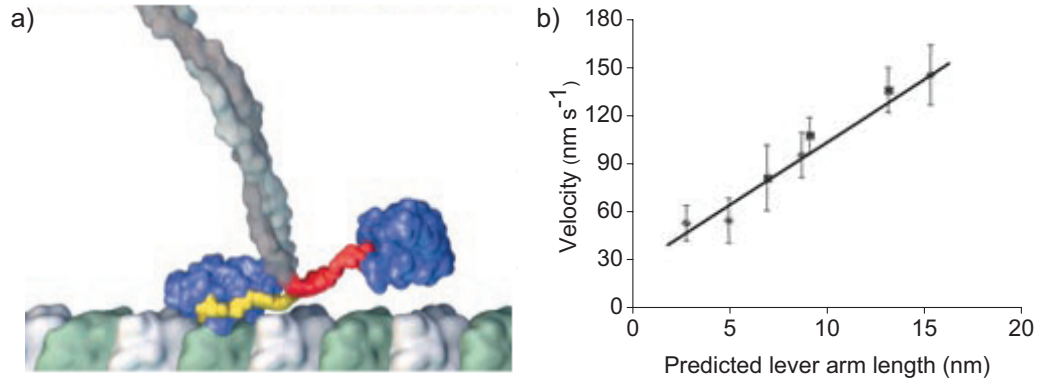


Figure 8. a) Conformational changes in the kinesin motor domain are amplified by the coiled-coil lever, causing the second head to swing forward (cargo not shown).[41] b) Kinesin velocity along microtubules depends on the coiled-coil domain length.[42]

Dynein, the third class of motor proteins, comprises a ~ 12 nm[44] antiparallel coiled-coil stalk domain that binds to microtubules via a small globular domain, a central globular head, and a cargo-binding stem (Figure 9a). As with kinesin, dynein also moves along microtubules in 8 nm steps.[45] The movement of dynein is not as well understood as for the other cytoskeletal motor proteins, but the microtubule-binding domain at one end of the coiled coil changes its affinity for microtubules depending on events at the headgroup, which is at the other end of the coiled coil (and vice versa), therefore structural changes must be transmitted along the length of the coiled coil. This implies a requirement for dynamic changes to helix–helix interactions.[46] It has recently been found that sliding the strands in the coiled-coil stalk by four amino acids couples the microtubule binding and headgroup activity.[47] It has also been observed that before the movement phase of each cycle, when dynein is tightly bound to the microtubule, the coiled-coil stalk is more flexible than after the powerstroke, when the coiled coil is straighter and has a lower standard deviation in its relative position, and is therefore thought to be more stable (Figure 9b). It is proposed that this flexibility may render the coiled coil capable of storing elastic energy when the molecule develops force against a load.[48] The length of the coiled-coil domain is highly conserved and is thought to be optimal for its force transduction role.[21]

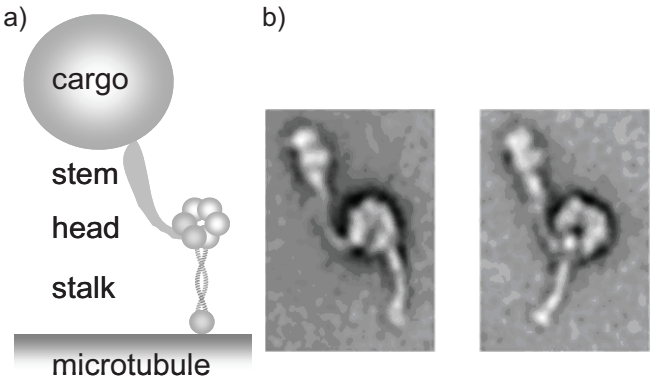


Figure 9. a) Dynein carries cargo along microtubules. b) Composite images of dynein from negative stained TEM. The coiled-coil stalk pre-power stroke (left) is more flexible than post-power stroke (right).[48]

The motor proteins discussed above all transport cargo along intracellular cables. Another method for intracellular transport that takes place in all eukaryotic cells is via transport vesicles. SNARE proteins are key components of this form of transport, as the dynamic coiled coil that forms between different SNARE proteins facilitates the docking and fusion of transport vesicles with organelles or the cell membrane. The SNARE proteins are a large family, with 27 SNARE proteins identified in a single unicellular parasite.[49] Although there is considerable variation in their structure and size, the coiled-coil domains are highly conserved, and it is thought that they all operate by way of the same mechanism. The SNARE proteins that are involved in the exocytosis of neurotransmitters from neurons are the best characterized. There is one type of SNARE protein connected to the transport vesicle membrane, another to the target membrane (in this case the neuronal membrane), and a third SNARE protein in the cytoplasm. A very stable coiled-coil complex forms between these three proteins, converging the membranes (Figure 10).[50] Assembly proceeds spontaneously from less structured monomers and results in a 6.5 nm coiled-coil heterotetramer.[16, 51, 52] The energy released by the formation of the stable four helix bundle overcomes the free energy barrier for fusion, producing enough force to disrupt the lipid bilayers, leading to membrane fusion, although the exact mechanism is unknown.[16, 52] The bundle is then ‘unzipped’ with the aid of four proteins and energy from ATP-hydrolysis so that the proteins can be used again.[53]

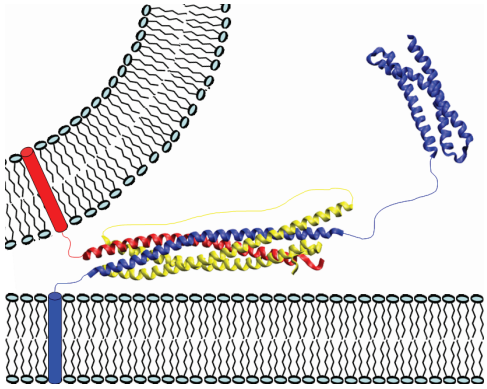


Figure 10. Structure of a SNARE protein complex featuring a coiled-coil tetramer that docks a transport vesicle to the target membrane and leads to membrane fusion and contents transfer. PDB codes 1sfc and 1br0.

A group of proteins, Rabs, are thought to act upstream of the SNARE coiled-coil complex formation to organize the fusion site.[54] Via conformational changes Rab proteins are switched between active and inactive forms, with this change catalyzed by specific guanine nucleotide exchange factors (GEFs). Coiled-coil proteins have recently been found to function as GEF catalysts, a role which is usually carried out by much more structurally complex proteins. The Sec2p GEF domain forms a 22 nm long parallel coiled-coil homodimer that makes use of the coiled-coil motif for catalysis in a very simple manner. A small mid-section of twenty five amino acids of the coiled-coil hydrophobic core packing is disrupted, and this region binds specifically to a Rab protein (Figure 11). The binding interface is mostly hydrophobic and buries ~ 30 nm2 of solvent-accessible surface. The binding induces extensive structural rearrangements in the Rab protein, which activates the protein. The amino acids from both helices of Sec2p that are involved in this binding interface are highly conserved in other GEFs whose mode of function is currently unknown, indicating that they also operate similarly to Sec2p.[55]

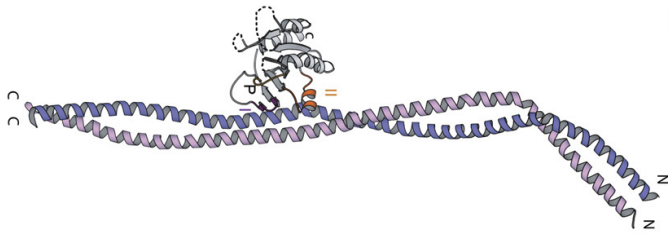


Figure 11. Crystal structure of the homodimeric coiled-coil GEF domain of Sec2p in complex with a Rab protein domain, which catalyzes the Rab's cellular transport modulation activity.[55]

Similarly to the transfer of cargo within and out of cells as discussed above, viruses also employ a dynamic aspect of coiled coils to transfer their contents across membranes; however the mechanism by which coiled-coil formation leads to this is rather dissimilar. Enveloped viruses (i.e. surrounded by a lipid membrane) such as influenza, Ebola or HIV fuse their membrane coats with cellular membranes to import their genomes into cells by

way of pH mediated coiled-coil extension.[56, 57] An extensively studied example is the entry of the influenza virus, which displays a parallel trimer surrounded by globular head domains as an 8 nm long 'spike' on the surface of the viral envelope at normal physiological pH (Figure 12a). In the initial steps of cell entry, viruses are internalized by endosomes, where the pH is gradually lowered to ~ 5. The pH change causes the globular head subunits to dissociate from the spike, triggering what was previously a loop region to change into the coiled-coil configuration, irreversibly extending the coiled-coil 'spike' to 13.5 nm (Figure 12b).[58-60] The folding of the coiled coil propels a hydrophobic fusion peptide from a buried, basal position 10 nm towards the target membrane,[58] inducing membrane fusion and hence the release of the viral RNA into the cell.[61] In effect the central coiled coil provides a spring-loaded hinge that is set off by a drop in pH.
Recent results indicate that the means of membrane entry of non-enveloped viruses also involves a coiled-coil spring-loaded hinge that brings a fusion sequence close to the target membrane, although the stimulus that releases the spring (i.e. that leads to coiled-coil formation) is not clear.[62]

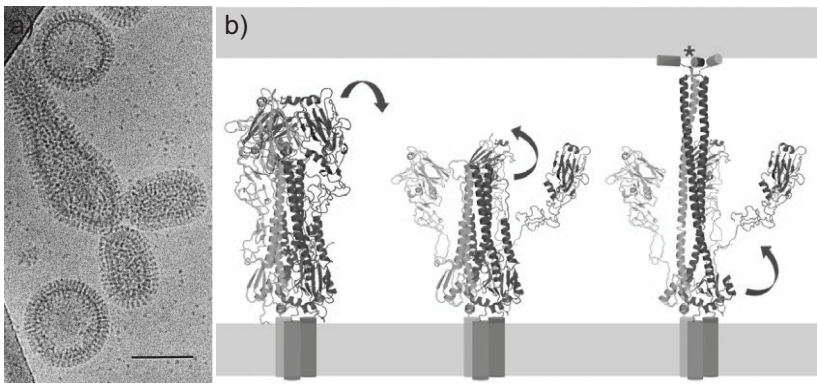


Figure 12. a) Cryo-TEM of influenza virions at 30 °C, pH 7.4 with the coiled-coil containing protein complex visible at the surface.[59] b) The drop in pH as a virus is encapsulated in endosomes dissociates globular head domains from the coiled-coil bundle (left), causing a loop domain to fold (center), thereby extending the coiled coil, and projecting a fusion peptide towards the endosome membrane (right). The crystallographically determined components are in ribbon representation.[60]

Whereas the coiled coils in motor proteins are dynamic in response to applied force, and enveloped viruses form a coiled coil in response to a pH drop, some proteins make use of the temperature dependent dissociation of coiled coils. Virulent bacteria are under constant pressure to sense their environment as they advance along their route of invasion experiencing changes in pH, temperature, and osmolarity.[63] As coiled coils respond to changes in the environment they may act as sensors to variations in the intracellular environment. Salmonella contains a protein, TlpA, with an N-terminus DNA-binding region and a coiled-coil domain of 250 amino acids.[63] This is similar to the b-ZIP domains of transcription factors, except that as well as functioning via molecular recognition these coiled-coil domains also function via temperature 'recognition'. At temperatures below 37 °C TlpA forms a homodimer that can bind to sequence-specific DNA, repressing its

activity. When the bacterium enters warm bodies, i.e. with temperatures above 37 °C, the homodimer is destabilized,[64] releasing the DNA, which is then available for replication.[65] Circular dichroism spectroscopy demonstrates that the temperature induced dimer to monomer transition of TlpA is reversible, and upon cooling both function and full α-helicity are regained.[65]

It is evident that by variations in the interfaces between α-helices (through different amino acid sequences), a remarkable assortment of properties emerge, and coiled coils are used in numerous ways in the cell. Coiled-coil structures provide one, two, and three dimensional mechanical stability to the interior and surfaces of cells via rods, mosaics, and scaffolding. The supramolecular structures are also involved in movement processes for which particular degrees of flexibility are essential. Natural coiled coils are utilized for their extremely thermostability in some cases, and their relative lability in others, switching structure in response to temperature or pH. Furthermore, coiled coils act as a molecular recognition system, catalyzing cell activities. The biological function of the coiled-coil motifs in many other proteins is not clear, and it is expected that several other functions will be elucidated in the future.

COILED COILS IN SYNTHETIC BIOLOGY

The functions of natural coiled coils discussed above took approximately 3.8 billion of years to develop.[66] Since the 1950s scientists have been reverse engineering nature: by studying the form and function of proteins, and tracing these back to amino acid sequences the 'rules' for their self-assembly can be obtained,[67, 68] allowing de novo peptide design, yielding novel form and function. In a synthetic sense this means designing molecules that organize into well-defined structures with specific functions.

Coiled coils are good candidates for the self assembly of smart biosynthetic nanostructures for many reasons: they have precisely defined size and shape (i.e. rods 2 nm in diameter with each heptad ~ 1 nm long) and surface functionality; the intra- and inter helical noncovalent interactions are relatively well understood; they can self-assemble into stable structures at low concentrations (sub-nanomolar[69]); coiled coils can be functionalized at the N- or C terminus or via solvent-exposed amino acids; and the affinity and specificity of the binding of coiled coils are very sensitive to the amino acid sequence. This rich array of controllable properties means that there is a coiled-coil 'building block' to suit many castles in the (supramolecular) sky.

Self-assembly that is inspired by α-helical coiled-coil peptides is discussed in terms of 'synthetic-biology space', as put forward by the Woolfson group, in which basic units bind covalently to form tectons, which hierarchically self-assemble via units and functional assemblies, and combine with other functional assemblies to culminate in systems.[1, 70] In this quadrant of synthetic biology the basic units are amino acids,

sequences of which covalently bind to form the tectons, α-helices. The α-helices bind noncovalently to form the units, coiled coils, which organize further into assemblies, and finally aspire to entire systems (Figure 1). The mapping and exploration of coiled-coil synthetic biology up to the current date is reviewed below. First units are discussed, then assemblies, and finally the first uses of coiled coils in systems are charted, and parallels are drawn between these advances and the sophistication of naturally occurring coiled-coil motifs.

Coiled-coil units

The initial aim of coiled-coil research was to understand the structures and binding of natural coiled coils. Peptides derived from transcription factors and other natural coiled coils have been mutated in order to delve into their binding properties. Once the rules mapping peptide primary sequence to intermolecular interactions had started to emerge the design aspect broadened from changing isolated residues in a natural sequence to designing completely de novo sequences, and the units have become more removed from native form and function as the possibilities of the unit are explored. Many aspects of coiled-coil binding have been tailored in coiled-coil units, namely coiled-coil length, stability, specificity of recognition partners, oligomerization number, strand orientation and conformation, with highlights touched upon in the following section.

To date the majority of the peptide units whose sequence to structure relationships have been investigated and modified have been short, usually with 3-5 heptad repeats. Generally peptides with more heptad repeats form more stable complexes. Very short homodimers with only two heptad repeats have been created by optimizing design criteria, i.e. by enhancing the hydrophobic packing, and intra- and intermolecular salt bridges, utilizing amino acids with high α-helix propensity, and using suitable capping moieties.[71, 72] The shortest identified coiled coils in nature also contain two heptad repeats,[7] and this appears to be the lower size limit.

A common goal is to design coiled coils with greater binding stability while retaining the other aspects of coiled-coil binding. This feature of unit self-assembly has primarily been targeted by optimizing the primary sequence. As an example, amino acid substitutions in the 37 residue coiled-coil domain of the c-Jun transcription factor[12] caused an increase in the melting temperature the Fos-Jun Heterodimer of 37 °C. By analyzing different amino acid substitutions it was concluded that the substitution of amino acids that increase the buried hydrophobic area and improve helix stability accelerate the formation of a partially-folded dimeric intermediate, and that after this intermediate is formed improved intermolecular coulombic interactions increase the thermodynamic stability of the final coiled-coil structure.[73] In another example the substitution of two amino acids in position a of the 34 residue coiled-coil domain of another DNA binding protein decreased the dissociation constant for homodimers by a factor of 105.[74]

Non-natural fluorinated amino acids, which have a large hydrophobic area, have been incorporated into recombinant coiled-coil peptides leading to increased stability with minimal structural perturbation of the final complex.[75, 76] For instance isoleucine residues in core positions of the bzip domain of peptides derived from the transcription factor GCN4 were substituted with 5,5,5-trifluoroisoleucine, resulting in an increase of 27 °C in the melting temperature while the affinity and specificity for DNA binding was similar to the hydrogenated counterparts.[76]

Another non-natural approach to increasing coiled-coil stability is the modification of amino acids. An example of this approach was the attachment of an azobenzene moiety as an intramolecular crosslinker between two residues in position f of a heterodimer, i.e. solvent exposed and parallel to the helix length. Irradiation of the peptide reversibly changed the conformation of the azobenzene cross-linker from trans to cis, thereby decreasing its length, and bringing it into line with the natural helical repeat length of the peptide, which increased its helicity and promoted coiled-coil folding.[77]

Metal binding to histidine and cysteine residues can also affect the stability of coiled coils. Divalent binding of metal ions to residues at positions i and i + 4 can be used to stabilize coiled coils, while i and i + 2 binding destabilizes coiled coils. Coordination of two peptides to a single metal ion can induce the coiled-coil complex, with this effect having been demonstrated with the metal ion at both solvent exposed and internal positions.[78]

Coiled-coil complexes are specific in terms of the sequences of the peptides that will bind, the number of strands that associate, and the orientation of the binding partners. The high degrees of binding specificity that can be designed into the coiled-coil interaction has been exemplified by the formation of three distinct heterodimers in solutions of six peptides.[79, 80] In one case the four heptad repeat peptides were based upon natural coiled-coil domains from transcription factors, and the selectivity was introduced by substituting a single amino acid in a core position. As well as substituting natural amino acids, non-natural, urea derived side chains were utilized to improve selectivity.[79]

Amino acids with charged side chains are important determinants of which peptides will form a coiled-coil complex, and controlling inter- or intra molecular coulomb interactions through pH or salt can be used to modulate coiled-coil binding by destabilizing certain complexes. Many hetero coiled coils gain their specificity by having charged strips bordering the hydrophobic core such that one helix is positively charged and the other negatively charged, hence preventing homo coils forming. In this way pH can be used to influence coulomb interactions such that hetero coiled coils form at neutral pH, and homo coiled coils at low[81] and high pH.[82]

This concept of pH controlled strand exchange has been developed further with iterative cycles specifically replacing one, two, or all three initial helices of a coiled-coil trimer.[83] The strand exchange can also be programmed to be accompanied by a switch from a parallel to antiparallel trimer.[84]

Alternatively to the electrostatic destabilization of particular helix combinations, the number of α-helices in a coiled-coil bundle can be changed by the stabilizing effect of steric packing in the hydrophobic core, which is the major driving force for coiled-coil formation. For example, an engineered form of a native coiled coil is predominantly two stranded, but the coiled-coil trimer becomes the most stable arrangement when one benzene molecule is bound in the hydrophobic core, as the increased buried hydrophobic surface renders the trimer the energetically preferred complex.[85]

The oligomerization state can also be varied by tuning the hydrophobicity by way of substituting amino acids in positions within the coiled-coil hydrophobic core. This was investigated by systematically substituting the 20 natural amino acids in the central a and d positions of a five heptad repeat peptide that forms homo coiled coils. The β-branched residues isoleucine, valine and threonine which have side chains with large hydrophobic areas promote trimer formation whereas amino acids with charged side chains favor two-stranded coiled coils.[86, 87]

Small changes in peptide sequence can also lead to different binding orientations. For instance the five heptad repeat coiled-coil domain from an osmosensory transporter binds as an antiparallel homodimer. When two charged residues in position a of the heptad repeat are replaced with isoleucine the hydrophobic packing is altered, interchain salt bridges are eliminated, and the dimer changes orientation from antiparallel to parallel, rendering the protein inactive in vivo.[88]

Considering the distribution and range of functions of coiled coils in vivo there are many potential ways in which controlling existing coiled-coil binding can influence in vivo function. For example there are research groups investigating coiled-coil forming peptides to specifically bind to the coiled-coil bundles essential to viral entry, with the aim of inhibiting them,[89, 90] or to bind to specific transcription factors to modulate the replication of DNA.[91]

Another aspect of coiled-coil unit self-assembly that has been investigated is to switch the secondary structure of the peptides, which can be programmed to fold into different structures in different environments. The most common conformational switch (other than coiled coil - random coil) is between coiled coils and β-sheets. This is generally achieved by incorporating amino acids with high β-sheet propensity or that are hydrophobic into solvent exposed f positions of coiled coils, and upon heating the α-helices undergo a rearrangement into β-sheets which aggregate into amyloid-like fibers.[92-94] In another approach, a peptide that forms homodimers at neutral pH was modified such that there was a lysine or glutamic acid face next to the hydrophobic core of the coiled-coil complex. Changing the pH led to these faces being charged, destabilizing the coiled coil, which rearranged into random coil or β-sheet structures.[95]

The final examples in this ‘coiled-coil unit’ section demonstrate that even without any larger scale assembly the units can be highly functional. Self-replicating complexes have

been developed in which coiled-coil folding catalyzes amide bond formation, producing replicates of the coiled-coil forming peptide. Two peptide fragments fold onto a full length peptide template, and an amide bond is formed between the two fragments via a cysteine thioester intermediate.[96] Subsequent developments included enhanced catalysis at reduced pH,[97] or at high ionic strength,[98] heterodimeric complexes,[99-101] a hypercycle, in which two self-replicating peptides catalyze each other's replication,[102] and a chirality-dependent self-replication cycle. In order for the cycle to continue the peptides must dissociate once the bond is formed, and to speed this up peptides one heptad repeat shorter were used,[103] or alternatively a proline kink was introduced to destabilize the coiled-coil complex.[104, 105] An interesting advance contains two self-assembling groups: peptides with nucleobases introduced as side chains. The complementary nucleobase interaction (via hydrogen bonding) enhanced the peptide self-replication reaction.[106]

The examples touched upon above demonstrate how researchers have taken the coiled-coil motif as a natural binding unit, deconstructed and rearranged it in many permutations to elucidate the mechanisms and subtleties of the binding, and in the process explored the wide variety of functions that can be chemically programmed into coiled-coil units. From the perspective of synthetic-systems chemists designed peptides have the advantage over natural peptides that the chemical, physical, and biological properties of the complex can be precisely defined over a broader range. For this reason it is predominantly designed peptides that are used to create higher order structures and systems. In the following sections an overview is given of the use of these functional building blocks to create one, two, and three-dimensional assemblies.

Coiled-coil Assemblies

Since 1997 coiled-coil based synthetic biology has been extended by the self-assembly of coiled-coil units into larger assemblies that contain multiple coiled-coil units.[107] As with the synthetic study of coiled-coil units, all of the coiled-coil assembly examples that follow use peptide lengths that would be considered short in nature (3-6 heptads). For the study of isolated coiled-coil units it is convenient to elucidate the binding properties with small molecules because they can be readily synthesized on solid support and because the effect of, for example, changing a single amino acid can more readily be identified. As the functional possibilities of coiled-coil assemblies are explored it is likely that there will be an expansion (via protein engineering) to longer coiled coils and de novo proteins with coiled-coil domains. In this section an overview is given of coiled-coil assemblies, with the structures categorized into those for which coiled-coil formation is the sole driving force for material organization, and those which contain two self-assembling entities.

Materials formed solely by coiled-coil folding

The first examples are of materials composed entirely of coiled coils and the following examples are assemblies that are formed from coiled-coil hybrids, but which nevertheless derive their higher order structure from coiled-coil folding. A well established mode of assembly is fibers and fibrils.[1, 108-112] This field takes inspiration from nature, in which coiled-coil proteins are often in the form of fibers, such as spacer rods or intermediate filaments. The rod-like structure of long native coiled coils is mimicked by using multiple short homo or hetero coiled-coil forming peptides which associate laterally[113] and in a staggered way such that each peptide is involved in two coiled-coil interactions simultaneously, leading to fibers, some up to hundreds of micrometers long. The fibers are generally composed of a bundle of coiled coils due to interactions between the amino acids on the outside of the coiled coil. To control this higher order structure more thought has to be put into the design of the amino acids in positions b, c, and f of the heptad repeat, an analogue to the decreased sequence variation in buried native coiled coils in comparison to non-buried motifs, e.g. in myosin filaments. Although the native rod structures can be emulated, the functions have by in large not been mimicked yet. With an eye to this current efforts are geared towards controlled design of the fiber morphology and related properties, for instance thinner and more flexible peptide fibers (Figure 13a).[114] The functionality of the fibers has been increased by conjugating additional molecules to the coiled-coil forming peptides, resulting in fibers coated with recruiting agents. These molecules on the surface of the fibers were able to bind to and hence localize proteins from solution (Figure 13b).[115] An additional dimension can be introduced by engineering kinks and branches into the fibers (Figure 13c).[116, 117] These coiled-coil fibers have been used to template silica layers at ambient temperature and physiological pH, which upon removal of the peptide (achieved most effectively by a protease), resulted in hollow silica tubes nanometers wide and microns long that are straight, kinked, or branched depending on the peptide template.[118] Alternatively, the fibrils can be induced to change to spherical objects at neutral pH,[119] or to reversibly dissociate at low pH.[120]

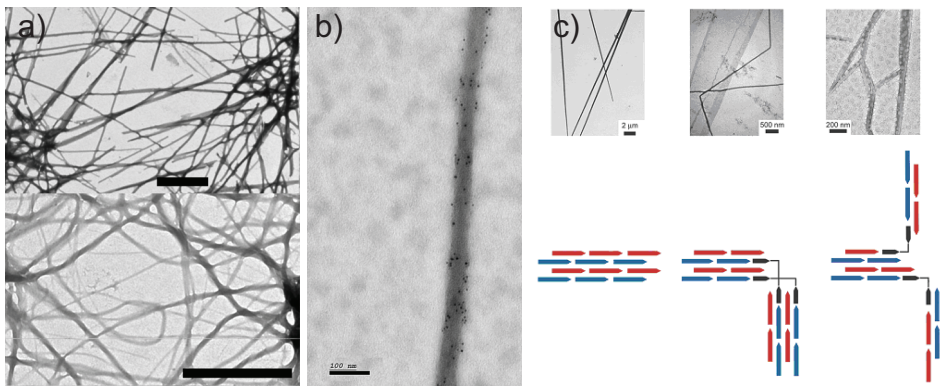


Figure 13. a) The rigidity of coiled-coil fibers can be programmed into the amino acid sequence. Negative stained TEM images, scale bars 1 µm.[114] b) TEM micrograph of a peptide fiber coated with recruited proteins. 5 nm gold particles were bound to the protein to enable visualization.[115] c) TEM images of straight, kinked, and branched coiled-coil fibers, with the modes of assembly shown schematically.[112]

Another method of accessing long coiled-coil rods has been to covalently link multiple coiled-coil forming peptides such that larger scale assemblies form upon complex formation. Helix-loop-helix peptides have been linked into four arm dendrimers via a sulfide bridge between cysteine residues in the loop region. These assemble into fibers with diameters of only ~ 5 nm, which are postulated to be one complex wide, and are many microns long. Heterofibers or homofibers can be formed depending on the pH dependent charge of the peptides (Figure 14).[121]

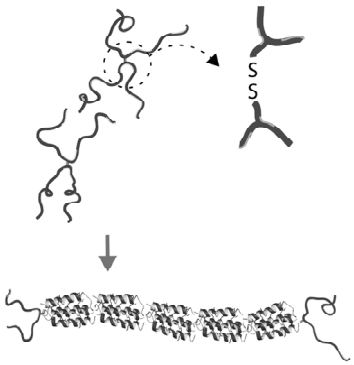


Figure 14. a) Two helix–loop–helix polypeptides are dimerized via cysteine residues and assemble into either homo- or heteroassociated fibers upon folding, depending on the pH value (pH 4.5 = homoassociated fibers, pH 7 = heteroassociated fibers).[121]

The majority of hierarchical coiled-coil structures are fibrous.[122] Dendrimers allow one to branch off from this direction and form three dimensional assemblies. Relatively complex self-assembly has been programmed with coiled-coil dendrimers: each peptide of a three armed dendrimer forms a dimer with a complementary peptide monomer, and the six-helix bundle then binds to three other dendrimer complexes through electrostatic interactions. In this way supramolecular porous sub-micron to micron sized spheres self-assembled. Silver colloids were formed within these 'nanoreactors', with diameters matching the pore sizes (Figure 15). As thiols have been shown to have a size-stabilizing effect on metallic colloids a cysteine residue was placed at position f in the coiled coil, such that the cysteine residues were orientated into the cavities.[122] This has certain parallels with the coiled-coil protein NuMa, which also forms dendrimers that self assemble into well defined three dimensional networks, creating a porous structural support (Figure 6),[33] although NuMa contains the longest known coiled coil, and this assembly is built up from the shortest known heterocoil length.

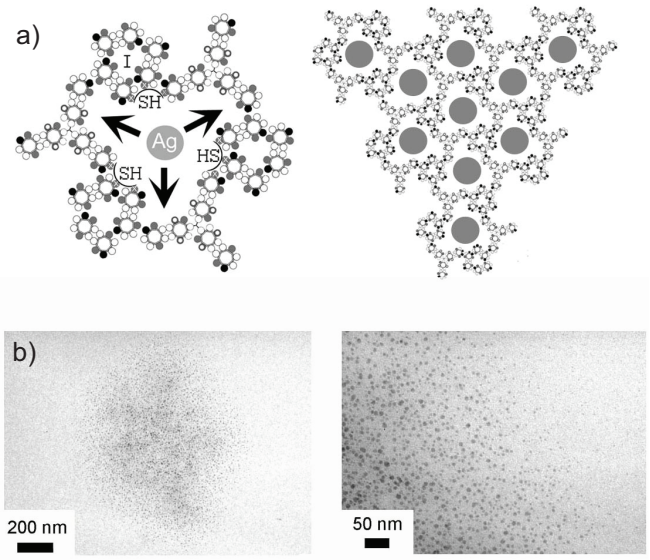


Figure 15. a) Schematics of coiled-coil dendrimers that form mesoscopic spheres with pores serving as reaction sites for nanoscopic silver particles. b) TEM images of the colloidal silver clusters formed in the cavities of the 3D coiled-coil cavities.[122]

Most self-assembly strategies using coiled coils are targeted at controlling the hydrophobic core and the charged residues bordering the core. The previous example varied from this in that the charged residues were designed for interactions between coiled coils. As an extension of this concept a complete departure from the standard coiled-coil binding follows. Amphipathic α-helical coiled-coil forming peptides were located at water-air interfaces, with the hydrophobic face of the helix oriented towards the air. Intra- and intermolecular cross-links between histidine residues stabilized the helices, which created a film at the interface, strengthening the foams. The films were disrupted by adding a metal chelator or by changing the pH to break the peptide-metal bond.[123] This is the only case in which the self-assembly of coiled-coil forming peptides is utilized not for their specific coiled-coil properties, but for their more general amphipathic property. This parallels the recently discovered coiled-coil GEF catalyst, in which the hydrophobic coiled-coil interface is temporarily disrupted and binds to a hydrophobic patch on a Rab protein.[55] An important difference is that the protein-protein interface remains highly specific, in contrast to this synthetic example.

The remainder of the assemblies in this section are composed of coiled-coil hybrids. The biological role of coiled coils in linking larger molecules and sub-cellular structures has been mimicked in the many instances of coiled-coil induced aggregation of nanoparticles. The first demonstration of this use of coiled coils was the decoration of gold nanoparticles with two different three heptad repeat peptides. Upon introduction of a complementary six heptad repeat peptide to the solution, a coiled coil formed, resulting in reversible networks of gold nanoparticles.[124] Utilizing the environmental sensitivity of coiled coils, conditional nanoparticle aggregation has also been investigated. Gold particles decorated with coiled-

coil forming peptides have been induced to aggregate only at low pH or in the presence of metal ions, both of which reduce the charge on multiple glutamic acid side chains (by protonation or chelation), allowing homocoils to form.[125-127] The same peptide also forms a heterocoil with a complimentary peptide dendrimer, which when added to solution induced gold particle aggregation with well defined spacing (Figure 16). The four armed dendrimer linker has a central disulfide bridge, which could be reduced in solution, re-dispersing the gold particles.[126]

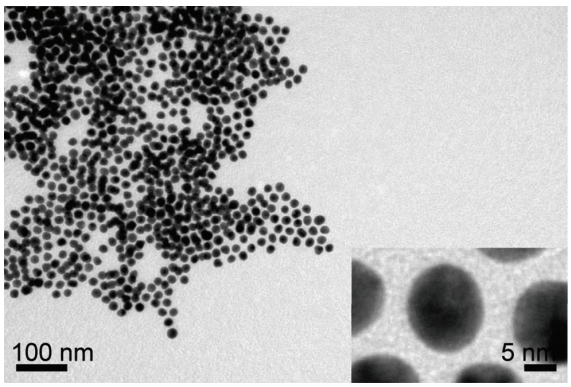


Figure 16. The aggregation of gold nanoparticles can be controlled by coiled-coil association/disassociation.[126]

The responsiveness of coiled-coil based assemblies is most frequently programmed by directly disrupting the binding. A recent example where the binding is indirectly targeted involves a hetero coiled coil (with a T_m > 85 °C) attached to gold nanocapsules which aggregated due to coiled-coil formation. By irradiating the sample with infrared radiation the gold nanoshells, which have a large photothermal response, produced enough heat to denature the coiled-coil complex, separating the nanoshells. When individual nanoshells were decorated in the same way with quantum dots, irradiation caused a large increase in quantum dot fluorescence, but the heat produced by the single nanocapsule did not dissociate the coiled coil (Figure 17).[128] This indirect photothermal control over coiled-coil assembly has no known parallels in nature.

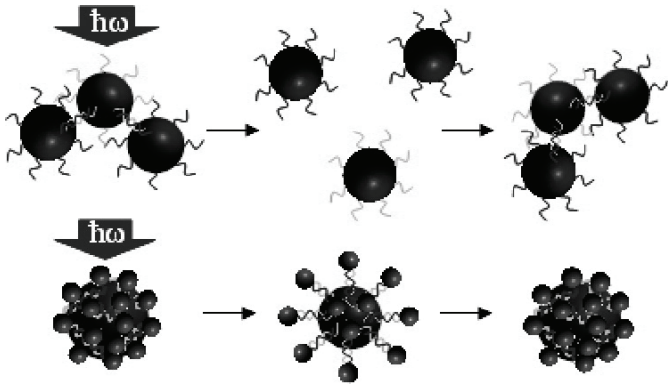


Figure 17. Cartoon of the dissociation of coiled coils by the heat released by illuminated gold nanoshells.[128]

Coiled coils can also be used to link other objects, for example, carbon nanotubes have been linked with gold nanoparticles when each is functionalized with complementary heterodimer forming peptides (Figure 18). In addition, the dimers were able to chelate cobalt via histidine residues.[69] The aim of this is to produce an interface for electrically conducting carbon nanotubes that will sense soluble biomolecular targets.

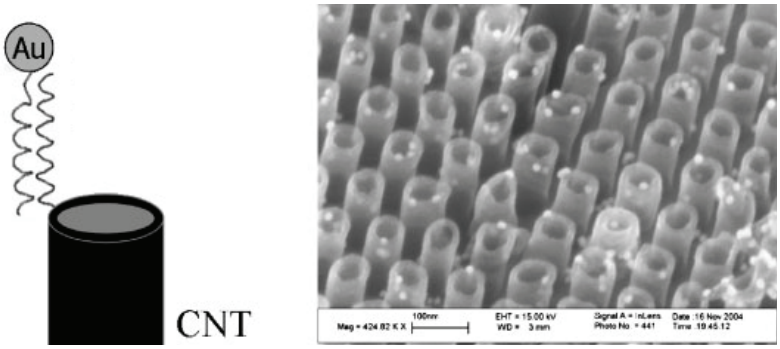


Figure 18. Cartoon and SEM image illustrating the reversible decoration of carbon nanotubes (CNTs) with gold nanoparticles by way of coiled-coil recognition.[69]

Since 1998 assemblies of coiled coils coupled with large water soluble polymer blocks have been investigated.[129] Currently the only materials assembled from coiled-coil hydrophilic hybrids have been hydrogels. As with the assemblies constructed entirely of coiled coils these materials have parallels to the structural function of cyto- and nucleoskeletal coiled-coil networks. In these constructs coiled-coil motifs flank a water soluble protein or polymer segment, and the coiled-coil interaction creates a randomly connected network. In the first example of this kind two coiled-coil forming peptides were linked by a long genetically engineered random coil polypeptide.[129] These artificial proteins form hydrogels via homodimer formation.[129-131] Shortly after this a more synthetic equivalent was demonstrated: a peptide-poly(ethylene glycol)-peptide hybrid that forms a hydrogel via homodimer formation.[132] The response of the coiled coil to temperature, pH, and metal ions allows the triblock hybrids to be switched between solution and gel states. Coiled-coil mediated hydrogels have also been created with the arms consisting of another water soluble polymer, N-(2-hydroxypropyl)methacrylamide, with the coiled-coil binding in a parallel orientation,[133] or an antiparallel orientation, which reduces the steric crowding of the polymer arms.[134] A recent review of peptide directed self-assembly of hydrogels, gives more details on hydrogels via coiled-coil formation.[135]

In contrast to the coiled-coil networks and scaffolds in nature, in which coiled coils constitute the structure, or ‘arms’ of the network (for example see spectrin in natural coiled coils), in the synthetic examples of networks mentioned above the coiled coils are used to connect the arms of the network together. There is one example, in which synthetic biology is entered close to the biology end of the spectrum, of a hydrogel with coiled-coil arms. A long α-helix from the intermediate filament keratin (a fibrous coiled-

coil structural protein) was expressed fused to a globular cell binding domain, and this hybrid was co-assembled with extracted keratins that form hydrogels through intermolecular coiled-coil association of α-helical segments (Figure 19). It was found that neurosphere-forming cells specifically adhered to the modified keratin hydrogel and actively proliferated with a high survival rate.[136]

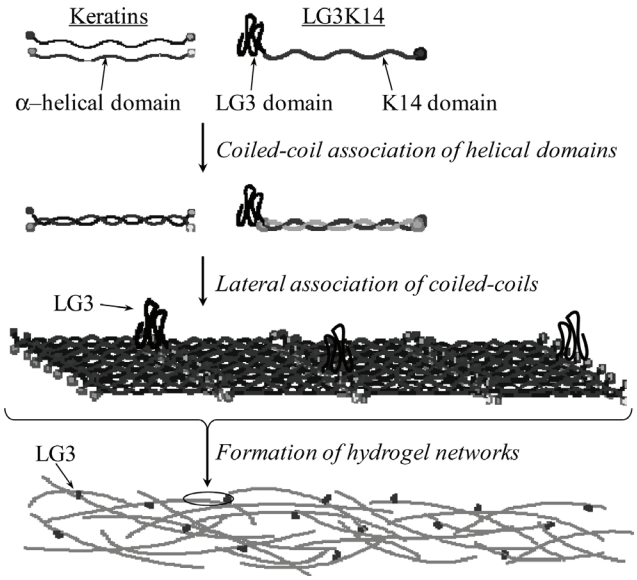


Figure 19. The fusion of a natural keratin peptide with a cell-binding domain modified the properties of the keratin hydrogel.[136]

Coiled-coil assemblies incorporating orthogonal self-assembly

Proteins, themselves hybrids of many self-assembled units, do not operate in isolation, they are embedded in cells, which are composed of self-assembled lipid compartments, self-assembled nucleotides etc. The complexity in coiled-coil based synthetic biology can be extended by coupling a wide variety of particles or molecules to coiled-coil forming peptides, leading to hierarchical self-assembly of "smart" nanostructures in which both coiled-coil formation plays a role and the properties of the other block/s.

An interesting hydrogel uses star-shaped poly(ethylene glycol) functionalized with a lysine rich peptide that folds into a coiled-coil homodimer which in turn binds to a polysaccharide segment (heparin) on a second star-shaped PEG by electrostatic interactions, hence leading to a hydrogel (Figure 20). This is one of the few examples in which coiled coils mediate self-assembly in a way other than by coiled-coil formation.[137]

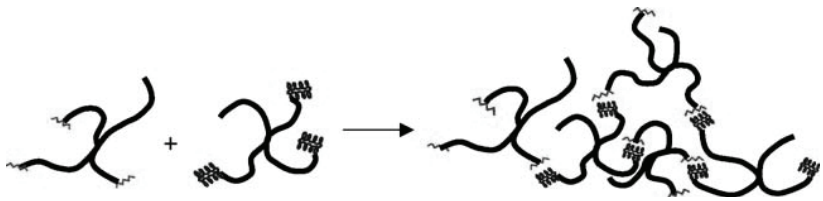


Figure 20. A hydrogels which contains coiled coils, but with the gelation caused by coiled-coil polysaccharide binding.[137]

Hydrogels have been constructed in which random coil polypeptide spacers are partially connected by coiled-coil forming peptides, and partially by an enzyme that dimerizes. Each protein building block has an additional function: the coiled coils are chelated with osmium moieties via histidine residues, rendering the hydrogels conductive, and in the dimeric form the enzyme uses electrons for the catalytic reduction of dioxygen to water. Thus, when the hydrogels are formed on electrodes this combination of functions allows the bioelectrocatalytic reduction of dioxygen to water, with possible application in fuel cells. (Figure 21).[138]

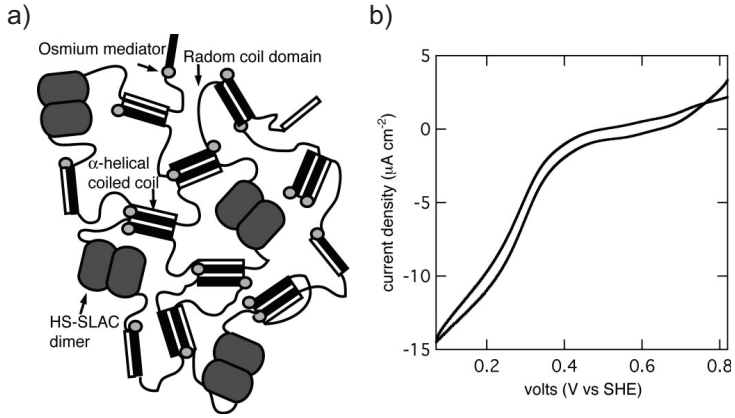


Figure 21. a) Diagram of a supramolecular hydrogel that relies on coiled-coil folding and enzyme dimerization to gelate. b) Bioelectrocatalysis of such a mixed hydrogel.[138]

Coiled-coil Systems

The goal of synthetic-biology is to create functional systems, which implies the interaction of multiple self-assembled components. The aim is therefore to incorporate units or assemblies, such as those discussed in the previous sections, with other self-assembled structures, such that functional systems emerge from the combination of the properties of the components, and the effects that they exert on one another. All of the systems developed to date have been rather basic, using coiled-coil units rather than assemblies. Additionally, each system aims to modify or model natural processes – there has not yet been a synthetic-biology system with an original purpose.

Biologists have made use of coiled-coil synthetic biology for some time. One technique used to visualize protein complexes in living cells is biomolecular fluorescence complementation. The concept is that moieties with highly specific associations are fused to protein fragments and the interaction of these moieties in vivo leads to the protein fragments forming a functional and fluorescent complex. Coiled-coil peptides which bind in a stable and specific manner such as the coiled-coil region from the GCN4 transcription factor and designed peptides have been used for such applications.[139, 140] Alternatively the interactions of native coiled-coil containing proteins can be visualized by fusing them with fragments of small fluorescent proteins.[141] As a specific tag-probe example, a hetero dimeric coiled-coil pair was utilized to label proteins in living cells. One of the peptides

was recombinantly attached to the surface exposed terminus of a transmembrane receptor protein. The corresponding peptide was synthesized with a fluorescent label, and added to the culture medium. Within one minute the fluorescently-labeled peptide had coated the cell surface as hetero coiled coils were formed. The formation of the coiled coil did not affect the receptor function, hence they were an efficient small tag-probe pair (Figure 23).[142]

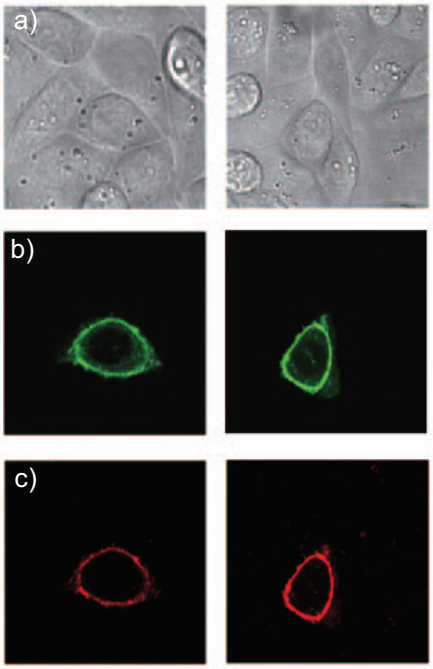


Figure 23. a,b) Cells were expressed bearing a coiled-coil tagged surface protein. Upon addition of the complementary peptide (three heptads, left; four heptads, right) the specific molecular recognition localized the peptide to the surface (c). The labeling was more effective with four heptad repeats on the probe peptide.[142]

Slightly more synthetic examples follow in which coiled-coil units and lipid assemblies are combined. In one case different coiled-coil forming peptides were added to solutions of liposomes. The positively charged peptides adsorbed to the surfaces of the liposomes and caused aggregation of the vesicles (Figure 24). Although the lipid packing was disturbed there was no liposome fusion or leakage. This model system could be used to study the interrelated effects of lipid membranes and coiled-coil peptides on one another.[143]

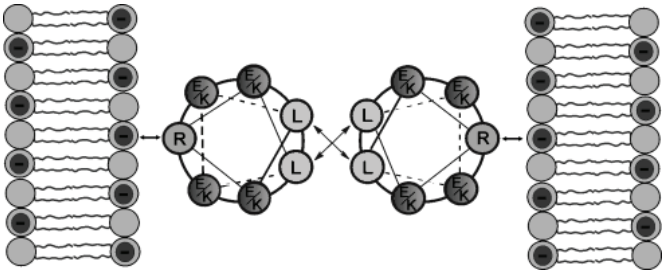


Figure 24. Coiled-coil folding and the interaction of the cationic coiled coil with negatively charged lipid membranes results in vesicle aggregation.[143]

As explained in the ‘native coiled coils’ section, enveloped viruses enter cells by way of a pH triggered conformational change involving a coiled-coil complex. Peptides that form an extremely stable complex with the viral envelope proteins may be an effective way to reduce viruses from infecting cells. Such inhibitors could be screened for with an efficient sensor platform. To that end a coiled-coil trimer based on a native viral protein was anchored to supported lipid bilayers and peptide binding to the coiled coil was monitored. The concept was demonstrated with two known inhibitor peptides and binding was monitored with AFM and ellipsometry, so there is some way to go to make this a practical system.[144]

A synthetic-biology system that is intended not to prevent, but to mimic viral membrane fusion has been developed. A peptide that forms an α-helical trimer at low pH was anchored in liposome bilayers via the C-terminus and displayed a tryptophan residue at the N-terminus. At low pH when the peptides have a helical configuration there is fusion of the liposomes, albeit very slowly and with contents leakage, which is proposed to occur due to tryptophan insertion in a nearby liposome, analogous to the fusion sequence in viral fusion proteins.

CONCLUSIONS

By combining the basic units of coiled coils – amino acids, in different sequences an amazing variety of coiled-coil unit, assembly, and system properties are possible. Changing just two amino acids in a sequence can alter factors such as the coiled-coil binding strength or hierarchical aggregation size by many orders of magnitude. This extreme variability has lead, over billions of years, to coiled coils performing a vast range of functions in every living cell. These functions include, but are certainly not limited to: controlling the binding of cellular components, structural edifices of varying dimensions, levers, force transducers, hinges, and clamps.

These many functions are fertile ground for creating synthetic-biology systems, with the important benefit that the rules for mapping amino acid sequences to coiled-coil assembly are relatively well understood. There is a pyramid of examples in which coiled coils are used as building blocks in synthetic biology. There have been many investigations of coiled coils as units, in which their binding specificity and stability are probed. Based on and building upon this knowledge the self-assembly of these units into higher order structures has been probed, both assemblies composed wholly of coiled coils, and those composed of coiled-coil hybrids. Also their dependence on environmental conditions has been explored. At the tip of the pyramid, an area which has yet to be explored to any great extent is combining coiled coils or coiled-coil hybrids with other self-assembled structures in order to compose functional systems.

Although intricate and with a wealth of function, self-assembly as observed in nature is not always the best solution to a particular challenge. By reverse engineering nature we discover tools with which we can construct structures with a wider scope than biology. We can construct coiled-coil hybrids that are unavailable to nature, and investigate self-assembly via pathways that are not possible naturally. We can use the assembly of coiled coils in nature, as developed slowly over billions of years, as a jumping board to new areas of synthetic biology.

SCOPE OF THIS THESIS

Each of the myriad coiled coils in nature operate in conjunction with other self-assembled units, be they motor domains, DNA-binding sequences, or lipid membranes. However, there have only been a limited number of coiled-coil assemblies or systems that mimic native coiled coils by incorporating orthogonal self-assembly. The aim of this thesis is therefore to explore this section of synthetic-biology space.

In order to achieve this, a range of hybrid molecules are synthesized which combine coiled-coil peptides with a hydrophobic component. In this way the highly specific coiled-coil self-assembly is juxtaposed with the non-specific, but structure-inducing aggregation of the hydrophobic section.

The same coiled-coil unit, made up of peptides 'E' and 'K', is used throughout the exploration, and is introduced in Chapter 2. Experimental characterization is compared and contrasted with a molecular dynamics simulation of the peptide binding. The results from the molecular dynamics simulation support the experimental results, briefly that the peptides E and K form a parallel coiled-coil dimer in aqueous solution. The added benefit of the molecular dynamics simulation is that each binding component is estimated, not just the cumulative average. In this way the E/K binding is understood in more depth, which helps to interpret results from subsequent chapters in which E and K are part of hybrid molecules.

In Chapter 3 the question is posed as to whether coiled-coil forming peptides are still able to fold if one is conjugated to an aggregating hydrophobic block. That is, if the self-assembly process can be balanced such that the intrinsic properties of both blocks persist when they are combined, and if so how they influence one another. To investigate this question the first hybrid is constructed by coupling peptide E with a short polystyrene chain. The self-assembly in solution is investigated of PS_9-E on its own and together with peptide K and a hydrophilic hybrid K-PEG_{77}. It is found that coiled-coil folding between E and K still occurs to a large extent when the peptides are conjugated with PS and/or PEG, resulting in linear noncovalent di- and triblock copolymers. Additionally, the intrinsic aggregation of polystyrene in aqueous solutions is not overpowered, and results in micelles. The morphology of the micelles is changed by reversibly unfolding the coiled-coil block.

The obvious question raised by the results of Chapter 3 is what is the limit of the hydrophobic block size? To approximate the hydrophobic block sizes that the peptides E and K are able to induce into well ordered aggregates, poly(γ-benzyl L-glutamate), or PBLG, was polymerized from peptide E. The synthesis and self-assembly of PBLG-E hybrids with polypeptide block lengths ranging from 36 monomers to 250 monomers are discussed in Chapter 4. By making use of the binding of E and K-PEG even the longest of these hybrids underwent ordered assembly into vesicles in aqueous solution. This system allows one to independently vary both hydrophobic and hydrophilic sections of the amphiphiles, and in this way disk-like micelles, and vesicles of different sizes, membrane

thicknesses and surface chemistries were accessed. The synthesis of polypeptide-*b*-peptides is novel, and as well as the self-assembly flexibility of this new class of peptide, this route has the advantage that the block copolymers are very easy to purify.

The thesis continues with methodology in Chapters 5 and 6, in which two novel techniques to produce polymersomes are presented. Every method to produce polymersomes results in different polymersome characteristics, and has different requirements regarding equipment, time, energy input etc., some of which are not compatible with particular research situations or block copolymers. Therefore a wide range of preparative techniques are beneficial. In Chapter 5 a detergent removal technique that has been used for three decades to form liposomes is adapted to block copolymers. This method will be particularly useful for incorporating biological material into the vesicles as it is a benign process. Chapter 6 adapts another vesicle formation method that has long been applied to liposomes to make it suitable for polymersomes, the 'water addition – solvent evaporation' procedure. The main advantages of this technique are that well defined polymersomes with low polydispersity indices are produced with a high capacity for tuning the polymersome sizes, and that it is very practical in terms of time and equipment, requiring only five minutes and a rotary evaporator.

Chapter 7 returns once again to the main thrust of the thesis: extending the orthogonal self-assembly of coiled-coil hybrids. In this Chapter the aspect under investigation is whether E/K coiled-coil folding can guide not just the self-assembly of the hydrophobic blocks to which they are covalently bound, but also separate supramolecular assemblies. E and K are conjugated to lipids, by which means they are anchored into the lipid bilayers of liposomes. The effect of E/K binding on the liposomes is studied and it is found that the system represents a minimal model for SNARE protein mediated membrane fusion. The coiled-coil hybrids mimic the structural components of SNARE proteins, and importantly they also induce liposomes fusion in a way that mimics native membrane fusion.

Chapter 8 presents an overview of the different approaches available to synthesize polymer-peptide block copolymers. There is a focus on contemporary activities, and the advantages and limitations of each approach are touched upon.

Finally, in Chapter 9 the results are summarized and discussed, and possibilities for future research are presented.

REFERENCES

1. Bromley, E. H. C.; Channon, K.; Moutevelis, E.; Woolfson, D. N. *ACS Chem. Biol.* **2008,** 3, (1), 38-50.
2. For sixty years beginning in the early 1930s, (Astbury, W.T. and A. Street, X-ray studies of the structure of hair, wool and related fibers. I. *General Trans. Roy. Soc A*, **1931**. 230, 75-101. Astbury, W.T. and H.J. Woods, X-ray studies on the structure of hair, wool and related fibers II: the molecular structure and elastic properties of hair keratin. *Philos. Trans. Roy. Soc. A,* **1933**. 232, 333-394.) research into understanding natural coiled coils simmered along with a scant output of ~ 5 publications per year. In the 1990's there was an explosion of research into coiled coils, with ~ 500 publications per year for the last 10 years. This sudden increase coincided with solid-phase peptide synthesis and Fmoc protected amino acids becoming affordable. The predominant focus of coiled-coil research is still on understanding the binding of native coiled coils, but, due in part to the insights gained in understanding native coiled coils, there is growing interest in utilizing rationally designed coiled coils for synthetic self-assembly.
3. Wolf, E.; Kim, P. S.; Berger, B. *Protein Sci.* **1997,** 6, (6), 1179-1189.
4. Barbara, K. E.; Willis, K. A.; Haley, T. M.; Deminoff, S. J.; Santangelo, G. M. *Mol. Genet. Genomics* **2007,** 278, (2), 135-147.
5. Rose, A.; Schraegle, S. J.; Stahlberg, E. A.; Meier, I. *BMC Evol. Biol.* **2005,** 5: 66.
6. Rose, A.; Meier, I. *Cell Mol. Life. Sci.* **2004,** 61, (16), 1996-2009.
7. Kohn, W. D.; Mant, C. T.; Hodges, R. S. *J. Biol. Chem.* **1997,** 272, (5), 2583-2586.
8. Blake, R. D., *Informational Biopolymers of Genes and Gene Expression: Properties and Evolution.* University Science Books: 2005; p 778.
9. Hurst, H. C. *Protein Profile* **1995,** 2, (2), 105-168.
10. Szilak, L.; Moitra, J.; Vinson, C. *Protein Sci.* **1997,** 6, (6), 1273-1283.
11. Gottschalk, K. E. *Structure* **2005,** 13, (5), 703-712.
12. Glover, J. N. M.; Harrison, S. C. *Nature* **1995,** 373, (6511), 257-261.
13. Shu, W.; Liu, J.; Ji, H.; Lu, M. *J. Mol. Biol.* **2000,** 299, (4), 1101.
14. Zizlsperger, N.; Malashkevich, V. N.; Pillay, S.; Keating, A. E. *Biochemistry* **2008,** 47, (45), 11858-11868.
15. White, G. E.; Erickson, H. P. *J. Struct. Biol.* **2006,** 154, (2), 111-121.
16. Parry, D. A. D.; Fraser, R. D. B.; Squire, J. M. *J. Struct. Biol.* **2008,** 163, (3), 258-269.
17. Peters, J.; Baumeister, W.; Lupas, A. *J. Mol. Biol.* **1996,** 257, (5), 1031-1041.
18. Peters, J.; Nitsch, M.; Kuhlmorgen, B.; Golbik, R.; Lupas, A.; Kellermann, J.; Engelhardt, H.; Pfander, J. P.; Muller, S.; Goldie, K.; Engel, A.; Stetter, K. O.; Baumeister, W. *J. Mol. Biol.* **1995,** 245, (4), 385-401.
19. Stetefeld, J.; Jenny, M.; Schulthess, T.; Landwehr, R.; Engel, J.; Kammerer, R. A. *Nat. Struct. Biol.* **2000,** 7, (9), 772-776.
20. Peters, J.; Baumeister, W.; Lupas, A. *J. Mol. Biol.* **1996,** 257, (5), 1031.
21. Burkhard, P.; Stetefeld, J.; Strelkov, S. V. *Trends Cell Biol.* **2001,** 11, (2), 82-88.
22. Engelhardt, H. *J. Struct. Biol.* **2007,** 160, (2), 115.
23. Herrmann, H.; Bar, H.; Kreplak, L.; Strelkov, S. V.; Aebi, U. *Nat. Rev. Mol. Cell Biol.* **2007,** 8, (7), 562-573.
24. Herrmann, H.; Aebi, U. *Annu. Rev. Bicochem.* **2004,** 73, 749-789.
25. Mucke, N.; Kreplak, L.; Kirmse, R.; Wedig, T.; Herrmann, H.; Aebi, U.; Langowski, J. *J.Mol. Biol.* **2004,** 335, (5), 1241-1250.
26. Ausmees, N. *J. Mol. Microbiol. Biotech.* **2006,** 11, (3-5), 152-158.
27. Margolin, W. *Curr. Biol.* **2004,** 14, (6), R242-R244.
28. Antoniou, C.; Lam, V. Q.; Fung, L. W. M. *Biochemistry* **2008,** 47, (40), 10765-10772.
29. De Matteis, M. A.; Morrow, J. S. *J. Cell Sci.* **2000,** 113, (13), 2331-2343.
30. Salomao, M.; Zhang, X. H.; Yang, Y.; Lee, S.; Hartwig, J. H.; Chasis, J. A.; Mohandas, N.; An, X. L. *Proc. Natl. Acad. Sci. U. S. A.* **2008,** 105, (23), 8026-8031.
31. Ausmees, N.; Kuhn, J. R.; Jacobs-Wagner, C. *Cell* **2003,** 115, (6), 705-713.
32. Lodish, H.; Berk, A.; Zipursky, L. S.; Matsudaira, P.; Baltimore, D.; Darnell, J., *Molecular Cell Biology*. 4th ed.; W. H. Freeman and Company: New York, Basingstoke, 2000.
33. Harborth, J.; Wang, J.; Gueth-Hallonet, C.; Weber, K.; Osborn, M. *Embo. J.* **1999,** 18, (6), 1689-1700.
34. Burghardt, T. P.; Hu, J. Y.; Ajtai, K. *Biophys. Chem.* **2007,** 131, (1-3), 15-28.

35. Ciudad, A.; Sancho, J. M.; Tsironis, G. P. *J. Biol. Phys.* **2006,** 32, (5), 455-463.
36. Uyeda, T. Q. P.; Warrick, H. M.; Kron, S. J.; Spudich, J. A. *Nature* **1991,** 352, (6333), 307-311.
37. Toba, S.; Watanabe, T. M.; Yamaguchi-Okimoto, L.; Toyoshima, Y. Y.; Higuchi, H. *Proc. Natl. Acad. Sci. U. S. A.* **2006,** 103, (15), 5741-5745.
38. Schwaiger, I.; Sattler, C.; Hostetter, D. R.; Rief, M. *Nat. Mater.* **2002,** 1, (4), 232.
39. Kreplak, L.; Nyland, L. R.; Contompasis, J. L.; Vigoreaux, J. O. *J. Mol. Biol.* **2009,** 386, (5), 1403.
40. Al-Khayat, H. A.; Morris, E. P.; Squire, J. M. *J. Struct. Biol.* **2009,** 166, (2), 183-194.
41. Vale, R. D.; Milligan, R. A. *Science* **2000,** 288, (5463), 88-95.
42. Endres, N. F.; Yoshioka, C.; Milligan, R. A.; Vale, R. D. *Nature* **2006,** 439, (7078), 875-878.
43. Lauzon, A. M.; Fagnant, P. M.; Warshaw, D. M.; Trybus, K. M. *Biophys. J.* **2001,** 80, (4), 1900-1904.
44. Mizuno, N.; Narita, A.; Kon, T.; Sutoh, K.; Kikkawa, M. *Proc. Natl. Acad. Sci. U. S. A.* **2007,** 104, (52), 20832-20837.
45. Sakakibara, H.; Kojima, H.; Sakai, Y.; Katayama, E.; Oiwa, K. *Nature* **1999,** 400, (6744), 586-590.
46. Burgess, S. A.; Knight, P. J. *Curr. Opin. Struct. Biol.* **2004,** 14, (2), 138.
47. Kon, T.; Imamula, K.; Roberts, A. J.; Ohkura, R.; Knight, P. J.; Gibbons, I. R.; Burgess, S. A.; Sutoh, K. *Nat. Struct. Mol. Biol.* **2009,** 16, (3), 325.
48. Burgess, S. A.; Walker, M. L.; Sakakibara, H.; Knight, P. J.; Oiwa, K. *Nature* **2003,** 421, (6924), 715-718.
49. Besteiro, S.; Coombs, G. H.; Mottram, J. C. *Bmc Genomics* **2006,** 7.
50. Lin, R. C.; Scheller, R. H. *Annu. Rev. Cell Dev. Bi.***2000,** 16, (1), 19-49.
51. Fasshauer, D.; Sutton, R. B.; Brunger, A. T.; Jahn, R. *Proc. Natl. Acad. Sci. U. S. A.* **1998,** 95, (26), 15781-15786.
52. Rizo, J.; Chen, X. C.; Arac, D. *Trends Cell Biol.* **2006,** 16, (7), 339-350.
53. Malsam, J.; Kreye, S.; Sollner, T. H. *Cell Mol. Life. Sci.* **2008,** 65, (18), 2814-2832.
54. Ungermann, C.; Langosch, D. *J. Cell Sci.* **2005,** 118, (17), 3819-3828.
55. Dong, G.; Medkova, M.; Novick, P.; Reinisch, K. M. *Molecular Cell* **2007,** 25, (3), 455-462.
56. Skehel, J. J.; Bayley, P. M.; Brown, E. B.; Martin, S. R.; Waterfield, M. D.; White, J. M.; Wilson, I. A.; Wiley, D. C. *Proc. Natl. Acad. Sci. U. S. A.* **1982,** 79, (4), 968-972.
57. Wilson, I. A.; Skehel, J. J.; Wiley, D. C. *Nature* **1981,** 289, (5796), 366-373.
58. Carr, C. M.; Kim, P. S. *Cell* **1993,** 73, (4), 823-832.
59. Shangguan, T.; Siegel, D. P.; Lear, J. D.; Axelsen, P. H.; Alford, D.; Bentz, J. *Biophys. J.* **1998,** 74, (1), 54-62.
60. Harrison, S. C. *Nat. Struc. Mol. Biol.* **2008,** 15, (7), 690-698.
61. Lupas, A. *Trends Biochem. Sci.* **1996,** 21, (10), 375.
62. Dormitzer, P. R.; Nason, E. B.; Prasad, B. V. V.; Harrison, S. C. *Nature* **2004,** 430, (7003), 1053-1058.
63. Hurme, R.; Berndt, K. D.; Namork, E.; Rhen, M. *J. Biol. Chem.* **1996,** 271, (21), 12626-12631.
64. Naik, R. R.; Kirkpatrick, S. M.; Stone, M. O. *Biosens. Bioelectron.* **2001,** 16, (9-12), 1051-1057.
65. Hurme, R.; Berndt, K. D.; Normark, S. J.; Rhen, M. *Cell* **1997,** 90, (1), 55-64.
66. Mojzsis, S. J.; Arrhenius, G.; McKeegan, K. D.; Harrison, T. M.; Nutman, A. P.; Friend, C. R. L. *Nature* **1996,** 384, (6604), 55-59.
67. Stretton, A. O. W. *Genetics* **2002,** 162, (2), 527-532.
68. Crick, F. H. C. *Nature* **1952,** 170, (4334), 882-883.
69. Contarino, M. R.; Sergi, M.; Harrington, A. E.; Lazareck, A.; Xu, J.; Chaiken, I. *J. Mol. Recognit.* **2006,** 19, (4), 363-371.
70. Channon, K.; Bromley, E. H. C.; Woolfson, D. N. *Curr. Opin. Struct. Biol.* **2008,** 18, (4), 491-498.
71. Burkhard, P.; Ivaninskii, S.; Lustig, A. *J. Mol. Biol.* **2002,** 318, (3), 901-910.
72. Dong, H.; Hartgerink, J. D. *Biomacromolecules* **2006,** 7, (3), 691-695.
73. Mason, J. M.; Hagemann, U. B.; Arndt, K. M. *J. Biol. Chem.* **2007,** 282, (32), 23015-23024.
74. Jean-Francois, N.; Frederic, G.; Raymund, W.; Benoit, C.; Lavigne, P. *J. Mol. Biol.* **2003,** 326, (5), 1577-1595.
75. Tang, Y.; Ghirlanda, G.; Vaidehi, N.; Kua, J.; Mainz, D. T.; Goddard, W. A.; DeGrado, W. F.; Tirrell, D. A. *Biochemistry* **2001,** 40, (9), 2790-2796.
76. Son, S.; Tanrikulu, I. C.; Tirrell, D. A. *Chembiochem* **2006,** 7, (8), 1251-1257.
77. Kumita, J. R.; Flint, D. G.; Woolley, G. A.; Smart, O. S. *Faraday Discuss.* **2003,** 122, 89-103.
78. Pagel, K.; Koksch, B. *Curr. Opin. Chem. Biol.* **2008,** 12, (6), 730-739.
79. Diss, M. L.; Kennan, A. J. *Org. Lett.* **2008,** 10, (17), 3797-3800.

80. Bromley, E. H. C.; Sessions, R. B.; Thomson, A. R.; Woolfson, D. N. *J. Am. Chem. Soc.* **2009,** 131, (3), 928-930.
81. Apostolovic, B.; Klok, H. A. *Biomacromolecules* **2008,** 9, (11), 3173-3180.
82. Unpublished data
83. Schnarr, N. A.; Kennan, A. J. *J. Am. Chem. Soc.* **2003,** 125, (43), 13046-13051.
84. Schnarr, N. A.; Kennan, A. J. *Org. Lett.* **2005,** 7, (3), 395-398.
85. Gonzalez, L.; Plecs, J. J.; Alber, T. *Nat. Struc. Biol.***1996,** 3, (6), 510-515.
86. Wagschal, K.; Tripet, B.; Lavigne, P.; Mant, C.; Hodges, R. S. *Protein Sci.* **1999,** 8, (11), 2312-2329.
87. Tripet, B.; Wagschal, K.; Lavigne, P.; Mant, C. T.; Hodges, R. S. *J.Mol. Biol.* **2000,** 300, (2), 377-402.
88. Tsatskis, Y.; Kwok, S. C.; Becker, E.; Gill, C.; Smith, M. N.; Keates, R. A. B.; Hodges, R. S.; Wood, J. M. *Biochemistry* **2008,** 47, (1), 60-72.
89. Liu, I. J.; Kao, C. L.; Hsieh, S. C.; Wey, M. T.; Kan, L. S.; Wang, W. K. *Antiviral Res.* **2009,** 81, (1), 82-87.
90. Tripet, B.; Kao, D. J.; Jeffers, S. A.; Holmes, K. V.; Hodges, R. S. *J. Struct. Biol.* **2006,** 155, (2), 176-194.
91. Jouaux, E. M.; Timm, B. B.; Arndt, K. M.; Exner, T. E. *J. Pept. Sci.* **2009,** 15, (1), 5-15.
92. Kammerer, R. A.; Steinmetz, M. O. *J. Struct. Biol.* **2006,** 155, (2), 146-153.
93. Ciani, B.; Hutchinson, E. G.; Sessions, R. B.; Woolfson, D. N. *J. Biol. Chem.* **2002,** 277, (12), 10150-10155.
94. Dong, H.; Hartgerink, J. D. *Biomacromolecules* **2007,** 8, (2), 617-623.
95. Pagel, K.; Wagner, S. C.; Araghi, R. R.; von Berlepsch, H.; Bottcher, C.; Koksch, B. *Chem.-Eur. J.* **2008,** 14, (36), 11442-11451.
96. Lee, D. H.; Granja, J. R.; Martinez, J. A.; Severin, K.; Ghadiri, M. R. *Nature* **1996,** 382, (6591), 525-528.
97. Yao, S.; Ghosh, I.; Zutshi, R.; Chmielewski, J. *J. Am. Chem. Soc.* **1997,** 119, (43), 10559-10560.
98. Yao, S.; Ghosh, I.; Zutshi, R.; Chmielewski, J. *Angew. Chem., Int. Edit.* **1998,** 37, (4), 478-481.
99. Kennan, A. J.; Haridas, V.; Severin, K.; Lee, D. H.; Ghadiri, M. R. *J. Am. Chem. Soc.* **2001,** 123, (9), 1797-1803.
100. Severin, K.; Lee, D. H.; Kennan, A. J.; Ghadiri, M. R. *Nature* **1997,** 389, (6652), 706-709.
101. Yao, S.; Chmielewski, J. *Biopolymers* **1999,** 51, (5), 370-375.
102. Lee, D. H.; Severin, K.; Yokobayashi, Y.; Ghadiri, M. R. *Nature* **1997,** 390, (6660), 591-594.
103. Issac, R.; Chmielewski, J. *J. Am. Chem. Soc.* **2002,** 124, (24), 6808-6809.
104. Li, X. Q.; Chmielewski, J. *J. Am. Chem. Soc.* **2003,** 125, (39), 11820-11821.
105. Issac, R.; Ham, Y.-W.; Chmielewski, J. *Curr. Opin. Struct. Biol.* **2001,** 11, (4), 458.
106. Matsumura, S.; Takahashi, T.; Ueno, A.; Mihara, H. *Chem.- Eur. J.* **2003,** 9, (19), 4829-4837.
107. Kojima, S.; Kuriki, Y.; Yoshida, T.; Yazaki, K.; Miura, K. *Proc. Jpn. Acad. Ser. B-Phys. Biol. Sci.* **1997,** 73, (1), 7-11.
108. Fairman, R.; Akerfeldt, K. S. *Curr. Opin. Struct. Biol.* **2005,** 15, (4), 453-463.
109. Yeates, T. O.; Padilla, J. E. *Curr. Opin. Struct. Biol.* **2002,** 12, (4), 464-470.
110. MacPhee, C. E.; Woolfson, D. N. *Curr. Opin. Solid St. M.* **2004,** 8, (2), 141-149.
111. Ulijn, R. V.; Smith, A. M. *Chem. Soc. Rev.* **2008,** 37, (4), 664-675.
112. Woolfson, D. N.; Ryadnov, M. G. *Curr. Opin. Chem. Biol.* **2006,** 10, (6), 559-567.
113. Lazar, K. L.; Miller-Auer, H.; Getz, G. S.; Orgel, J.; Meredith, S. C. *Biochemistry* **2005,** 44, (38), 12681-12689.
114. Papapostolou, D.; Brornley, E. H. C.; Bano, C.; Woolfson, D. N. *J. Am. Chem. Soc.* **2008,** 130, (15), 5124-5130.
115. Ryadnov, M. G.; Woolfson, D. N. *J. Am. Chem. Soc.* **2004,** 126, (24), 7454-7455.
116. Ryadnov, M. G.; Woolfson, D. N. *Angew. Chem., Int. Edt.* **2003,** 42, (26), 3021-3023.
117. Ryadnov, M. G.; Woolfson, D. N. *Nat. Mater.* **2003,** 2, (5), 329-332.
118. Holmstrom, S. C.; King, P. J. S.; Ryadnov, M. G.; Butler, M. F.; Mann, S.; Woolfson, D. N. *Langmuir* **2008,** 24, (20), 11778-11783.
119. Potekhin, S. A.; Melnik, T. N.; Popov, V.; Lanina, N. F.; Vazina, A. A.; Rigler, P.; Verdini, A. S.; Corradin, G.; Kajava, A. V. *Chem. Biol.* **2001,** 8, (11), 1025-1032.
120. Zimenkov, Y.; Dublin, S. N.; Ni, R.; Tu, R. S.; Breedveld, V.; Apkarian, R. P.; Conticello, V. P. *J. Am. Chem. Soc.* **2006,** 128, (21), 6770-6771.
121. Aili, D.; Tai, F. I.; Enander, K.; Baltzer, L.; Liedberg, B. *Angew. Chem., Int. Edt.* **2008,** 47, (30), 5554-5556.

122. Ryadnov, M. G. *Angew. Chem., Int. Edt.* **2007,** 46, (6), 969-972.
123. Dexter, A. F.; Middelberg, A. P. J. *J. Phys. Chem. C* **2007,** 111, (28), 10484-10492.
124. Ryadnov, M. G.; Ceyhan, B.; Niemeyer, C. M.; Woolfson, D. N. *J. Am. Chem. Soc.* **2003,** 125, (31), 9388-9394.
125. Aili, D.; Enander, K.; Rydberg, J.; Nesterenko, I.; Bjorefors, F.; Baltzer, L.; Liedberg, B. *J. Am. Chem. Soc.* **2008,** 130, (17), 5780-5788.
126. Aili, D.; Enander, K.; Baltzer, L.; Liedberg, B. *Nano Lett.* **2008,** 8, (8), 2473-2478.
127. Stevens, M. M.; Flynn, N. T.; Wang, C.; Tirrell, D. A.; Langer, R. *Adv. Mater.* **2004,** 16, (11), 915-918.
128. Slocik, J. M.; Tam, F.; Halas, N. J.; Naik, R. R. *Nano Lett.* **2007,** 7, (4), 1054-1058.
129. Petka, W. A.; Harden, J. L.; McGrath, K. P.; Wirtz, D.; Tirrell, D. A. *Science* **1998,** 281, (5375), 389-392.
130. Wang, C.; Kopecek, J.; Stewart, R. J. *Biomacromolecules* **2001,** 2, (3), 912-920.
131. Stevens, M. M.; Allen, S.; Davies, M. C.; Roberts, C. J.; Sakata, J. K.; Tendler, S. J. B.; Tirrell, D. A.; Williams, P. M. *Biomacromolecules* **2005,** 6, (3), 1266-1271.
132. Wang, C.; Stewart, R. J.; Kopecek, J. *Nature* **1999,** 397, (6718), 417-420.
133. Yang, J. Y.; Xu, C. Y.; Kopeckova, P.; Kopecek, J. *Macromol. Biosci.* **2006,** 6, (3), 201-209.
134. Yang, J. Y.; Xu, C. Y.; Wang, C.; Kopecek, J. *Biomacromolecules* **2006,** 7, (4), 1187-1195.
135. Kopecek, J.; Yang, J. *Acta Biomater.* **2009,** 5, (3), 805.
136. Nakaji-Hirabayashi, T.; Kato, K.; Iwata, H. *Biomacromolecules* **2008,** 9, (5), 1411-1416.
137. Zhang, L.; Furst, E. M.; Kiick, K. L. *J. Control. Release* **2006,** 114, (2), 130-142.
138. Wheeldon, I. R.; Gallaway, J. W.; Barton, S. C.; Banta, S. *Proc. Natl. Acad. Sci. U. S. A.* **2008,** 105, (40), 15275-15280.
139. Marsden, H. R.; Korobko, A. V.; van Leeuwen, E. N. M.; Pouget, E. M.; Veen, S. J.; Sommerdijk, N.; Kros, A. *J. Am. Chem. Soc.* **2008,** 130, (29), 9386-9393.
140. Kerppola, T. K. *Nat. Rev. Mol. Cell Biol.* **2006,** 7, (6), 449-456.
141. Mizuno, T.; Murao, K.; Tanabe, Y.; Oda, M.; Tanaka, T. *J. Am. Chem. Soc.* **2007,** 129, (37), 11378-11383.
142. Hu, C. D.; Kerppola, T. K. *Nat. Biotech.* **2003,** 21, (5), 539-545.
143. Yano, Y.; Yano, A.; Oishi, S.; Sugimoto, Y.; Tsujimoto, G.; Fujii, N.; Matsuzaki, K. *ACS Chem. Biol.* **2008,** 3, (6), 341-345.
144. Vagt, T.; Zschornig, O.; Huster, D.; Koksch, B. *Chemphyschem* **2006,** 7, (6), 1361-13

UNDERSTANDING THE BINDING OF THE E/K PEPTIDE DIMER IN AQUEOUS SOLUTION, A COMBINED EXPERIMENTAL AND COMPUTATIONAL STUDY

Coiled coils are composed of α-helical peptides that bind together with an affinity and specificity that is very sensitive to the amino acid sequence. This potential to link the amino acid sequence to peptide form and function makes them valuable building blocks for nanostructures with novel functions. The design criteria for coiled coils are relatively well understood, though still incomplete, therefore to maximize their use in supramolecular chemistry it is important to extend the general design criteria to an understanding of the contribution of each amino acid to the coiled-coil binding. In this Chapter experimental techniques are combined with molecular dynamics simulations to quantify the parallel coiled-coil heterodimer formation of the peptides E and K. It is shown firstly that the simulations accurately predict the peptide tertiary and quaternary structures; and secondly, by breaking down the binding energy of each amino acid, that the simulations provide useful insights into the importance of particular residues to the coiled-coil binding. For example, the van der Waals energies of the terminal core forming residues drive the binding of E and K, while the charged residues bordering the core, contrary to previous assumptions, destabilize the dimer. K is optimally designed, but E is energetically more favorable in monomeric form, hence the sequence could be redesigned to stabilize the heterodimer. The computational results complement and extend the experimental results, demonstrating that this method will be useful to connect peptide sequence to the function of complex designed coiled-coil building blocks.

INTRODUCTION

Coiled coils consist of α-helical peptides that fold together due to shielding of hydrophobic residues and through electrostatic interactions between charged residues on adjacent coils.[1] The archetypal coiled-coil forming sequence has a heptad repeat of amino acids, represented by **abcdefg**, with positions **a** and **d** being hydrophobic residues that form a 'hydrophobic face' when the peptide is in the α-helical conformation.[2] The packing of two or more of these hydrophobic faces together results in the helices wrapping around one another in a left-handed supercoil.[3] In this conformation the charged amino acids **e** and **g** border the core, and the electrostatic attractions or repulsions between these confer alignment and specificity to a particular combination of helices (Figure 1).[2] The noncovalent association of the peptides is sensitive to changes in pH, temperature and salt content.[4-7]

The coiled-coil motif is a common structure in nature, with up to 10% of eukaryotic proteins containing sequences predicted to adopt the coiled-coil motif.[8] The coiled-coil domain has a diverse array of functions in different proteins, for example acting as spacers between functional head and tail domains, forming filaments and networks, operating as flexible connectors, tethering vesicles, facilitating membrane fusion, and acting as temperature sensors by unfolding above a certain temperature.[9] Because of the response of coiled coils to changes in the cellular environment it is expected that more regulatory functions of the coiled-coil motif will be discovered. In natural coiled coils there can be some variation in the placement of hydrophobic, hydrophilic, and neutral residues at certain positions in the heptad repeat, and indeed some variation could be essential to balance the need for both stability and specificity.[10, 11]

The coiled-coil motif is on one hand very simple – it is a cylinder with well defined size, shape, and surface functionality, it consists only of α-helix secondary structure, and is readily identified by circular dichroism; and on the other hand the binding properties can be controlled through design of the amino acid sequence and also post-synthesis by external stimuli such at temperature, salt and pH.[4-7] This combined simplicity and functionality has lead to their use as 'natural' molecular tools in nanotechnology. Applications of coiled coils to date include those in the bionanotechnology field, such as affinity purification and biosensors,[12] conformationally defined combinatorial libraries,[13] the directed assembly of extracellular receptor domains,[14] and the creation of miniature antibodies.[15] A burgeoning area of interest is their incorporation into hybrid macromolecules, as their well-defined structure and responsiveness allow precise control over nano-, micro-, and macrostructure. Examples are hydrogels,[16-18] controlled aggregation of gold nanoparticles,[19] the formation of fibers[20-23] and fractal structures,[24] incorporation into hierarchically self-assembling block copolymers,[25] and in liposome fusion systems.[26]

With this increasing complexity of biomaterials that incorporate coiled coils the peptides are not acting in isolation, the binding properties – stability, specificity, aggregation number, and orientation – are also influenced by the self assembly of neighboring groups. The current coiled coil design rules have been sufficient for a number of applications, but as seen in nature, there are numerous functions that they can undertake, and in order to make full use of the potential of coiled coils in biomaterials there is a need for a quantitative measure of the coiled-coil binding.

This Chapter combines experimental and computational results to understand in greater detail why one peptide dimer 'binds' while another will not by looking at the contributions of each amino acid in the heptad repeat in a quantitative way, beyond the 'hydrophobic', 'neutral', or 'hydrophilic' qualifications. The van der Waals and coulomb contributions of each residue to the dimer binding is calculated. This is the first time that the contributions of each amino acid to coiled-coil binding have been presented.

It is demonstrated that these computational techniques can use amino acid sequences as input and from these accurately calculate the intermolecular structural and binding properties of coiled-coil forming peptides. These techniques can now be used to predict the binding in more complex applications of coiled-coil forming peptides, for example peptide containing hybrids, which will focus advances in this expanding field.

RESULTS AND DISCUSSION

Peptide design

The peptide sequences used in this study are based on an α-helical coiled-coil pair shown by Litowski and Hodges to exclusively form parallel heterodimers with high conformational stability.[27-30] The compositions of the peptides are shown in Table 1. At three heptad repeats they are amongst the shortest peptides that form stable coiled-coil heterodimers.

Table 1. Peptide sequences.

Name	Structure[a]	M_n[b]
K	Ac-WG(KIAALKE)$_3$G-NH$_2$	2620
E	Ac-YG(EIAALEK)$_3$-NH$_2$	2543

[a] Ac = acetyl. The sequences are written using the one-letter amino acid code. [b] M_n (molecular weight) values of the hybrid molecules were calculated from MALDI-TOF spectra.

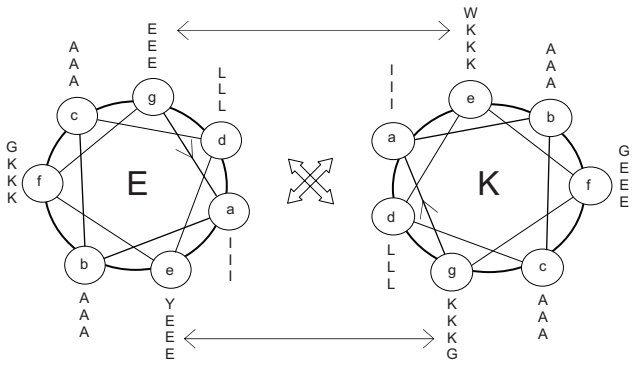


Figure 1. Helical wheel diagram of peptides E and K. Peptides E and K propagate into the page from the N-terminus to the C-terminus. The potential inter-helical electrostatic interactions are demonstrated by thin arrows and the inter-helical hydrophobic core packing by open arrows.

This pair incorporates design criteria for each position in the heptad repeat (Figure 1) in order to maximize the stability of the parallel heterodimeric α-helical coiled coil. The hydrophobic core (positions **a** and **d** in the amino acid heptad repeat), has been found previously to be most stabilized by β-branched amino acids at position **a** [31], in this case isoleucine, and that leucine is the most stabilizing residue at position **d,**[32] as is the case with these peptides. This combination of isoleucine and leucine in the hydrophobic core sterically fit well together in a 'knobs in holes' manner.[27]

Heterodimerization was programmed by incorporating charged residues at positions **e** and **g**, bordering the hydrophobic core, with these being lysine for peptide K and glutamic acid for peptide E. The experiments are carried out at pH 7.0, where the side chains of all lysine residues should be protonated, and hence positively charged, and the side chains of all glutamic acid residues should be deprotonated and hence negatively charged.[33] In this way it is thought that homodimers are destabilized by electrostatic repulsions and heterodimers are stabilized by electrostatic attractions. The peptides used in this study

were based on a pair that were three heptad repeats long. The individual peptides did not form homodimers, but when combined they formed heterodimers. Peptides were also synthesized with four heptad repeats and these did self-associate,[28] demonstrating the fine balance required between the stabilization provided by the hydrophobic core and the specificity imparted by the charged amino acids at these side positions.

Positions **b** and **c** , away from the hydrophobic face, were occupied by alanine residues, which are known to increase the likelihood that a peptide adopts an α-helical configuration.[34]

The final position in the heptad repeat, position **f**, was occupied by either lysine or glutamic acid, the opposite of what is in positions **e** and **g**, thus decreasing the overall net charge on a single peptide and increasing the solubility.[28]

The peptides also include N-terminal fluorescent amino acids tryptophan and tyrosine to enable characterization of the peptide orientation (parallel or antiparallel) by fluorescence spectroscopy. These are separated from the three heptad repeats by a glycine spacer to reduce possible end-fraying effects of the tryptophan and tyrosine. Peptide E also has a C-terminal glycine residue to act as a spacer between the peptide and polymers in future hybrid studies.[25]

First the experimental results are discussed in terms of peptide structure and binding, followed by the results from the computer simulations, again divided into structural and binding properties.

Experimental Results – Structural Properties

Circular Dichroism.

Peptide E has a predominantly random coil structure in phosphate buffered saline (PBS, pH 7.0), while K is predominantly α-helical, as determined by their circular dichroism (CD) spectra (Figure 2a). With an equimolar mixture of E and K, denoted E/K, the intensity at 222 nm, which is directly proportional to the amount of helical structure, [35] increased. The ellipticity ratio, $[\theta]_{222}/[\theta]_{208,}$ also increased to 1.01 (Table 1), indicative of the formation of coiled coils.[36]

The peptide interaction was further analyzed by recording CD spectra after diluting the samples 1:1 (v/v) with trifluoroethanol (TFE). TFE is known to enhance intramolecular α-helicity while disrupting intermolecular interactions.[37] In this solvent mixture the % α-helicity of E and K increased and their ellipticity ratios were 0.80 and 0.81 respectively, which is in the range of monomeric helices. For the mixture there is a significant decrease in the $[\theta]_{222}/[\theta]_{208}$ ratio from benign buffer to 50% TFE, decreasing from 1.01 to 0.81, as the intermolecular coiling is destabilized and single coils with the same % α-helicity as the individual peptides are formed (Table 1).

These results confirm that individually the peptides do not self associate, which is due to electrostatic repulsions overcoming the stability provided by the forming of the hydrophobic core. When the peptides are combined they assemble into hetero coiled coils

as the electrostatic interactions no longer negate the stability provided by the hydrophobic core. These results are in accordance with the findings of Litowski and. Additionally, the spectra are nearly identical to those of E and K without the fluorophores (Figure 2b), showing that the additional fluorescent amino acids do not significantly affect the secondary and quaternary structures of the peptides.

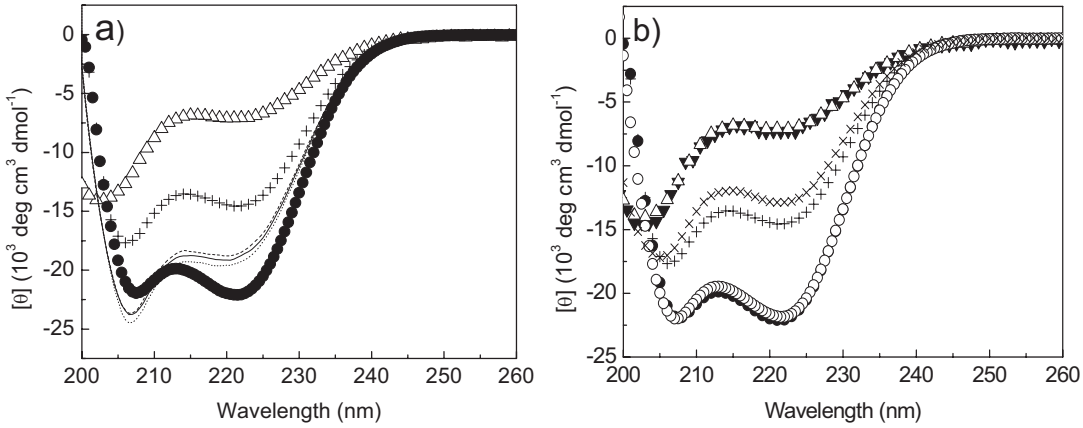


*Figure 2.*a) CD spectroscopic data of E (Δ), K (+), and an equimolar mixture of E and K (●) in PBS. E (- -), K (···), and an equimolar mixture of E and K (—) in 1:1 (v/v) PBS:TFE. b) CD Spectroscopic Data of E (Δ), K (+), and E/K (●) compared to E(-Tyr) (▼), K(-Trp, Gly) (×), and E(-Tyr)/K(-Trp, Gly) (○) in PBS. [Total Peptide] = 200 μM, 25 °C.

Table 1. CD spectroscopic data of the synthetic peptides used in this study.

name[a]	$[\theta]_{222}$		% α-helix[b]		$[\theta]_{222}/[\theta]_{208}$		Coiled coil[c]
	PBS	50% TFE	PBS	50% TFE	PBS	50% TFE	
K	14580	19265	45	60	0.83	0.81	-
E	6662	18472	21	58	0.68	0.80	-
K/E	23308	18760	73	59	1.01	0.81	+

[a] A/B refers to mixtures of the stated compounds with equimolar concentrations. [b] The percentage α-helicity is the ratio of the observed $[\theta]_{222}$ to the predicted $[\theta]_{222}$ for an α-helical peptide of *n* residues x 100. The predicted α-helicity is calculated from $[\theta]_{222}$ = -40 000 x (1-4.6/*n*).[35] [c] The + sign signifies a significant decrease in the $[\theta]_{222}/[\theta]_{208}$ ratio from benign to 50% TFE in PBS, indicative of the folded coiled-coil structure in PBS. [Total Peptide] = 200 μM, 50 mM phosphate, 100 mM KCl, pH 7.0, 25 °C.

FRET spectroscopy

The orientation of the two peptides within the E/K coiled-coil complex was confirmed by measuring the fluorescence resonance energy transfer (FRET) between the donor, tyrosine, on peptide E, and the acceptor, tryptophan, on peptide K. In order to minimize the influence on the peptide structure the natural amino acids tyrosine and tryptophan were used as a FRET pair and introduced them at the ends of the peptides in the **e** position of the heptad repeat. The peptide structure was only nominally modified, as was proven with CD. Both fluorophores are at the N-termini of the peptides, and the Förster distance ($R_o \approx$ 1 nm)[38] is much less than the length of the peptides, which stringently ensures that FRET can only occur when the peptides are in the parallel orientation, not when they are in the antiparallel orientation.

Figure 3 shows emission spectra (excitation at 275 nm) of peptides E and K, E/K in PBS, and E/K in 1:1 PBS:TFE. At 275 nm both tyrosine and tryptophan are excited. In 1:1 PBS:TFE there should be no intermolecular interaction between the peptides (as confirmed with CD), and hence no significant energy transfer between the donor and the acceptor because the distances between them are too great. The spectrum of E/K in 1:1 PBS:TFE in Figure 3 shows contributions from both tyrosine and tryptophan, confirming that there is no FRET between the peptides. In benign buffer the emission spectrum of an equimolar mixture of E and K shows a predominantly K signal. This means that there is efficient energy transfer between the donor (tyrosine) on E and the acceptor (tryptophan) on K, and therefore the peptides E and K form a parallel coiled coil in solution.

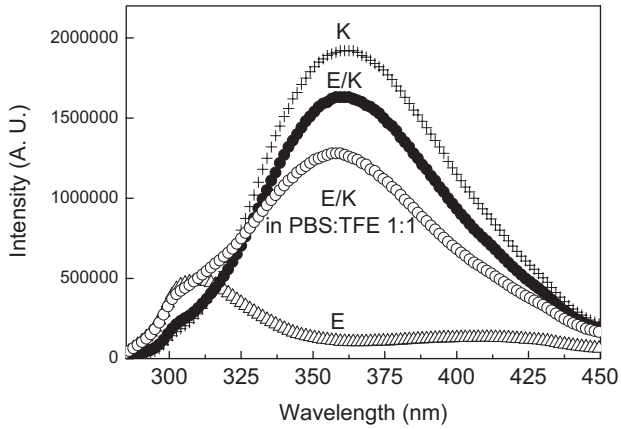


Figure 3. Fluorescence emission spectra of E (Δ), K (+), and an equimolar mixture of E and K (●) in PBS, and in 1:1 (v/v) PBS:TFE (○). [Total Peptide] = 100 μM, 25 °C.

Experimental Results – Binding Properties

Thermodynamic parameters of the thermally and chemically induced equilibrium unfolding were determined by monitoring the resistance of the E/K coiled-coil complex to unfolding as a function of the denaturant GdnHCl concentration, and of increasing temperature.

GdnHCl

The thermodynamic stability of the E/K was determined by measuring the molar ellipticity at 222 nm as a function of GdnHCl concentration. At this wavelength the molar ellipticity is directly proportional to the amount of helical structure.[35] In the folded state, i.e. in benign buffer, the E/K coil is 73% helical. At a GdnHCl concentration of 5.5 M the molar ellipticity at 222 nm of the E/K mixture had dropped to 6% helicity and had stopped decreasing (Figure 4a), indicating that the coiled coil had dissociated and the peptides were predominantly unfolded. The denaturation curve is sigmoidal with a single inflection point, consistent with a two-state equilibrium in which intermediates (folded monomers) are minimally populated at equilibrium.[39] To calculate the conformational stability of the E/K dimer in the absence of denaturant a dimer/monomer equilibrium was used. From the transition zone of the unfolding curve the free energy associated with unfolding as a

function of GdnHCl concentration can be measured, as plotted in Figure 4b. By linear extrapolation to zero GdnHCl concentration the free energy of unfolding at 25 °C in benign buffer was calculated to be 11.7 kcal mol^{-1}.[40] The dissociation constant at 25 °C calculated from this free energy value is 2.5 x 10^{-9} M.

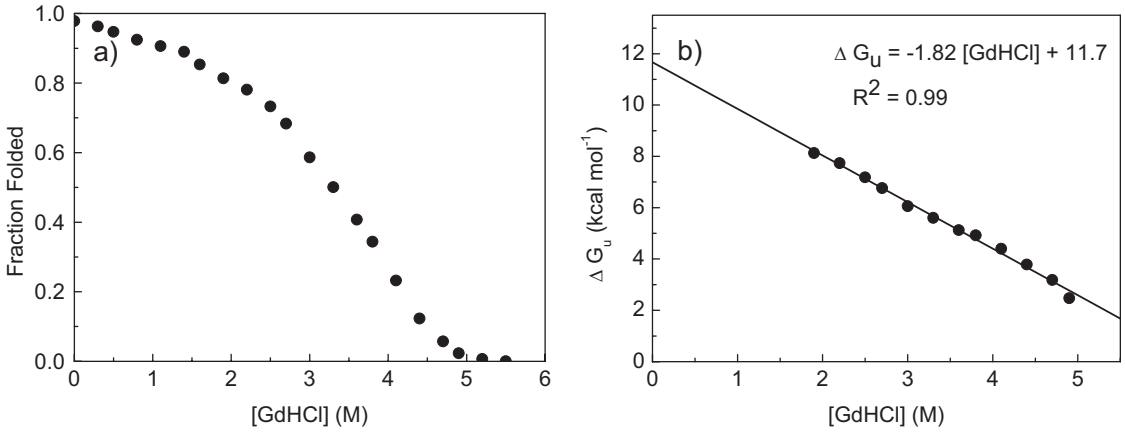


Figure 4. a) GdnHCl unfolding curve of E/K in PBS, 25 °C as followed by CD. The degree of folding in benign buffer is set to fraction folded = 1. [Total Peptide] = 200 μM. b) Gibbs free energy associated with the unfolding of E/K as a function of GdnHCl. The least-squares fit has an intercept of 11.7 kcal mol^{-1}.

Temperature

The thermal denaturation of proteins and peptides provides information about the type and cooperativity of the interactions stabilizing their structures.[39] Figure 5a shows how the folding of the E/K coiled coil changes with temperature. The curve corresponds to a smooth cooperative transition from an α-helical coiled-coil structure to peptides in the random coil conformation. The transition is completely reversed by lowering the temperature. At this concentration the T_m, the temperature at which half of the peptide is in the unfolded form, is 62 °C.

Figure 5c shows that the enthalpy associated with the thermal unfolding of the E/K coiled coil increases linearly with temperature. This is the expected behavior for a two state transition.[41] The gradient of this plot is the change in heat capacity between folded dimers and unfolded monomers.[42] The positive value (0.30 kcal mol^{-1} K^{-1}) of the heat capacity indicates that nonpolar surfaces are being exposed to water upon disassociation of the dimer.[43] It can be concluded that the burial of the bulky non-polar side chains of leucine and isoleucine residues contributes to the stabilization of the E/K dimer as opposed to monomeric peptides.

Using the heat capacity value the change in free energy of unfolding at different temperatures can be calculated (Figure 5d). At 25 °C this value is 11.0 kcal mol^{-1}. This is close to the value of 11.7 kcal mol^{-1} measured using GdnHCl denaturation. The dissociation constant at 25 °C calculated from this ΔG^{H_2O} value is 8.0 x 10^{-9} M.

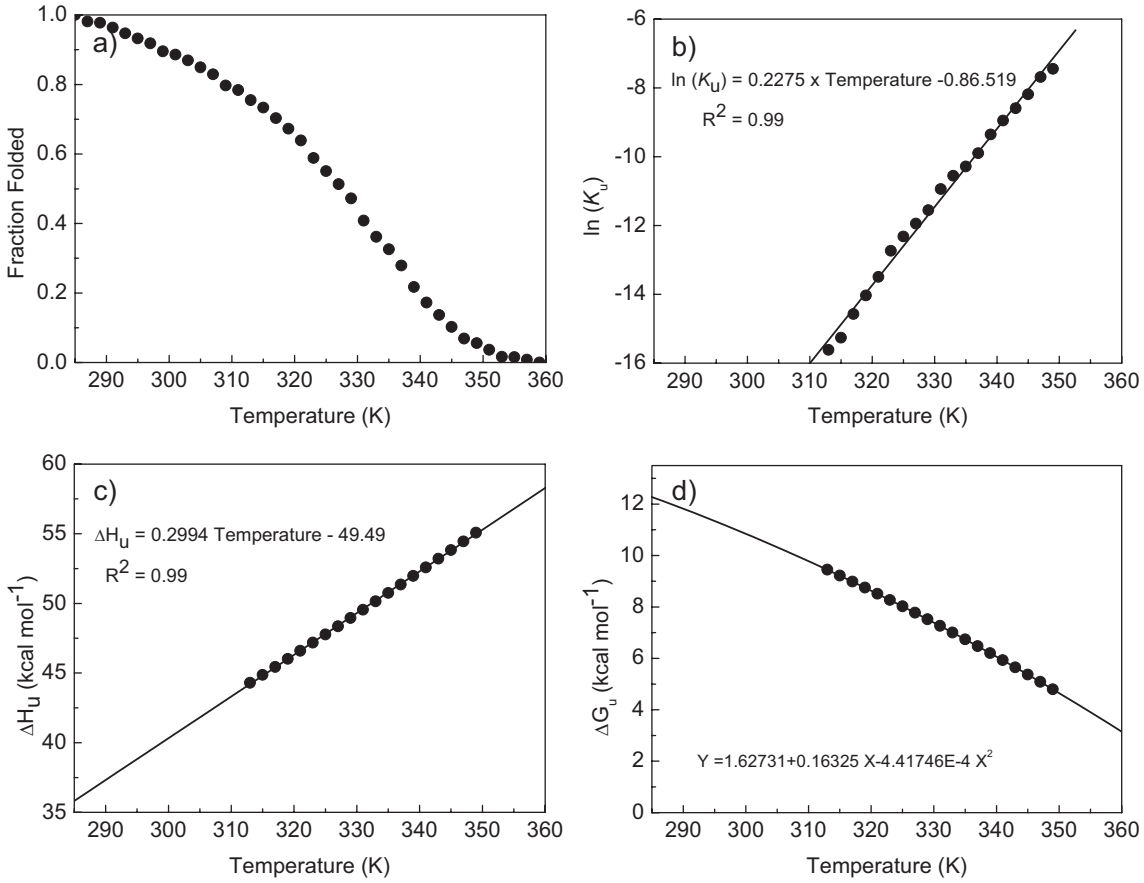


Figure 5. a) Thermal unfolding curve of E/K in 50 mM phosphate, 100 mM KCl, pH 7.0, as followed by CD. [Total Peptide] = 40 μM. b) Van't Hoff plot of the thermal denaturation of E/K. c) Dependence of the enthalpy of unfolding of E/K on temperature. ΔH_u values were obtained using the derivative of the van't Hoff plot. d) Free energy associated with the unfolding of E/K as a function of temperature. The least-squares fit gives a ΔG^{H_2O} value at 25 °C of 11.0 kcal mol^{-1}.

Results of Computer Simulations

The design of the amino acid sequences of E and K, i.e. the placement of amino acids with particular properties at certain positions of the heptad repeat, was based on trends observed experimentally. The E/K coiled-coil interaction has been well characterized on a molecular level: E and K bind to form parallel heterodimers with a free energy of unfolding at 25 °C of ~ 11 kcal mol^{-1}, and a dissociation constant of ~ 10^{-9} M. Molecular dynamics (MD) simulations of the individual peptides and the E/K dimer were then carried out with two goals in mind: first, to see if the structures observed experimentally could be predicted theoretically by the van der Waals and coulomb interactions of the residues; and second, in order to understand in a quantitative way the contributions of the different amino acids to the coiled-coil interaction. If the coiled-coil binding can be understood using MD simulations, sequence designs can be tested for stability before synthesis and characterization.

Structural Properties

For the simulations the experimental conditions were mimicked by immersing the peptides in water with counter ions. Initially, the molecular dynamics of the individual peptides E and K were simulated. Figure 6 shows the starting peptide structures and snapshots at 2 ns. E changes structure significantly over the simulation time, departing from the standard helical structure. K remains largely α-helical, with the largest changes at the N- and C-termini. These results concur with the CD data: both methods demonstrate that E in isolation has a random coil secondary structure, while K is α-helical. This means that the repulsion between the charged glutamic acid side chains in positions **e** and **g** of peptide E is more disruptive to the hydrogen bonding that maintains the α-helicity than the charged lysine side chains in peptide K.

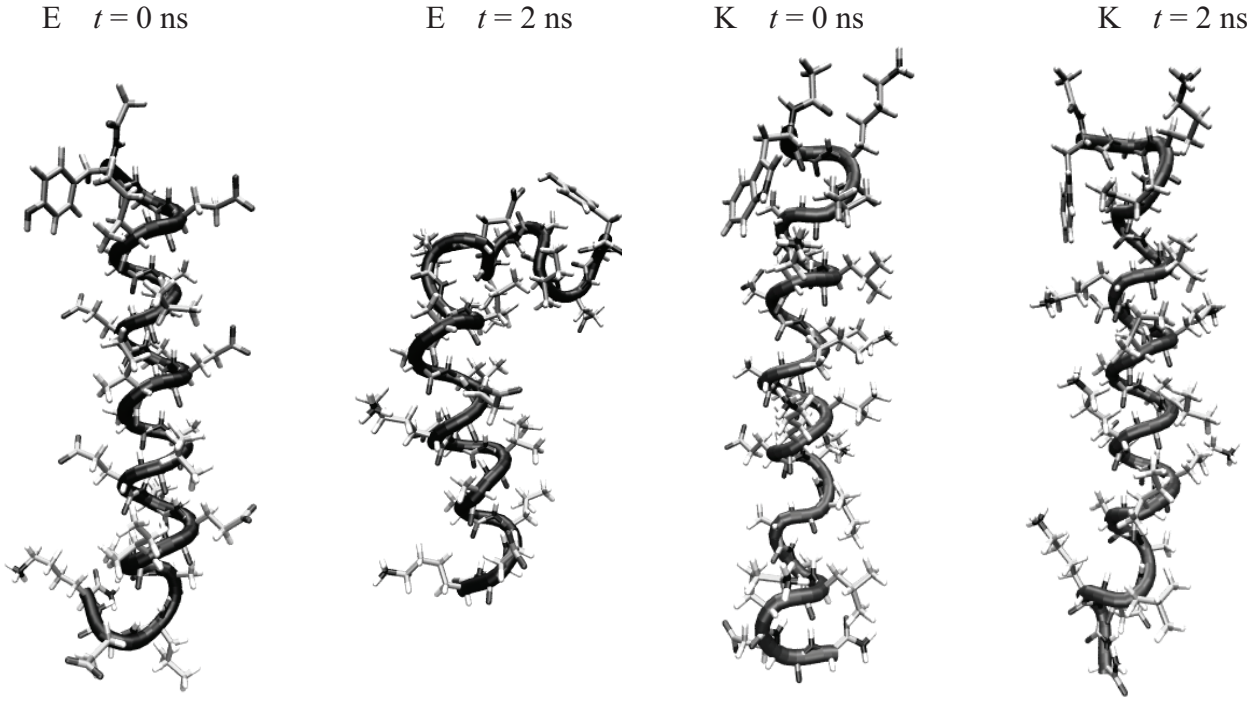


Figure 6. Snapshots of the MD simulations of the peptide monomers in solution. The two left-most Figures shows the initial configuration of peptide E and the final configuration at t = 2.0 ns. The two right-most Figures show the initial configuration of peptide K and the final configuration at t = 2.0 ns. The initial α-helical configurations were constructed in the program Chemsite.[44] Water molecules and counter ions are not shown for simplicity and the backbone is indicated by the blue (E) and red (K) ribbons.

The computed E/K dimer conformation at t = 1.5 ns is shown in Figure 7. Unlike the individual peptides, the structure of the dimer does not alter significantly with time. The peptides are stable as a parallel α-helical dimer, as predicted by the design of the amino acid sequence and as confirmed by circular dichroism, FRET, and also as observed in the structure determined by NMR spectroscopy of IAAL-E3/K3 [27], which have very similar amino acid sequences. As seen in Figure 7b, the peptides interact through the packing

together of isoleucine and leucine residues forming a hydrophobic core away from the water molecules. E and K are staggered, with the C-terminus of peptide K being lower than that of E, again mirroring the results of the structure of IAAL-E3/K3 determined by NMRspectroscopy.[27]

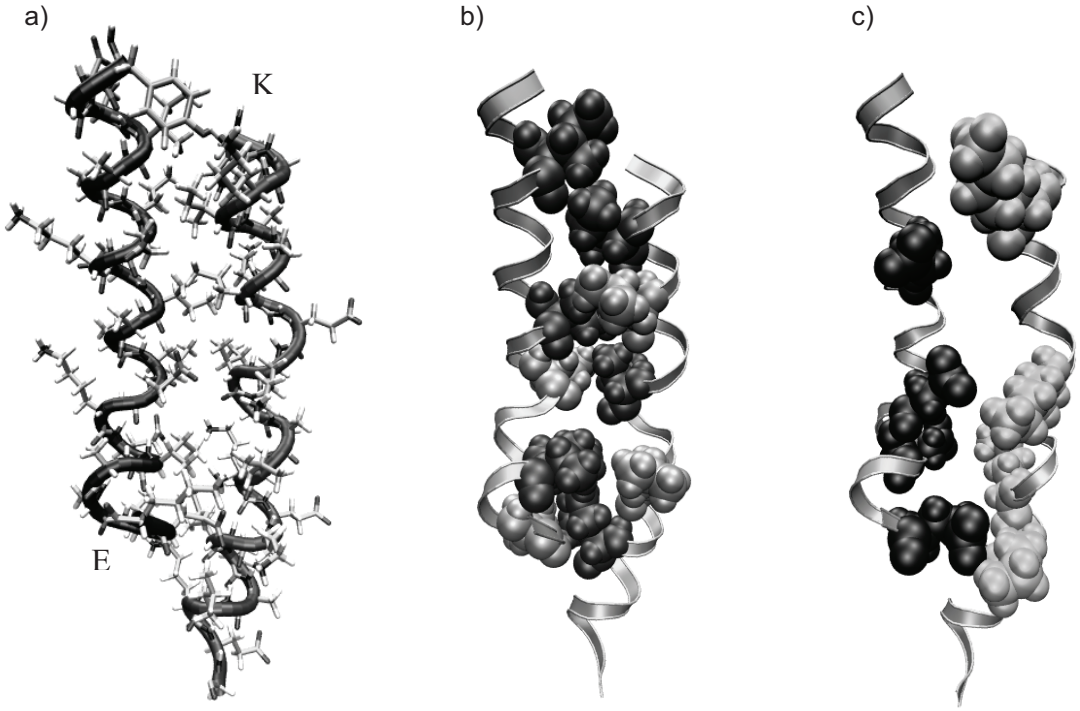


Figure 7. a) Snapshot of the MD simulation of the E-K dimer at t = 1.5 ns. Water molecules are not shown for simplicity and the tubes indicate the peptide backbones. b) Important hydrophobic interactions. Peptide backbones are indicated by the ribbons, isoleucine = dark, leucine = light. c) Important electrostatic interactions. Glutamic acid = dark, lysine = light.

The average tyrosine-tryptophan distance in the heterodimer is 3.5 Å with little variance over the simulation time. This is in agreement with experimental FRET results that revealed that the dimer assumed a parallel orientation.

Core-forming hydrophobic residues

The close-contact intermolecular distances for the core forming leucine and isoleucine residues are shown in Table 2. The close contact pairs are very near one another, on average 2.7 Å, and with little variance over the simulation time. In coiled-coil dimers with parallel conformation the **a** and **a'** residues are purported to pack together in a side-to-side manner, as are the residues at positions **d** and **d'**[45] (Figure 1). In this simulation for the packing of the hydrophobic core, all of the **a** - **a'** distances are less than 3 Å, i.e. the residues are closely packed, but none of the **d** to **d'** distances are less than 3 Å. This means that the helices are slightly twisted from the classical representation of the coiled-coil parallel dimer (Figure 8). All of the possible **a** – (**d**-1)' and **d** – **a**' distances are also within

3 Å. This type of packing is attributed to antiparallel coiled-coil dimers [46], but is also consistent with the 'knobs into holes' core packing model purported by Crick for coiled coils of either orientation.[3] In this model the residues in positions **a** and **d** pack together in a 'knobs into holes' manner, in which each is surrounded by four residues of the opposing strand. The simple "**a** pairs with **a'** and **d** pairs with **d'**" rule does not take into account the close packing of the entire interface.

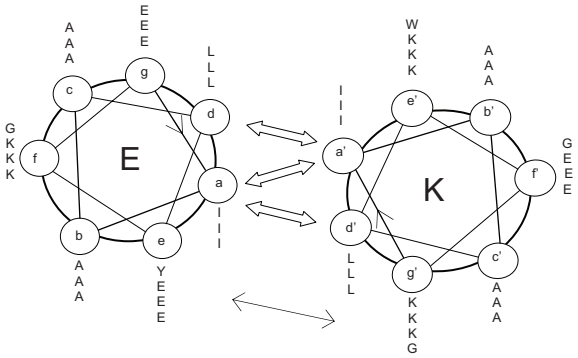


Figure 8. Helical wheel representation of the E/K parallel dimer, with arrows showing the close interhelical distances (< 5 Å) as simulated by molecular dynamics (thin arrow between charged residues, open arrows between residues in the hydrophobic core). Peptides E and K propagate into the page from the N-terminus to the C-terminus.

Core-bordering charged residues

Interhelical salt-bridges ($i \rightarrow i' + 5$ and $i \rightarrow i' + 2$) are often assumed to contribute to the stability of coiled coils. However, taking a cut-off distance of 5 Å for the salt bridges, only four of the ten possible $i \rightarrow i' + 5$, and $i \rightarrow i' + 2$ interactions are present (Table 2). There is some precedent for this: for the peptide pair upon which E and K are based an NMR structure is available, with the authors alleging lysine glutamic acid salt-bridging pairs with the rather long distances of between 9.3 and 16.7 Å.[27,47]. Additionally, fewer intermolecular ion pairs than would be anticipated from the amino acid sequence were observed in the x-ray structure of the extensively studied GCN4 leucine zipper.[45] The fact that in the current simulations only 40% of the distances between glutamic acid and lysine charged side chains are within distances for which salt-bridges are to be expected indicates that the role of charged residues in stabilizing coiled coils is not as extensive as is commonly assumed.

Table 2. The Tyr-Trp intermolecular distance, the close-contact intermolecular hydrophobic distances, and all Glu-Lys distances of the E/K dimer in solution obtained from the MD trajectory. Distances are based on the closest contact interatomic distances between the respective fragments. Averages and standard deviations were taken over the final 500 ps of the trajectory.

E	K	*R* (Å)	Type
1-Tyr	1-Trp	3.5 ± 0.7	
4-Ile	4-Ile	2.9 ± 0.8	a – a'
7-Leu	4-Ile	2.7 ± 0.4	d – a'
11-Ile	7-Leu	2.4 ± 0.2	a – (d-1)'
11-Ile	11-Ile	2.6 ± 0.4	a – a'
14-Leu	11-Ile	2.6 ± 0.6	d – a'
18-Ile	14-Leu	2.6 ± 0.4	a – (d-1)'
18-Ile	18-Ile	2.7 ± 0.4	a – a'
21-Leu	18-Ile	2.8 ± 0.5	d – a'
3-Glu	8-Lys	14.1 ± 1.5	i – i' + 5
8-Glu	3-Lys	2.1 ± 0.6	i – i' + 5
8-Glu	10-Lys	8.6 ± 1.1	i – i' + 2
10-Glu	8-Lys	7.6 ± 0.8	i – i' + 2
10-Glu	15-Lys	12.9 ± 1.1	i – i' + 5
15-Glu	10-Lys	4.1 ± 1.1	i – i' + 5
15-Glu	17-Lys	11.6 ± 0.7	i – i' + 2
17-Glu	15-Lys	4.8 ± 0.9	i – i' + 2
17-Glu	22-Lys	10.4 ± 1.6	i – i' + 5
22-Glu	17-Lys	2.1 ± 0.5	i – i' + 5

The molecular dynamics simulations result in the same peptide intra- and intermolecular structures as observed experimentally, and indicate that the packing of the dimer may be slightly twisted from the classical representation. The large distances between most charged side chains indicate that salt-bridges may not play a major role in stabilizing the dimer. The three dimensional arrangement of peptides is a result of a balance of forces that promote and oppose the compactly folded conformation,[48] and further insights into the peptide binding are obtained by analyzing the energetic contributions to the dimerization.

Binding Properties

The total energy of binding is calculated to be -15.2 kcal mol^{-1}, as shown in Table 3. Although the simulated total binding energy is in the same range as the values obtained from experiments, namely -11.7 kcal mol^{-1} and -11.0 kcal mol^{-1}, it should be noted that only a rough comparison of the values is possible because the simulations lack an entropic term. This would reduce the simulated value, bringing it in the direction of the experimental values. In contrast to the experiments, which gave an overall binding energy, MD simulations also readily allow access to the binding energy components of the different types of residues.

Table 3 breaks down the contribution of each class of residue to the total dimer energy in terms of van der Waals and coulomb energies. It is seen that overall the van der Waals energy is binding, and specifically that the van der Waals interactions of the hydrophobic core-forming isoleucine and leucine residues contribute the most to coiled-coil binding. This supports the conclusion from the temperature induced dimer unfolding that the packing of bulky hydrophobic side chains contributes to the binding energy. In contrast the coulomb energy is non-binding, and the largest anti-binding component is the coulomb repulsion of the glutamic acid and lysine residues. The helix stabilizing residues barely contribute to the overall binding energy; they have the same energy in monomer or dimer form. The 'other' category also contributes to the binding energy, but as seen in the next section this arises from an end-capping moiety, not from amino acid residues.

Table 3. Van der Waals (VdW), coulomb and total contributions to the E/K dimer binding energy grouped per residue type. Hydrophilic: Glu, Lys; hydrophobic: Ile, Leu; helix-stabilizing: Ala, Gly; other: acetyl, Tyr, Trp, NH_2. Grouping of the residues is based on the work by Hodges and Litowski.[28]

Type of Residues	Number of Residues	VdW (kcal mol^{-1})	Coulomb (kcal mol^{-1})	Total (kcal mol^{-1})
Hydrophilic	18	-12.1	23.2	11.1
Hydrophobic	12	-20.0	1.6	-18.4
Helix-stabilizing	15	-0.1	1.2	1.1
Other	6	-3.1	-5.9	-9.0
Total	51	-35.3	20.1	-15.2

In order to probe in more detail the influence of specific residues Table 4 lists the contributions of the van der Waals and coulomb components of each residue to the binding energy of the E/K dimer. The van der Waals interactions are similarly binding for peptides E and K, but E electrostatically destabilizes the dimer while K electrostatically stabilizes it. In isolation E is more random coil than K, and it is seen that the simulated energy changes are greater upon forming a dimer for E rather than K.

Van der Waals Interactions

The van der Waals contribution of amino acids in peptide K, and to some extent E, is dependent on the position along the helix. At the N- and C-termini the van der Waals interactions stabilize dimer binding, and while those in the middle sections destabilize dimer binding, regardless of the position on the helical wheel (Figure 9). It is generally assumed that the middle section of coiled coils are the most stable,[36] but in this case the simulations predict that while the middle sections are the most helical, the most favorable van der Waals interactions in the dimer are the end sections. This reflects the changes in residue packing for different parts of the peptides when going from monomer to dimer form.

Table 4. Van der Waals (VdW), coulomb and total residue contributions to the E/K dimer binding energy. Calculations were obtained from the monomer and dimer MD trajectories and treated according to equations outlined in the computational details.

			E					K		
	Index	Residue	VdW	Coulomb	Total	Index	Residue	VdW	Coulomb	Total
		acetyl	0.3	-0.2	0.1		acetyl	-1.1	0.9	-0.1
e	1	Tyr	-2.2	2.0	-0.2	1	Trp	-0.3	-0.1	-0.4
f	2	Gly	-0.7	0.6	-0.1	2	Gly	-1.1	1.3	0.2
g	3	Glu	-0.7	-0.2	-0.9	3	Lys	-4.1	-3.3	-7.4
a	4	Ile	-1.9	0.1	-1.8	4	Ile	-4.7	1.4	-3.3
b	5	Ala	-0.6	-0.4	-1.0	5	Ala	0.4	-1.1	-0.8
c	6	Ala	-2.2	1.7	-0.4	6	Ala	-0.6	-0.6	-1.2
d	7	Leu	-1.1	-0.5	-1.6	7	Leu	-2.6	1.6	-1.0
e	8	Glu	-2.6	8.4	5.8	8	Lys	1.7	1.4	3.1
f	9	Lys	-1.8	-1.3	-3.0	9	Glu	2.3	-3.2	-0.9
g	10	Glu	-0.3	5.2	4.9	10	Lys	1.8	-0.4	1.4
a	11	Ile	-1.3	0.8	-0.5	11	Ile	0.9	0.1	0.9
b	12	Ala	0.2	-0.9	-0.6	12	Ala	2.4	0.8	3.2
c	13	Ala	0.8	0.7	1.6	13	Ala	2.3	-0.1	2.2
d	14	Leu	1.3	-1.2	0.2	14	Leu	0.3	-0.1	0.2
e	15	Glu	1.1	0.0	1.1	15	Lys	-0.7	1.1	0.4
f	16	Lys	1.3	-0.2	1.2	16	Glu	-0.3	0.8	0.5
g	17	Glu	-0.4	13.7	13.3	17	Lys	-2.8	-1.8	-4.6
a	18	Ile	-1.8	-2.6	-4.4	18	Ile	-4.3	-2.6	-6.9
b	19	Ala	1.1	1.2	2.3	19	Ala	-1.7	-0.1	-1.9
c	20	Ala	2.4	0.8	3.1	20	Ala	-2.9	-2.3	-5.2
d	21	Leu	-2.7	5.4	2.7	21	Leu	-2.0	-0.9	-3.0
e	22	Glu	-4.4	0.4	-4.0	22	Lys	-0.3	1.0	0.7
f	23	Lys	-1.1	-1.1	-2.2	23	Glu	-0.7	2.5	1.8
g		NH_2	0.3	-1.9	-1.6	24	Gly	0.1	-0.4	-0.3
							NH_2	-0.1	-6.6	-6.7
Total			-17.0	30.8	13.8	Total		-18.3	-10.6	-28.9

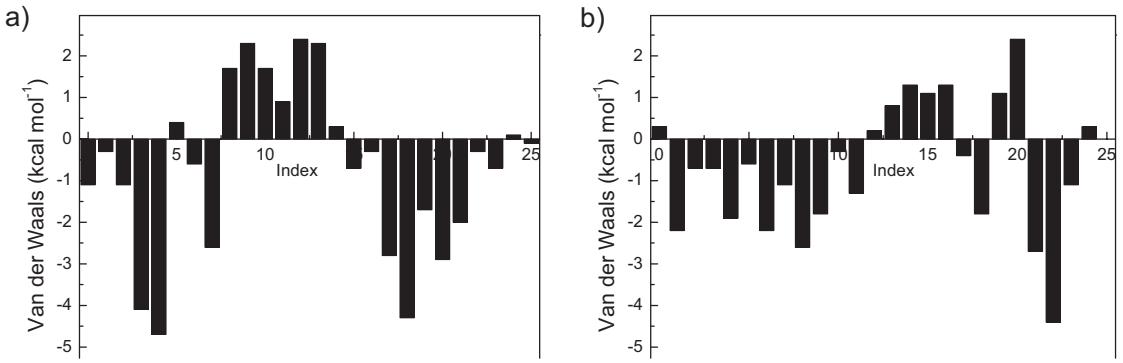


Figure 9. The van der Waals contribution of each residue of peptide K (a), and peptide E (b) to E/K dimer binding.

Coulomb Interactions

It is known that the placement of charged residues along the edge of the hydrophobic core can determine heterodimeric vs. homodimeric peptide association, through destabilizing one quaternary structure.[10] However, whether the electrostatic interactions not only destabilize the homodimeric form, but also stabilize the heterodimeric form is a matter of contention, as is indeed whether salt-bridges form at all.[49, 50] In general for protein and peptide folding electrostatic attraction contributes only moderately to the free energy of folding, while electrostatic repulsion strongly opposes folding.[51] These simulations are in line with this general observation, as there are four detractors to the binding energy that are particularly strong, notably glutamic acid residues at positions **e** and **g**, whereas no amino acid makes a very strong (> -5 kcal mol^{-1}) stabilizing coulomb contribution to the E/K complex formation.

It should be noted that the amide capping moiety at the C-terminus of peptide K displayed the only significant coulomb stabilization (-6.6 kcal mol^{-1}). The C-termini of peptides are often amidated, which it thought to prevent repulsions between charged carboxylic acid termini. In the simulation of the coiled-coil complex the NH_2 group is in close proximity to the carbonyl of alanine in position 20 forming an intramolecular hydrogen-bond that is stable for the duration of the run.

The glutamic acid residues with the highest anti-binding coulomb interactions (positions 8 and 17, 8.4 kcal mol^{-1} and 13.7 kcal mol^{-1} respectively) form close-contacts with charged lysine side-chains (Table 2), but this obviously does not recover the desolvation penalty. Indeed, salt bridges only rarely provide stabilization for protein folding due to under-recovery of desolvation energy.[51] The present simulations find that out of the 10 possible salt-bridges, only 4 are within the distances expected of a salt-bridge, and of the 8 residues involved in these close-contacts only 3 are stabilizing. Therefore in this system the Glu-Lys interaction is important for inferring specificity, i.e. destabilizing homodimers, [52] but does not contribute to stabilizing heterodimers as the majority of the charged side-chains have a lower energy when surrounded by a water solvation shell.

The long-standing hypothesis of the leucine zipper postulates that the sequestering of the hydrophobic residues at positions **a** and **d** drives the dimerization, which is stabilized or destabilized by the placement of charged residues bordering the hydrophobic core.[53] A variation is offered on this: the sequestering of the hydrophobic leucine and isoleucine residues at positions **a** and **d** of E and K drives the dimerization, and heterodimers are destabilized to some extent and homodimers are fully destabilized by the placement of charged glutamic acid and lysine residues bordering the hydrophobic core. This behavior has also been observed for the widely studied stable GCN4 dimer, for which the electrostatic contribution to the dimer was found to be destabilizing using continuum calculations.[54]

By combining experimental work with simulations more detailed information regarding the contribution of specific residues to the stability of the dimer can be obtained. The role of each residue is quantified, and this is not always as one would expect from the coiled-

coil design principles. This allows one to suggest changes in the primary sequence to yield more stable quaternary structures. There is a balance between stability and specificity of coiled-coil dimers, with both positive and negative design being important. Peptide K is energetically more stable as part of the E/K heterocoil than as a monomer (Table 4). There are no residues that have very large destabilizing effects on the dimer. Therefore K seems to be well designed to form E/K heterocoils. If residues were altered to provide greater stability to the E/K heterocoil there would be the danger that K homocoils would be stable. To increase the stability of the heterocoil while maintaining specificity one should focus on the glutamic acid residues of peptide E, which is more stable as a monomer than as a dimer.

CONCLUSIONS

Peptides E and K were designed to form parallel heterodimers in PBS (pH 7.0, 25 °C). K is positively charged and E is negatively charged, and CD experiments show that E is random coil while K is α-helical, i.e. neither can form a homodimeric coiled coil because of charge repulsion. When E and K are combined they interact to form a heterodimeric α-helical coiled-coil complex. FRET experiments revealed that the peptides bind with a parallel orientation. The dissociation energy of the E/K dimer was probed with CD by determining how much energy (temperature or a denaturing salt) is required to disrupt the dimers, and was found to be approximately 11 kcal mol^{-1}. The measured change in heat capacity can be accounted for by burial of bulky leucine and isoleucine non-polar side-chains, therefore experiments predict that stabilization of the dimer is provided by the formation of the hydrophobic core. The computer simulations backed up the experimental results: E is not helical by itself while K is. When combined E and K are in close proximity in the form of a parallel α-helical heterodimer. The binding energy is -15.2 kcal mol^{-1}, with the formation of the hydrophobic core being the largest determinant in the creation of the coiled-coil dimer. In addition to confirming the experimental findings, the computer simulations provide insights into the binding contributions and importance of particular types of amino acids in the peptide sequence.

The largest contribution to the dimer binding energy is the van der Waals interaction of the hydrophobic core-forming residues at the ends of the peptides. It is generally assumed that the middle section of coiled coils are the most stable, but from the simulations it was concluded that the end sections of the dimer have the most favorable van der Waals interactions in comparison to the monomers. Overall the glutamic acid and lysine residues are energetically more stable in monomeric form, and in particular glutamic acid residues display highly unfavorable intra- and interhelical electrostatic repulsions. However, when E and K are in the dimeric form due to the formation of the hydrophobic core the charged residues bordering the hydrophobic core are energetically more stable in close proximity. While the charged amino acids do not contribute overall to the dimer binding, they are important for binding specificity, preventing homodimer formation. The helix stabilizing residues barely contribute to the overall binding energy; they have the same energy in monomer or dimer form.

A challenge in protein and peptide design is to choose a primary structure that will code for particular tertiary and quaternary structures. The largest advances in this area have been in the area of coiled-coil forming peptides.[55] The computational results accurately predicted the oligomerization, direction of coiling, specificity and stability of the coiled-coil tertiary structure, and move beyond the experimental results to quantify the involvement of each amino acid in the peptide sequences. This approach improves the ability to design functional coiled-coil units, widening the scope of their use.

EXPERIMENTAL SECTION

Experimental Details

Materials and Methods

Materials

Fmoc-protected amino acids were purchased from Novabiochem. All other reagents and solvents were obtained at the highest purity available from Sigma-Aldrich or BioSolve Ltd. and used without further purification. Phosphate buffered saline, PBS: 30 mM $K_2HPO_4.3H_2O$, 19 mM KH_2PO_4, 100 mM KCl, pH 7.0.

General Methods

RP-HPLC was performed with a Shimadzu HPLC system with two LC-8A pumps, and an SPD-10AVP UV-VIS detector. Samples were eluted with a linear gradient from A to B, A being 0.1% (v/v) TFA in water, and B acetonitrile. Purification was performed on a Vydac C4 reversed phase column (214TP1022, 22 mm diameter, 250 mm length, 10.00 μM particle size) with a flow rate of 20 mL min^{-1}. Sample elution was monitored by UV detection at 214 nm and 256 nm. For verification of sample purity a reversed phase Vydac C4 column (214TP54, 4.6 mm diameter, 250 mm length, 5.00 μM particle size) was used with a flow rate of 1 mL min^{-1}. Sample elution was monitored by UV detection at 214 nm and 256 nm.

MALDI-TOF mass spectra were acquired using an Applied Biosystems Voyager System 6069 MALDI-TOF spectrometer with an ACH matrix. Samples were dissolved in 1:1 (v/v) 0.1% TFA in water:acetonitrile (TA), at concentrations of ~0.3 mg mL^{-1} for K and E. Solutions for spots consisted of (v/v) 1:10 sample solution: 10 mg mL^{-1} ACH in TA.

^{1}H-NMR spectra were recorded on a Bruker AV-500 spectrometer using the residual proton resonance of deuterated water or acetonitrile for calibration.

Solid-Phase Peptide Synthesis

The peptides E and K were prepared using standard Fmoc chemistry on an Applied Biosystems 431A automated peptide synthesizer. The peptides were synthesized on Sieber-Amide resin. HCTU was used to activate the amino acids derivatives. The peptides were acetylated. Cleavage and deprotection was carried out using 95:2.5:2.5 (v/v) TFA:water:TIS for 1-3 hours. The cleavage mixture and three subsequent rinses of the resin with the TFA mixture were added drop-wise to cold diethylether. The white precipitate was compacted with centrifugation and the supernatant removed. This was repeated three times with the addition of fresh diethylether. The pellets were dried in air or under reduced pressure.

The crude products were purified by RP-HPLC, with gradient elution 35% to 50% B over 20 minutes. After purification all compounds were lyophilized from water to give white material with the following yields: E, K ~40%. The peptides were characterized by MALDI-TOF MS (K: *m/z* = 2621 $[M+H]^+$, E: *m/z* = 2544 $[M+H]^+$), RP-HPLC, and ^{1}H-

NMR. For each compound the purity was estimated from RP-HPLC to be greater than 95%.

Characterization of peptide folding

Fluorescence Spectroscopy

Fluorescence measurements were performed using a FS920 fluorometer from Edinburgh Instruments with a DTMS-300X excitation monochromator and a peltier-controlled thermostatic cell. All spectra were obtained at 25 °C using a quartz cuvette with a 1 cm path length. Excitation and emission slits were 5 nm. Emission spectra were measured from 250 nm to 450 nm in 0.5 nm steps at a fixed excitation wavelength of 275 nm. The sampling time was 0.5 s at each wavelength. The spectra were corrected by subtraction of PBS or 50% TFE spectra. The concentration of E or K was 100 μM in each measurement.

Circular Dichroism Spectroscopy

CD spectra were obtained using a Jasco J-815 spectropolarimeter equipped with a peltier-controlled thermostatic cell. The ellipticity is given as mean residue molar ellipticity, [θ] (10^3 deg cm^2 $dmol^{-1}$), calculated by Eqn. (1),

$$[\theta] = (\theta_{obs} \text{ x MRW})/(10\ l\ c) \quad (1)$$

Where θ_{obs} is the ellipticity in millidegrees, MRW is the mean residue molecular weight, l is the path length of the cuvette in cm and c is the peptide concentration in mg/mL.

A 1.0 mm quartz cuvette was used. Spectra were recorded from 260 nm to 200 nm at 25°C. Data was collected at 0.5 nm intervals with a 1 nm bandwidth and 1 s readings. Each spectrum was the average of 5 scans. For analysis each spectrum had the appropriate background spectrum (buffer or 50% TFE) subtracted.

Temperature dependent CD spectra were obtained using an external temperature sensor immersed in the sample. The temperature was controlled with the internal sensor and measured with the external sensor. A 10 mm quartz cuvette was used, and the solutions were stirred at 900 rpm. Spectra were recorded from 260 nm to 200 nm, with data collected at 0.5 nm intervals with a 1 nm bandwidth and 1 s readings. Each spectrum was one scan. The temperature range was 6 °C to 96 °C with a temperature gradient of 2.0 °C/minute and a 60 s delay after reaching the set temperature. The solutions took 5 minutes to return to 6 °C. The spectrum of PBS at 6 °C (average of 5 scans) was subtracted from each spectrum.

The data was analyzed using a two-state unfolding model to determine the fraction folded using Eqn. (2),

$$F_F = ([\theta] - [\theta]_U) / ([\theta]_F - [\theta]_U) \quad (2)$$

Where $[\theta]$ is the observed molar ellipticity, $[\theta]_U$ is the ellipticity of the denatured state, as determined from the plateau of the ellipticity vs. temperature curve, and $[\theta]_F$ is the ellipticity of the folded state at that temperature as determined from a linear fit of the initial stages of the ellipticity vs. temperature curve ($[\theta]_F = -23956 + 131.5$ x T).

The fraction unfolded, F_U, was calculated by Eqn. (3),

$$F_U = (1 - F_F) \quad (3)$$

The dimer dissociation constant in the transition zone was calculated using Eqn. (4),

$$K_U = 2\, P_t F_U^2 / F_F \quad (4)$$

where P_t is the total peptide concentration. By taking the derivative of ln(Ku) vs. Temperature and using this in the van't Hoff equation, Eqn. (5), the change in enthalpy associated with unfolding with temperature can be plotted:

$$\mathrm{d}\ln(K_U) / \mathrm{d}T = \Delta H_U / RT^2 \quad (5)$$

The gradient of this plot ΔC_P, is the difference in heat capacity between the folded and unfolded forms, and can be used in the Gibbs-Helmholtz equation adapted to a monomer-dimer equilibrium, Eqn. (6), to obtain the Gibbs free energy of unfolding as a function of temperature

$$\Delta G_U = \Delta H_m (1 - T/T_m) + \Delta C_p [T - T_m - T\ln(T/T_m)] - RT\ln[P_t] \quad (6)$$

where T_m and H_m, the temperature and enthalpy at the midpoint of the transition, as determined by the maximum of derivative of the ellipticity vs. temperature graph.

The GdnHCl denaturation CD data was obtained by observing the ellipticity at 222 nm in a 1 mm quartz cuvette at 25 °C. Data was collected at 0.5 nm intervals with a 1 nm bandwidth and 1 s readings. Each spectrum was the average of 5 scans.

For data analysis the dimer dissociation constant in the transition zone was calculated in the same way as for temperature denaturation, with $[\theta]_U$ being the ellipticity of the plateau of the ellipticity vs. [GdnHCl] curve and assuming a linear dependency of $[\theta]_F$ with respect to denaturant concentration ($[\theta]_F$ = -1648 + 1314.1 x [GdnHCl]).

The Gibbs free energy of unfolding in the transition zone was calculated using:

$$\Delta G_U = -RT\ln(K_U) \quad (7)$$

ΔG_U decreases linearly with increasing [GdnHCl], so by extrapolating a least-squares fit of

$$\Delta G_U = \Delta G_U^{PBS} - m\,[\mathrm{GdnHCl}] \quad (8)$$

to zero the free energy of unfolding in PBS can be calculated, and from this value the dimer dissociation constant in PBS can be calculated using equation 7.

Computational Details

Binding Energies

For the calculation of the binding energy the potential energy difference between the dimer in solution and the sum of the potential energies of the monomers in solution is computed. The binding energy is defined as follows:

$$\Delta E_{bind}^{E,K} = \left\{\left\langle E_{pot}^{E}\right\rangle + \left\langle E_{pot}^{K}\right\rangle\right\}_{dimer} - \left\{\left\langle E_{pot}^{E}\right\rangle + \left\langle E_{pot}^{K}\right\rangle\right\}_{monomer}. \quad (1)$$

Here $\left\langle E_{pot}^{E}\right\rangle$ denotes the average potential energy of the E-peptide and the accolades indicate the simulation from which the energy values were taken, i.e. either the simulation of the dimer in solution or the simulations of the monomer in solution. In this way one is able to quantify the energetic change when the two peptides form a dimer. The binding

energy can be further split up in terms due the van der Waals, electrostatic and valence interactions. In formulas this would read:

$$\Delta E_{\text{bind}}^{\text{E,K}} = \Delta E_{\text{VdW}}^{\text{E,K}} + \Delta E_{\text{Elec}}^{\text{E,K}} + \Delta E_{\text{valence}}^{\text{E,K}}, \tag{2}$$

where the van der Waals contribution is computed as

$$\Delta E_{\text{VdW}}^{\text{E,K}} = \left\{ \left\langle E_{\text{VdW}}^{\text{E}} \right\rangle + \left\langle E_{\text{VdW}}^{\text{K}} \right\rangle \right\}_{\text{dimer}} - \left\{ \left\langle E_{\text{VdW}}^{\text{E}} \right\rangle + \left\langle E_{\text{VdW}}^{\text{K}} \right\rangle \right\}_{\text{monomer}}. \tag{3}$$

The electrostatic and valence contributions are calculated in the same way as Eqn. (3). In a similar fashion one can write down the separate peptide contributions to the binding energy as

$$\Delta E_{\text{bind}}^{\text{E,K}} = \Delta E_{\text{bind}}^{\text{E}} + \Delta E_{\text{bind}}^{\text{K}}, \tag{4}$$

where

$$\Delta E_{\text{bind}}^{\text{E}} = \left\{ \left\langle E_{\text{pot}}^{\text{E}} \right\rangle \right\}_{\text{dimer}} - \left\{ \left\langle E_{\text{pot}}^{\text{E}} \right\rangle \right\}_{\text{monomer}}, \tag{5}$$

and

$$\Delta E_{\text{bind}}^{\text{K}} = \left\{ \left\langle E_{\text{pot}}^{\text{K}} \right\rangle \right\}_{\text{dimer}} - \left\{ \left\langle E_{\text{pot}}^{\text{K}} \right\rangle \right\}_{\text{monomer}}. \tag{6}$$

The van der Waals and electrostatic energy contributions can be further partitioned among the amino acid residues of the E and K peptides. For example for the E peptide one would get for the van der Waals contribution:

$$\Delta E_{\text{VdW}}^{\text{E}} = \sum_{i=1}^{n} \left[\left\{ \left\langle E_{\text{VdW}}^{i} \right\rangle \right\}_{\text{dimer}} - \left\{ \left\langle E_{\text{VdW}}^{i} \right\rangle \right\}_{\text{monomer}} \right], \tag{7}$$

where the summation runs over all the amino acid residues of the E-peptide.

In practice, for every time frame the energy of the total simulation box is computed and from this is subtracted both the energy of the isolated fragment (i.e. residue or total peptide) and the energy of the simulation box without the fragment. Averages were then taken over the time frames. Since the fragments bear a net charge a simple distance cutoff was used to compute the electrostatic interactions.

Models and Methods

Constant pressure Molecular Dynamics (MD) simulations were performed on the E and K peptides, and on the dimer in aqueous solution using the 1999 release of the AMBER force field.[56, 57] Water was described by the TIP3P water model[58] augmented with a Urey-Bradley cross term. A similar combination of AMBER/TIP3P was recently used by us and other authors in MD simulation studies of a single peptide chain and peptide aggregates in aqueous solution.[59, 60] A cutoff of 9.0 Å was used for all non-bonded interactions and electrostatic interactions were computed using a smooth particle mesh Ewald summation. All calculations were performed with the TINKER software package.[61]

Molecular models of the experimentally used E and K peptides with charged lysine (Lys) and glutamate (Glu) residues were built and minimized with the Chemsite program.[44] It was checked that the resulting structures adopted α-helical conformations. Subsequently, the optimized structures of E and K were both ‘soaked’ into an equilibrated water box

sufficiently large to ensure that periodic images of the peptide did not interact. Water molecules overlapping with the peptide were removed by hand. In the case of the E peptide the edges of the simulation box were 49.6 Å x 35.8 Å x 27.8 Å and the box contained 1523 water molecules. For the K peptide the edges were the same and the number of water molecules was 1506. For every Lys residue along the peptide chain a chloride ion was added to simulation boxes in and for every Glu residue a sodium ion. This ensured that the total net charge of the simulation box was zero in all cases. The initial position of the ion was chosen randomly as long as it did not overlap with the peptide structure or was too close to a water molecule. The pressure was maintained at ambient values by employing the Berendsen barostat.[62] The Beeman algorithm was used to integrate the equation of motion with a time step of 0.5 fs. No intramolecular constraints were employed. The total number of atoms in both simulation boxes is less than 5000, which should result in a fast equilibration of the system. 2.0 ns MD NPT simulations of the E and K peptides in aqueous solution were then performed. Statistical averages were recorded over the final 500 ps of the run.

An initial structure of the dimer of E and K was built with the XMakemol program [63] in such a way that the interstrand Lys-Glu interactions were as favorable as possible. The resulting dimer structure was ‘soaked’ into an equilibrated water box, again ensuring that periodic images did not interact. The resulting box edges were 65.1 Å x 44.6 Å x 37.9 Å and the box contained 3363 water molecules. Initially, a 0.1 ns constraint MD simulation was performed in order to let the peptide dimer adjust to the aqueous water shell. Five interstrand Glu-Lys distances along the backbone were constrained by fixing the CO-HN side-chain interatomic distance to 3.0 Å using a simple flat-welled harmonic potential. After the constraint was released a 1.5 ns MD simulation was performed. Statistical averages were collected over the final 500 ps of the run.

REFERENCES

1. Yu, Y. B. *Adv. Drug Deliv. Rev.* **2002,** 54, (8), 1113-1129.
2. Mason, J. M.; Arndt, K. M. *Chembiochem* **2004,** 5, (2), 170-176.
3. Crick, F. H. C. *Acta Crystallogra.* **1953,** 6, (8-9), 689-697.
4. Schnarr, N. A.; Kennan, A. J. *J. Am. Chem. Soc.* **2003,** 125, (21), 6364-6365.
5. Stevens, M. M.; Allen, S.; Sakata, J. K.; Davies, M. C.; Roberts, C. J.; Tendler, S. J. B.; Tirrell, D. A.; Williams, P. M. *Langmuir* **2004,** 20, (18), 7747-7752.
6. Naik, R. R.; Kirkpatrick, S. M.; Stone, M. O. *Biosens. Bioelectron.* **2001,** 16, (9-12), 1051-1057.
7. Wendt, H.; Leder, L.; Harma, H.; Jelesarov, I.; Baici, A.; Bosshard, H. R. *Biochemistry* **1997,** 36, (1), 204-213.
8. Liu, J. F.; Rost, B. *Protein Sci.* **2001,** 10, (10), 1970-1979.
9. Rose, A.; Meier, I. *Cell. Mol. Life Sci.* **2004,** 61, (16), 1996-2009.
10. Woolfson, D. N., The design of coiled-coil structures and assemblies. In *Fibrous Proteins: Coiled-Coils, Collagen And Elastomers*, Elsevier Academic Press Inc: San Diego, 2005; Vol. 70, pp 79-+.
11. Mason, J. M.; Muller, K. M.; Arndt, K. M. *Biochemistry* **2007,** 46, (16), 4804-4814.
12. Chao, H. M.; Bautista, D. L.; Litowski, J.; Irvin, R. T.; Hodges, R. S. *J. Chromatogra. B* **1998,** 715, (1), 307-329.
13. Li, C. Z.; Plugariu, C. G.; Bajgier, J.; White, J. R.; Liefer, K. M.; Wu, S. J.; Chaiken, I. *J. Mol. Recognit.* **2002,** 15, (1), 33-43.
14. Behncken, S. N.; Billestrup, N.; Brown, R.; Amstrup, J.; Conway-Campbell, B.; Waters, M. J. *J.Biol. Chem.* **2000,** 275, (22), 17000-17007.
15. Pack, P.; Pluckthun, A. *Biochemistry* **1992,** 31, (6), 1579-1584.
16. Petka, W. A.; Harden, J. L.; McGrath, K. P.; Wirtz, D.; Tirrell, D. A. *Science* **1998,** 281, (5375), 389-392.
17. Shen, W.; Zhang, K. C.; Kornfield, J. A.; Tirrell, D. A. *Nat. Mater.* **2006,** 5, (2), 153-158.
18. Wang, C.; Stewart, R. J.; Kopecek, J. *Nature* **1999,** 397, (6718), 417-420.
19. Stevens, M. M.; Flynn, N. T.; Wang, C.; Tirrell, D. A.; Langer, R. *Adv. Mater.* **2004,** 16, (11), 915-918.
20. Ryadnov, M. G.; Woolfson, D. N. *Nat. Mater.* **2003,** 2, (5), 329-332.
21. Zhou, M.; Bentley, D.; Ghosh, I. *J. Am. Chem. Soc.* **2004,** 126, (3), 734-735.
22. Dublin, S. N.; Conticello, V. P. *J. Am. Chem. Soc.* **2008,** 130, (1), 49-+.
23. Potekhin, S. A.; Melnik, T. N.; Popov, V.; Lanina, N. F.; Vazina, A. A.; Rigler, P.; Verdini, A. S.; Corradin, G.; Kajava, A. V. *Chem. Biol.* **2001,** 8, (11), 1025-1032.
24. Lomander, A.; Hwang, W. M.; Zhang, S. G. *Nano Letters* **2005,** 5, (7), 1255-1260.
25. Marsden, H. R.; Korobko, A. V.; van Leeuwen, E. N. M.; Pouget, E. M.; Veen, S. J.; Sommerdijk, N.; Kros, A. *J. Am. Chem. Soc.* **2008,** 130, (29), 9386-9393.
26. Marsden, H. R.; Elbers, N. A.; Bomans, P. H. H.; Sommerdijk, N.; Kros, A. *Angew. Chem., Int. Ed.* **2009,** 48, (13), 2330-2333.
27. Lindhout, D. A.; Litowski, J. R.; Mercier, P.; Hodges, R. S.; Sykes, B. D. *Biopolymers* **2004,** 75, (5), 367-375.
28. Litowski, J. R.; Hodges, R. S. *J. Biol. Chem.* **2002,** 277, (40), 37272-37279.
29. Klok. **2008**.
31. Wagschal, K.; Tripet, B.; Lavigne, P.; Mant, C.; Hodges, R. S. *Protein Sci.* **1999,** 8, (11), 2312-2329.
32. Moitra, J.; Szilak, L.; Krylov, D.; Vinson, C. *Biochemistry* **1997,** 36, (41), 12567-12573.
34. Lyu, P. C.; Liff, M. I.; Marky, L. A.; Kallenbach, N. R. *Science* **1990,** 250, (4981), 669-673.
35. Chen, Y. H.; Yang, J. T.; Chau, K. H. *Biochemistry* **1974,** 13, (16), 3350-3359.
36. Zhou, N. E.; Kay, C. M.; Hodges, R. S. *J.Biol. Chem.* **1992,** 267, (4), 2664-2670.
37. Lau, S. Y. M.; Taneja, A. K.; Hodges, R. S. *J.Biol. Chem.* **1984,** 259, (21), 3253-3261.
38. Eisinger, J.; Feuer, B.; Lamola, A. A. *Biochemistry* **1969,** 8, (10), 3908-&.
39. Boice, J. A.; Dieckmann, G. R.; DeGrado, W. F.; Fairman, R. *Biochemistry* **1996,** 35, (46), 14480-14485.
40. The free energy of dimer unfolding measured by Litowski and Hodges was 9.6 $kcalmol^{-1}$, however, they did not take into account the linear section at the beginning of the denaturation curve. If the current data is treated in the same way a value of 9.2 $kcalmol^{-1}$ is obtained. The glycine, tryptophan and tyrosine residues were added to the peptides investigated by Litowski and Hodges for FRET purposes, and are not designed to contribute to the coiled-coil formation, but were expected not to

disrupt the coiled coil. The similar values of 9.6 and 9.2 kcal mol^{-1} indicate that the effect of the glycine, tryptophan and tyrosine residues is indeed minimal.
41. Privalov, P. L.; Tiktopulo, E. I.; Tischenko, V. M. *J. Mol. Biol.***1979,** 127, (2), 203-216.
42. Defrancesco, R.; Pastore, A.; Vecchio, G.; Cortese, R. *Biochemistry* **1991,** 30, (1), 143-147.
43. Sturtevant, J. M. *Proc. Natl. Acad. Sci. U.S.A.* **1977,** 74, (6), 2236-2240.
44. ChemSW, I. *ChemSite - Computer-Aided Chemistry Modeling*.
45. Oshea, E. K.; Klemm, J. D.; Kim, P. S.; Alber, T. *Science* **1991,** 254, (5031), 539-544.
46. Oakley, M. G.; Hollenbeck, J. J. *Curr. Opin. Struc. Biol.* **2001,** 11, (4), 450-457.
47. The NMR structure was obtained by constraining the Leu Ile distances, which results in closer Lys Glu distances (the distances are greater at the ends of the dimer where there are fewer constraints)
48. Jelesarov, I.; Durr, E.; Thomas, R. M.; Bosshard, H. R. *Biochemistry* **1998,** 37, (20), 7539-7550.
49. Lumb, K. J.; Kim, P. S. *Science* **1995,** 268, (5209), 436-439.
50. Meier, M.; Burkhard, P. *J. Structural Biol.* **2006,** 155, (2), 116-129.
51. Sheinerman, F. B.; Honig, B. *J.Mol. Biol.* **2002,** 318, (1), 161.
52. When the charges of peptides E and K are eliminated (by lowering the pH for E and raising the pH for K) homocoils form, data not shown.
53. McLachlan, A. D.; Stewart, M. *J. Mol. Biol.* **1975,** 98, (2), 293-304.
54. Hendsch, Z. S.; Tidor, B. *Protein Sci.* **1999,** 8, (7), 1381-1392.
55. Chad A. Mirkin, C. M. N., *Nanobiotechnology ll: More Concepts and Applications*. Wiley-VCH: 2007.
56. Cornell, W. D.; Cieplak, P.; Bayly, C. I.; Gould, I. R.; Merz, K. M.; Ferguson, D. M.; Spellmeyer, D. C.; Fox, T.; Caldwell, J. W.; Kollman, P. A. *J. Am. Chem. Soc.* **1995,** 117, (19), 5179-5197.
57. Wang, J. M.; Cieplak, P.; Kollman, P. A. *J. Comp. Chem.* **2000,** 21, (12), 1049-1074.
58. Walser, R.; Hunenberger, P. H.; van Gunsteren, W. F. *Proteins* **2001,** 43, (4), 509-519.
59. Monti, S.; Bronco, S.; Cappelli, C. *J.Phys. Chem. B* **2005,** 109, (22), 11389-11398.
60. Handgraaf, J. W.; Zerbetto, F. *Proteins* **2006,** 64, (3), 711-718.
61. Ponder, J. W. *TINKER - Software Tools for Molecular Design, Version 4.1*, 1990-2003.
62. Berendsen, H. J. C.; Postma, J. P. M.; Vangunsteren, W. F.; Dinola, A.; Haak, J. R. *J. Chem. Phys.* **1984,** 81, (8), 3684-3690.
63. Hodges, M. P. *XMakemol: a program for visualizing atomic and molecular systems, version 5*, 2001.

NONCOVALENT TRIBLOCK COPOLYMERS BASED ON A COILED-COIL PEPTIDE MOTIF

The formation of a noncovalent triblock copolymer based on a coiled-coil peptide motif is demonstrated in solution. A specific peptide pair (E and K) able to assemble into heterocoiled coils was chosen as the middle block of the polymer and conjugated to poly(ethylene glycol) (PEG) and polystyrene (PS) as the outer blocks. Mixing equimolar amounts of the polymer-peptide block copolymers PS-E and K-PEG resulted in the formation of coiled-coil complexes between the peptides and subsequently in the formation of the amphiphilic triblock copolymer PS-E/K-PEG. Aqueous self-assembly of the separate peptides (E and K), the block copolymers (PS-E and K-PEG), and equimolar mixtures thereof was studied by circular dichroism, dynamic light scattering, and cryogenic transmission electron microscopy. It was found that the noncovalent PS-E/K-PEG copolymer assembled into rod-like micelles, while in all other cases, spherical micelles were observed. Temperature-dependent studies revealed the reversible nature of the coiled-coil complex and the influence of this on the morphology of the aggregate. A possible mechanism for these transitions based on the interfacial free energy and the free energy of the hydrophobic blocks is discussed. The self-assembly of the polymer-peptide conjugates is compared to that of polystyrene-*b*-poly(ethylene glycol), emphasizing the importance of the coiled-coil peptide block in determining micellar structure and dynamic behavior.

INTRODUCTION

Amphiphilic block copolymers derived from synthetic monomers can self-assemble into well-defined assemblies, such as micelles, vesicles, and networks.[1] Researchers are increasingly focusing on the use of peptide- and protein-based segments as replacements for one of the traditional polymer blocks because polymers based on amino acids have the ability to adopt structures with precisely defined shapes and spatial distributions of functionality, making them attractive building blocks for the bottom-up approach to the production of nanostructures.[2] It has been demonstrated that the degree of control over the organization of polymer assemblies can be increased not only by using well-defined building blocks but also, more recently, by utilizing noncovalent bonding motifs within the block copolymer.[3] On the basis of this principle, supramolecular polymers have been

constructed using metal-ligand coordination, hydrogen bonding, and π-π interactions.[4] In this manner, it is possible to obtain dynamic systems based on supramolecular interactions in which the association constants are controlled by external parameters such as temperature, solvent, and concentration. Although dynamic reversible assemblies based on noncovalent interactions are ubiquitously present in nature,[5] examples of synthetic assemblies in aqueous systems bearing these properties are rare.[6] As an example from nature, several specific peptide sequences have been demonstrated to generate precisely defined noncovalent complexes. A prominent motif in nature is the coiled-coil assembly of helical peptides, which is found in up to 10% of eukaryotic proteins,[7] including transcription factors, motor proteins, chaperone proteins, and viral fusion proteins. Coiled coils are formed through the coiling of two or more α-helical peptides around each other in a very specific manner that produces a stable complex in aqueous solution.[8] The oligomerization state (2-7 peptides[9]), size (~ 2 nm[10] to 200 nm[11]), direction of binding (parallel[12] or antiparallel[13]), choice of homo- [14] or heterobinding,[15] and stability[14] can be controlled by careful selection of the amino acids (natural or synthetic[16]) that constitute the peptides. The noncovalent association of these peptides is sensitive to changes in external parameters (e.g., pH, temperature, ionic strength, and solvent), which affect both the electrostatic and hydrophobic interactions, and this responsiveness permits control over the association state of the peptides.[17] As a result, incorporation of coiled-coil forming peptides into hybrid macromolecules is a vital field of research, as it allows enhanced control over nano-, micro-, and macrostructure.

Coiled coils have previously been applied to connect proteins[18] and hydrophilic polymers,[19] forming hydrogels. In these constructs, coiled-coil motifs flank a water-soluble protein or polymer segment, and the coiled-coil interaction creates a randomly connected network. This peptide motif has also been employed to reassemble complementary protein segments, restoring the original function of the proteins.[20] Aggregation of gold particles decorated with coiled-coil-forming peptides has been accomplished as a result of the interparticle peptide-peptide interaction.[21] Coiled-coil-forming peptides that associate in a staggered way, such that each peptide is involved in two coiled-coil interactions simultaneously, have been used to create fibers [22] having lengths as great as hundreds of micrometers.[23] Fractal structures have also been observed in solutions of coiled coils cross-linked through cysteine residues.[24] In all of these examples, assembly of the nanostructures is driven solely by the coiled-coil peptide interaction. The coiled-coil motif has also been connected to a poly(ethylene glycol) (PEG) block.[25] The PEG wraps around the peptide without inhibiting the formation of coiled-coil complexes. These hydrophilic hybrids do not exhibit any higher-order assembly. In this work, the complexity in this field is extended by incorporating a hydrophobic block and a hydrophilic block into peptide-polymer hybrids, thereby demonstrating hierarchical self-assembly of “smart” nanostructures in which both coiled-coil formation and, for the first time, hydrophobic-block-induced aggregation into larger assemblies coexist and influence the final structures that form.

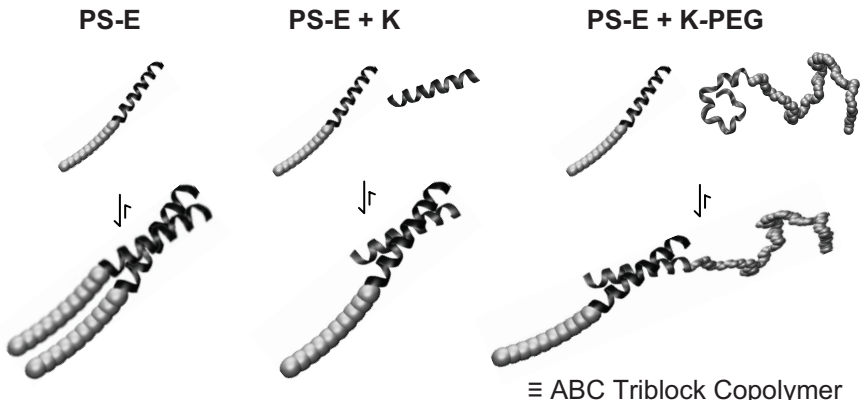


Figure 1. Schematic representation of the hierarchical self-assembly of the hybrids PS-E and K-PEG containing complementary peptide blocks. PS is polystyrene, PEG is poly(ethylene glycol), and E and K are peptides.

Using as a basis an α-helical coiled-coil pair (E and K) that exclusively forms parallel heterodimers,[8,26] a pair of polymer-peptide block copolymers were designed, PS-E and K-PEG (Table 1), containing polystyrene (PS) and PEG blocks, respectively, as the synthetic polymers. These molecules undergo two levels of self-assembly upon dispersion in solution: the specific association of the peptide pair leads to the formation of the new amphiphilic hybrid ABC triblock copolymer PS-E/K-PEG (Figure 1), which subsequently self-assembles into rod-like micelles. Reversible dissociation of the coiled coil was induced by temperature control, resulting in the transition of the rod-like micelles into spherical micelles. The self-assembly behavior of the peptides and the block copolymer PS-PEG was also studied for comparison. These experiments were used to emphasize the influence of the coiled-coil peptide interaction on the formation of the PS-E/K-PEG complex and subsequent formation of the rod-like micelles as well as on the ability to change the morphology of the self-assembled nanostructures.

RESULTS AND DISCUSSION

Peptide and Polymer-b-Peptide Design

The objective was to design a dynamic noncovalent triblock copolymer able to assemble into well-defined aggregates in aqueous solution. In order to create an amphiphile, it was chosen to design one of the outer blocks to be hydrophobic and the other to be hydrophilic in nature. The coiled-coil motif was chosen to control the self-assembly process and was used as the middle block in order to bring the hydrophobic and hydrophilic blocks together to give the noncovalent triblock copolymer PS-E/K-PEG. The pair of 22-mer peptides E and K was selected on the basis of the well-defined shape, size, and stability of the peptide parallel heterodimer.[8,26] Typically, α-helical peptides able to form a coiled-coil motif consist of a heptad repeat sequence (abcdefg).[27] This peptide pair, whose members each contain only three heptad repeats, is amongst the shortest that exclusively forms stable heterodimers. The peptides E and K chosen for this study are designed to favor heterodimer formation over homodimerization because of the presence of oppositely charged residues at the e and g positions.[27] In this way, potential homodimer formation is destabilized whereas the E/K heterodimer is stabilized through electrostatic interactions. The charged residues at position f have charges opposite those at positions e and g in order to increase the solubility and reduce the net charges of the peptides. The hydrophobic core (positions a and d) contains isoleucine and leucine, which pack together well in a "knobs-into-holes" fashion.[28] Alanine is present in the remaining two positions in order to increase the helical propensity of the peptides (Table 1). Since the peptides E and K are designed to form parallel dimers, the polymers must be conjugated at opposite ends of the peptides if formation of a coiled-coil complex is to result in a linear ABC triblock copolymer. Therefore, peptide E was conjugated at the N-terminus with hydrophobic monocarboxy terminated polystyrene to give the block copolymer PS-E, which had a polydispersity index (PDI) of 1.01. In order to form a hydrophilic corona upon self-assembly, peptide K was conjugated at the C-terminus to poly(ethylene glycol), resulting in K-PEG (PDI = 1.05). To show the importance of the coiled-coil motif on the self-assembly process, PS-PEG (PDI = 1.03), which has block lengths similar to those in the hybrid PS-E/K-PEG complex, was synthesized for comparison. All of the peptides and polymer-peptide hybrids were prepared by solid-phase peptide synthesis protocols using standard Fmoc chemistry. Sieber amide resins were used for the syntheses of E, K, and PS-E. In the synthesis of PS-E, monocarboxy-terminated polystyrene (PSCOOH) with a number-average molecular weight (M_n) of 2400 g mol-1 and a PDI of 1.20 was coupled to the N-terminus of E on the resin for 5 days. For K-PEG, K was synthesized on a PAP tentagel resin that was preloaded with a PEG block (Fmoc-NH-PEG-OH, M_n = 3400 g mol^{-1}, PDI = 1.02). All of the compounds were purified using precipitation protocols and reversed-phase high-performance liquid chromatography (RP-HPLC) and then characterized using NMR spectroscopy and matrix-assisted laser desorption ionization-time-of-flight (MALDI-TOF) mass spectrometry (Figures A1-A3 in the Appendices).

Table 1. Peptide Sequences and Hybrid Compositions.

Name	Structure[a]	M_n (g/mol)[b]	PDI
K	Ac-$(KIAALKE)_3$G-NH_2	2378	-
E	Ac-G$(EIAALEK)_3$-NH_2	2380	-
K-PEG	Ac-$(KIAALKE)_3$G-PEG_{77}	5832	1.05
PS-E	PS_9-G$(EIAALEK)_3$-NH_2	3341	1.01
PS-PEG	PS_{11}-PEG_{74}	4500	1.03

[a] PEG = poly(ethylene glycol), PS = polystyrene, Ac = acetyl. The sequences are written using the one-letter amino acid code. [b] Determined by MALDI-TOF mass spectrometry.

Peptide Self-Assembly

The secondary and quaternary structures of the peptides in buffered solution were evaluated by circular dichroism (CD) spectroscopy. Peptide E adopts a predominantly random-coil conformation, while K exhibits a predominantly α-helical spectrum. Both peptides exist in the monomeric state, as indicated by the observed ellipticity ratios ($[\theta]_{222}/[\theta]_{208}$) of 0.59 and 0.74, respectively[29] (Figure 2a and Table 2). When peptides E and K were combined in an equimolar ratio, denoted E/K, a typical α-helical CD spectrum was exhibited, with minima at 208 and 222 nm (Figure 2a). The ellipticity ratio was determined to be 0.94, consistent with interacting α-helices[29] (Table 2). This clearly shows that E and K specifically interact to form a heterodimeric α-helical coiled coil. The formation of the dimeric species was confirmed by determining the molecular weights using sedimentation equilibria, revealing that separate solutions of E and K are purely monomeric while the mixture of E/K exists as dimers (Table 3).

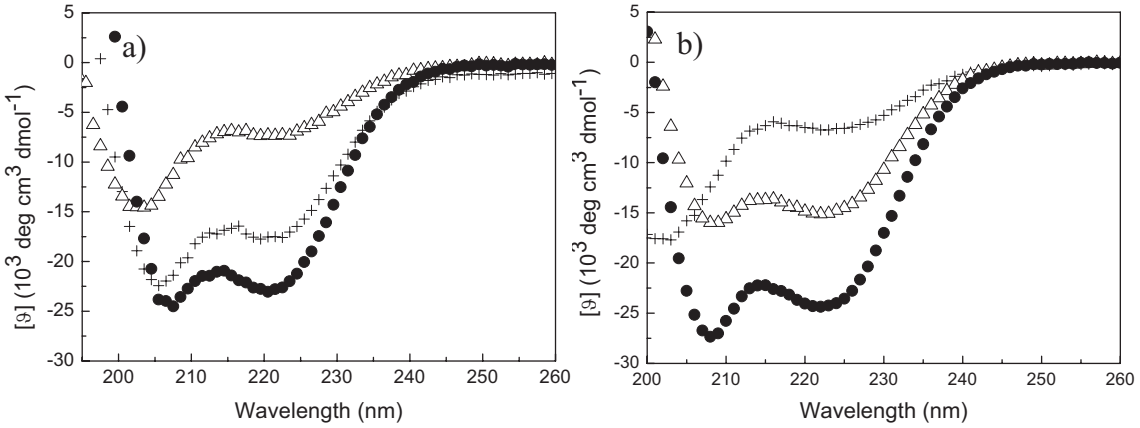


Figure 2. CD spectra of (a) E (Δ), K (+), and an equimolar mixture of E and K (●) and (b) PS-E (Δ), K-PEG (+), and an equimolar mixture of PS-E and K-PEG (●). Conditions: [total peptide] = 150-210 μM, PBS, 25 °C.

Table 2. CD Spectroscopic Data of Synthetic Peptides, Polymer-b-Peptides, and Mixtures Thereof.

Sample[a]	$[\theta]_{222}/[\theta]_{208}$		% α-helicity[b]	Coiled coil[c]
	PBS	50% TFE	PBS	
K	0.74	0.77	56	-
E	0.59	0.80	22	-
E/K	0.94	0.78	74	+
K-PEG	0.53	0.75	37	-
PS-E	0.95	0.78	48	+
E/K-PEG	0.86	0.79	37	+
PS-E/K	0.91	0.79	33	+
PS-E/K-PEG	0.89	0.77	77	+

[a] A/B refers to a mixture having equimolar concentrations of compounds A and B. [b] The % α-helicity is 100 times the ratio of the $[\theta]_{222}$ value observed in PBS to the $[\theta]_{222}$ value predicted for an α-helical peptide of n residues. The predicted α-helicity is calculated using the formula $[\theta]_{222} = -40000(1 - 4.6/n)$.[30] [c] The + sign signifies a significant decrease in the $[\theta]_{222}/[\theta]_{208}$ ratio in going from PBS to 50% TFE in PBS, indicative of the folded coiled-coil structure in PBS.[8] Conditions: [total peptide] = 150-210 μM, T = 25 °C.

Table 3. Sedimentation equilibrium data of the peptides used in this study.

name	Calculated monomeric molecular weight (g/mol)	observed molecular weight (g/mol)	oligomerization state
K	2378	2675	Monomer
E	2380	2446	Monomer
K/E	2379	4069	Dimer

Polymer-Peptide Self-Assembly

Circular Dichroism

As discussed in the Introduction, the function of the peptide blocks is to control the behavior of the synthetic polymer blocks, i.e., to assemble them into a supramolecular ABC triblock copolymer. However, the interaction between the peptides E and K can be influenced by the presence of the synthetic polymers. CD spectroscopy (Figure 2b and Table 2) showed that K-PEG adopts a random-coil secondary structure, probably due to wrapping of the PEG around the peptide.[25] A comparison of the hydrodynamic diameters (D_h) of K and K-PEG (5.1 vs. 5.4 nm) supported this interpretation. This tight packing of the PEG chain around K results in a different environment for the peptide, disturbing the hydrogen bonding that maintains the helical secondary structure in peptides. An opposite effect was observed when PS was conjugated to peptide E to form PS-E. While E adopts a random-coil conformation in solution, the spectrum of the PS-E conjugate was typical of those for interacting helices (ellipticity ratio of 0.95, 48% α-helicity). Stabilization of the α-helical structure in collagen-like peptides by hydrophobic alkyl tails has been demonstrated previously,[31] and in the present study, this observation is attributed to PS-induced aggregation (see below) that results in forced close contact of multiple E peptides and subsequent coiled-coil folding between E peptides. Mixing PS-E with K-PEG to form

PS-E/K-PEG produced increases in the ellipticity ratio and the % α-helicity (to 0.89 and 77%, respectively), indicating the formation of a coiled-coil complex similar to E/K.32 CD spectra were also recorded after the samples were diluted 1:1 (v/v) with trifluoroethanol (TFE), as TFE is known to enhance α-helicity while disrupting quaternary structures.[33] Therefore, adding TFE to monomeric peptides increases the ellipticity ratio to ~80%, while addition of TFE to coiled coils reduces this ratio to ~80%. As expected for PS-E/K-PEG, a significant decrease in the ellipticity ratio (to 0.77) was observed, which is typical of the transition from coiled coils to single helices with nearly maximum α-helicity. Combining these results shows that the ability of the peptides E and K to form heterocoiled coils is almost completely retained upon conjugation with two vastly different polymer chains. These findings imply the formation of a noncovalent ABC triblock copolymer (PS-E/K-PEG) with an amphiphilic nature.

Dynamic Light Scattering

Next, the process of self-assembly of the noncovalent PS-E/K-PEG complex into larger structures was studied using dynamic light scattering (DLS) and electron microscopy. The peptides, polymer-*b*-peptide conjugates, and mixtures thereof were dialyzed into phosphate buffered saline (PBS) starting from dimethylformamide (DMF). As expected, DLS did not show any aggregate formation for water-soluble E, K, and K-PEG or for the complexes E/K and E/K-PEG. In contrast, all of the samples containing PS assembled into defined aggregates. For PS-E, a D_h value of 16.2 $\pm$ 3.3 nm was observed (Figure 3 and Table 3). Mixing PS-E with K resulted in a small decrease in D_h (to 13.7 $\pm$ 3.2 nm). This occurred because complexation of K with E results increases the ratio of the area of the headgroup to the volume of the hydrophobic block and thus effectively decreases the packing parameter, resulting in a reduced radius for the spherical micelles.34 Combining equimolar amounts of PS-E with K-PEG increased the area of the hydrophilic headgroup of the resulting PS-E/K-PEG complex, and as a result, larger aggregates, having a D_h of 39.7 $\pm$ 11.3 nm, were observed. This large increase in micellar size was not expected on the basis of traditional packing-parameter considerations, and another model was adapted in order to explain the observations (see below).

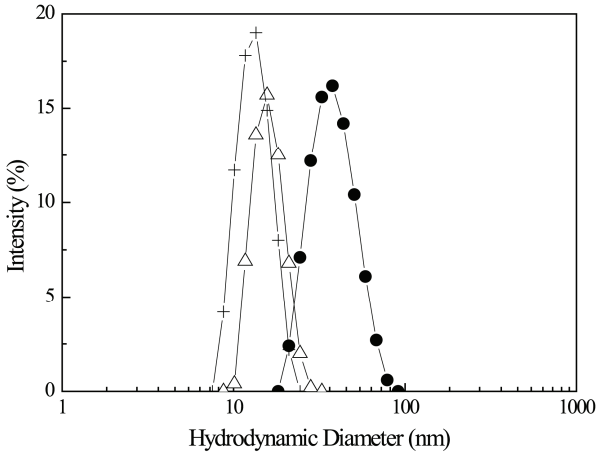


Figure 3. DLS intensity distributions for PS-E (Δ), PS-E/K (+), and a mixture of PS-E and K-PEG (●). Conditions: [total peptide] = 150-210 μM, PBS, 25 °C.

Cryogenic Transmission Electron Microscopy

Further insight into the morphologies of the assemblies was obtained by cryogenic transmission electron microscopy (cryo-TEM). These studies revealed the presence of aggregates for PS-E and the complexes PS-E/K and PS-E/K-PEG (Figure 4A-F). The micrographs showed that PS-E and PS-E/K assembled into spherical micelles with mean effective diameters (D_{eff}) of 15 $\pm$ 2 and 13 $\pm$ 3 nm, respectively (the size distributions of these micelles are presented in Figure A8 in the Appendices). In contrast, the noncovalent amphiphilic ABC triblock copolymer PS-E/K-PEG assembled into rod-like micelles with dimensions (length × width) of (42 $\pm$ 10 nm) × (8 $\pm$ 1 nm) and an average apparent aspect ratio of 5.35 Moreover, careful examination of the cryo-TEM images revealed that high electron-density regions separated by low-density regions were present along the rod. On the basis of the molecular structure of the ABC block copolymer, it is proposed that the rod-like micelles of PS-E/K-PEG are composed of a hydrophobic PS core with a corona of E/K-PEG. The high-density regions within the corona are attributed to clustering of multiple coiled-coil segments along the aggregates, while the low-density regions are attributed to hydrated PEG chains that cannot be visualized by cryo-TEM. It is therefore also proposed that the peptide clusters are separated by PEG-rich domains, as these have been shown to fold around coiled-coil-forming peptides without affecting their ability to associate.[36] Approximately 5% of the observed rods showed a lower intensity in the core of the assembly (Figure 4E and the white box in 4C), likely arising from less-efficient removal of DMF during dialysis. This results in an increased electron-density contrast between the coiled-coil clusters and the PS core, rendering the core visible. In addition, the extra solvation of the PS core most probably allows for better microphase separation of the blocks, in contrast to the majority of the micelles. The mean diameter of the core of these cylinder-like structures, as determined from the density profiles of 16 of these rods, was well-defined, with a well-defined distance between the two walls of 4.7 $\pm$ 0.5 nm, which is close to the calculated diameter of a solvated PS_9 core (4.2 nm).[37]

These results complement the DLS measurements, as demonstrated by the calculation of effective diameter distributions for the aggregates in cryo-TEM images (Table 4). Significantly, as the ellipticity ratios of PS-E/K and PS-E/K-PEG are nearly identical (Table 2), the observed morphological differences can be attributed completely to the presence of the PEG segment in the latter complex. Finally, the structural integrities of all of the micellar forms were maintained for at least 9 months when the micelles were stored at 4 °C.

In order to study the influence of the coiled-coil complex on the self-assembly behavior, PS_{11}-PEG_{74} was studied. Upon dispersion in PBS, the exclusive formation of spherical micelles was observed. Cryo-TEM revealed a polystyrene core with a mean effective diameter of 12 $\pm$ 3 nm, and DLS gave an overall hydrodynamic diameter of 20.6 $\pm$ 4.5 nm (Figures A5 and A6 in the Appendices).

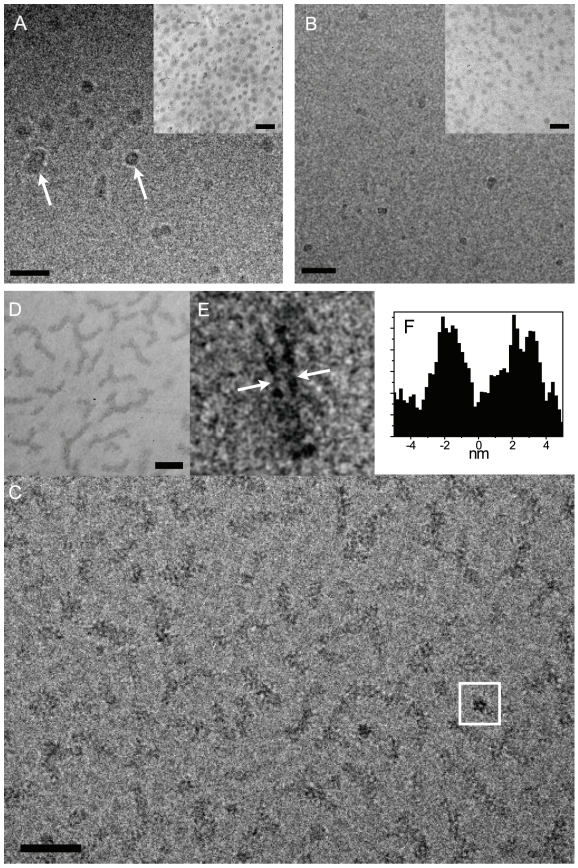


Figure 4. Cryo-TEM images of (A) PS-E, (B) PS-E/K, and (C) PS-E/ K-PEG, with 50 nm scale bars. Conditions: [total peptide] ~1500 μM, PBS. Arrows in (A) show ice particles arising from vacuum contamination. The insets in (A) and (B) and the image in (D) are phosphotungstic acid (PTA)-stained samples ([total peptide] = 150-210 μM, 50 mM phosphate, 100 mM KCl, pH 7.0, 25 °C). The micrographs in (C) and (E) show that the rods of PS-E/K-PEG are formed by small dots organized along the rod. Approximately 5% of the rods show a lower electron density in the core [viewed lengthwise in (E) and perpendicularly down the cylinder axis in the white box in (C)]. (F) The intensity profile of these rods shows a mean core diameter of 4.7 nm (representing an average calculated from 16 different profiles with a standard deviation of 0.5 nm).

Table 4. Number-Average Particle Diameters (with Standard Deviations) and Theoretical Diameters of the Aggregating Systems Investigated in This Study

Sample	Morphology	D_h (nm) [a]	D (nm) [b]	D (nm)[e]
PS-E	spherical	16.2 ± 3.3	15 ± 2	15
PS-E/K	spherical	13.7 ± 3.2	13 ± 3	13
PS-E/K-PEG	rod-like	39.7 ± 11.3	42 ± 10 x 8 ± 1[c]	length x 17
PS-E/K-PEG[f]	spherical	21.0 ± 4.4	14 ± 2[d]	18
PS-PEG	spherical	20.6 ± 4.5	12 ± 3	20

[a] Hydrodynamic diameter, as determined by DLS. The DLS data revealed a log-normal distribution of sizes. [b] Mean effective diameter, as determined from measurements of objects in TEM images. TEM size distributions are shown in Figure A8 in the Appendices. For PEG-containing samples, the dimensions obtained from TEM are smaller than those from DLS or the model, indicating that the PEG is not observed using TEM. [c] Dimensions (length × width) of the rod-like micelles. [d] PTA-stained sample. [e] Theoretical diameter, as determined using the model explained in the Appendices. [f] After annealing.

Temperature-Dependent Self-Assembly

Circular Dichroism

The temperature dependence of the assemblies was tested in order to gain insight into the dynamics and reversibility of the systems. Coiled-coil peptide complexes typically are temperature sensitive,[17] and the mixture E/K showed a melting temperature of 50 °C, as determined from the inflection point of the observed decrease in ellipticity at 222 nm (Figure 5a). The rod-like micelles composed of PS-E/K-PEG did not have a clear melting temperature, underlining the stabilizing effect of the micelles (Figure 5A). However, when the temperature reached 96 °C, the ellipticity ratio of PS-E/K-PEG mixture had decreased to less than 0.75 (Figure 5b), indicating that the peptides were no longer forming a coiled-coil complex. At this high temperature, the mixture exhibited a random-coil spectrum (Figure 5c), confirming that the specific interaction between E and K was lost, resulting in a full separation of PS-E from K-PEG (see below). When the mixture was cooled, the coiled-coil structure of PS-E/K-PEG was fully regained, as demonstrated by both the reproduction of the melting profile without hysteresis and the identical CD spectra before and after annealing (Figure 5c). These results show that the process of coiled-coil unfolding/dissociation is reversible and fast, and that the peptide structures are in equilibrium. The different shapes of the melting curves for the hybrids compared to that for E/K (Figures 5a and A9) indicates that the hybrids unfold and dissociate in a way that is atypical for coiled-coil motifs. The initial linear part of the CD melting curves corresponds to changes in helicity in the peptide complex (for example, end-fraying or unimolecular rearrangement) that occur before the onset of the cooperative unfolding and dissociation corresponding to the sigmoidal decrease in helicity seen in the E/K profile.[38] The fact that the initial linear parts of the CD melting curves for the hybrids extended from 30 °C for E/K to 70 °C for all three forms of micelle means that the PS core imparts stability with respect to cooperative folding of the peptide components by retaining them in close proximity. Although there was no clear cooperative dissociation phase for the

peptides in the micellar form, when the temperature reached 70 °C, the ellipticity ratio had decreased to a value less than that for which one can expect the coiled-coil motif to exist, indicating that the peptide complexes do not dissociate in the usual cooperative way but instead fray from one end to another or that the increasing magnitude of structural vibrations gradually dissociates the peptide complexes.[38]

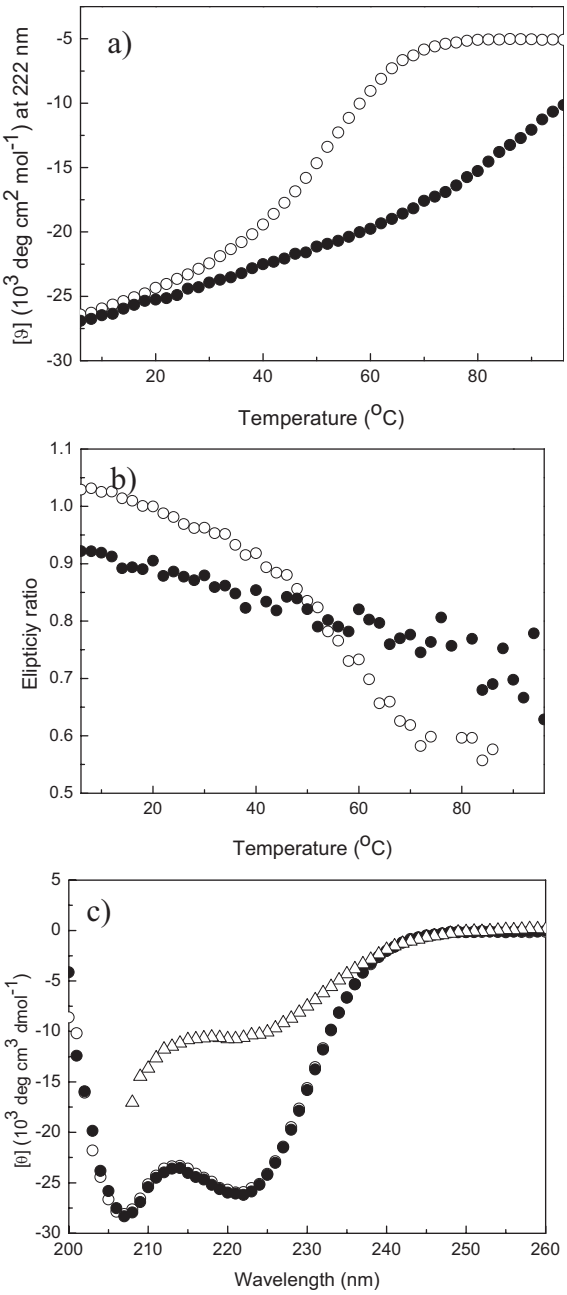


Figure 5. (a) Temperature dependence of the ellipticities ([θ] at 222 nm for E/K (○) and PS-E/K-PEG (●). (b) Temperature dependence of the ellipticity ratios for E/K (○) and PS-E/K-PEG (●). (c) CD spectra of PS-E/K-PEG at 6 °C (●), 96 °C (Δ), and after cooling back to 6 °C (○). Conditions: heating and cooling rates of 2 °C min-1, [total peptide] = 150-210 μM, PBS.

Dynamic Light Scattering

DLS of the annealed solutions of PS-E/K-PEG revealed that D_h for the rod-like micelles decreased to 21.0 $\pm$ 4.4 nm after cooling to 4 °C (Figure 6a, Table 3). Indeed, TEM revealed a conversion to spherical micelles (Figure 6b) having an average size of 14 $\pm$ 2 nm, and rod-like micelles were no longer observed. These results indicate that although the temperature-dependent assembly of the coiled-coil peptide motif is fully reversible, morphological transitions of the entire assembly are subject to more-complex kinetics.

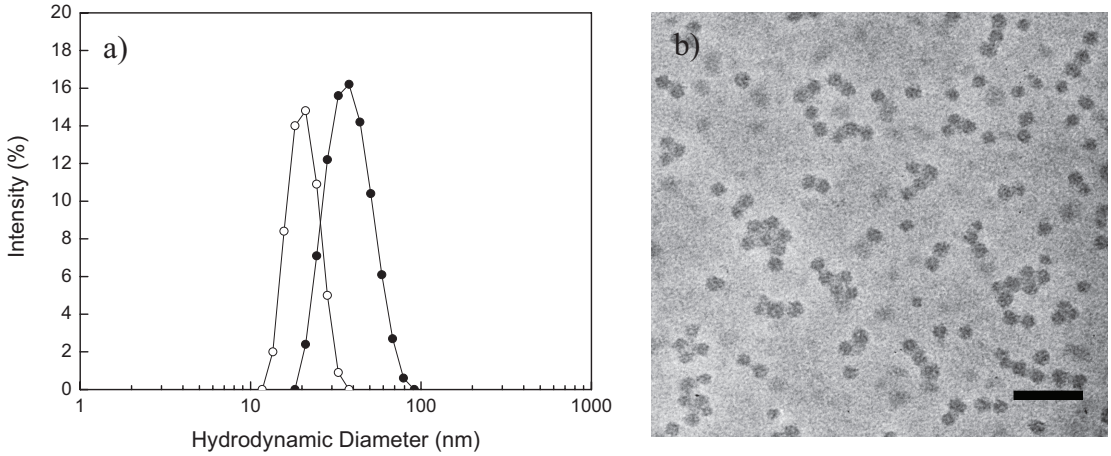


Figure 6. (a) Size distributions obtained from DLS of PS-E/K-PEG before (●) and after (○) a heating-cooling cycle. (b) PTA-stained TEM image of PS-E/K-PEG after annealing, with a scale bar of 50 nm. Conditions: [total peptide] = 270 μM, PBS, 25 °C.

A more detailed inspection of the temperature-dependent DLS data (Figure A10 in the Appendices) revealed that the rod-like micelles are stable up to ~ 45 °C. Between 45 and 75 °C, a transition of the aggregate morphology occurs, resulting in a 50% decrease in D_h. As 97% of the PS blocks have a glass transition temperature (T_g) lower than 45 °C, melting of the polystyrene core is unlikely to be the cause for this transition.[39] Temperature-dependent DLS data for the PEG homopolymer (PEG_{77}) did not reveal a significant decrease in size with increasing temperature (Figure A10), so a temperature-induced collapse of PEG chains is also unlikely to trigger the change in aggregate size. Hence, the observed size decrease must be a consequence of the temperature-dependent dissociation of the peptides (Figure 5a). In contrast, thermal cycling of PS-PEG micelles revealed the stability of these assemblies, with only a slight, reversible decrease of 2 nm in D_h (from 23 to 21 nm) upon cycling of the temperature between 4 and 90 °C (Figure A7 in the Appendices). The formation of thermally stable spherical PS-PEG micelles is in accord with the results of previous studies of the aqueous self-assembly of PS-PEG with block lengths or polystyrene weight fractions similar to those used in this study.[40]

SUMMARY AND DISCUSSION

Experimental

The experimental results have shown that the hybrids PS-E and K-PEG undergo two levels of self-assembly: the peptides interact to produce a noncovalent triblock copolymer, which then arranges into rod-like micelles. The hydrophobic PS block forms the core, which is shielded from the aqueous buffer by clusters of coiled-coil peptides around which PEG is closely folded. The dissociation of the PS-E/K-PEG complex at high temperature leads to a change in the micellar morphology, yielding spherical micelles composed of PS-E with K-PEG free in solution, i.e., the system now behaves like the PS-E sample. When the peptides are cooled, they re-coil (as seen with CD), resulting in spherical micelles coated with PEG. The high-temperature rearrangement of the rod-like micelles studded with clusters of coiled coils into spherical PS-E micelles results in homogenous dispersion of E over the surface. Hence, when K-PEG starts to re-coil with the PS-E micelles, the PEG block forms a layer outside the peptide shell. These conclusions are supported by DLS and cryo-TEM data. DLS shows that the hydrodynamic diameter of the annealed PS-E/K-PEG spherical micelles is larger than that of PS-E/K, and the difference fits with the dimensions of the PEG block used. In contrast, similar diameters were found with TEM since PEG is not visible, further confirming that PS-E/K-PEG micelles are composed of a PS core, a peptide layer, and a PEG outer layer. The micelles remain spherical upon subsequent heating and cooling cycles, indicating that these micelles are at thermodynamic equilibrium. A schematic representation of the behavior of the triblock copolymer is shown in Figure 7.

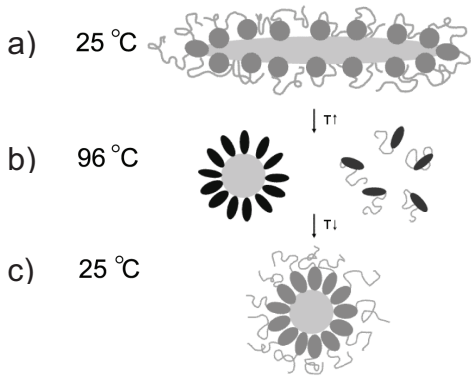


Figure 7. Idealized schematic cross-section representation of the temperature- dependent self-assembly of PS-E/K-PEG. (a) Rod-like micelles are composed of a PS core and an E/K-PEG corona. (a) Heating leads to the formation of spherical micelles with a PS core and an E corona. K-PEG is in solution. (c) When the spherical micelles are cooled, they have a PS core and an E/K-PEG corona.

The distinct difference in the self-assembly behaviors of noncovalent PS-E/K-PEG and covalent PS-PEG highlights the influence of the coiled-coil block on these processes, as

shown by the observed morphologies and temperature-dependent dynamic behaviors. In summary, PS-E/K-PEG self-assembles into dynamic rod-like micelles that are able to undergo a transition in micellar morphology, while PS-PEG organizes into static spherical micelles (see below). Thus, inclusion of the reversible noncovalent connecting block provides access to an unusual micellar morphology and encodes "smartness" into the nanostructures, allowing them to respond to environmental changes.

Model

Because direct dissolution of PS-E in buffer is not possible, micelles are produced by the gradual removal of the organic cosolvent from the amphiphile solutions. However, the presence of solvent in the core41 and the low degree of polymerization of the PS block (which has a low average T_g of 11 °C)[39] may lead to equilibrated micelles with mobile hydrophobic blocks. As a result, the micellar morphology becomes sensitive to external factors such as temperature, buffer concentration, interaction between monomers, and so on. The dimensions of the PS-PEG, PS-E, and PS-E/K micelles, as measured by DLS and TEM at temperatures above the T_g of the PS part, are in accordance with those of micelles having a disordered polystyrene core surrounded by a PEG or coiled-coil peptide shell. The packing parameters of PS-PEG, PS-E, and PS-E/K micelles predict the formation of micelles with spherical morphology. PS-E/K self-assembles into slightly smaller micelles than PS-E does, as the larger size of the hydrophilic block causes greater curvature in the self-assembled nanostructures and, in addition, E/K charge neutralization reduces stretching of the PS core. For the PS-E/K-PEG complex, a spherical micellar morphology for the thermodynamically favored structures is *expected* on the basis of the simple packing parameter model, as the ratio of the hydrophilic and hydrophobic block lengths increases.[34] However, for this complex, the observed morphology formed during dialysis is the rod-like structure. The packing parameter was originally designed to predict the morphology and size of nanostructures formed from lipids.[34] However, this approach has proven to be ill-suited for block copolymers like the ones considered here, as it cannot accommodate headgroup complexity such as flexibility and dynamic behavior. To qualitatively explain all of the observed morphologies and the transition from rod-like to spherical micelles, a theoretical model was adapted (see the Appendices) initially designed for charged, flexible diblock copolymers.[42] Currently, no simple model for determining the phase diagram of triblock copolymers with a rigid middle block exists. In view of the limitations of available models, the most practical model was adapted that can predict the different morphologies and transitions between them as well as the micellar dimensions that arise from the complex, noncovalent hybrids studied in this work. In order to treat the PS-E/K-PEG triblock copolymer as a diblock one, E/K-PEG was considered to be a single block. It was also assumed that the excess of salt present in the buffer neutralizes the charges of the E, K, and E/K blocks and that polymers follow the statistics of flexible neutral chains. The size of the PS core and the overall size of the micelle are established from the interplay between the free energy of the hydrophilic block (E, E/K, or E/K-PEG)

and the interfacial energy between the core and corona. For PS-PEG, PS-E, and PS-E/K complexes, the free energy of the hydrophilic group comprises the free energies of the PEG or peptide conformations and of short-range interactions between molecules. All of the spherical morphologies observed in this study are predicted by this model. PS-E and PS-E/K complexes are either in the region of spherical micelles or in the region of degenerate structures where rod-like micelles, spherical micelles, and lamella have the same free energy. Only spheres are observed because the translational entropy favors the formation of smaller objects. For comparison, PS-PEG is in a region where micelles can only be spherical. The model predicts that increasing the length of the water soluble block (through complexation of PS-E with K-PEG) leads exclusively to rod-like morphology. This is due to the low free energy of the short-range interactions between monomers per hydrophilic E/K-PEG block. This means that the PEG chains are more compact than those in PS-PEG. Temperature annealing of the rod-like complex transforms the structure into degenerate spheres. This is possible because at high temperature, the E/K complex dissociates and K-PEG leaves the micelle. The reduced amount of organic solvent in the PS core decreases the conformational entropy of PS and increases the interfacial energy. Therefore, the PS-E rearranges into degenerate spheres with a tightly packed polystyrene core. When the system is cooled, K-PEG re-coils with the PS-E micelles, but because the polystyrene core is now locked in a frozen equilibrium (tightly packed), the PS molecules are unable to rearrange into the rod-like structure upon condensation of K-PEG onto the spherical PS-E micelles or with further temperature annealing. As summarized in Table 3, the model correctly predicts the form of PS-PEG, PS-E, PS-E/K, and PS-E/K-PEG micelles and includes the transition of PS-E/K-PEG from rod-like to spherical micelles upon annealing. The micellar diameters estimated by this model are in surprisingly close agreement with the experimental results. However, the model overestimates the diameter of the rod-like micelles, indicating that it requires further tuning in order to account for the complexity of the triblock copolymer and the end-capping energy.

CONCLUSIONS

This work represents the first account of a noncovalent triblock copolymer composed of hydrophobic and hydrophilic polymers united via a peptide complex. The hierarchical self-assembly in solution of two complementary polymer-*b*-peptides (PS-E and K-PEG) utilizes the coiled-coil-forming propensities of the peptides, resulting in the formation of an amphiphilic triblock copolymer (PS-E/K-PEG) able to assemble into rod-like micelles. The dynamic nature of these micelles was shown by annealing of the amphiphile above the coiled-coil transition temperature. The release of the hydrophilic hybrid led to a transformation to spherical micelles that persisted upon re-coiling of the peptides, demonstrating the reversibility of the noncovalent block linker. As the macromolecular entities that are connected to the peptides are open to choice and additional methods for influencing the peptidic interaction exist, this peptide motif is a promising building block for the bottom-up approach to the formation of “smart” block copolymer structures in aqueous solutions.

EXPERIMENTAL SECTION

Materials and Methods

Materials

Fmoc-protected amino acids were purchased from Novabiochem. Tentagel PAP resin was purchased from Rapp Polymere. Monocarboxy terminated polystyrene was purchased from Polymer Source Inc.. All other reagents and solvents were obtained at the highest purity available from Sigma-Aldrich or BioSolve Ltd. and used without further purification. Phosphate buffered saline, PBS: 30 mM $K_2HPO_4.3H_2O$, 19 mM KH_2PO_4, 100 mM KCl, pH 7.0.

General Methods

HPLC was performed with a Shimadzu HPLC system with two LC-8A pumps, and an SPD-10AVP UV-VIS detector. Sample elution was monitored by UV detection at 214 nm and 256 nm. Samples were eluted with a linear gradient from A to B, A being 0.1% (v/v) TFA in water, and B acetonitrile. Purification of the peptides and hybrids was performed on a Vydac C4 reversed phase column (214TP1022, 22 mm diameter, 250 mm length, 10.00 μM particle size) with a flow rate of 20 mL min^{-1}. For verification of sample purity a reversed phase Vydac C4 column (214TP54, 4.6 mm diameter, 250 mm length, 5.00 μM particle size) was used with a flow rate of 1 mL min^{-1}. Sample elution was additionally monitored by an light evaporative light scattering detector. PS-PEG was purified on an Alltech Alltima Silica 5u column (22 mm diameter, 250 mm length) with a flow rate of 10 mL min^{-1} and a linear gradient from A to B, A being methanol, and B dichloromethane.

MALDI-TOF mass spectra were acquired using an Applied Biosystems Voyager System 6069 MALDI-TOF spectrometer. Samples were dissolved in 1:1 (v/v) 0.1% TFA in water:acetonitrile (TA), at concentrations of ~0.3 mg mL^{-1} for K and E, ~6 mg mL^{-1} for K-PEG and PS-PEG, and ~3 mg mL^{-1} for PS-E and PEG. Solutions for spots consisted of (v/v) 1:10 sample solution: 10 mg mL^{-1} ACH in TA. For K-PEG and PS-E one part 0.1% AgTFA in THF was added to facilitate ionization, and for the PS-E solutions 10 parts of THF were added. PSCOOH was dissolved at ~ 2 mg mL^{-1} in a dithranol solution (20 mg mL^{-1} dithranol in $CHCl_3$).

^{1}H-NMR spectra were recorded on a Bruker AV-500 spectrometer and a Bruker DPX300 spectrometer using the residual proton resonance of deuterated water, acetonitrile, or chloroform for calibration.

GPC was preformed with a Shimadzu system equipped with a refractive index detector. A Polymer Laboratories column was used (3M-RESI-001-74, 7.5 mm diameter, 300 mm length) with DMF as the eluent, at 60 ºC, and a flow rate of 1 mL min^{-1}. PEG standards were used for mass calibration.

Synthesis

Solid-Phase Peptide Synthesis of K, E, K-PEG, PS-E

The peptide components of K, E, PS-E, and K-PEG were prepared using standard Fmoc chemistry on an Applied Biosystems 431A automated peptide synthesizer. E, K, and the peptide component of PS-E were synthesized on Sieber-Amide resin, while the peptide section of K-PEG was prepared on Tentagel PAP resin. HCTU was used to activate the amino acid derivatives. K, E and K-PEG were acetylated at the N-terminus. After the peptide component of PS-E was prepared, the resin was removed from the reaction vessel, swollen in 1:1 (v/v) DMF:NMP, and Fmoc deprotected. PS was coupled to the N-terminus by shaking 4 equivalents of PSCOOH M_n 2400 g mol^{-1} (PDI 1.20), 4 equivalents of HCTU, and 8 equivalents of DIPEA (predissolved in DMF) with the resin for five days. Cleavage and deprotection of the compounds was carried out using 95:2.5:2.5 (v/v) TFA:water:TIS for 1-3 hours. The cleavage mixture and three subsequent rinses of the resin with the TFA mixture were added drop-wise to cold diethylether, or cold methanol for PS-E. With K, E, and K-PEG the white precipitate was compacted with centrifugation and the supernatant removed. This was repeated three times with the addition of fresh diethylether. The pellets were dried in air or under reduced pressure. For PS-E the solution was evaporated to dryness with toluene addition 5 times throughout the evaporation. The slightly yellow material was dried under reduced pressure.

The crude products of the K, E, and PS-E syntheses were purified by RP-HPLC, with gradient elution 35% to 50% B over 20 minutes for K and E, and 50% to 100% B over 30 minutes for PS-E. K-PEG was purified by dialysis from Spectra/Por® regenerated cellulose dialysis tubing with a molecular weight cut of 3500 g mol^{-1}. After purification all compounds were lyophilized from water (or in the case of PS-E, from a water/acetonitrile mixture) to give white material with the following yields: K, E ~ 40%, K-PEG, PS-E ~ 10%. The compounds were characterized by MALDI-TOF MS (K: m/z = 2379 $[M+H]^+$, E: m/z = 2381 $[M+H]^+$), RP-HPLC, and ^{1}H-NMR. The chromatograms and spectra for PS-E and K-PEG are shown in Figures A1–A3.For each compound the purity was estimated from RP-HPLC to be greater than 95%.

Synthesis of PS-PEG

Cleavage of NH_2-PEG_{74}-OH from Tentagel PAP resin was carried out using TFA for 15 hours. The cleavage mixture and three subsequent rinses of the resin with TFA were added drop-wise to cold diethylether. The white precipitate was compacted with centrifugation and the supernatant removed. This was repeated three times with the addition of fresh diethylether. The pellets were dried under reduced pressure. Residual acid was removed by dissolving the powder in Milli-Q water and shaking with Amberlite resin IRA-410 (OH) for 5 minutes. Lyophilizing resulted in a white powder at 80% yield. MALDI-TOF MS: M_n = 3321 gmol^{-1}.

Monocarboxy terminated polystyrene was coupled to the poly(ethylene glycol) via the amine terminus by shaking 1 equivalent of PSCOOH (MALDI-TOF MS: M_n = 1286 g

mol^{-1}, FTIR (thin film from $CHCl_3$): 1706 cm^{-1} (C=O stretch)), 1.2 equivalents of PYBOP, and 2.4 equivalents of DIPEA (predissolved in DMF, 2 minutes activation, FTIR (thin film from $CHCl_3$): 1811 cm^{-1} (C=O stretch)) with 1.4 equivalents of poly(ethylene glycol) for 15 hours.

The crude product was purified by silica HPLC, with gradient elution 100% to 90% B over 30 minutes, followed by a Bio-Beads column using chloroform as the eluent. Lyophilizing resulted in PS_{11}-PEG_{74} in the form of a white powder at 13% yield. MALDI-TOF MS: M_n = 4500 g mol^{-1}. ^{1}H-NMR (300 MHz, $CDCl_3$, δ): 7.15-6.64 (bm, 53H, PS), 3.64 (s, 296H, PEG). FTIR (thin film from $CHCl_3$): 1672 cm^{-1} (C=O stretch, Amide I band). GPC (DMF): 8.2 minutes, PDI = 1.03.

Preparation of the Micellar Suspensions

The compounds were dissolved at 1 mg mL^{-1} of peptide in DMF for the preparation of the stock solution. The stock solutions were combined in 1:1 ratios. PS-PEG was dissolved at 1 mg mL^{-1} in DMF. Dialysis tubing of molecular weight cut-off of 1000 g/mol was rinsed with water, then DMF, and the samples were dialyzed against buffer (50 mM PO4, 100 mM KCl, pH 7.0) at room temperature for at least 24 hours with at least 5 changes of buffer.

The aggregation numbers of the spherical micelles of PS-E and PS-E/K are estimated to be 270 and 110 based on the aggregate sizes observed with electron microscopy and the calculated molecular/complex volume using the program ChemDraw. PS-E/K-PEG rod-like micelles are estimated to contain 640 complexes, while the spherical PS-E/K-PEG micelles are estimated to contain 230 complexes.

Characterization of Micellar Suspensions

Circular Dichroism Spectroscopy

CD spectra were obtained as detailed in the experimental section of Chapter 2.

Dynamic Light Scattering

Experimental diffusion coefficients, D, were measured at 25 °C by dynamic light scattering using a Malvern Zetasizer Nano ZS equipped with a peltier-controlled thermostatic cell holder. The laser wavelength was 633 nm and the scattering angle was 173˚. The Stokes-Einstein relationship $D = k_BT/3\pi\eta D_h$ was used to estimate the hydrodynamic radius, D_h. Here k_B is the Boltzmann constant, and η is the solvent viscosity. Temperature dependent DLS distributions were measured from 4 °C to 90 °C with parameters optimized at each temperature.

Analytical Ultracentrifugation

Apparent molecular masses were determined by sedimentation profiles using a Beckmann XL-A ultracentrifuge at 20 °C. The peptides were dissolved in 50 mM phosphate, 100 mM KCl, pH 7.0 buffer at 1.0 mg/mL. For each sample three different concentrations where

used, namely those concentrations at which the optical density (O.D.) was 0.1, 0.3 and 0.5 respectively. The absorption of each sample was first checked with an UV-VIS photospectrometer and diluted with the buffer to reach the necessary concentration. The samples where then loaded into a charcoal/epoxy 6-channel 12 mm centerpiece, equipped with quartz windows against the buffer as a reference. The samples where then loaded into the analytical ultracentrifuge and allowed to equilibrate at three different rotor speeds namely, 25000 rpm, 33000 rpm and 40000 rpm. Data were fit to a single species, with high correlation factors, R, and random residuals.

Transmission Electron Microscopy

TEM was conducted on a JEOL 1010 instrument with an accelerating voltage of 60 kV. Samples for TEM were prepared by placing a drop of each solution on carbon-coated copper grids. After ~ 10 minutes the droplet was removed from the edge of the grid. A drop of 2% PTA stain was applied and removed after 2 minutes. Negative images are shown in order to retain image quality.

Cryogenic Transmission Electron Microscopy

Samples for cryogenic TEM were concentrated by centrifuging in Centricon centrifugal filter devices MWCO 3000 g mol^{-1} at 4˚C. Sample stability was verified by DLS and TEM.

The cryogenic transmission microscopy measurements were performed on a FEI Technai 20 (type Sphera*)* TEM or on a Titan Krios (FEI). A Gatan cryo-holder operating at ~ -170 °C was used for the cryo-TEM measurements. The Technai 20 is equipped with a LaB_6 filament operating at 200kV and the images were recorded using a 1kx1k Gatan CCD camera. The Titan Krios is equipped with a field emission gun (FEG) operating at 300 kV. Images were recorded using a 2k x 2k Gatan CCD camera equipped with a post column Gatan energy filter (GIF). The sample vitrification procedure was carried out using an automated vitrification robot: a FEI Vitrobot Mark III. TEM grids, both 200 mesh carbon coated copper grids and R2/2 Quantifoil Jena grids were purchased from Aurion. Copper grids bearing lacey carbon films were home made using 200 mesh copper grids from Aurion. Grids were treated with a surface plasma treatment using a Cressington 208 carbon coater operating at 25 A for 40 seconds prior to the vitrification procedure.

REFERENCES

1. (a) Zhang, L.; Eisenberg, A. *Science* **1995**, *268*, 1728–1731. (b) Cameron, N. S.; Corbierre, M. K.; Eisenberg, A. *Can. J. Chem.* **1999**, *77*, 1311–1326.
2. (a) Vandermeulen, G. W. M.; Klok, H.-A. *Macromol. Biosci.* **2004**, *4*, 383–398. (b) Cornelissen, J. J. L. M.; Fischer, M.; Sommerdijk, N. A. J. M.; Nolte, R. J. M. *Science* **1998**, *280*, 1427–1430. (c) Kros, A.; Jesse, W.; Metselaar, G. A.; Cornelissen, J. J. L. M. *Angew. Chem., Int. Ed.* **2005**, *44*, 4349–4352. (d) Klok, H.-A. *Angew. Chem., Int. Ed.* **2002**, *41*, 1509–1513. (e) Bellomo, E. G.; Wyrsta, M. D.; Pakstis, L.; Pochan, D. J.; Deming, T. J. *Nat. Mater.* **2004**, *3*, 244–248. (f) Boerakker, M. J.; Botterhuis, N. E.; Bomans, P. H. H.; Frederik, P. M.; Meijer, E. M.; Nolte, R. J. M.; Sommerdijk, N. A. J. M. *Chem.Eur. J.* **2006**, *12*, 6071–6080. (g) Billot, J.-P.; Douy, A.; Gallot, B. *Makromol. Chem.* **1976**, *177*, 1889–1893. (h) Vriezema, D. M.; Kros, A.; De Gelder, R.; Cornelissen, J. J. L. M.; Rowan, A. E.; Nolte, R. J. M. *Macromolecules* **2004**, *37*, 4736–4739.
3. (a) Shimizu, L. S. *Polym. Int.* **2007**, *56*, 444–452. (b) Sivakova, S.; Rowan, S. J. *Chem. Soc. Rev.* **2005**, *34*, 9–21.
4. (a) Brunsveld, L.; Folmer, B. J. B.; Meijer, E. W.; Sijbesma, R. P. *Chem. Rev.* **2001**, *101*, 4071–4097, and references cited therein. (b) Xu, J.; Fogleman, E. A.; Craig, S. L. *Macromolecules* **2004**, *37*, 1863– 1870. (c) Ilhan, F.; Galow, T. H.; Gray, M.; Clavier, G.; Rotello, V. M. *J. Am. Chem. Soc.* **2000**, *122*, 5895–5896. (d) Guillet, P.; Fustin, C.- A.; Lohmeijer, B. G. G.; Schubert, U. S.; Gohy, J.-F. *Macromolecules* **2006**, *39*, 5484–5488.
5. (a) Ohlson, S.; Strandh, M.; Nilshans, H. *J. Mol. Recognit.* **1997**, *10*, 135–138. (b) Vandermerwe, P. A.; Barday, A. N. *Trends Biochem. Sci.* **1994**, *19*, 354–358.
6. Gohy, J.-F.; Lohmeijer, B. G. G.; Alexeev, A.; Wang, X. S.; Manners, I.; Winnik, M. A.; Schubert, U. S. *Chem.Eur. J.* **2004**, *10*, 4315–4323.
7. Liu, J.; Rost, B. *Protein Sci.* **2001**, *10*, 1970–1979.
8. Litowski, J. R.; Hodges, R. S. *J. Biol. Chem.* **2002**, *277*, 37272–37279.
9. Liu, J.; Deng, Y.; Cheng, C.-S.; Kallenbach, N. R.; Lu, M. *Proc. Natl. Acad. Sci. U.S.A.* **2006**, *103*, 15457–15462.
10. (a) Dong, H.; Hartgerink, J. D. *Biomacromolecules* **2006**, *7*, 691–695. (b) Burkhard, P.; Meier, M.; Lustig, A. *Protein Sci.* **2000**, *9*, 2294–2301.
11. Kohn, W. D.; Mant, C. T.; Hodges, R. S. *J. Biol. Chem.* **1997**, *272*, 2583–2586.
12. Woolfson, D. N. *Adv. Protein Chem.* **2005**, *70*, 79–112.
13. Oakley, M. G.; Hollenbeck, J. J. *Curr. Opin. Struct. Biol.* **2001**, *11*, 450–457. (b) Hadley, E. B.; Testa, O. D.; Woolfson, D. N.; Gellman, S. H. *Proc. Natl. Acad. Sci. U.S.A.* **2008**, *105*, 530–535.
14. Yu, Y. B. *Adv. Drug Delivery Rev.* **2002**, *54*, 1113–1129.
15. Acharya, A.; Ruvinov, S. B.; Gal, J.; Moll, J. R.; Vinson, C. *Biochemistry* **2002**, *41*, 14122–14131.
16. Tang, Y.; Ghirlanda, G.; Vaidehi, N.; Kua, J.; Mainz, D. T.; Goddard, W. A., III; DeGrado, W. F.; Tirrell, D. A. *Biochemistry* **2001**, *40*, 2790–2796. (b) Ryan, S. J.; Kennan, A. J. *J. Am. Chem. Soc.* **2007**, *129*, 10255–10260.
17. (a) Schnarr, N. A.; Kennan, A. J. *J. Am. Chem. Soc.* **2003**, *125*, 6364–6365. (b) Stevens, M. M.; Allen, S.; Sakata, J. K.; Davies, M. C.; Roberts, C. J.; Tendler, S. J. B.; Tirrell, D. A.; Williams, P. M. *Langmuir* **2004**, *20*, 7747–7752. (c) Naik, R. R.; Kirkpatrick, S. M.; Stone, M. O. *Biosens. Bioelectron.* **2001**, *16*, 1051–1057. (d) Wendt, H.; Leder, L.; Harma, H.; Jelesarov, I.; Baici, A.; Bosshard, H. R. *Biochemistry* **1997**, *36*, 204–213.
18. (a) Petka, W. A.; Harden, J. L.; McGrath, K. P.; Wirtz, D.; Tirrell, D. A. *Science* **1998**, *281*, 389–392. (b) Shen, W.; Zhang, K.; Kornfield, J. A.; Tirrell, D. A. *Nat. Mater.* **2006**, *5*, 153–158.
19. Wang, C.; Stewart, R. J.; Kopeček, J. *Nature* **1999**, *397*, 417–420.
20. (a) Ghosh, I.; Hamilton, A. D.; Regan, L. *J. Am. Chem. Soc.* **2000**, *122*, 5658–5659. (b) Yuzawa, S.; Mizuno, T.; Tanaka, T. *Chem.Eur. J.* **2006**, *12*, 7345–7352. (c) Chelur, D. S.; Chalfie, M. *Proc. Natl. Acad. Sci. U.S.A.* **2007**, *104*, 2283–2288.
21. Stevens, M. M.; Flynn, N. T.; Wang, C.; Tirrell, D. A.; Langer, R. *Adv. Mater.* **2004**, *16*, 915–918.
22. (a) Zhou, M.; Bentley, D.; Ghosh, I. *J. Am. Chem. Soc.* **2004**, *126*, 734–735. (b) Dublin, S. N.; Conticello, V. P. *J. Am. Chem. Soc.* **2008**, *130*, 49–51. (c) Potekhin, S. A.; Melnik, T. N.; Popov, V.; Lanina, N. F.; Vazina, A. A.; Rigler, P.; Verdini, A. S.; Corradin, G.; Kajava, A. V. *Chem. Biol.* **2001**, *8*, 1025–1032.
23. Ryadnov, M. G.; Woolfson, D. N. *Nat. Mater.* **2003**, *2*, 329–332.
24. Lomander, A.; Hwang, W.; Zhang, S. *Nano Lett.* **2005**, *5*, 1255–1260.

25. (a) Vandermeulen, G. W. M.; Hinderberger, D.; Xu, H.; Sheiko, S. S.; Jeschke, G.; Klok, H.-A. *ChemPhysChem* **2004**, *5*, 488–494. (b) Klok, H.-A.; Vandermeulen, G. W. M.; Nuhn, H.; Ro¨sler, A.; Hamley, I. W.; Castelletto, V.; Xu, H.; Sheiko, S. S. *Faraday Discuss.* **2005**, *128*, 29–41. (c) Pechar, M.; Kopečková, P.; Joss, L.; Kopeček, J. *Macromol. Biosci.* **2002**, *2*, 199–206.
26. (a) The peptide pair has a free energy of unfolding ($\Delta G H_2O$) value of 9.6 kcal mol^{-1}. (b) Lindhout, D. A.; Litowski, J. R.; Mercier, P.; Hodges, R. S.; Sykes, B. D. *Biopolymers* **2004**, *75*, 367–375. The amino acid sequences of K and E are based on those of IAAL K3 and IAAL E3, but each has a terminal glycine residue that was included as a spacer between the peptide and the polymer in the hybrids. See also Figure A4 in the Appendices.
27. Mason, J. M.; Arndt, K. M. *ChemBioChem* **2004**, *5*, 170–176.
28. Crick, F. H. C. *Acta Crystallogr.* **1953**, *6*, 689–697.
29. Zhou, N. E.; Kay, C. M.; Hodges, R. S. *J. Biol. Chem.* **1992**, *267*, 2664–2670.
30. Chen, Y. H.; Yang, J. T.; Chau, K. H. *Biochemistry* **1974**, *13*, 3350–3359.
31. Fields, G. B.; Lauer, J. L.; Dori, Y.; Forns, P.; Yu, Y.-C.; Tirrell, M. *biopolymers* **1998**, *47*, 143–151.
32. It should be noted that the CD spectrum of PS-E/K-PEG is not the average of the spectra of PS-E and K-PEG, as would be observed if the peptide blocks were not interacting. The observed amount of helicity is more than double what would be observed if PS-E remained homocoiled in the presence of K-PEG.
33. Lau, S. Y.; Taneja, A. K.; Hodges, R. S. *J. Biol. Chem.* **1984**, *259*, 13253–13261.
34. Israelachvili, J. N.; Mitchell, D. J.; Ninham, B. W. *J. Chem. Soc., Faraday Trans. 1* **1976**, *72*, 1525–1568.
35. On the basis of a comparison of the DLS and TEM data (Table 3), it is believed that the PEG segments do not contribute to the contrast observed in TEM; therefore, the true aspect ratio would be smaller.
36. The measured D_h of K-PEG (5.4 nm) is only slightly larger than that of K (5.1 nm). Also see ref 25a.
37. See the theoretical model section in the Appendices.
38. Dragan, A. I.; Privalov, P. L. *J. Mol. Biol.* **2002**, *321*, 891–908.
39. Claudy, P.; Lètoffè, J. M.; Camberlain, Y.; Pascault, J. P. *Polym. Bull.* **1983**, *9*, 208–215.
40. (a) Mortensen, K.; Brown, W.; Almdal, K.; Alami, E.; Jada, A. *Langmuir* **1997**, *13*, 3635–3645. PS-PEG with block sizes similar to those used in this study (1000 and 3000 g mol^{-1} for PS and PEG, respectively, compared to 1000 and 3500 g mol^{-1} in PS-E and KPEG) forms spherical micelles in D_2O with no intermicellar interactions in the concentration range used in this study that were detectable by small-angle neutron scattering or static or dynamic light scattering. The micelles were very stable with respect to temperature, showing minimal structural changes (a 5% reduction in core size and a somewhat swollen corona) upon heating from ambient temperature to 95 °C. (b) Brown, G. J.; Richards, R. W.; Heenan, R. K. *Polymer* **2001**, *42*, 7663–7673. Small-angle neutron scattering experiments studying aqueous self-assembly of PS-PEG (M_n = 8500 g mol^{-1}) with a PS weight fraction of 0.15 were found to assemble exclusively into spherical micelles. In contrast, PS-E/K-PEG has a similar PS weight fraction (0.11) and forms rod-like micelles.
41. Zhang, L. F.; Eisenberg, A. *Polym. Adv. Technol.* **1998**, *9*, 677–699.
42. Netz, R. R. *Europhys. Lett.* **1999**, *47*, 391–397.

APPENDICES

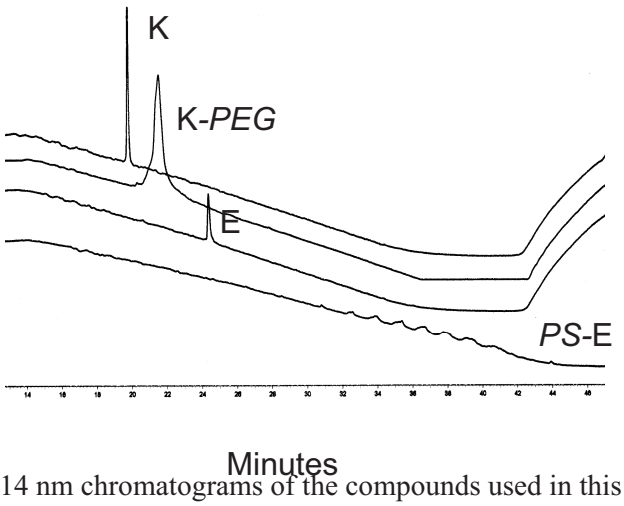
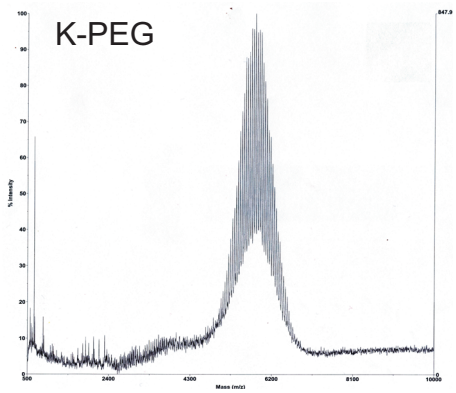


Figure A1. RP-HPLC 214 nm chromatograms of the compounds used in this study.
K, E, and K-PEG: 10% to 90% B over 25 minutes. PS-E: 10% to 100% B over 30 minutes.



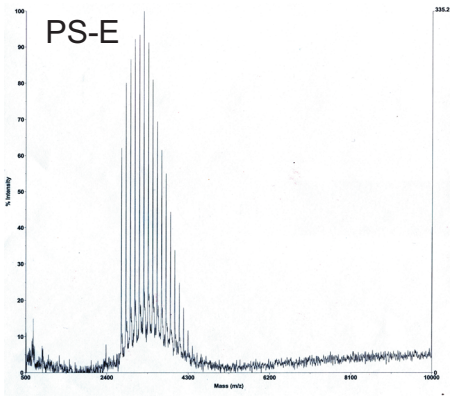
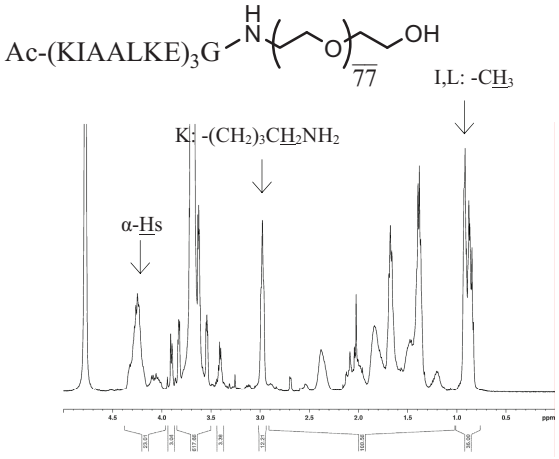


Figure A2. MALDI-TOF mass spectra of the compounds used in this study.

K-PEG



PS-E

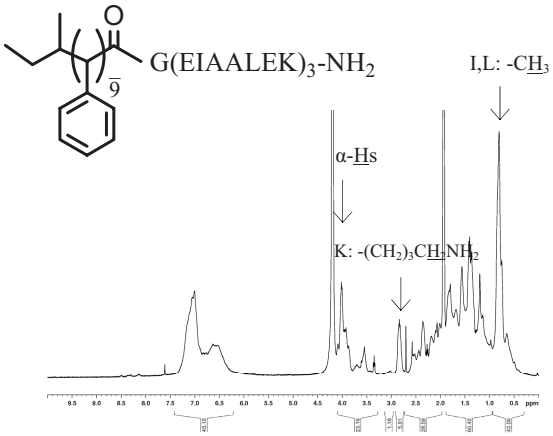


Figure A3. ^{1}H-NMR spectra

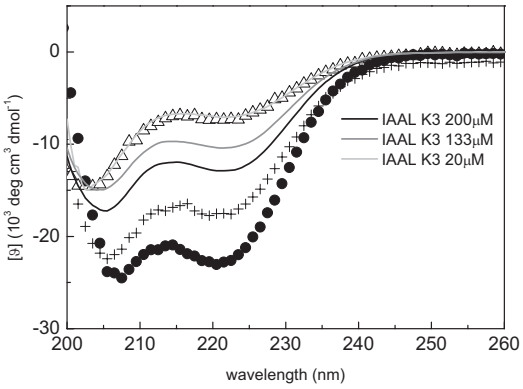


Figure A4. Comparison of K with IAAL K3. CD spectra of K (+), E (Δ), E/K (•) and IAAL K3 that was synthesized for this study (solid lines). [total peptide] = 200 μM unless otherwise stated, PBS, 25˚C.

The amino acid sequence of K was based upon, but is not identical to that of IAAL K3 (Litowski J. R.; Hodges, R. S. *J. Biol. Chem.* **2002**, 40, 37272-37279). K has a C-terminal glycine residue which was included as a spacer between the peptide and polymer in the hybrids. When IAAL K3 was synthesized for this study it had a similar helicity to that reported by Hodges and Litwoski (41% compared to 36%). Interestingly the amount of helicity of IAAL K3 increases with concentration.

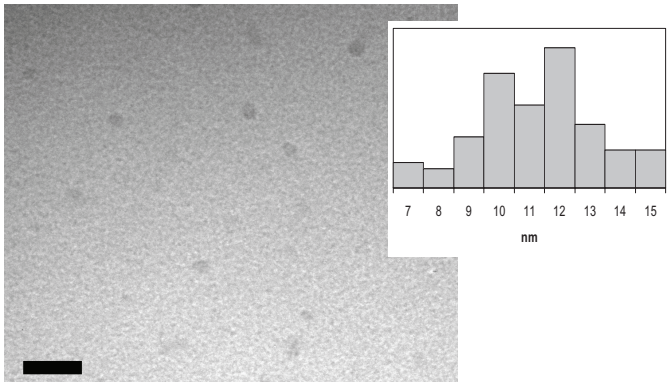


Figure A5. Cryogenic TEM of PS-PEG, with size distribution inset. Scale bar = 50nm. ([PS-PEG] = 440 μM, PBS, 25 °C.) 100 measurements.

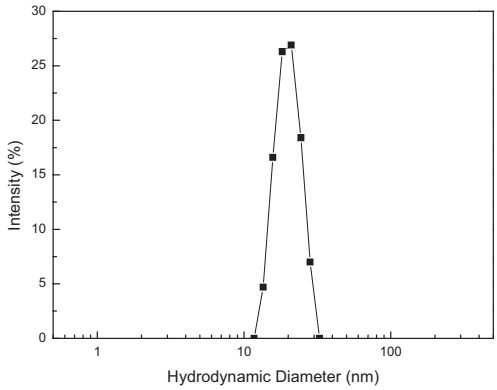


Figure A6. DLS intensity distribution of PS-PEG. ([PS-PEG] = 440 μM, PBS, 25 °C).

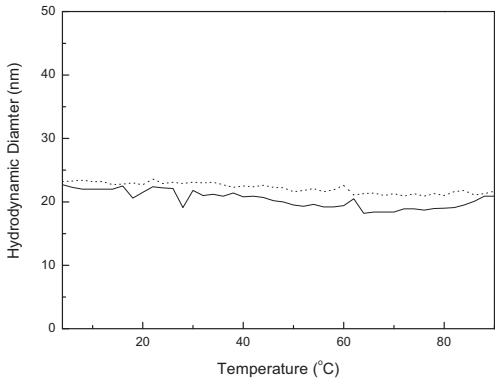


Figure A7. Temperature dependent DLS data for PS-PEG with heating (—) and cooling (····). ([PS-PEG] = 440 μM, PBS, 25 °C).

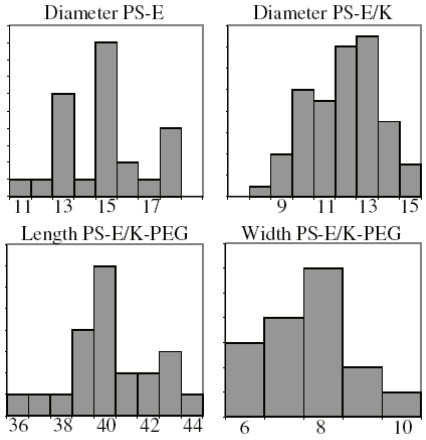


Figure A8. Size distribution of the diameters of PS-E (N=27) and PS-E/K (N=73), and distribution of the lengths (N=22) and widths (N=16) of the worm-like micelles of PS-E/K-PEG. The dimensions are given in nm.

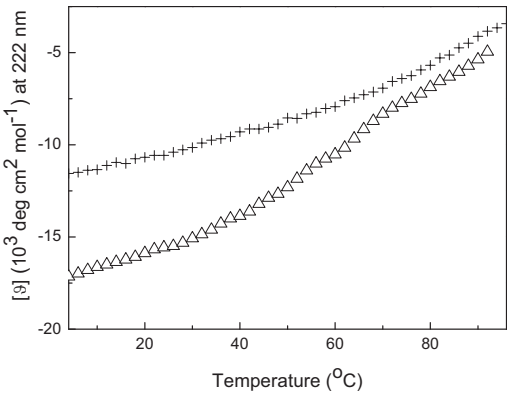


Figure A9. Temperature dependent ellipticity at 222 nm for PS-E (Δ) and PS-E/K (+) recorded at 222nm. ([Total Peptide] = 150-210 μM, PBS).

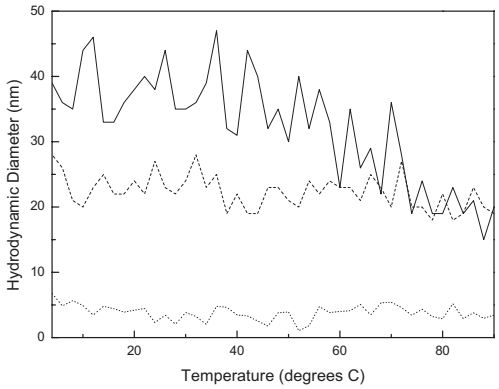


Figure A10. Temperature dependent DLS of PS-E/K-PEG with heating (—), PS-E/K-PEG with cooling (---), and PEG with heating (···). ([Total Peptide] ~ 200 μM, 50 mM PBS).

Theoretical Model

As observed by CD, at about 60 °C the PS-E/K-PEG complex dissociates into PS-E and K-PEG subunits that do not interact with each other. On the micellar scale, at elevated temperature, the rod-like PS-E/K-PEG micelles transform into PS-E spherical micelles suspended in the buffer solution with the K-PEG hybrid. When the solution temperature decreases E/K re-bond, but due to the reduction of solvent in the core and the increase of the surface tension between PS and buffer the PS blocks are no longer mobile and the transition from spherical morphology back to rod-like does not occur.

Being inspired by work of Netz (Netz, R. R. *Europhys. Lett.* **1999**, 47, 391-397.), calculations were made of the free energy of the equilibrium aggregates in the strong segregation limit (Bates, F.S.; Fredrickson, G.H. *Annu. Rev. Phys. Chem.* **1990**, 41, 525-57) when the Flory-Huggins interaction parameter χ has a large value corresponding to no mixing between the PS blocks and peptides/PEG. In this case, the interface between the PS domain and the buffer soluble macromolecules forms, and can be characterized by surface tension defined (Helfand, E.; Tagami, Y. *J Chem. Phys.* **1972**, 56, 3592-3601) as $\gamma=k_BT/a^2(\chi/6)^{1/2}$ where a is the Kuhn length of polystyrene. To simplify the model and to reduce it to the level of di-block copolymer, a few assumptions were made.

First, in all cases only neutral block copolymers are considered. For PS-E and PS-E/K complexes with charged E and K peptides, this assumption is justified by the high concentration of salt in the buffer which may strongly screen inter- and intramolecular electrostatic interactions of E and K peptides.

Second, it is assumed that the second virial coefficient and the statistical properties of E, E/K, and E/K-PEG complexes to be the same and as those of flexible chains. However, for PS-E/K-PEG micelles the neutral PEG block may have a different virial coefficient and conformational free energy compared to those of the peptides, due to the difference in rigidity of the blocks. Using this assumption the model predicts the dimensions of the rod-like and spherical micelles experimentally observed, however a more accurate description of PS-E/K-PEG structures requires treatment of this macromolecule as an ABC triblock copolymer with each block having different physical properties.

Third, with regards to the previous assumptions, the temperature annealing plays a role by reducing the hydrophilic block length (from E/K-PEG to E) and the size of corona in the case of the PS-E/K-PEG sample. The PS core becomes frozen when the temperature is lowered.

For the strong segregation limit, as it was mentioned by Bates and Fredrickson[3], the domain size can be estimated from the balance of the interfacial energy and the chain free energy. The free energy per chain in this case can be written:

$$\frac{F}{k_bT}=\frac{3}{2}\frac{R_s^2}{a_s^{\,2}N_s}+\frac{\upsilon_s f}{2}\frac{N_s^2}{V_s}+\frac{\gamma a_c^{\,3}dN_c}{k_bTR_c}$$

where the first term on the right hand side is the entropic contribution from the corona, the second term is the free energy of the short range interaction between monomers of the corona, and the last contribution comes from the interfacial energy. γ is the interfacial tension between the melt of hydrophobic blocks and the solvent and f is the aggregation number. R_s (s = E, E/K, E/K-PEG or PEG) is the size of the corona, R_c (c = PS) is the size of core, a denotes the Kuhn length, and N_s/N_c is the polymerization index of the corona/core block respectively. υ_s is the second virial coefficient of the hydrophilic block, and

$$V_s = fa^3 N_c \left[\left(\frac{R_s}{R_c} + 1 \right)^d - 1 \right]$$

is the volume of the corona, which depends on the dimension of the secondary structure: d = 1 (lamella), d = 2 (rod), d = 3 (sphere).

Following (Netz, R. R. *Europhys. Lett.* **1999**, 47, 391-397.), two limits are considered when the size of the corona is much larger than the size of core, $R_s/R_c >> 1$, or vice versa, $R_s/R_c << 1$. Under these limits functions can be solved to provide the sizes of the core and corona as well as the minimum free energy of the micellar structure. For the complexes containing PEG the limit of $R_s/R_c >> 1$ was used. Experimentally, for PS-E and PS-E/K complexes the size of the PS core is in the same order of magnitude as the peptide corona, $R_c \approx R_s$. For this reason the micellar properties of PS-E and PS-E/K at both limits are calculated.

After minimization of the free energy over the size of the corona, R_s, and further over the core size, R_c, the size of the core is obtained:

$$R_c = \begin{cases} c_1 \left(\dfrac{\gamma}{k_B T} \right)^{1/3} a_c a_s^{2/3} N_c^{1/3} N_s^{1/3} \left(\dfrac{2}{\upsilon_s} \left(\dfrac{\gamma}{k_B T} \right)^{2/3} a_c^5 a_s^{-2/3} N_c^{5/3} N_s^{-7/3} \right)^{\frac{2}{5}}, & R_s << R_c \\ c_d \left(\dfrac{\gamma}{k_B T} \right)^{1/3} a_c a_s^{2/3} N_c^{1/3} N_s^{1/3} \left(\dfrac{2}{\upsilon_s} \left(\dfrac{\gamma}{k_B T} \right)^{2/3} a_c^5 a_s^{-2/3} N_c^{5/3} N_s^{-7/3} \right)^{\frac{2}{2+3d}}, & R_s >> R_c \end{cases}$$

where c_d are the coefficients of the order of unity. The size of the corona is derived from the first derivation of the free energy with respect to the corona size.

$$R_s = \begin{cases} \left(\dfrac{1}{6} \dfrac{\upsilon_s N_s^3 a_s^2 R_c}{d a_c^3 N_c} \right)^{\frac{1}{3}}, & R_s << R_c \\ \left(\dfrac{d}{6} \dfrac{\upsilon_s N_s^3 a_s^2 R_c^d}{a_c^3 N_c} \right)^{\frac{1}{2+d}}, & R_s >> R_c \end{cases}$$

The minimal free energy of the aggregate becomes:

$$F/k_bT = \begin{cases} \left(\frac{5}{2}\right)3^{\frac{1}{5}}\left(\frac{\gamma}{k_BT}\right)^{2/3} a_c^2 a_s^{-2/3} N_c^{2/3} N_s^{-1/3} \left(\frac{2}{\upsilon_s}\left(\frac{\gamma}{k_BT}\right)^{2/3} a_c^5 a_s^{-2/3} N_c^{5/3} N_s^{-7/3}\right)^{-\frac{2}{5}}, & R_s << R_c \\ \left(1+\frac{3}{2}d\right)\left(\frac{d}{3}\right)^{-\frac{d}{2+3d}}\left(\frac{\gamma}{k_BT}\right)^{2/3} a_c^2 a_s^{-2/3} N_c^{2/3} N_s^{-1/3} \left(\frac{2}{\upsilon_s}\left(\frac{\gamma}{k_BT}\right)^{2/3} a_c^5 a_s^{-2/3} N_c^{5/3} N_s^{-7/3}\right)^{-\frac{2}{2+3d}}, & R_s >> R_c \end{cases}$$

In the limit of a small corona, $R_s << R_c$, the free energy does not depend on the symmetry of the aggregate: spheres, rods and lamellae have the same free energy. This phase is known as a degenerate phase where all morphologies can be observed at high polymer concentrations at the same time. However, at low polymer concentrations only spheres are formed.

For the opposite limit, $R_s >> R_c$, the rod-like structures are possible when:

$$0.008 < \frac{2}{\upsilon_s}\left(\frac{\gamma}{k_BT}\right)^{2/3} a_c^5 a_s^{-2/3} N_c^{5/3} N_s^{-7/3} < 0.038$$

estimated by equating free energies of different aggregates. PS-E/K-PEG falls within these values. This last equation shows that rods can be assembled by tuning the parameters of the hydrophobic/hydrophilic blocks as well as the interface tension and the interaction between chains within the corona. For PS-PEG, PS-E and PS-E/K the ratio between parameters falls out of the region of rod-like structures and only spherical micelles form.

The rod-like structure of the PS-E/K-PEG aggregates can be changed into spherical micelles by dissociation of the PS-E/K-PEG into PS-E and K-PEG (as observed experimentally at elevated temperature). Upon reassociation of K-PEG with the PS-E spherical micelles there is no transition back to rod-like micelles because the surface tension is too high.

To evaluate the dimensions of the experimentally observed self-assembled structures, the model presented above was used. The number of statistical Kuhn units (Nc, Ns) was chosen to match the model with experimental data and values given in the literature (each statistical unit is equivalent to two monomer units, i.e. two styrene or ethylene glycol units or several amino acids). The Kuhn length was taken to be 0.9-1.15 nm (PS), and 1.05-1.55 nm (PEG, peptides). These numbers are within the reported values for PS and PEG, which lie between 0.5 and 2 nm. The second virial coefficient is unknown for peptides, but the values were chosen to be close to the volume of the monomer. To calculate the interfacial tension for the strong segregation limit, χ = 140. The results of these calculations are presented in the Table A1.

Table A1. Parameters of the molecules, and properties of the micelles that they form as predicted by the model.

Polymer	Limit	a_c [nm]	a_s [nm]	N_c	N_s	V_s [nm^3]	D_c [PS] [nm]	R_s [pept+PEG] [nm]	D [nm]	Morph
PS-E	$R_s >> R_c$	0.9	1.35	4	4	25.70	3.86	4.86	13.6	spheres
PS-E	$R_s << R_c$	0.9	1.35	4	4	0.12	12.34	1.57	15.5	spheres
PS-E/K	$R_s >> R_c$	0.9	1.15	4	4	15.9	3.74	4.47	12.7	spheres
PS-E/K	$R_s << R_c$	0.9	1.35	4	4	0.12	10.54	1.54	13.6	spheres
PS-E/K-PEG	$R_s >> R_c$	0.95	1.05	4	45	0.043	4.20	6.57	17.3	rods
PS-E/K-PEG[1]	$R_s >> R_c$	0.9	1.15	4	45	0.120	3.74	6.97	17.7	spheres
PS-PEG	$R_s >> R_c$	0.95	1.05	5	40	0.850	6.01	7.18	20.4	spheres

The results represented in the Table agree with the experimental findings (Table 3, main text). Although, the model does not take into account the morphology of peptides, it can predict the dimensions of micelles using estimates of the statistical parameters of molecules. The model explains the decrease in size of spherical PS-E micelles when E/K complexation occurs by the decrease of the peptide's rigidity and the decrease in the second virial coefficient (for the $R_s << R_c$ limit). For the opposite limit $R_s >> R_c$ the dimension of spherical micelles is very similar. For rod-like micelles, the end-capping energy should be included in the model, as this may play an important role for short rods close to the transition boundaries. The segregation between peptides and PEG blocks may be considered in more complicated models for the tri-block copolymers where the rigidity of peptides and their structure are known. [1]After annealing PS-E/K-PEG spherical micelles are no longer in equilibrium.

UNITING POLYPEPTIDES WITH SEQUENCE-DESIGNED PEPTIDES: SYNTHESIS AND SELF-ASSEMBLY OF POLY(γ-BENZYL L-GLUTAMATE)-*b*-COILED-COIL PEPTIDE COPOLYMERS

A novel class of amphiphilic block copolymers has been synthesized, in which for the first time an N-carboxyanhydride (NCA) polymerization is initiated from a designed peptide. In this series of amphiphiles the hydrophobic block is poly(γ-benzyl L-glutamate) (PBLG), and the hydrophilic block is a coiled-coil forming peptide (denoted E). The synthetic approach was to synthesize the coiled-coil forming peptide on the solid phase, followed by NCA polymerization of γ-benzyl L-glutamate initiated from the N-terminal amine of the peptide on the solid support. The polypeptide-*b*-peptide was then cleaved from the resin, requiring no further purification. Peptide E contains 22 amino acids, while the average length of the PBLG block ranged from 36-250 residues. This synthetic approach was applied to create a modular system, in which the different PBLG block lengths are able to be connected noncovalently with various hydrophilic blocks via the specific coiled-coil folding of E with K or K-poly(ethylene glycol), where K is a peptide of complementary amino acid sequence to E. In this way nanostructures could be formed in water at neutral pH over the entire compositional range, which has not been demonstrated previously with such large PBLG blocks. It was found that the size, morphology (polymersomes or bicelles), and surface functionality could be specified by combining the appropriate modular building blocks. The self-assembled structures were characterized by means of dynamic light scattering, circular dichroism, scanning electron microscopy, cryogenic-transmission electron microscopy, fluorescence spectroscopy, and zeta-potential measurements. Finally, as the polymersomes are able to encapsulate water soluble compounds, and the surface of the polymersomes is easily functionalized via the coiled-coil binding, it is expected that these peptide-based polymersomes will be able to act as delivery vehicles to specific targets in the body.

INTRODUCTION

For materials scientists polypeptides are a fertile area for investigation as they can be programmed with the ability to adopt specific intra- and intermolecular conformations, which may allow heightened levels of control over the morphologies and properties of the self-assembled structures. The structure and functional properties of proteins and peptides are determined by their primary sequence of amino acids. Materials scientists are still unable to design the complex structures found in nature. Yet there has been some progress, particularly in understanding the folding of silks, elastins, collagens, and coiled-coil motifs.[1]

Two methods for the synthesis of peptides are the ring-opening polymerization (ROP) of amino acid *N*-carboxyanhydrides (NCAs), and solid-phase synthesis. The ROP of NCAs is the most common method of synthesizing polypeptides containing a single amino acid residue.[2] The polymers can be readily prepared, and have no detectable racemization at the chiral centers.[3] Blocks based on glutamic acid (γ-benzyl L-glutamate) have been commonly synthesized as their polymerization is known to be the best controlled, and because they form well-defined rod-like α-helical secondary structures both in the solid-state and solution.[4] They have been initiated from traditional linear coil polymers,[5] polymer dendrimers,[6,7] modified lipids,[8] and polypeptides themselves synthesized by the ROP of NCAs.[9] Most commonly initiators with primary amine end-groups are used,[3] although the polymerization can also be initiated with transition metal-amine functionalized polymers.[10] Block copolymers have also been synthesized in the reverse manner, i.e. the ROP of NCA, followed by polymerization of another monomer from the polypeptide.[11,12] The ROP of NCAs has the disadvantage of multiple side-reactions and termination reactions, resulting in polypeptides with a wide range of polymer lengths. To reduce the range of lengths, which are likely to have different self-assembly properties, fractionation is often applied.[3] Additionally the abundance of side-reactions leads to contamination with homopolymers, which has to be separated from the desired block copolymers.[3]

There have been many studies of PBLG containing block copolymers in organic solution, but due to the hydrophobicity of PBLG blocks, there have only been limited reports of PBLG block copolymers in aqueous solution. Spherical,[13-15] cylindrical,[14] and whisker-like[16] micelles, solid spheres,[17] and vesicles[18,19] have been observed in aqueous solution from block copolymers which incorporate a PBLG block.

Using solid-phase synthesis protocols, peptides are designed with an exact molecular weight and specific amino acid sequence, which can result in a well defined shape and functionality. Importantly, the functionality can be more complex compared to NCA-based peptides, hence they are very interesting for incorporation into block-copolymers. The class of coiled-coil forming peptides, for which the design rules for the sequence-to-structure relationships are relatively well understood,[20] are accessible by solid-phase synthesis, and are of specific interest.

Coiled-coil forming peptides are strongly complementary in spatial packing and inter-peptide electrostatic interactions and form highly specific noncovalent complexes in aqueous solution. By designing the amino acid sequence appropriately many aspects of coiled-coil binding can be specified, such as the oligomerization state, complex size, orientation of binding, homo- or heterobinding, and stability. In Chapters 2 and 3 the coiled-coil peptide pair E and K were shown to form stable parallel heterodimers.[21,22] E and K fold to form amphipathic α-helices, and when E and K are mixed the driving force for the dimer structure is the shielding of the hydrophobic faces of the α-helices from the aqueous solution. The specificity of the complex is determined by the electrostatic interactions between the charged side chains of lysine and glutamic acid residues bordering the hydrophobic core. This renders the heterodimers energetically favorable and homodimers energetically unfavorable. The E/K heterodimer has been shown to retain the specific coiled-coil binding upon conjugation of macromolecules to E and/or K.[21-23]

In this Chapter, the combination of solid-phase synthesis with ROP to build up polypeptide-*b*-peptides is demonstrated for the first time. This new synthetic approach gives access to peptides that are not possible to synthesize using only solid-phase synthesis or only ROP. The large size range of polypeptides can be united with the complex functionality of sequence-specific peptides, leading to peptides with an increased range of potential properties.

The potential of this novel combination of peptide classes is demonstrated by the creation of a modular system with which one can mix-and-match hydrophobic and hydrophilic peptide blocks, with resultant control over the size, morphology, and surface functionality of the structures that self-assemble in aqueous solution.

In the polypeptide-*b*-peptides presented here one block is composed of hydrophobic PBLG, and the other block is composed of the hydrophilic coiled-coil forming designed peptide E (Table 1). The block copolymers are made by a two step process. Initially peptide E was synthesized using solid-phase synthesis protocols. While still anchored to the resin the amine terminus was used to initiate the ROP of γ-benzyl L-glutamate N-carboxyanhydride. This gives access to polypeptide-*b*-peptides with well-defined block sizes and functionalities. Additionally, it overcomes one of the main disadvantages of NCA polymerization, as any PBLG homopolymer that is formed as a side product can be readily washed away from the resin. PBLG-E block copolymers were synthesized with a range of hydrophobic block lengths, and cleaved from the resin, requiring no further purification.

Peptide E was chosen as the sequence-specific block because it folds into a stable coiled-coil dimer with peptide, K, due to their amino acid sequence designs, and the E/K pair was shown in the previous chapter to retain its coiled-coil binding upon conjugation of macromolecules to E and/or K. In Chapter 2 a short polystyrene chain with an average length of 9 monomers is coupled to the N-terminus of peptide E (denoted PS-E). PS-E forms spherical micelles in aqueous solution, and via coiled-coil folding with peptide K or K-poly(ethylene glycol)$_{77}$ the corona can be altered, resulting in larger spherical micelles,

or rod-like micelles. Furthermore, the E/K complex was shown to reversibly dissociate upon raising the temperature, again leading to a change in the self-assembled structures. Thus, by utilizing a coiled-coil forming peptide as the hydrophilic block of a block copolymer one can obtain a high degree of control over the hydrophilic block/s, and hence the nanostructures that form. However, the self-assembly of amphiphilic block copolymers depends not only on the corona chains, but also to a large extent on the hydrophobic blocks. As of yet, the conjugation of a range of hydrophobic block lengths to designed peptides has not been demonstrated. By combining polypeptides with sequence-designed peptides as presented here, we are able to create a modular system in which the hydrophobic PBLG length is readily controlled by ROP, and the hydrophilic block/s are readily controlled by coiled-coil folding (Figure 1), allowing one to piece together different components to access a range of self-assembled structures.

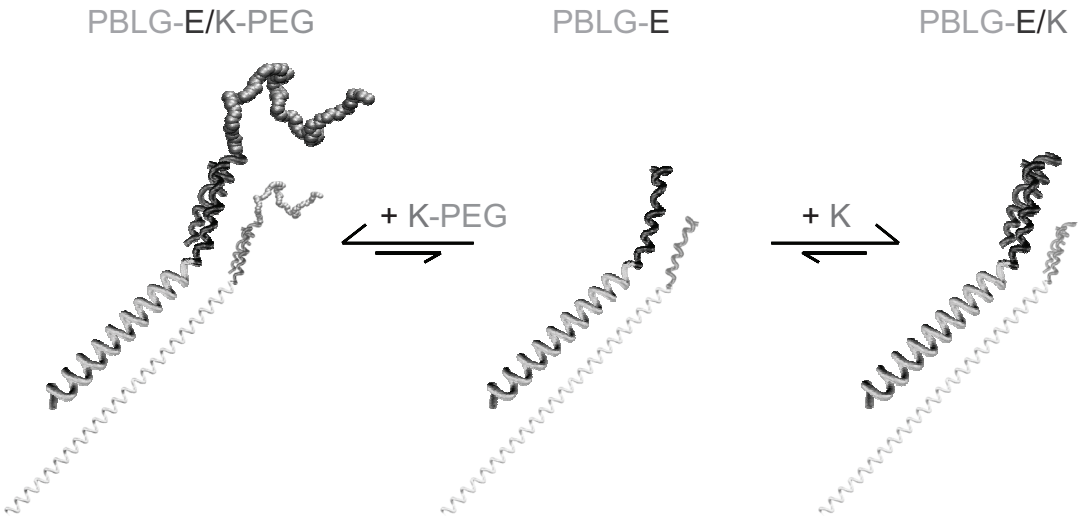


Figure 1. Schematic representation of a selection of the noncovalent amphiphiles obtained via the coiled-coil interaction between the building blocks.

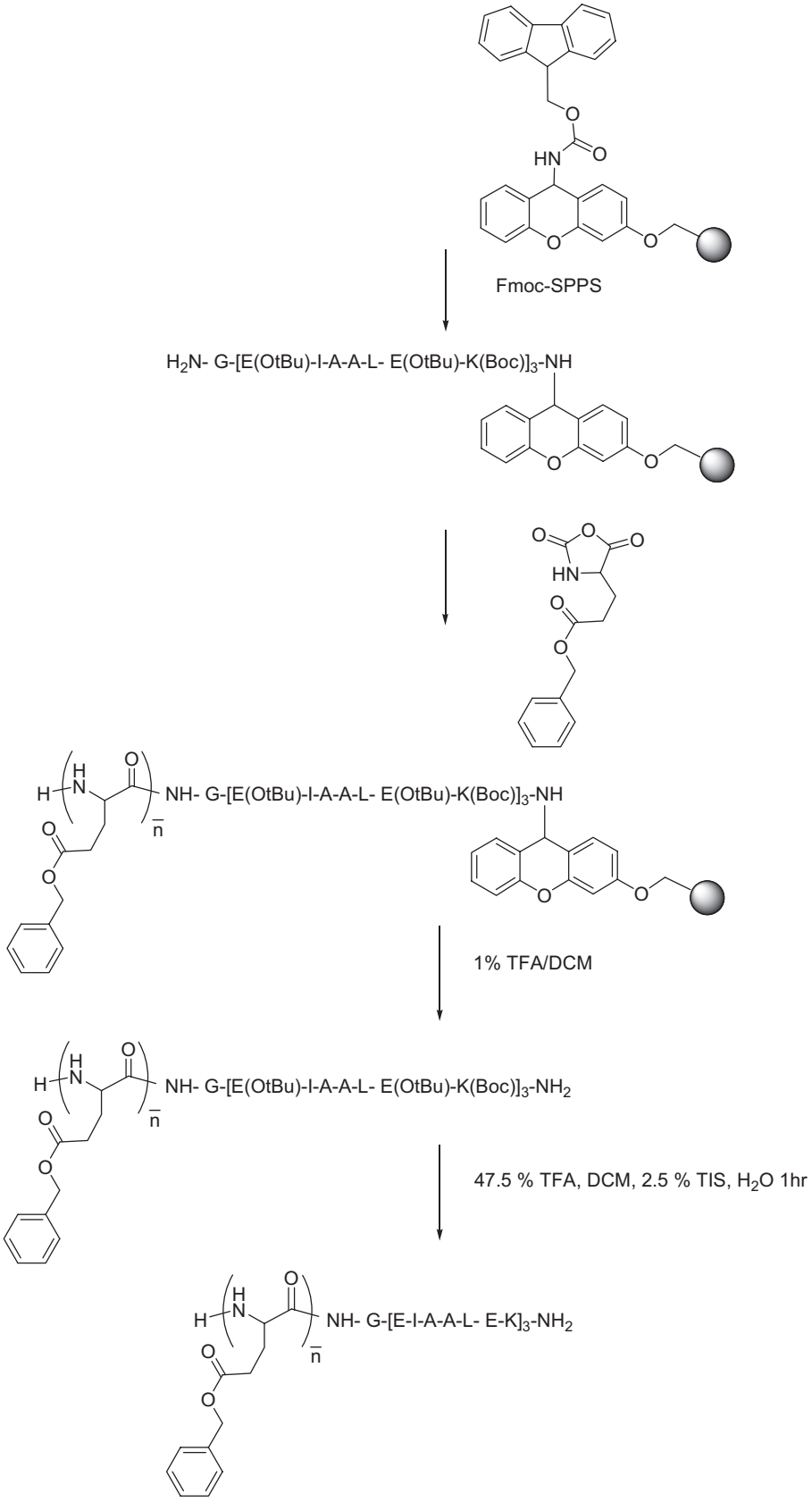
RESULTS AND DISCUSSION

Synthesis and Characterization of the protected PBLG-E block copolymer series

Poly(α-amino acid)s can be prepared by the ROP of NCAs starting from nucleophilic attack of the C_5 carbonyl group of the NCA by an initiator such as amines, alkoxide anions, alcohols, transitions metals, and water.[24] In the current approach to synthesize polypeptide-*b*-peptides, the coiled-coil peptide block E is first synthesized on a Sieber amide resin using standard Fmoc solid-phase peptide protocols, and the N-terminal Fmoc group is removed. ROP of the BLG-NCA is then initiated by the deprotected N-terminal amine of peptide E while still anchored to the resin (Scheme 1). The polymerization was conducted by shaking the resin-bound peptide with the NCA in DCM at room temperature under an argon atmosphere for one to three days. When all the BLG-NCA monomer was consumed, the resin was drained and washed thoroughly with DCM, NMP, and DMF. Typically 8% of the NCA monomer formed short oligomers during the polymerization reaction, due to trace amounts of water. These impurities were easily removed from the desired product by extensive washing of the resin.

The protected polypeptide-*b*-peptides were released from the solid support by shaking 10 times (2 minutes each) in 99:1 (v/v) DCM:TFA, with subsequent precipitation in cold methanol. The purity of each fraction was ascertained with GPC, from which it was found that within each synthesis the longer PBLG-E polypeptide-*b*-peptides were cleaved first from the resin, with a progressive shortening of the PBLG chain with each fraction collected, until finally peptide fragments from the solid-phase peptide synthesis of E were cleaved. In this way polypeptide-*b*-peptides with a lower polydispersity index (PDI) can be obtained by selecting which fractions to combine. Due to the washing away of homo-PBLG while the block copolymer is still attached to the resin, and the cleavage of peptide fragments from the resin only after the bulk of PBLG-E molecules have been cleaved, no further purification was necessary. The GPC chromatographs of the PBLG-E series are shown in Figure 2. Peaks are monomodal and the PDIs range from 1.1 for the hybrid with the shortest PBLG block to 1.7 for the hybrid with the longest PBLG block.

Scheme 1. Synthesis of PBLG-E by solid-phase peptide synthesis followed by N-carboxyanhydride ring-opening polymerization initiated from the N-terminal amine of the resin-bound peptide.



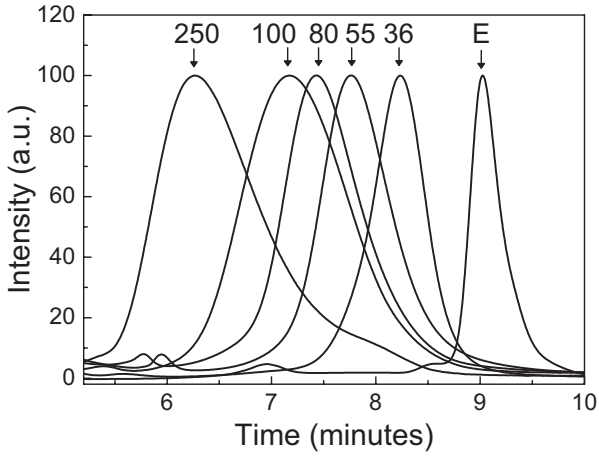


Figure 2. GPC chromatographs of the coiled-coil forming peptide E (not purified), and PBLG-E polypeptide-*b*-peptides in the protected form. The numbers above each trace refer to the degree of polymerization of the PBLG block.

Synthesis and Characterization of the PBLG-E block copolymer series

The protecting groups from the glutamic acid and lysine residues of peptide E were selectively removed using a mixture of TFA, DCM, water, and TIS, while retaining the benzyl protecting groups of the PBLG block, and the amphiphilic polypeptide-*b*-peptide was precipitated in cold methanol. The complete removal of the protecting groups was confirmed by the disappearance of the peak from the methyl groups of the OtBu and Boc moieties at 1.5 ppm from ^{1}H NMR spectra. To determine the degree of polymerization and M_n of the PBLG blocks, spectra were obtained for each compound in deuterated dichloromethane with increasing amounts of trifluoroacetic acid, ensuring the absence of aggregation of the amphiphilic block copolymer and hence that accurate peak comparisons between E and PBLG blocks could be made.[25-27] The peak arising from the leucine and isoleucine methyl protons of the E block was compared to the peak arising from the benzyl protons of the PBLG block (Figure 3). The degree of polymerization of the PBLG blocks determined using ^{1}H NMR spectroscopy matched the data obtained by GPC, indicating that the polystyrene standards used for GPC molecular weight comparison are reliable for these hybrids. The molecular characteristics of the compounds used in this study are shown in Table 1. The hydrophilic peptide E has 22 amino acid residues, while the hydrophobic PBLG block ranges from 36 to 250 benzyl glutamate residues.[28]

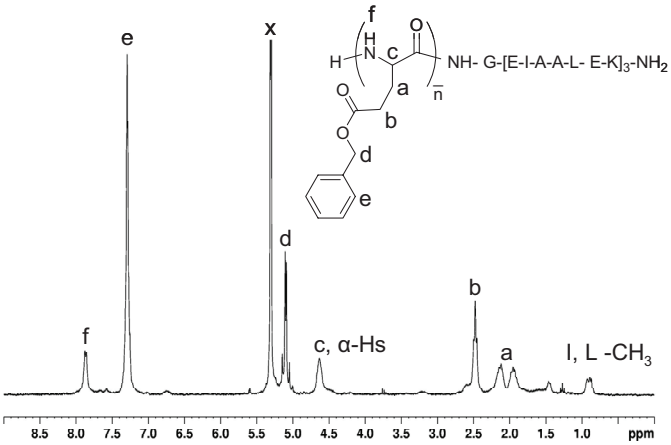


Figure 3. ^{1}H-NMR spectrum of $PBLG_{36}$-E in 7:3 (v/v) DCM-d_3:TFA with the proton assignments. X is from DCM.

Table 1. Molecular Characteristics of the Compounds used in this Study

Name	Structure	Yield (%)	M_n (g/mol)	PDI[3]
K	Ac-(K I A A L K E)$_3$G-NH_2	~ 40	2378.0[1]	
E	Ac-G(E I A A L E K)$_3$-NH_2	~ 40	2380.6[1]	
PEG-K	Ac-(K I A A L K E)$_3$G-PEG_{77}	~ 10	5832[1,2]	1.05[1]
$PBLG_{36}$-E	$PBLG_{36}$-G(E I A A L E K)$_3$-NH_2	28	10230[2,3]	1.1
$PBLG_{55}$-E	$PBLG_{55}$-G(E I A A L E K)$_3$-NH_2	30	14396[2,3]	1.3
$PBLG_{80}$-E	$PBLG_{80}$-G(E I A A L E K)$_3$-NH_2	56	19877[2,3]	1.4
$PBLG_{100}$-E	$PBLG_{100}$-G(E I A A L E K)$_3$-NH_2	69	24262[2,3]	1.4
$PBLG_{250}$-E	$PBLG_{250}$-G(E I A A L E K)$_3$-NH_2	74	57148[2,3]	1.7

[1] Obtained from MALDI-TOF MS. [2] Based on a comparison of ^{1}H-NMR peaks. [3] GPC calibrated with polystyrene standards. PEG: poly(ethylene glycol), PBLG: poly(γ-benzyl L-glutamate), amino acids in the designed peptides are represented by their one letter codes, Ac: acetyl.

Self-Assembling Properties of the Polypeptide-b-Peptides and Polymer Mixtures in Aqueous Solution

The synthesis and self-assembly of rod-rod block copolymers is an emerging topic in polymer chemistry, and the well-defined shapes of rod polymers leads to novel self-assembly properties. PBLG is hydrophobic and with a degree of polymerization (n) larger than 10 has an α-helical secondary structure,[29] resulting in a rod-like molecular shape. The length of PBLG α-helices is n x 1.5 nm[30] while the diameter is ~ 2 nm,[31] hence in the α-helical configuration the PBLG rod-like blocks in this study range in average length from 5.4 to 37.5 nm long. The peptide E was chosen as the hydrophilic block because it forms an α-helical coiled-coil dimer with K, a peptide with a complementary amino acid sequence (see Chapters 2 and 3). E/K is one of the shortest pairs of coiled-coil forming peptides that specifically forms heterodimers. E and K form complexes with a well defined rod-like geometry of cylinders 3.5 nm long with approximately the same diameter

as PBLG rods.[33] Poly(ethylene glycol) is a hydrophilic coil polymer, and the PEG used in this study, with an average of 77 monomers, has an average diameter of approximately 5 nm,[34] although it is more compact when attached to peptide K.[21] The peptides K and the hybrid K-PEG are predominantly hydrophilic and do not aggregate in aqueous solutions.[35] Due to the amphiphilic nature of the rod-rod PBLG-E polypeptide-*b*-peptides and the noncovalent complexes PBLG-E/K and PBLG-E/K-PEG, it was expected that the PBLG and hydrophilic blocks would phase separate in aqueous solution. The self-assembling characteristics of the PBLG-E series, both in isolation and with equimolar amounts of K or K-PEG were studied in phosphate buffered saline solution (PBS) at pH 7.0. The PBLG-E polypeptide-*b*-peptides, having large hydrophobic PBLG blocks, were not soluble in aqueous solutions. The standard methods for inducing self-assembly,[36] namely film hydration, or solvent injection followed by dialysis were ineffective as the PBLG-E block copolymers precipitated. Better results were achieved by injecting PBS into a tetrahydrofuran (THF) solution of the polymer with sonication. PBS is selective for the hydrophilic E, E/K, and E/K-PEG blocks and induces aggregation of the PBLG blocks. The initial ratio of THF to PBS was such that the E/K coiled coil is stable (Figure A1), and the THF was subsequently removed by continuous sonication for two hours in an open vessel. An example of circular dichroism spectra of the polymers and polymer mixtures is given in the Appendices (Figure A2).

Particle Sizes

The aggregation of the individual polypeptide-*b*-peptides (PBLG-E) was investigated with dynamic light scattering (DLS), as well as with the equimolar addition of the complementary peptide K or K-PEG. It was found that when the PBLG block length was 80 monomers or shorter the pure PBLG-E polypeptide-*b*-peptides had a suitable balance of hydrophobicity and hydrophilicity to form ordered supramolecular structures in aqueous solution. For $PLBG_{100}$-E, complexation with K resulted in a noncovalent block copolymer with a corona sufficient to form ordered structures. The amphiphilic block copolymer with the longest hydrophobic block, $PBLG_{250}$-E, required association with K-PEG in order to have a large enough corona to aggregate in an ordered manner. The average hydrodynamic diameter of the structures that self-assembled from the polymers and polymer mixtures ranged from 100 nm to 400 nm, and were significantly larger than the calculated sizes of spherical micelles. All size distributions were monomodal and the polydispersity index (PDI) of the samples was 0.35 or less.

As shown in Figure 4, increasing the PBLG block length resulted in larger aggregates. Additionally, for a particular PBLG block length, increasing the size of the head-group (going from E to E/K and E/K-PEG) leads to a smaller hydrodynamic diameter of the particles. These trends can both be explained by classical packing parameter considerations: the larger the head-group is in comparison to the hydrophobic PBLG, the greater is the curvature of the aggregate surface, and hence the particle size decreases.[37] The packing parameter was originally designed to predict the morphology and size of

nanostructures formed from lipids, and this approach is not always suited to block copolymers because it does not take into account the complexity of the interfacial energy and interaction free-energies of the blocks.[21] That being said, it is sufficient to explain the trends observed in the assembly of this system. This may be because in the case of both lipid structures and structures formed from the PLBG-E series the influence of stretching of the hydrophobic chains is minimal (lipid tails are stretched,[38] and the PBLG rods have a very well defined structure and size with no change in configuration expected upon aggregation[39]), hence the role of deformation of the core block on the free-energy of the structure is reduced.

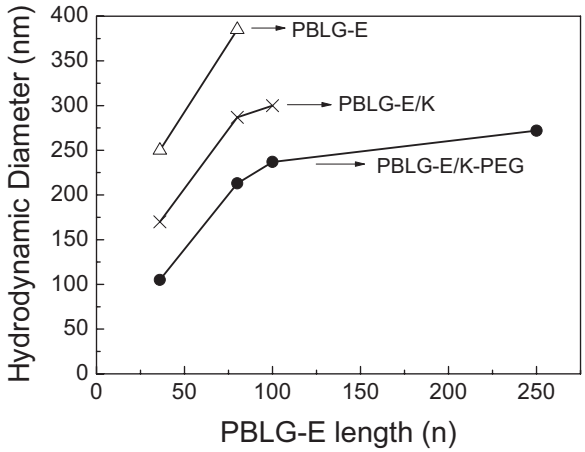


Figure 4. Typical hydrodynamic diameters of the self-assembled structures formed by the polypeptide-*b*-peptides and noncovalent complexes. ([Total Peptide] = 50 μM, PBS, 25 °C).

Particle Morphology

Information about the morphology of the supramolecular structures that formed was obtained by electron microscopy. The effects of PBLG chain length and the relative size of the corona on the ability of the molecules to controllably self-assemble as observed by scanning electron microscopy (SEM) were consistent with the DLS observations (Figure 5). Combining the shortest PBLG length with an E or E/K hydrophilic block results in spherical objects assembling in PBS, which collapse when dried (Figure 5A, B). $PBLG_{36}$-E/K-PEG has the same hydrophobic block length, but forms smaller structures, as explained in the DLS section, which are stable upon drying. This sample also contained disk-like aggregates, *vide infra*. To obtain further insight into the internal structure of the assemblies cryo-TEM studies were performed for a selection of the self-assembled structures (Figure 6). The shortest hybrid, $PBLG_{36}$-E, has a low PDI of 1.1, and self-assembles into vesicles with rather uniform membrane thicknesses, that seem to be independent of the vesicle diameter. The thicknesses observed increase slightly with increasing size of the hydrophilic block/s: 17.2 $\pm$ 2.6 nm for $PBLG_{36}$-E, 18.5 $\pm$ 2.4 nm for $PBLG_{36}$-E/K, and 21.5 $\pm$ 2.2 nm for $PBLG_{36}$-E/K-PEG (Figure 6A, B, C). The observed membrane thicknesses are in remarkably close accordance with the calculated bilayer

thicknesses, as seen in Table 2. These results show that the rigid hydrophobic PBLG rods are able to assemble into very well-defined bilayers through coupling to the water soluble peptide rods. In contrast to other block copolymer vesicles,[40] there does not appear to be any interdigitation of the two layers of the hydrophobic block, presumably due to the rod-like structure of the PBLG and the comparable diameter of the tail and corona rods.

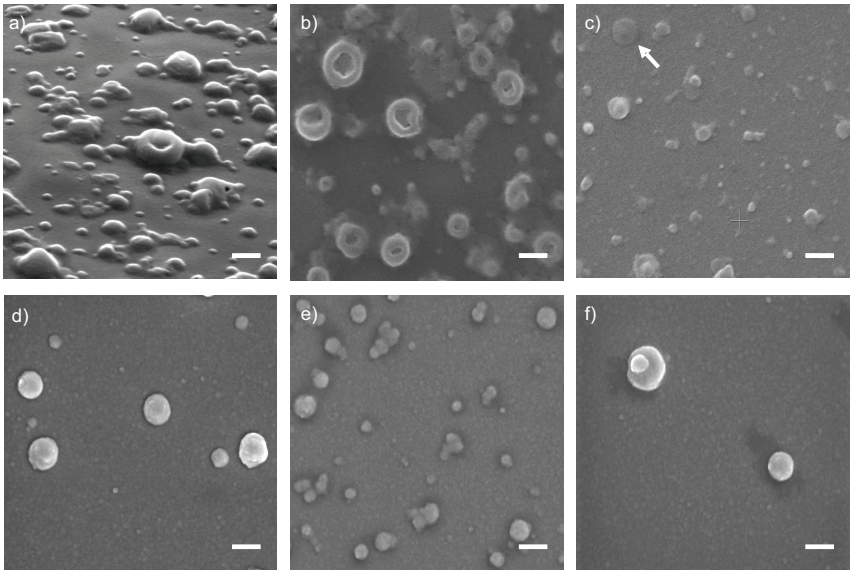


Figure 5. SEM images of the particles formed from (a) $PBLG_{36}$-E, (b) $PBLG_{36}$-E/K, (c) $PBLG_{36}$-E/K-PEG, (d) $PBLG_{100}$-E/K, (e) $PBLG_{100}$-E/K-PEG, (f) $PBLG_{250}$-E/K-PEG. Scale bars = 200 nm. ([Total Peptide] = 50 μM, PBS, 25 °C).

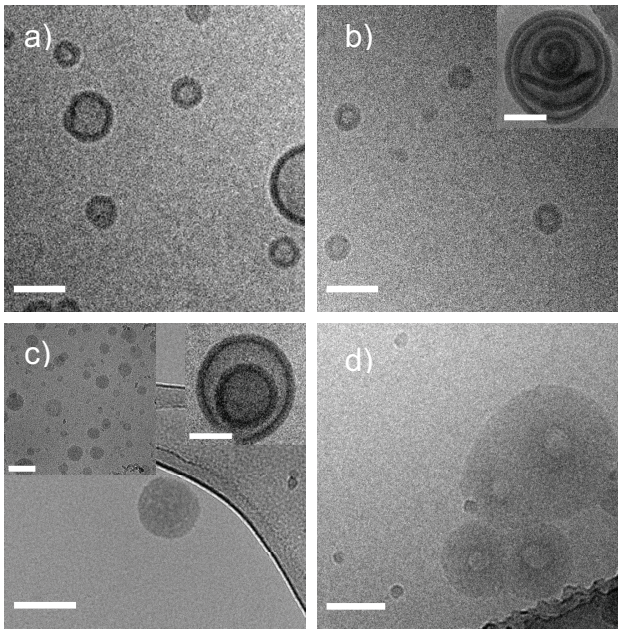


Figure 6. Cryo-TEM images of $PBLG_{36}$E (a), $PBLG_{36}$E/K (b), $PBLG_{36}$E/K-PEG (c), and $PBLG_{100}$E/K-PEG (d). Scale bars = 100 nm. ([Total Peptide] = ~ 1500 μM, PBS).

Table 2. Experimental and theoretical membrane thicknesses of the vesicles.

Sample	Membrane thickness	
	experimental (nm)[a]	theoretical (nm)[b]
$PBLG_{36}$-E	17.2 ± 2.6 nm	18
$PBLG_{36}$-E/K	18.5 ± 2.4 nm	18
$PBLG_{36}$-E/K-PEG	21.5 ± 2.2 nm	24
$PBLG_{100}$-E/K-PEG	68 ± 22 nm	42

[a] Determined by cryo-TEM. [b] PBLG length: n x 1.5 nm,[90] E and E/K length 3.5 nm,[27] PEG length: ~ 3 nm.[30]

In addition to polymersomes, disks of uniform height and density were observed in the SEM and cryo-TEM images of $PBLG_{36}$E/K-PEG (arrows, Figure 5C and Figure 6C). This is the sample with the shortest PBLG block and the longest hydrophilic component in comparison to the PBLG block. Presumably polymeric bicelles are observed only for this noncovalent block-copolymer because the length of the PBLG block is short enough that the hydrophilic blocks are able to fold over any exposed PBLG on the sides of the discs, shielding it from the aqueous buffer.[41] This eliminates the energetic need for the bilayers to close the hydrophobic sides by curving to form vesicles. This possibility was tested with computer modeling, which confirmed that PEG is able to cover the average length of the extended α-helical PBLG block without any chain stretching, i.e. while still in the random coil configuration (Figure 7). A theoretical study has found that for rod-coil block copolymers the only stable micellar form has disk-like cores and relatively large corona thicknesses. The disk-like core reduces the core-corona interfacial free energy of the rod blocks, as in this geometry the rods pack well together, and only large coil blocks can deform enough to balance the interfacial free energy.[39]

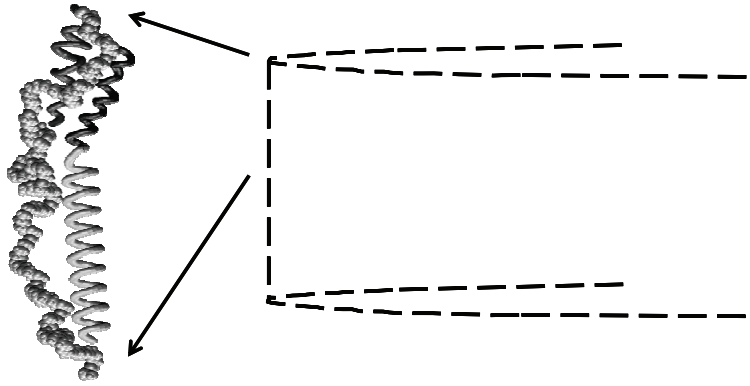


Figure 7. The space filling model of the $PBLG_{36}$-E/K-PEG complex illustrates that without chain stretching PEG readily extends the length of the coiled-coil peptides and the PBLG block. The E/K dimer structure is based on the work of Litowski and Hodges,[33] the PBLG adopts and α-helix, and the PEG has a random coil conformation. The $PBLG_{36}$-E/K-PEG model was built with Molden version 4.6,[42] and the image generated with VMD version 1.8.6.[43]

For the polypeptide-*b*-peptides and noncovalent complexes with longer PBLG lengths the SEM images exclusively show spherical objects that withstand the drying process (Figure 5D, E, F). Cryo-TEM was also conducted on the structures assembled from the complex $PBLG_{100}$-E/K-PEG. As seen in Figure 6D the spherical particles were observed to contain aqueous interiors, and have very bulky membranes of variable thickness (≈ 68 $\pm$ 22 nm). The range of membrane thicknesses likely arises from the polydispersity of molecular lengths in this sample. GPC of the protected polypeptide-*b*-peptide yielded a PDI of 1.4, and it was estimated that 95% of the $PBLG_{100}$-E lengths are between 9 nm and 80 nm when in the α-helical conformation.

An advantage of polymersomes over liposomes is that their membrane thickness varies depending on the composition, molecular weight, and degree of stretching of the blocks. The hydrophobic core of lipid bilayers is always approximately 3-4 nm thick, regardless of the lipid composition,[44] while the membrane thickness of polymersomes ranges from 3-5 nm[45] to 200 nm (in 1:1 v/v TFA/DCM).[46] In the present series the nature of the membrane can be dictated by the choice of hydrophobic and hydrophilic components, and the thickness of the membrane of $PBLG_{100}$-E/K-PEG vesicles is the largest reported for polymersomes in aqueous solutions.

Encapsulation

To demonstrate the ability of the supramolecular structures to encapsulate water soluble compounds, samples were prepared in the presence of the water soluble fluorescent dye rhodamine B. Following sonication the unencapsulated rhodamine B was removed by FPLC. The samples for which DLS indicated ordered structures (monomodal intensity distributions and PDI < 0.35) exhibited rhodamine B fluorescence (Figure A3), confirming that the polypeptide-*b*-peptides and noncovalent complexes had a suitable balance of the hydrophilic block size to the hydrophobic PBLG block to lead to controlled assembly, and that these self-assembled structures had aqueous interiors, i.e. were vesicles. As expected, the samples that did not show well defined assembly by DLS ($PBLG_{100}$-E, $PBLG_{250}$-E, and $PBLG_{250}$-E/K) contained insignificant amounts of rhodamine B, as verified by fluorescence spectroscopy (Figure A3). The hydrodynamic diameter of the nanocapsules did not change for at least 10 – 20 months at 4 °C as determined by DLS, showing the extensive stability of the samples.[47] As well as the particle size and morphology, the surface functionality was also retained over the same measurement period, with PBLG-E samples (having a net charge per molecule of -3) displaying a negative zeta potential, and PBLG-E/K and PBLG-E/K-PEG samples (with no net charge per complex) having zeta potentials closer to zero (Table A1).

CONCLUSIONS

A new class of peptides, polypeptide-*b*-peptides, has been synthesized by a straightforward synthetic approach. The ROP polymerization of an amino acid NCA is initiated from the N-terminal amine of a sequence specific peptide while still on the solid support. The concept is demonstrated by the solid-supported polymerization of γ-benzyl L-glutamate NCA from the coiled-coil forming peptide E, which was synthesized using standard solid-phase peptide synthesis protocols. Cleavage of the diblock from the resin and precipitation yielded block copolymers requiring no further purification. The polypeptide-*b*-peptides had PBLG block lengths ranging from 36 to 250 monomers. The chemical structure of the polypeptide-*b*-peptides was confirmed by GPC, NMR, FTIR, and MALDI-TOF MS. This new class of peptides will broaden the scope of peptide-based nanostructures, as the combination of polypeptides with designed peptides enables control over both the peptide size and functionality, which are both determining factors in molecular self-assembly. This potential is investigated by selecting 4 molecular building blocks and showing that a variety of structures could be accessed, relying on the size of the PBLG block and the noncovalent coiled-coil interaction of peptide E with the complementary peptide K or the hybrid K-PEG. Polymersomes with a range of sizes, membrane thicknesses, and surface functionality were formed, as well as disk-like micelles. The structures were characterized by means of CD, DLS, SEM, cryo-TEM, fluorescence spectroscopy, and zeta potential measurements. It was found that the diameters of the structures increased with decreasing hydrophilic to hydrophobic block size ratios, as is typical for traditional surfactants such as lipids. The form of the polymersome membrane depended on the length of the PBLG block, with the shortest PBLG length forming very well-defined membranes that were twice the calculated molecular length. The structures were demonstrated to encapsulate water soluble compounds, hence there is potential for use of these materials as drug delivery devices, and through E/K complexation the outside of the polymersomes can be decorated with targeting/stealth molecules.

EXPERIMENTAL SECTION

Materials and Methods

Materials

Fmoc-protected amino acids were purchased from Novabiochem. Tentagel PAP resin was purchased from Rapp Polymere. All other reagents and solvents were obtained at the highest purity available from Sigma-Aldrich or BioSolve Ltd. and used without further purification. Phosphate buffered saline, PBS: 30 mM $K_2HPO_4.3H_2O$, 19 mM KH_2PO_4, 100 mM KCl, pH 7.0.

General Methods

Gel permeation chromatography (GPC) was performed with a Shimadzu system equipped with a refractive index detector. A Polymer Laboratories column was used (3M-RESI-001-74, 7.5 mm diameter, 300 mm length) with DMF as the eluent, at 60 ºC, and a flow rate of 1 mL min^{-1}. Both the coiled-coil peptide and PBLG are soluble in DMF, and the runs were conducted at 60 ºC to prevent aggregation. The molecular weights were calibrated using polystyrene standards.

^{1}H-NMR spectra recorded on a Bruker AV-500 spectrometer and a Bruker DPX300 spectrometer at room temperature. The residual proton resonance of deuterated dichloromethane was used for calibration. In order to ensure that there were no aggregation artifacts in the spectra that were analyzed for molecular weight determination a range of ^{1}H-NMR spectra of the deprotected hybrids were recorded, from deuterated dichloromethane to 1:1 (v/v) deuterated dichloromethane:trifluoroacetic acid.

MALDI-TOF mass spectra were acquired using an Applied Biosystems Voyager System 6069 MALDI-TOF spectrometer. Samples were dissolved in 1:1 (v/v) 0.1% TFA in water:acetonitrile (TA), at concentrations of ~10 mg mL^{-1}. Solutions for spots consisted of (v/v) 1:10 sample solution: 10 mg mL^{-1} α-Cyano-4-hydroxycinnamic acid (ACH) in TA.

FT-IR spectra were recorded on a BIORAD FTS-60A instrument equipped with a deuterated-triglycine-sulphate (DTGS) detector at a resolution of 20 cm^{-1}. The compounds were dried from dichloromethane onto an attenuated total reflectance (ATR) ZnSe crystal. A clean ATR ZnSe crystal was used as the background.

Synthesis

Solid-Phase Peptide Synthesis of the coiled-coil forming peptides E, K, and K-PEG

The peptides E and K, and the hybrid K-PEG were prepared and characterized as described in Chapter 3. After the peptide E was prepared, the resin was removed from the reaction vessel, swollen in 1:1 (v/v) DMF:NMP, and Fmoc deprotected. The amount of successfully synthesized E on a given weight of peptide-resin was estimated using the mass added to the resin during the synthesis of E, and by integration of HPLC peaks from an LCMS run of a test cleavage of 10 mg of resin-bound peptide.

Synthesis of γ-benzyl L-glutamate N-carboxyanhydride (BLG-NCA)

A suspension of γ-benzyl L-glutamate (ca. 5.0 g, 21.1 mmol) in anhydrous ethyl acetate was heated to reflux (120 °C) under an argon atmosphere with vigorous stirring. Triphosgene (ca. 2.1 g, 7.0 mmol) was added quickly and stirring was continued for 3 hours, until the suspension became clear. If the suspension remained turbid a small quantity of triphosgene was added every 15 minutes. The solution was filtered and concentrated to one third of the initial volume (oily yellow liquid). The product was transferred to a glovebox under an argon atmosphere and precipitated in hexane, filtered, recrystallized, and dried. ^{1}H NMR (300 MHz, $CDCl_3$, δ): 7.3 (aromatic H, m); 5.1 (benzylic CH_2, s), 2.6 (γ-CH_2, t), 2.2 (β-CH_2, m), 4.4 (α-CH, t), 6.8 (N-H, br).

Solid-Phase Synthesis of Poly (γ-benzyl L-glutamate)-block-E (PBLG-E)

Poly(γ-benzyl L-glutamate) was synthesized via a one-pot NCA polymerization of γ-benzyl L-glutamate *N*-carboxyanhydride, initiated from the amine at the N-terminus of the peptide E while still on the resin. The resin-bound peptide was dried with reduced pressure at 40 °C overnight, and then in argon with reduced pressure for 5 hours. Under an argon atmosphere the peptide-resin was swollen in DCM (2.5 wt% NCA to DCM), and subsequently the appropriate weight of NCA (determined from the mass loading and HPLC peak integration) was added. The flask was shaken for 24 – 65hrs. A small volume of DCM was drained from the reaction vessel and the contents analyzed with FT-IR spectroscopy, showing that no NCA monomer remained (as determined by the absence of the carbonyl stretching absorption band of the C_2 carbonyl at 2000 – 1800 cm^{-1}, which is released as CO_2 during the reaction). The resin was drained and washed profusely with DCM, NMP, DMF, and finally with DCM. The initial DCM washes were dried to collect any homopolymer that formed in solution. The yields of the resin-bound block copolypeptides were 85% - 92%.

The hybrid material was cleaved in the protected form from the resin using 1:99 (v/v) TFA:DCM for 2 minutes, 10 times. Each cleavage mixture was precipitated drop-wise in cold methanol. The white precipitate was compacted with centrifugation and the supernatant removed. This was repeated three times with the addition of fresh methanol. The pellets were dried under reduced pressure. Molecular weights and their distributions of the protected PBLG-E polypeptide-*b*-peptides were determined using gel permeation chromatography.

The OtBu and BOC protecting groups of the glutamic acid and lysine residues of the E block were removed by stirring the block copolymer in 47.5:47.5:2.5:2.5 (v/v) TFA:DCM:water:TIS for 1 hour, and the product was precipitated drop-wise in cold methanol. The white precipitate was compacted with centrifugation and the supernatant removed. This was repeated three times with the addition of fresh methanol. The pellets were dried under reduced pressure, with yields ranging from 28% for the block copolymer with the shortest average PBLG length, which does not sediment well in cold methanol, to 74% for the block copolymer with longest PBLG block, which is the most hydrophobic of

the series. The purity and molecular weights of the deprotected polypeptide-*b*-peptides were checked using ^{1}H-NMR spectra. The absolute masses of the polypeptide-*b*-peptides with shorter PBLG blocks were determined using MALDI-TOF mass spectrometry. The yield and molecular weight of the compounds used in this study as determined by GPC, NMR, and MALDI-TOF spectroscopy are given in Table 1. The secondary structure of the polypeptide-*b*-peptides was determined using FT-IR spectroscopy.

Preparation of PBLG-E suspensions

0.1 μmol of each compound (PBLG-E, or PBLG-E and K, or PBLG-E and K-PEG) was dissolved in 200 μL tetrahydrofuran (THF). 2 mL of phosphate buffered saline (PBS, 50 mM PO_4, 100 mM KCl, pH 7.0) was added and the sample was immediately sonicated with an open lid for 2 hours in a Branson 1510 bath sonicator with an output of 70 W and 42 kHz. The final concentration of each polymer was 50 μM.

For the encapsulation of rhodamine B in the vesicles the samples were prepared as described above, with the addition of rhodamine B (0.2 mg mL^{-1}, 0.418 mM) to the buffer. The unencapsulated rhodamine B was removed over a fast protein liquid chromatography (FPLC) column. FPLC was performed with an Äkta prime, Amarsham Pharmacia Biotech apparatus with a Pharmacia XK 26 column (135 mm x 25 mm) packed with Sephadex G50-fine. PBS was used as the eluent. The flow rate was 5 mL min^{-1}, UV sensitivity was set on 0.1 AU, 1%, the conductivity was set on 15-20 mS cm^{-1} and the wavelength for UV recording was 254 nm. The amount of encapsulated rhodamine B in each sample was determined by fluorescence spectroscopy, with excitation at 555 nm, and emission monitored from 563 – 650 nm with 5 nm slits using a Cary-50 Spectrophotometer.

Characterization of PBLG-E suspensions

Dynamic Light Scattering

Dynamic light scattering was conducted as detailed in the experimental section of Chapter 3.

Scanning Electron Microscopy

Scanning electron microscopy (SEM) was conducted on a Nova NanoSEM FEI instrument with an accelerating voltage of 10 kV and spot size of 3.5. Samples for SEM were prepared by placing 5 μL of the solution on SEM stubs with a TEM grid on the carbon tape. After 30 minutes the excess buffer was removed. Samples were coated with gold for one minute, resulting in a layer ~ 15 nm thick.

Cryogenic Transmission Electron Microscopy

Cryogenic TEM was conducted as detailed in the experimental section of Chapter 3. Copper grids bearing lacey carbon films resulted in a greater number of self-assembled structures in the vitrified ice.

Zeta Potentials

Zeta potentials were measured at 25 °C using the same instrument. The laser wavelength was 633 nm and the scattering angle was 173˚. A Malvern universal dip cell (ZEN1002) was used, and the samples were diluted ten-fold with 1 mM NaCl to reduce the ionic strength of the buffer.

Circular Dichroism Spectroscopy

CD spectra were obtained as detailed in the experimental section of Chapter 2. For analysis each spectrum had the appropriate background spectrum (buffer or buffer/THF) subtracted.

REFERENCES

1. van Hest, J. C. M.; Tirrell, D. A. *Chem. Commun.* **2001**, (19), 1897-1904.
2. Smeenk, J. M.; Ayres, L.; Stunnenberg, H. G.; van Hest, J. C. M. *Macromol. Symp.* **2005,** 225, 1-8.
3. Deming, T. J., Polypeptide and polypeptide hybrid copolymer synthesis via NCA polymerization. In *Peptide Hybrid Polymers*, Springer-Verlag Berlin: Berlin, 2006; Vol. 202, pp 1-18.
4. Gallot, B. *Prog. Polym. Sci.* **1996,** 21, (6), 1035-1088.
5. Caillol, S.; Lecommandoux, S.; Mingotaud, A. F.; Schappacher, M.; Soum, A.; Bryson, N.; Meyrueix, R. *Macromolecules* **2003,** 36, (4), 1118-1124.
6. Huang, H.; Dong, C. M.; Wei, Y. *Comb. Chem. High. T. Scr.* **2007,** 10, (5), 368-376.
7. Higashi, N.; Koga, T.; Niwa, M. *Langmuir* **2000,** 16, (7), 3482-3486.
8. Dimitrov, I. V.; Berlinova, I. V.; Iliev, P. V.; Vladimirov, N. G. *Macromolecules* **2008,** 41, (3), 1045-1049.
9. Sun, J.; Chen, X. S.; Lu, T. C.; Liu, S.; Tian, H. Y.; Guo, Z. P.; Jing, X. B. *Langmuir* **2008,** 24, (18), 10099-10106.
10. Brzezinska, K. R.; Deming, T. J. *Macromolecules* **2001,** 34, (13), 4348-4354.
11. Kros, A.; Jesse, W.; Metselaar, G. A.; Cornelissen, J. J. L. M. *Angew. Chem., Int. Edit.* **2005,** 44, (28), 4349-4352.
12. Imanishi, Y. *J. Macromol. Sci. Chem.* **1984,** A21, (8-9), 1137-1163.
13. Jeong, Y. I.; Cheon, J. B.; Kim, S. H.; Nah, J. W.; Lee, Y. M.; Sung, Y. K.; Akaike, T.; Cho, C. S. *J. Control. Release* **1998,** 51, (2-3), 169-178.
14. Thunemann, A. F.; Kubowicz, S.; von Berlepsch, H.; Mohwald, H. *Langmuir* **2006,** 22, (6), 2506-2510.
15. Cai, C.; Lin, J.; Chen, T.; Wang, X.-S.; Lina, S. *Chem. Commun.* **2009**.
16. Tang, D. M.; Lin, J. P.; Lin, S. L.; Zhang, S. N.; Chen, T.; Tian, X. H. *Macromol. Rapid. Comm.* **2004,** 25, (13), 1241-1246.
17. Morikawa, M.; Kimizuka, N. *Chem. Commun.* **2005**, (38), 4866-4868.
18. Iatrou, H.; Frielinghaus, H.; Hanski, S.; Ferderigos, N.; Ruokolainen, J.; Ikkala, O.; Richter, D.; Mays, J.; Hadjichristidis, N. *Biomacromolecules* **2007,** 8, (7), 2173-2181.
19. Kuo, S. W.; Lee, H. F.; Huang, C. F.; Huang, C. J.; Chang, F. C. *J. Polym. Sci. Pol. Chem.* **2008,** 46, (9), 3108-3119.
20. Woolfson, D. N., The design of coiled-coil structures and assemblies. In *Fibrous Proteins: Coiled-Coils, Collagen And Elastomers*, Elsevier Academic Press Inc: San Diego, 2005; Vol. 70, pp 79-+.
21. Marsden, H. R.; Korobko, A. V.; van Leeuwen, E. N. M.; Pouget, E. M.; Veen, S. J.; Sommerdijk, N. A. J. M.; Kros, A. *J. Am. Chem. Soc.* **2008,** 130, (29), 9386-9393.
22. Robson Marsden., H.; Elbers., N. A.; Bomans., P. H. H.; Sommerdijk., N. A. J. M.; Kros, A. *Angew. Chem., Int. Ed.* **2009,** 48, (13), 2330-2333.
23. Yano, Y.; Yano, A.; Oishi, S.; Sugimoto, Y.; Tsujimoto, G.; Fujii, N.; Matsuzaki, K. *ACS Chem. Biol.* **2008,** 3, (6), 341-345.
24. Blout, E. R.; Karlson, R. H. *J. Am. Chem. Soc.* **1956,** 78, (5), 941-946.
25. Note that when PBLG-E is in the α-helical conformation, e.g. in DCM or DMSO, the α-H resonance peak is at 4.0 ppm, and by adding TFA the peak position is shifted low-field to 4.7 ppm, indicating that the hybrids have random coil conformation in this solvent mixture, and are not aggregated.
26. Higashi, N.; Kawahara, J.; Niwa, M. *J. Colloid. Interf. Sci.* **2005,** 288, (1), 83-87.
27. Bradbury, E. M.; Cranerob.C; Goldman, H.; Rattle, H. W. E. *Nature* **1968,** 217, (5131), 812-816.
28. See supporting information
29. Rinaudo, M.; Domard, A. *Biopolymers* **1976,** 15, (11), 2185-2199.
30. Murthy, N. S.; Knox, J. R.; Samulski, E. T. *J. Chem. Phys.* **1976,** 65, (11), 4835-4839.
31. Chang, Y. C.; Frank, C. W. *Langmuir* **1996,** 12, (24), 5824-5829.
33. Lindhout, D. A.; Litowski, J. R.; Mercier, P.; Hodges, R. S.; Sykes, B. D. *Biopolymers* **2004,** 75, (5), 367-375.
34. The hydrodynamic diameter of the PEG block was determine by DLS.
35. Kaiser, E.; Colescot.Rl; Bossinge.Cd; Cook, P. I. *Anal. Biochem.* **1970,** 34, (2), 595-598.
36. Kita-Tokarczyk, K.; Grumelard, J.; Haefele, T.; Meier, W. *Polymer* **2005,** 46, (11), 3540-3563.
37. Israelachvili, J. N.; Mitchell, D. J.; Ninham, B. W. *J. Chem. Soc. Farad. T. 2* **1976,** 72, 1525-1568.

38. Opsteen, J. A.; Cornelissen, J. J. L. M.; van Hest, J. C. M. *Pure Appl. Chem.* **2004,** 76, (7-8), 1309-1319.
39. Halperin, A. *Macromolecules* **1990,** 23, (10), 2724-2731.
40. Srinivas, G.; Discher, D. E.; Klein, M. L. *Nat. Mater.* **2004,** 3, (9), 638-644.
41. There is likely to be sorting within the bicelles such that the polymer-*b*-peptides with shorter hydrophobic blocks are located at the rim. The shortest PBLG length in the $PBLG_{36}$-E polymer-b-peptide is 23 monomers (as determined by MALDI-TOF MS), which corresponds to an alpha-helical length of ~ 3.5 nm. The persistence length of bulk PBLG is ~ 2 nm, and increases when under thermodynamic confinement, as is the case in this nanophase separated system. (Floudas G. and Speiss H. W. *Macromol. Rapid Commun.* **2009**, 30, 278-298). It is possible that the PBLG rods are kinked, further reducing/eliminating the area of solvent exposed PBLG.
42. Noordik, G. S. a. J. H. *J. Comput.-Aided Mol. Design* **2000,** 14, 123-134.
43. Humphrey, W., Dalke, A. and Schulten, K. *J. Molec. Graphics* **1996,** 14, 33-38.
44. Discher, B. M.; Hammer, D. A.; Bates, F. S.; Discher, D. E. *Curr. Opin. Colloid In.* **2000,** 5, (1-2), 125-131.
45. Schillen, K.; Bryskhe, K.; Mel'nikova, Y. S. *Macromolecules* **1999,** 32, (20), 6885-6888.
46. Jenekhe, S. A.; Chen, X. L. *Science* **1998,** 279, (5358), 1903-1907.
47. The hydrodynamic diameter of $PBLG_{36}$-E, $PBLG_{36}$-E/K and $PBLG_{36}$-E/K-PEG was monitored over ten months, while the remainder of the samples were monitored (and were stable) over twenty months.
48. Discher, D. E.; Eisenberg, A. *Science* **2002,** 297, (5583), 967-973.
49. Aranda-Espinoza, H.; Bermudez, H.; Bates, F. S.; Discher, D. E. *Phys. Rev. Lett.* **2001,** 87, (20).
50. Antonietti, M.; Forster, S. *Adv. Mater.* **2003,** 15, (16), 1323-1333.

APPENDICES

Characterization of the PBLG-E block copolymer series

It was possible to characterize the PBLG-E polypeptide-*b*-peptides with the shortest PBLG blocks by MALDI-TOF MS. The masses observed do not correspond to an integer multiple of benzyl glutamate monomers in the PBLG chain. Additionally, the Kaiser test was negative (Kaiser, E.; Colescot.Rl; Bossinge.Cd; Cook, P. I. *Anal. Biochem.* **1970**, 34, (2), 595-598). These results indicate that the polymer chains do not end in a primary amine, as would be expected by the "amine" mechanism of ring-opening polymerization, but that another reaction, such as the "activated monomer" mechanism, has capped the growing chains. This is also consistent with the fact that there is not 100% monomer conversion, but some degree of oligomer formation. A given polymerization can alternate between these two mechanisms, and ROPs of NCAs using amines as initiators are notorious for their variable chain-end functionality and formation of homopolymer (Klok, H. A. *Angew. Chem., Int. Ed.* **2002**, 41, (9), 1509-1513. Deming, T. J., *Polypeptide and polypeptide hybrid copolymer synthesis via NCA polymerization*. **2006**; Vol. 202).

PBLG-E adopts a typical α-helical structure in the solid state as is evident from the amide I and amide II positions in FT-IR spectra (1651.1 cm^{-1} and 1546.9 cm^{-1} respectively). There is no shoulder on the amide I vibration, indicating that there is no random coil secondary structure in the hybrid, and thus that the secondary structure of E is helical in the solid state. The half width at half maximum of the amide II absorption depends on the stability of the α-helix, and at ~14cm^{-1} for the amide II band, this is on a par with the most stable helices (Nevskaya, N. A.; Chirgadze, Y. N. *Biopolymers 1976*, 15, (4), 637-648).

Self-assembling properties of the block copolymers and polymer mixtures in solution

Effect of THF on E/K and PBLG secondary and quaternary structures

The E/K heterodimer is a noncovalent complex driven by the packing of leucine and isoleucine residues forming a hydrophobic core in order to reduce contact with the aqueous environment. In PBS E/K exhibits a typical α-helical circular dichroism (CD) spectrum, with minima at 208 nm and 222 nm. The ellipticity ratio was 1.00 (Figure A2, thick line), consistent with interacting α-helices (Zhou, N. E.; Kay, C. M.; Hodges, R. S. *J. Biol. Chem.* **1992**, 267, (4), 2664-2670). Upon the addition of THF, the secondary structure of the peptides remains α-helical, but the intermolecular interaction is disrupted, as evidenced by the decreasing ellipticity ratio (Figure A2). This is because adding THF to PBS reduces the polarity of the solvent so there is a decreased energetic penalty associated with the hydrophobic residues being exposed to the solvent.

PBLG is α-helical in THF, and aggregates in aqueous solutions. Samples were prepared using 5, 10, 20, 30, and 40 (v/v)% THF in PBS. Between 10 and 30% THF the particles had similar appearances, whereas with more THF the particles were larger (DLS) and had a different appearance (negative stained TEM, not shown). Based on these observations the initial ratio of THF:PBS was fixed at 10:90 (v/v). This strikes a balance between the necessity to perform experiments in an environment allowing coiled-coil pairing between

E and K, and the need for mobility of the hydrophobic PBLG blocks in order to reduce the formation of macro-aggregates.

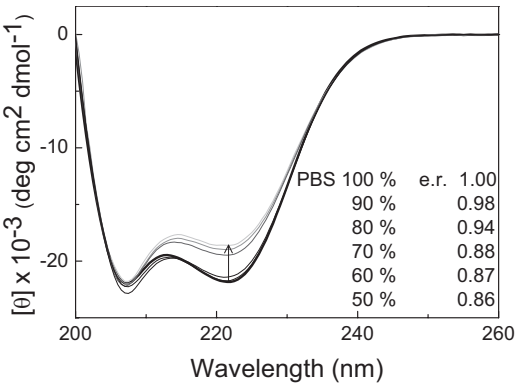


Figure A1. CD spectra of E/K in mixtures of PBS and THF. The intensity at 222 nm decreases with increasing THF concentrations (arrow). [Total Peptide] = ~ 0.5 mg mL^{-1}, PBS, 25 °C.

Peptide structure in the supramolecular assemblies

Circular dichroism (CD) spectra of the polypeptide-*b*-peptides and polymer mixtures in aqueous buffer after sonication are typical for aggregated α-helices: there is dampening of the spectrum and a red-shift of the 222 nm minimum compared to the typical solution spectra of α-helices. (Long, M. M.; Urry, D. W.; Stoeckenius, W. *Biochemical and Biophysical Research Communications* **1977**, 75, (3), 725-731. Frost, D. W. H.; Yip, C. M.; Chakrabartty, A. *Biopolymers* **2005**, 80, (1), 26-33. Potekhin, S. A.; Melnik, T. N.; Popov, V.; Lanina, N. F.; Vazina, A. A.; Rigler, P.; Verdini, A. S.; Corradin, G.; Kajava, A. V. *Chemistry & Biology* **2001**, 8, (11), 1025-1032. Pandya, M. J.; Spooner, G. M.; Sunde, M.; Thorpe, J. R.; Rodger, A.; Woolfson, D. N. *Biochemistry* **2000**, 39, (30), 8728-8734. Higashi, N.; Yamamoto, T.; Yokoyama, K.; Niwa, M. *Macromolecules* 1995, 28, (7), 2585-2587. Mattice, W. L.; Mccord, R. W.; Shippey, P. M. *Biopolymers* **1979**, 18, (3), 723-730. Cho, C. S.; Kobayashi, A.; Goto, M.; Akaike, T. *Thin Solid Films* 1995, 264, (1), 82-88. Urry, D. W. *Biochimica Et Biophysica Acta* **1972**, 265, (1), 115-&). The CD spectra of $PBLG_{36}$-E, $PBLG_{36}$-E/K, and $PBLG_{36}$-E/K-PEG are given in Figure S3. For $PBLG_{36}$-E the 222 nm peak is red-shifted, and both peaks are dampened. This is typical for membrane proteins, and the spectral artifacts are attributed to the particulate nature of the suspension (Long, M. M.; Urry, D. W.; Stoeckenius, W. *Biochemical and Biophysical Research Communications* **1977**, 75, (3), 725-731). For soluble proteins and peptides the intensity at 222 nm is directly proportional to the amount of helical structure (Chen, Y. H.; Yang, J. T.; Chau, K. H. *Biochemistry* **1974**, 13, (16), 3350-3359), but in this case the spectra are distorted due to the tight packing and therefore the amount of helical structure cannot be determined. Upon combining K with $PBLG_{36}$-E ($PBLG_{36}$-E/K) the distortions in the spectrum are reduced. With the addition of K-PEG ($PBLG_{36}$-E/K-PEG), the position of the minima is only slightly red-shifted (223 nm), and there is less dampening of the CD signal. These results show that as the size of the hydrophilic block/s increases in comparison to the hydrophobic PBLG block the helices become less constricted, yielding more standard CD spectra. Although the E/K complex can not be directly observed due to juxtaposition of the spectra of E/K with that of PBLG, it is clear that the molecules interact as the spectra are markedly different from the average of the individual components.

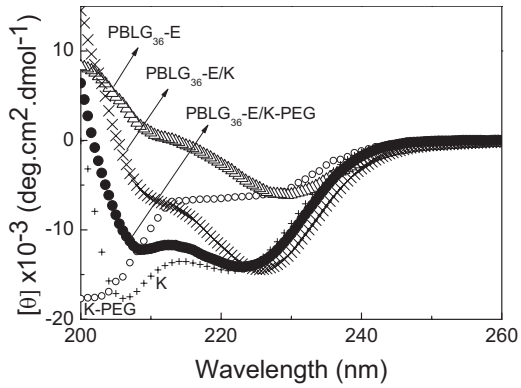


Figure A2. CD spectra of K (+), K-PEG (○), $PBLG_{36}$-E (Δ), $PBLG_{36}$-E/K (x), and $PBLG_{36}$-E/K-PEG (●) in PBS. [Total Peptide] = 50 μM, PBS, 25 °C.

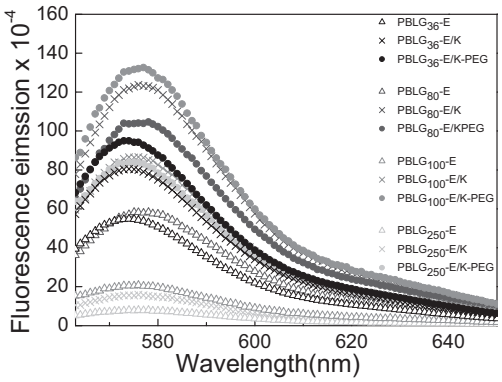


Figure A3. Fluorescence emission spectra of the polypeptide-*b*-peptides and polymer mixture suspensions. [Total Peptide] = 0.467 – 1.812 μM, PBS, 0.2 mg/mL rhodamine B, 25 °C.

Table A1. Zeta Potential of the Supramolecular Assemblies

Sample[a]	Zeta potential (mV)
$PBLG_{36}$-E	-26.1
$PBLG_{36}$-E/K	-9.5
$PBLG_{36}$-E/K-PEG	-7.2
$PBLG_{80}$-E	-28.5
$PBLG_{80}$-E/K	-10.2
$PBLG_{80}$-E K-PEG	-12.1
$PBLG_{100}$-E/K	-5.0
$PBLG_{100}$-E K-PEG	-5.7
$PBLG_{250}$-E K-PEG	-5.7

[a] [Total Peptide] = 0.0467 – 0.1812 μM, PBS: 5 mM phosphate, 10 mM KCl, pH 7.0, 0.02 mg/mL rhodamine B, 25 °C.

DETERGENT AIDED POLYMERSOME PREPARATION

Until now, most preparative methods used to form polymeric vesicles involve either organic cosolvents and/or sonication. In this Chapter a detergent aided method to produce polymersomes is demonstrate for the first time. Peptidic polymersomes were formed from the rod-rod block copolymer $PBLG_{36}$-E, where PBLG is hydrophobic poly(γ-benzyl L-glutamate) and E is a hydrophilic designed peptide. The block copolymer was first solubilized by cholate micelles in aqueous buffer, after which the concentration of detergent was reduced by dilution, transforming the particle morphology in solution from mixed micelles to polymersomes. The polymersome formation was monitored with dynamic light scattering and confirmed with transmission electron microscopy. Polymersomes with average diameters of ~ 300 nm were observed, as well as discs with average diameters of ~ 100 nm. This technique will be particularly useful when delicate biomacromolecules such as (membrane) proteins, peptides, or nucleic acids are to be encapsulated in the polymersomes, as the detergent used is compatible with these compounds, and the possible denaturing effect of sonication or organic solvents on the biological activity of the molecule of interest is avoided.

INTRODUCTION

Polymersomes are structurally similar to viral capsids in many ways, and are now being designed to perform in a similar way to viruses: to carry, protect, target, and release cargo.[1] This cargo is increasingly biological substances such as proteins, peptides or nucleic acids, intended for biomedical activity in the body.[2] The advantage of polymersomes over the traditional nanocapsules, liposomes, is that their membranes are more stable, leading to an enhanced ability to carry and protect cargo. The targeting and release properties of polymersomes also have more potential to be tailored to the intended application than liposomes, owing to the wide range of block copolymers available.

There are currently two classes of polymersome preparations: solvent free, and with organic solvents.[3] In the first class the block copolymer is hydrated to form polymersomes. Some block copolymers require no agitation during hydration, while others require stirring, vortexing, extrusion, electric current or sonication. Other block copolymers are too hydrophobic to undergo controlled aggregation in aqueous solution, and need to be first dissolved in an organic solvent which is then mixed with/exchanged for an aqueous solution.

In the growing number of cases in which biological molecules – macromolecules whose functions depend on intra and intermolecular structures – are to be incorporated into the polymersome membrane or aqueous interior, organic solvents or high energy input cannot always be used as they would degrade the activity of the cargo. Thus, a dilemma remains: for polymersomes that are intended to incorporate sensitive biological substances, but are unable to form vesicles directly in water, or cannot be sonicated, there is currently no suitable method available.

However, a third class of vesicle formation has been used for nearly forty years to create liposomes: the detergent removal technique.[4] This has been the preferred preparation method for liposomes incorporating biological substances as it does not diminish the biological activity.[5]

The first step of this method is to solubilize the water insoluble phospholipid that is to constitute the liposomes in a detergent (water soluble surfactant). Low molecular weight detergents typically have a large hydrophilic section in comparison to the hydrophobic section, and form micellar structures with highly curved interfaces. Amphiphiles such as phospholipids and certain block copolymers have a larger hydrophobic component in comparison to the polar section, and form lamellar assemblies, such as vesicles. When bilayer-forming phospholipids are solubilized by a large excess of high curvature detergent molecules, at a concentration higher than the critical micelle concentration (c.m.c.) of the detergent, mixed micelles result – micelles composed of the detergent, with the bilayer-forming lipid as an 'impurity'. The detergent in the micelles is in equilibrium with the detergent monomers in the aqueous phase, with the exchange rate in the microsecond range for medium chain detergent molecules.[5] The exchange rate of the lipid between aggregates is dramatically lower than that of the detergent, on the order of seconds to hours,[6-8] due to the poor solubility of the larger hydrophobic block in water. The second step is to alter conditions such that the morphology of self-assembled particles is no longer directed by the molecular properties of the detergent, but rather by those of the phospholipid. The mixed micelles are slowly diluted below the c.m.c. of the detergent by adding aqueous solution, and as the micellar-monomer equilibrium is maintained, the amount of detergent in the micelles is reduced. As the proportion of bilayer-forming molecules in the mixed micelles increases, new, lower curvature structures evolve. With lipids the departure from high curvature micelles passes through sheets, which near the c.m.c. of the detergent close to eliminate hydrophobic edge exposure to water, culminating in vesicles.[9]

Although certain phospholipids and block copolymers share molecular characteristics such that they each assemble into vesicles, their interaction parameters between the hydrophilic and hydrophobic components and the aqueous solvent are very different, which affects the self-assembly process.[8] In this Chapter the detergent removal method is adapted for the first time to block copolymers to create polymersomes. The polymer specific adaptations are explained, making this biomacromolecule-friendly technique readily applicable to create biomacromolecule-containing polymersomes in the future.

RESULTS AND DISCUSSION

While phospholipids are typically ~ 2 nm long and somewhat flexible, the amphiphilic block copolymer $PBLG_{36}$-E used in this study has an average length of ~ 8 nm and is relatively rigid. Both the poly(γ-benzyl L-glutamate) block, denoted $PBLG_{36}$, and the peptide E (amino acid sequence $G(EIAALEK)_3$) adopt an α-helical conformation. The hydrophobic $PBLG_{36}$ block has an average length of 4.5 nm, and peptide E is water soluble and ~ 3.5 nm long. In Chapter 4 it was shown that $PBLG_{36}$-E forms bilayered vesicles in aqueous solution. Due to the large hydrophobic block size none of the common solvent free polymersome preparation methods, i.e. bulk/film hydration, sonication etc., which all require hydration of a macroscopic phase of the block copolymer, have been successful. In this Chapter sodium cholate is used as the detergent to solubilize the block copolymer. Sodium cholate is a low molecular weight rigid disc-like anionic detergent with a c.m.c. of ~ 10 mM in 100 mM NaCl aqueous solution at 25 °C[10] that is often used to immobilize and/or encapsulate proteins in liposomes.[5] The relative sizes of cholate, a phospholipid typically used to prepare liposomes by the detergent removal method, and $PBLG_{36}$-E are illustrated in Figure 1. From the size disparity between the block copolymer and the phospholipid and detergent it can be readily appreciated that the balance of self-assembling forces between the micelle- and vesicle-forming molecules is very different when using this method to prepare liposomes or polymersomes.

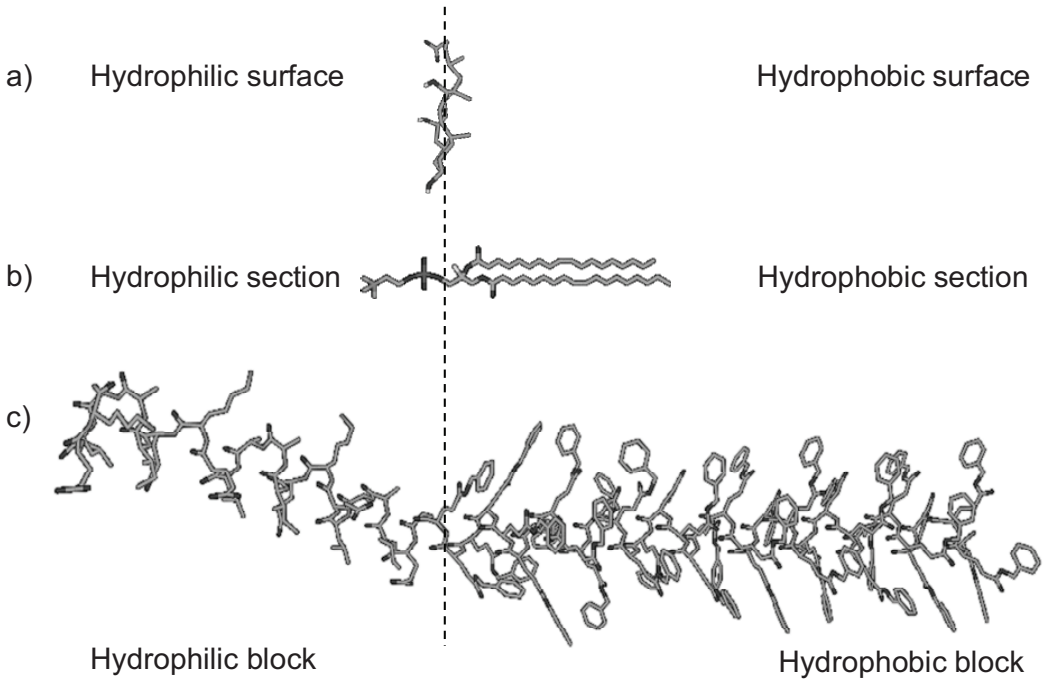


Figure 1. The molecular shape, amphiphilic nature, and relative size of cholate, DOPC (1,2-dioleoyl-sn-glycero-3-phosphocholine), and $PBLG_{36}$-E are illustrated in a), b) and c) respectively. The molecules are depicted approximately to scale, with the hydrophilic sections of the molecules aligned on the left side of the dashed line and the hydrophobic sections on the right.

The process of making polymersomes starts with forming mixed micelles of the detergent molecule and the block copolymer from a $PBLG_{36}$-E film and an aqueous solution of cholate micelles. The aggregation number of cholate micelles is quite variable, with micelles containing between 2 and 30 molecules.[10-12] Cholate micelles (200 mM in PBS, 25 °C) were determined by dynamic light scattering (DLS) to have an average hydrodynamic diameter of 2 nm, in agreement with reported values,[13] and a size range of about 1 – 5 nm (Figure 2a). Using the detergent dilution method to produce liposomes, lipid:cholate molar ratios on the order of 1:2 are typically employed.[14,15] In comparison to lipids, the block copolymer has a much larger surface area to be encapsulated and therefore a $PBLG_{36}$-E:cholate molar ratio of 1:4000 (0.05 mM $PBLG_{36}$:200 mM cholate) was chosen. Thin films of $PBLG_{36}$-E were hydrated in aqueous cholate solutions for 24 hours with occasional gentle agitation to solubilize the block copolymer. Since many cholate molecules are required to shield the large hydrophobic PBLG block from the aqueous solution, a departure from pure cholate micellar morphology is expected.[15,17] This was observed by transmission electron microscopy (TEM), with images of the mixed micelle stage containing a majority of pure cholate micelles, and some larger particles between 5 and 20 nm in diameter (Figure 2b). With the low block copolymer:cholate ratio employed in the current preparation conditions the size distribution of the mixed micelle population as determined by DLS does not vary significantly from that of pure cholate micelles (Figure 2). The size distributions of mixed micelle solutions were stable for at least 4 days as determined by DLS.

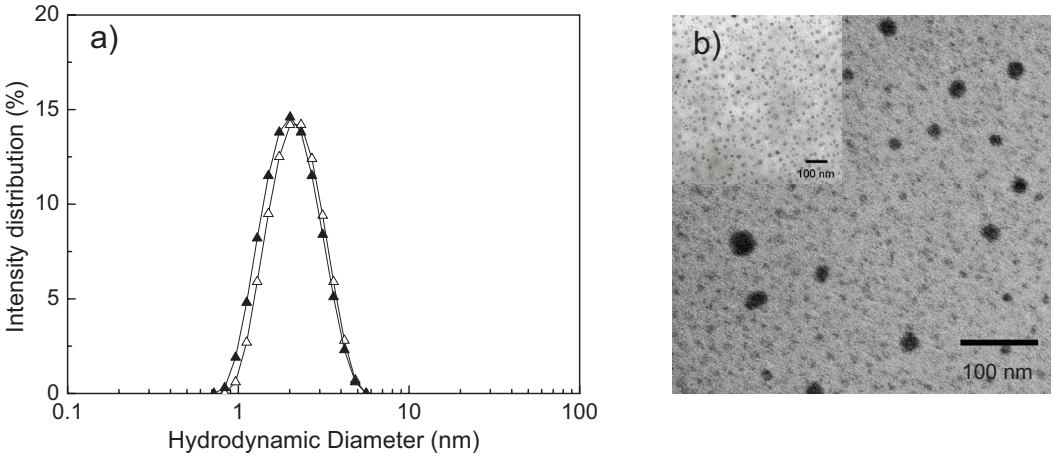


Figure 2. a) DLS intensity distributions of sodium cholate (Δ) and sodium cholate:$PBLG_{36}$-E 1:4000 (▲). b) PTA stained TEM image of a sodium cholate:$PBLG_{36}$-E 1:4000 mixture showing micelles and mixed micelles. Inset: PTA stained TEM image of pure cholate micelles. Conditions: 200 mM cholate, 0.05 mM $PBLG_{36}$-E in PBS, 25 °C.

The second step in the formation of vesicles is the dilution of the mixed micelles such that detergent molecules are gradually removed from the micelles and the morphology of the structures shifts from being dominated by the self-assembling properties of the detergent to those of the block copolymer. This was achieved by diluting the mixed micelle solution from 200 mM cholate, well above the c.m.c., to 2 mM, below the c.m.c.. The solution was

stirred rapidly during detergent dilution in order to prevent uncontrolled aggregation, similar to the preparation of liposomes using the detergent dilution method.[18] Moreover, well-defined size distributions were observed with DLS only when the aqueous solution was added gradually (over 30 minutes or longer). After this dilution step the particle sizes had increased from 2 nm to larger structures with a bimodal distribution as observed with DLS. The average D_h of the predominant structure was ~ 350 nm, and the D_h of the second population averaged ~ 100 nm (Figure 3a). This size distribution is most likely due to the range of molecular lengths and self-assembling characteristics of the block copolymer ($PBLG_{\geq 22, \leq 46}$, PDI = 1.1[19]).

For detergent/phospholipid systems the initial mixed micelles increase in dimension upon dilution and finally form liposomes around the c.m.c. of the detergent.[9] This means that the intrinsic self-assembly of the lipid only fully emerges, and liposomes assemble, when the detergent concentration becomes too low to form micelles. The energetic determinants of supramolecular vesicle formation are different for block copolymers as compared to lipids, and it is not clear if the spatial and temporal route from micelles to vesicles is the same. DLS was therefore conducted during detergent dilution to gain insight into the route to vesicle formation. PBS was added incrementally to mixed micelles (200 mM cholate) and the development of the size distributions was monitored. From the first PBS addition (170 mM cholate) the transition to the final polymersome size was already observed (Figure 3b), which is in marked contrast to the temporal pathway of liposome formation. As more PBS was added the number of vesicles gradually increased and there was a simultaneous decrease in the number of micelles. As the detergent concentration passed below the c.m.c. of cholate (10 mM), micelles were no longer detected.[20] The cholate concentration at which the first polymersomes are detected is approximately 15 x its c.m.c., implying that the determining factor in the micelle-to-vesicle transition for this polymer is not the dispersion of the micelles at the c.m.c. of the detergent.

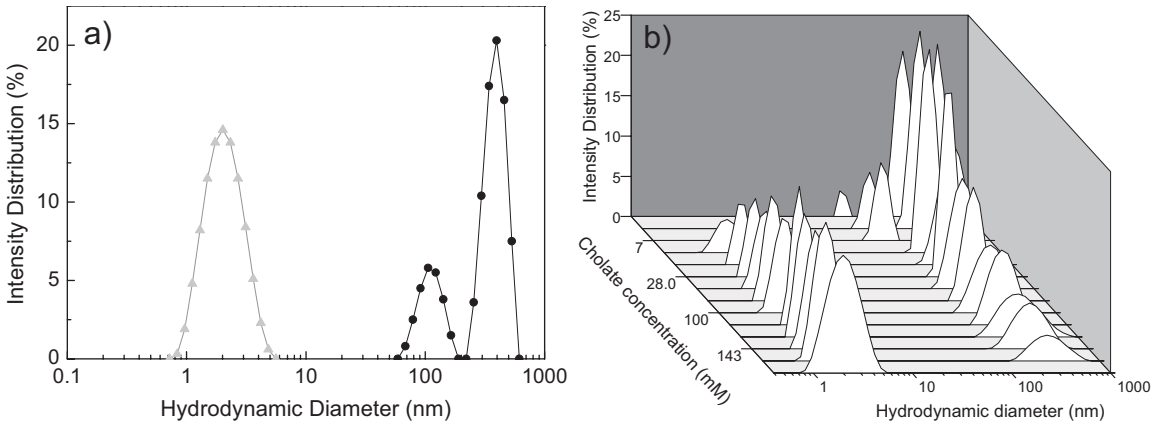


Figure 3. a) DLS intensity distributions during vesicle preparation: (▲) cholate:$PBLG_{36}$-E mixed micelles, (●) polymersomes formed after diluting the mixed micelles to 2 mM detergent. b) Evolution of micelle/polymersome diameters as a function of cholate concentration during dilution from 200 mM to 2 mM. Initial conditions: 200 mM cholate, 0.05 mM $PBLG_{36}$-E in PBS, 25 °C.

In fact, it was not necessary to dilute the samples below the c.m.c. of the micelles as the vesicle population was stable before all micelles (many of which would be pure cholate micelles) had dispersed, as seen in Figure 3b. In order to avoid unnecessary dilution of the polymersome suspensions it was preferred to dilute the cholate from 200 to 20 mM, with the vesicle size distribution not significantly different from samples that had been diluted below the c.m.c. of the detergent (Figure 4a). After detergent dilution to 20 mM, TEM revealed polymersomes with diameters matching the DLS distribution, and membrane thicknesses of ~ 15 – 20 nm, which is in close agreement with the calculated average bilayer thickness of 18 nm (Figure 4b). In addition to polymersomes, another bilayered structure, discs, were observed. The diameter of the of discs was ~ 100 nm, which is also consistent with the DLS results.

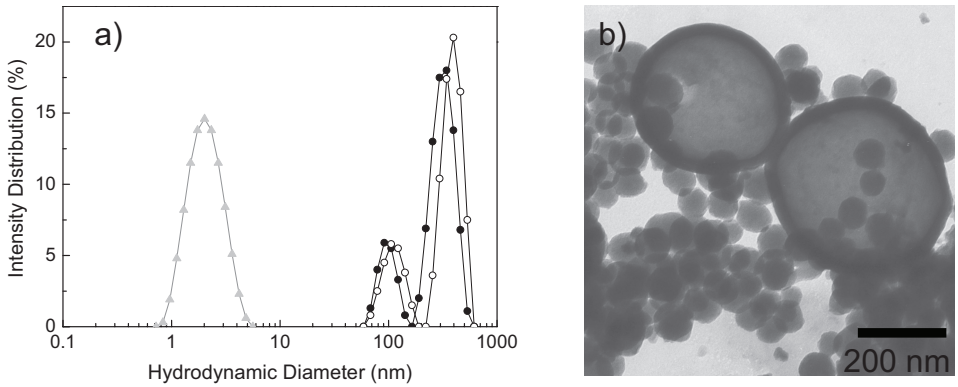


Figure 4. a) DLS intensity distributions during vesicle preparation: (▲) cholate:$PBLG_{36}$-E mixed micelles, (○) polymersomes formed after diluting the mixed micelles to 2 mM detergent, (●) polymersomes formed after diluting the mixed micelles to 20 mM detergent. b) OsO_4 stained TEM image of polymersomes and polymer discs after diluting the mixed micelles to 20 mM. Initial conditions: 200 mM cholate, 0.05 mM $PBLG_{36}$-E in PBS, 25 °C.

These results show that the relative influence and function of the detergent on the vesicle self-assembly process is clearly different for phospholipids and these block copolymers. In order to verify that it is dilution, i.e. removal of detergent from the mixed micelles, not only stirring that induces self-assembly of the block copolymer a preparation with 200 mM cholate was stirred without dilution. A population of larger particles does emerge (Figure 5), although the detected size distribution is quite variable and the rate of formation is reduced at least four-fold, with the large particles still forming after two hours, whereas with dilution and stirring all of the polymer has assembled into bilayered structures within half an hour. This shows that with a $PBLG_{36}$-E:cholate ratio of 1:4000 each polymer is effectively isolated from one another and removal of cholate molecules from the mixed micelles facilitates complete structural conversion.

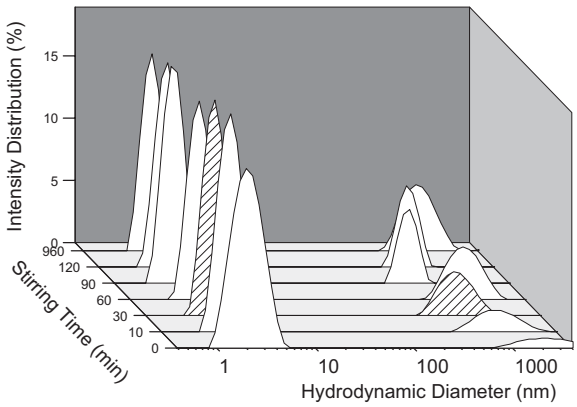


Figure 5. Evolution of micelle/polymersome diameters as a function of time, without dilution. The size distribution after the standard duration of stirring is thatched. Conditions: 200 mM cholate, 0.05 mM $PBLG_{36}$-E in PBS, 25 °C, stirring at 700 rpm. D_h intensity distributions determined by DLS.

A possible explanation of the observed results is as follows. In the mixed micelle stage the large hydrophobic PBLG block is shielded from the aqueous environment by a layer of disc-like cholate molecules.[12] Due to the high exchange rate of cholate between micelles and solution,[21,22] detergent depleted 'sticky patches' temporarily appear, allowing the block copolymer to exert its native self-assembling propensities, and leading to coalescence between detergent coated block copolymers. Due to its large hydrophobic block, $PBLG_{36}$-E exhibits very strong phase separation in comparison to phospholipids in aqueous solution, with similar block copolymers having exchange rates between pure micelles ranging from hours to non-detectable.[23-25] Once a number of $PBLG_{36}$-E molecules self-assemble, it is unlikely that the reverse process would occur. As a control experiment, $PBLG_{36}$-E polymersomes were prepared and cholate was added to a final concentration of 200 mM. The polymersome/micelle suspension was stirred for 30 minutes (the standard duration of dilution), and no significant changes in the polymersome population were observed with DLS. In essence, for this polymersome assembly process the important aspect of the detergent is that it provides a means of solubilizing the block copolymer and dampening its strong aggregation tendency en route to polymersomes. The micelle-to-monomer transition of the detergent does not induce polymersome formation. In more general terms, the initial detergent concentration should be high enough to completely solubilize the block copolymer, and to accelerate the structural conversion the mixed micelles should be diluted until the transformation of the block copolymer into vesicles is complete, with the precise detergent concentration dependent on the block copolymer used.

Because detergents may interact with other molecules in the environment to which the polymersomes are applied, in some instances detergent removal may be desired after detergent dilution. Therefore dialysis was used to reduce the detergent concentration

outside the polymersomes from 20 mM to ~ 0.1 μM. The size distribution did not change significantly during dialysis (Figure 6a), and was stable for 9 days at 4 °C. After this time aggregation was apparent by DLS, with the limited stability presumably arising from residual cholate trapped within the polymersomes. After vesicles have formed in solution the enclosed detergent will not diffuse out of the assembly as readily as from micellar or lamellar sheet morphologies. Thus, the rate of detergent removal depends on how readily the detergent diffuses through the vesicle membrane, and the rate of amphiphile flip-flop between the bilayers.[5] These polymersomes have relatively thick and rigid bilayers, and the rate of flip-flop is expected to be insignificant; hence the rate detergent removal depends almost entirely on the diffusion of entrapped cholate through the $PBLG_{36}$-E membrane, and it is expected to be more difficult to remove residual detergent from polymersomes than from liposomes.[26] Following dialysis for 48 hours the polymersomes were solubilized and it was observed with NMR spectroscopy that < 0.5% of the cholate remained after dialysis. From the NMR spectra it was also seen that the recovery of $PBLG_{36}$-E after dialysis was nearly quantitative (80%).

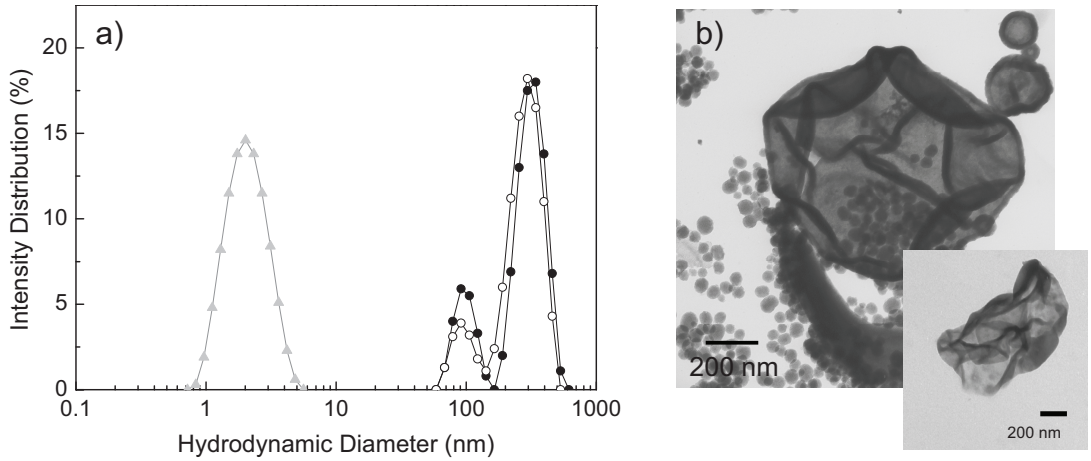


Figure 5. a) DLS intensity distributions during vesicle preparation: (▲) cholate:$PBLG_{36}$-E mixed micelles, (●) polymersomes formed after diluting the mixed micelles to 20 mM detergent, (○) polymersomes after detergent removal by dialysis. b) OsO_4 stained TEM images of polymersomes and micelles after diluting the mixed micelles to 20 mM, inset: polymersomes after detergent removal by dialysis. Initial conditions: 200 mM cholate, 0.05 mM $PBLG_{36}$-E in PBS, 25 °C.

CONCLUSIONS

It was demonstrated that the detergent removal technique, which has been used to produce liposomes for three decades[27], can also be used to produce polymersomes. The dilution of cholate/$PBLG_{36}$-E mixed micelles leads to a controlled transition from micelles to polymersomes with average diameters of ~ 350 nm, as well as polymers discs with average diameters of ~ 100 nm. While in the case of liposome formation the micelle-to-vesicle transition is controlled by the break-up of detergent micelles, this block copolymer dictates the self-assembled structures of the two-component system more forcibly, and the micelle-to-vesicle transition is determined by the self-assembly of predominantly detergent covered hydrophobic polymer blocks well above the c.m.c. of the detergent. The detergent is an agent to modulate the force of the phase separation such that well-ordered nanophase separation can occur in aqueous solution rather than the uncontrolled precipitation that occurs without a shielding layer. As the utility of the detergent is restricted to its ability to solubilize the polymer the method is termed 'detergent aided polymersome preparation'. This new pathway to produce polymersomes increases the possible applications of polymersomes as it does not require high energy input (for example sonication) or possibly damaging organic solvents, thus it is compatible with labile biomacromolecules.

Other than the benign nature of the detergent removal method, another advantage of this route has traditionally been that is it possible to control the liposome size and homogeneity. This can be achieved by varying the rate of detergent dilution,[9,18] using different classes of detergent[15,28,29] or vesicle-forming lipid,[18,27] varying the initial detergent:lipid ratios[15] and concentrations,[9] and by changing the pH[27] and ionic strength[30] of the aqueous solution. The effect of these parameters on polymersome properties, the structural evolution during the formation of vesicles, and the applicability of this method to other block copolymers will be the subject of future investigation.

EXPERIMENTAL SECTION

Materials and Methods

$PBLG_{36}$-E was synthesized as described in Chapter 4. The amino acid sequence of the E block was $G(EIAALEK)_3$-NH_2. The average molecular weight of $PBLG_{36}$-E was 10230 g mol^{-1}, and the PDI was 1.1. Sodium cholate was obtained from Fluka, and tetrahydrofuran was from Biosolve. Phosphate buffered saline, PBS: 8 mM $Na_2HPO_4.2H_2O$, 20 mM KH_2PO_4, 30 mM KCl, 137 mM NaCl, pH 7.2.

Preparation of Polymersome Suspensions

Preparation of mixed micelles

0.01 μmol of $PBLG_{36}$-E was used to create a uniform polymer film in a 100 mL round-bottomed flask (100 μL of a 1 mg ml^{-1} $PBLG_{36}$-E stock solution in THF, with the THF was subsequently removed on a rotary evaporator under reduced pressure). 200 μL of a 200 mM sodium cholate solution in PBS was added to the round-bottomed flask, which was then gently agitated until the polymer film was solubilized and the suspension was homogenous.

Detergent Dilution

The mixed micelle suspension was diluted ten-fold by the addition of 1.8 mL of 15 mM PBS over ½ hour using a syringe pump (NE-300, just infusion, Prosense B.V.), while stirring at 700 rpm.

Removing Detergent

The majority of the detergent was removed by means of dialysis (MWCO 7000 g mol^{-1} Slide-A-Lyser dialysis cassette from Therm Scientific), thoroughly rinsed with water then PBS. Samples were dialyzed against PBS for at least 48 hours with two changes of buffer).

$PBLG_{36}$-E and cholate Quantification

After dialysis (against water) the amount of $PBLG_{36}$-E and cholate in the samples was quantified by NMR spectroscopy (^{1}H-NMR spectra were recorded on a Bruker AV-400 spectrometer, in 7:3 (v/v) DMF-d_7:TFA to prevent block copolymer aggregation. A residual DMF proton resonance was used for ppm calibration, and HMDS as an internal calibrant to quantify the amount of $PBLG_{36}$-E and cholate). It was found that 80% of the original polymer material was present after dialysis, and no cholate could be detected (sensitivity ~ 0.25 μmol).

Characterization of Polymersome Suspensions

Dynamic Light Scattering

Dynamic light scattering was conducted as detailed in the experimental section of Chapter 3.

Transmission Electron Microscopy

Transmission electron microscopy (TEM) was conducted on a JEOL 1010 instrument with an accelerating voltage of 60 kV. Samples for TEM were prepared by placing 5 μL of each solution on carbon-coated copper grids. After ~ 5 minutes the droplet was removed from the edge of the grid. 5 μL of 2% PTA stain or 2% OsO_4 stain was applied and the excess was removed after 2 minutes.

REFERENCES

1. Discher, D. E.; Ortiz, V.; Srinivas, G.; Klein, M. L.; Kim, Y.; David, C. A.; Cai, S. S.; Photos, P.; Ahmed, F. *Prog. Polym. Sci.* **2007,** 32, (8-9), 838-857.
2. Christian, D. A.; Cai, S.; Bowen, D. M.; Kim, Y.; Pajerowski, J. D.; Discher, D. E. *Eur. J. Pharm. Biopharm.* **2009,** 71, (3), 463-474.
3. Kita-Tokarczyk, K.; Grumelard, J.; Haefele, T.; Meier, W. *Polymer* **2005,** 46, (11), 3540-3563.
4. Kagawa, Y.; Racker, E. *J. Biol. Chem.* **1971,** 246, (17), 5477-&.
5. Ollivon, M.; Lesieur, S.; Grabielle-Madelmont, C.; Paternostre, M. *BBA Biomembranes* **2000,** 1508, (1-2), 34-50.
6. Thomas, M. J.; Pang, K.; Chen, Q.; Lyles, D.; Hantgan, R.; Waite, M. *BBA Biomembranes* **1999,** 1417, (1), 144-156.
7. Fullington, D. A.; Nichols, J. W. *Biochemistry* **1993,** 32, (47), 12678-12684.
8. Discher, D. E.; Ahmed, F. *Annu. Rev. Biomed. Eng.* **2006,** 8, 323-341.
9. Wacker, M.; Schubert, R. *Int. J.Pharm.* **1998,** 162, (1-2), 171-175.
10. Garidel, P.; Hildebrand, A.; Neubert, R.; Blume, A. *Langmuir* **2000,** 16, (12), 5267-5275.
11. Hofmann, A. F.; Small, D. M. *Annu. Rev. Med.* **1967,** 18, 333-&.
12. Warren, D. B.; Chalmers, D. K.; Hutchison, K.; Dang, W. B.; Pouton, C. W. *Colloid. Surface. A* **2006,** 280, (1-3), 182-193.
13. Hildebrand, A.; Garidel, P.; Neubert, R.; Blume, A. *Langmuir* **2004,** 20, (2), 320-328.
14. Milsmann, M. H. W.; Schwendener, R. A.; Weder, H. G. *Biochim. Biophys. Acta* **1978,** 512, (1), 147-155.
15. Zumbuehl, O.; Weder, H. G. *Biochim. Biophys. Acta* **1981,** 640, (1), 252-262.
17. Small, D. M.; Penkett, S. A.; Chapman, D. *BBA Lipid. Lipid Met.* **1969,** 176, (1), 178.
18. Jiskoot, W.; Teerlink, T.; Beuvery, E. C.; Crommelin, D. J. A. *Pharm. Weekblad* **1986,** 8, (5), 259-265.
19. The degrees of polymerization were calculated from MALDI-TOF spectra, and the PDI was calculated from MALDI-TOF spectra and GPC .
20. Because micelles scatter less light than the much larger vesicles it expected that the micelles exist in the solution after they can no longer be detected by DLS.
21. Li, C. Y.; Zimmerman, C. L.; Wiedmann, T. S. *Pharm. Res.* **1996,** 13, (4), 535-541.
22. Wiedmann, T. S.; Liang, W.; Herrington, H. *Lipids* **2004,** 39, (1), 51-58.
23. Wang, Y. M.; Balaji, R.; Quirk, R. P.; Mattice, W. L. *Polym. Bull.* **1992,** 28, (3), 333-338.
24. Creutz, S.; van Stam, J.; Antoun, S.; De Schryver, F. C.; Jerome, R. *Macromolecules* **1997,** 30, (14), 4078.
25. Battaglia, G.; Ryan, A. J. *J. Phys. Chem. B* **2006,** 110, (21), 10272.
26. Pata, V.; Ahmed, F.; Discher, D. E.; Dan, N. *Langmuir* **2004,** 20, (10), 3888-3893.
27. Rhoden, V.; Goldin, S. M. *Biochemistry* **1979,** 18, (19), 4173-4176.
28. Kashiwagi, H.; Ueno, M. *Yakugaku Zasshi* **2008,** 128, (5), 669-680.
29. Rotenberg, M.; Lichtenberg, D. *J. Col. Interf. Sci.* **1991,** 144, (2), 591-594.
30. Leng, J.; Egelhaaf, S. U.; Cates, M. E. *Biophys. J.* **2003,** 85, (3), 1624-1646.

RAPID PREPARATION OF POLYMERSOMES BY A WATER ADDITION – SOLVENT EVAPORATION METHOD

In this Chapter a water addition – solvent evaporation method to produce polymersomes is demonstrated for the first time. The process involves solubilizing an amphiphilic block copolymer in an appropriate volatile organic solvent (THF), mixing it with an aqueous solution, and then evaporating the organic solvent under reduced. The parameters that influence the formation and size of the polymersomes are easily controlled, thus polymersomes are formed, tuned, and stabilized in less than five minutes. The method was demonstrated with a series of peptidic block copolymers, where the hydrophilic block is a charged designed peptide, and the hydrophobic block is poly(γ-benzyl L-glutamate) with varying degrees of polymerization (35 – 100 monomers), and the polymersome formation was monitored and confirmed with dynamic light scattering, optical microscopy, and transmission electron microscopy. The scope of the technique was also probed with noncovalent peptidic polymer complexes, and fully synthetic charged and non-charged coil-coil block copolymers of varying length. The method was found to be very robust with regards to salt concentration and initial mixing, and the polymersome size could be precisely adjusted, with the same block copolymer forming polymersomes ranging from ~ 200 nm to ~ 2 μm in diameter. Given the simplicity and versatility of the water addition – solvent evaporation method it is a very appealing new tool for polymersome preparation.

INTRODUCTION

Vesicles formed from lipids have been prepared since the early 1960s.[1,2] During these decades many techniques have been developed to prepare lipid vesicles, such as film rehydration, bulk rehydration, electroformation, solvent injection, aqueous phase injection, emulsion based methods (solvent evaporation or dialysis), and detergent dialysis. There are many variations on these methods, and also techniques to modify preformed vesicles such as vortexing, freeze-thawing, extrusion, or sonication have been applied.[3] Each of these methods results in lipid vesicles with different properties, and a remarkable range of properties are accessible: diameters from 25 nm to 100 μm, unilamellar or multilamellar vesicles, vesicles with relatively narrow or broad size distributions, vesicles encapsulating varying amounts of water soluble compounds, or incorporating material within the membrane, and vesicles with or without (residual) organic solvent. As a result, the physical properties required by a specific application often dictate which method of

vesicle formation should be applied. For example, for tumor targeting and retention purposes 100 nm vesicles are favored,[4] while for the study of membrane mimics giant vesicles are preferred, and the same method cannot be used to make these different types of vesicles. In addition to the final vesicle characteristics, each technique has associated advantages/disadvantages such as the use of organic solvents, high energy input, availability of specific equipment, or the time required for preparation. These aspects also frequently direct the choice of vesicle preparation method. For instance, when biomolecules are involved physiological ionic strength buffer is often required, and sonication or organic solvents cannot be used.

While lipid-based vesicles are the most extensively studied, other amphiphiles can assemble into vesicles as well. Examples are block copolymers and modified cyclodextrins. Polymer vesicles are particularly interesting as there is a profusion of choice regarding block composition and length, which results in a large variety of potential vesicle properties. Research into polymer vesicles, referred to herein as 'polymersomes', has been carried out since 1995,[5] and the remarkable vesicle properties arising from the choice of polymers have only been partially revealed. In order to allow the potential of polymersomes to be more fully exposed, the variety of preparation techniques that allows one to access different polymersomes needs to be extended. Not all methods used to assemble lipids into vesicles can be transferred directly to polymers due to their different physical/chemical properties, for example many block copolymers cannot be directly hydrated as lipids can. Hence techniques used for lipids are tailored to polymers, or new procedures are developed. The earliest method to prepare polymersomes, and currently the most commonly used, is to dissolve the polymer in an organic solvent and slowly add water, followed by dialysis to remove the organic solvent.[5-7] Other methods are solvent injection followed by dialysis,[8] bulk and film rehydration,[7] direct hydration,[9] electroformation,[10,11] dewetting from a template,[12] and a microfluidic double emulsion technique.[13]

Here a new method is presented, the 'water addition – solvent evaporation' method, to prepare polymersomes. The method is inspired by a rapid liposome preparation technique and is adapted to meet the requirements of block copolymers.[14] The advantages of this method are that the polymersome sizes can be readily and precisely tuned over a wide range; it is a robust method that can be applied to many different types of block copolymers; and finally it is very practical, as the process is complete in less than five minutes, uses standard laboratory equipment, and does not require high energy input.

RESULTS AND DISCUSSION

The new technique for preparing polymersomes consists of three steps: (I) the block copolymer is dissolved in THF, (II) the aqueous phase is added all at once and gently mixed, (III) the THF is removed by rotary evaporation under reduced pressure.

The method is initially demonstrated with the amphiphilic rod-rod block copolymer $PBLG_{50}$-K, in which PBLG is poly(γ-benzyl L-glutamate), and K is a charged peptide with 22 amino acid residues. Using the standard conditions (PBS, one minute vortexing, evaporation at 20 °C) $PBLG_{50}$-K self-assembled into large structures with an average hydrodynamic diameter of ~ 1200 nm, and a low size distribution (PDI 0.06) (Figure 1a). The particles were spherical and when the water soluble dye rhodamine B was added to the buffer it was observed by fluorescence microscopy to be encapsulated within the structures (Figure 1b), confirming that the block copolymer assembled into polymersomes. With transmission electron microscopy (TEM) it was established that polymersomes were the predominant structure, with the only other morphology being a very small quantity of spherical micelles. The average diameter of the polymersomes as measured by optical microscopy and dynamic light scattering were in agreement with one another, while the sizes of the dried polymersomes observed with electron microscopy were ~ 50 % smaller, likely due to deflation while drying.

The polymersome formation process and the extent to which $PBLG_{50}$-K polymersome sizes could be tuned were investigated, proceeding through the three parts of the method.

(I) Dissolving the polymer in THF

The water addition – solvent evaporation method was modified from a rapid liposome preparation technique.[14] For this method the lipids are also dissolved in an organic solvent, the aqueous phase quickly added, and the organic solvent removed by rotary evaporation under reduced pressure. However, the organic solvent used in the rapid liposome method is chloroform, which is immiscible with water, and liposomes form during evaporation. Many block copolymers, including the PBLG-peptide series used in this study, are not soluble in chloroform because of the hydrophilicity of the corona forming block. THF is a polar organic solvent that dissolves a wider range of polymer blocks. As it also has a low boiling point (66 °C), it is suitable to use in a solvent evaporation method. Unlike chloroform, THF is miscible with water; hence the block copolymers are exposed to a high water content upon addition of the aqueous phase, and aggregation induced by the hydrophobic block is expected before solvent evaporation.[18] Therefore the block copolymer specific adaptations mean that the current method has a different mechanism of vesicle formation to the rapid preparation of liposomes and is therefore quite dissimilar.

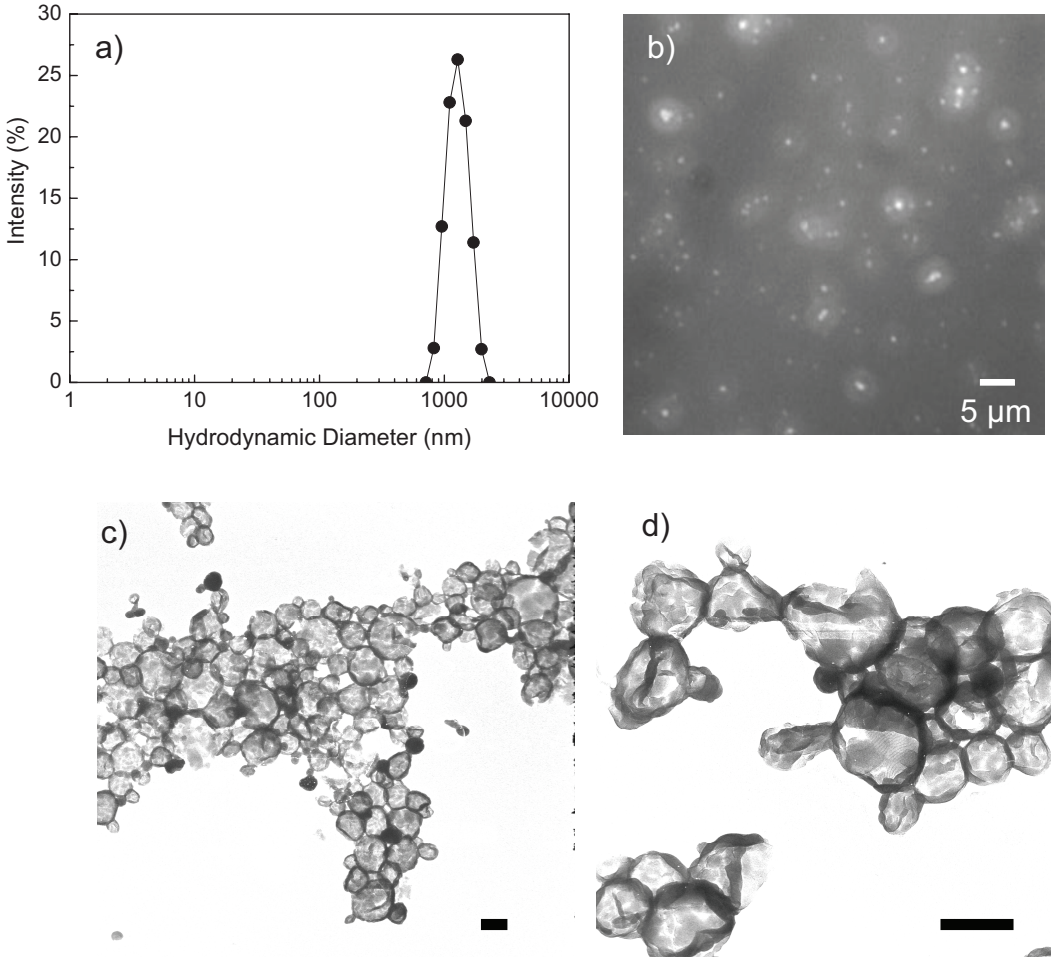


Figure 1. a) DLS intensity distribution for $PBLG_{50}$-K polymersomes prepared with the standard conditions. b) Fluorescence microscope image of $PBLG_{50}$-K polymersomes with encapsulated rhodamine B. c,d) TEM images of PTA stained $PBLG_{50}$-K polymersomes. Scale bars = 500 nm. Conditions: 2 mL THF, 0.02 μmol $PBLG_{50}$-K, 3 mL PBS, vortexing 1 minute at 200 rpm, THF evaporated for 2 minutes at 20 °C.

(II) Addition of aqueous buffer

To demonstrate the self-assembly process, $PBLG_{50}$-K samples were monitored with dynamic light scattering (DLS) and optical microscopy throughout the polymersome formation procedure. $PBLG_{50}$-K has a hydrodynamic diameter (D_h) of 8 nm in THF, in accordance with the theoretical value for molecularly dispersed block copolymer.[19] Upon addition of PBS large particles with a narrow size distribution (PDI ~ 0.06) were observed in the THF/PBS mixture (Figure 2a), which contained a polar interior (Figure 2b), suggesting that the block copolymer already assembles into polymersomes in the mixed solvent phase.

Additionally, it was observed by DLS and optical microscopy that the aggregate size continued to increase after the initial rapid structure formation (Figure 2c, d). This sustained size increase could be caused by three phenomena, operating either alone or in

tandem: ripening, fusion, or aggregation (see Figure A1). In general, polymersomes in mixed solvent systems increase in size in response to water addition in order to reduce the interfacial free energy between the core and solvent in the corona (if the core is still mobile).[20] This often occurs by fusion of smaller polymersomes, with low growth rates when the water content is high, as is the case in this system.[21,22]

In an attempt to observe the transition from molecularly dispersed block copolymer to polymersomes of ~ 1 μm, DLS was carried out as PBS was added incrementally to the THF solution (Figure 2c inset).[23] At a critical water content of ~ 5 v/v % PBS to THF the solvent quality of the mixture is sufficiently poor for the hydrophobic PBLG block that it aggregates, leading to microphase separation, and nanostructure formation. For PBLG-K (or PBLG-E, *vide infra*) block copolymers with shorter PBLG blocks, the onset of PBLG induced aggregation occurs at higher PBS/THF ratios. As more PBS is added the solvent becomes increasingly poor for the PBLG block and the structures continue to increase in size.[24] The trend of increasing particle size upon PBS addition is reliable, but the exact values for D_h should not be over interpreted due to the juxtaposition of the aforementioned kinetic growth effect, and because the size of the jumps in water content can affect the water volume at which structural transitions occur.[6,22]

During polymersome preparation, the introduction of the aqueous phase is generally the most critical step in the process, being the point at which precipitation of the block copolymer is likely to occur. In the present case polymersomes form upon PBS addition, and the manner in which samples are treated prior to THF removal may be expected to influence the final structures. Under the standard conditions the aqueous phase is added to the organic phase and then gently vortexed for one minute at a speed such that the phases are mixed but not agitated. Simply leaving the samples for one minute without mixing also resulted in well-defined final polymersomes, with similar sizes to those prepared with the mixing step (average D_h ~ 1000 nm, PDI 0.01, Figure 3). The THF can also be evaporated directly after addition of the aqueous phase (Figure 3). The inevitable mixing upon addition of the aqueous phase and during solvent evaporation is therefore adequate to yield polymersomes with a narrow size range. However, if the THF solution and PBS were mixed with high energy input by vortexing the flask for 1 minute at 2000 rpm such that the solution is strongly agitated, the material precipitated. Therefore, within practical limits, the structure formation is relatively insensitive to the way in which the organic and aqueous phases are combined, and no special care is required at this stage. Although the mixing step is not necessary with this block copolymer, the polymersome size distribution was found to be slightly less reproducible without the mixing step for a different block copolymer series (*vide infra*), therefore it was included to standardize the procedure.

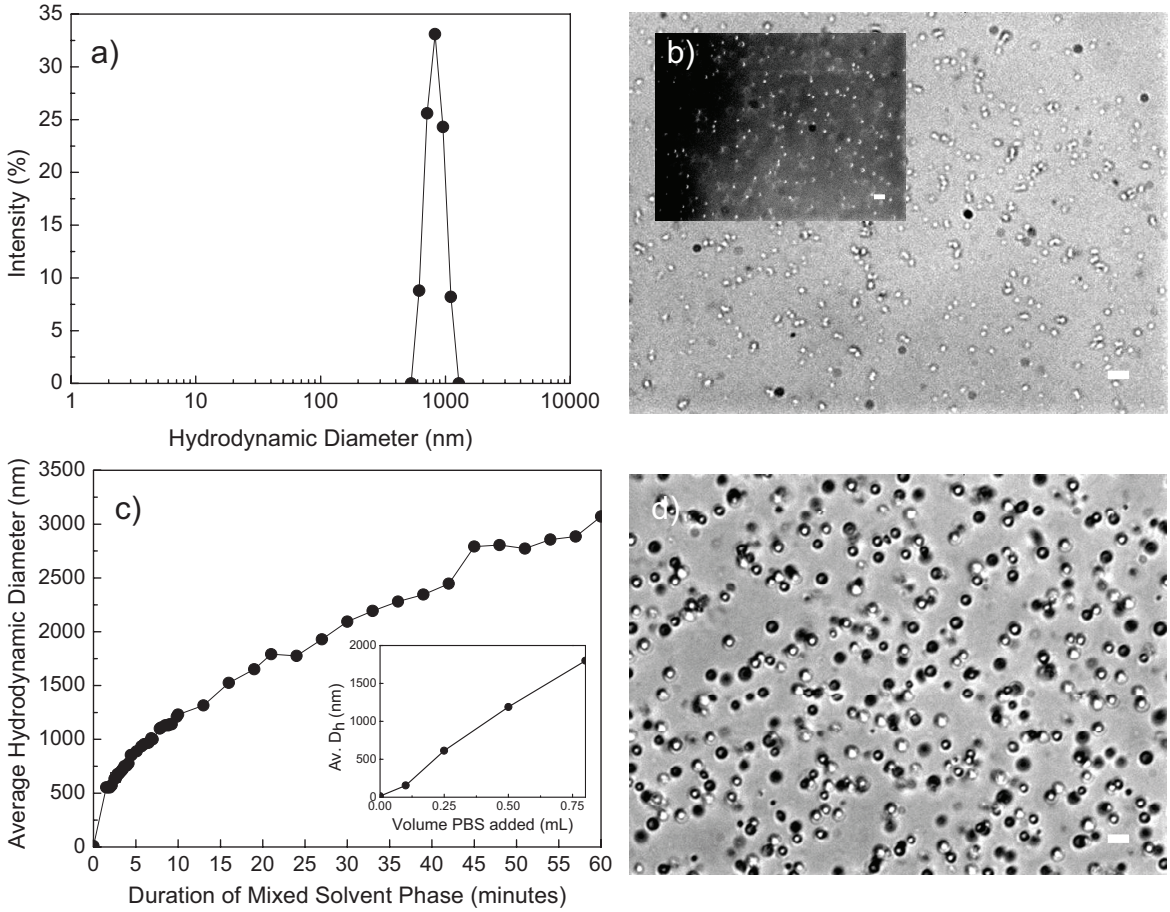


Figure 2. Particle characteristics in 2:3 v/v THF:PBS prior to THF evaporation: a) D_h distribution of $PBLG_{50}K$ polymersomes measured ~ 5 minutes after addition of the PBS. b) Optical bright field and fluorescence (inset) microscope images of $PBLG_{50}$-K polymersomes ~ 2 minutes after addition of PBS. Scale bar = 5 μm. c) The change in average D_h of $PBLG_{50}K$ assemblies with time after addition of PBS. Note that the initial points are subruns from DLS. Inset, average D_h during incremental PBS addition. d) Optical microscope image of $PBLG_{50}$-K particles ~ 30 minutes after addition of PBS. Scale bar = 5 μm.

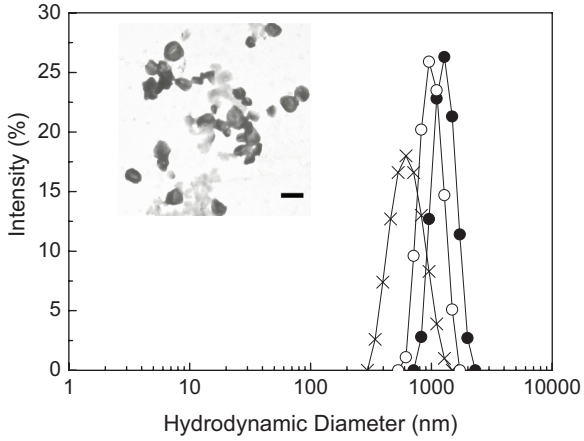


Figure 3. DLS intensity distributions for $PBLG_{50}$-K polymersomes prepared with 1 minute of vortexing at 200 rpm prior to THF evaporation (●), 1 minute without mixing (○), and immediate evaporation (×). Inset: PTA stained $PBLG_{50}$-K polymersomes prepared with immediate evaporation. Scale bar = 500 nm.

(III) Evaporation of the organic solvent

Many block copolymers cannot be hydrated from the bulk phase, thereby necessitating dispersal in an organic solvent followed by introduction of the aqueous phase. Since it is not possible to remove all of the organic solvent, all polymersomes prepared using solvent displacement techniques contain residual organic solvent. The advantages of removing the THF by rotary evaporation under reduced pressure are that it is very rapid, and the polymersome sizes can be adjusted and frozen during the same step (*vide infra*). The disadvantage is that more THF is likely to remain compared to removal by dialysis, which is the typical method for extracting the organic solvent. The samples were evaporated for 30 seconds after the boiling of THF subsided, with 97% of the THF removed at 20 °C, as determined by NMR spectroscopy, and insignificant volumes of water evaporated. After the majority of the THF has been evaporated the particle size does not change for at least four months at 4 °C, presumably because the PBLG blocks are frozen in the poor solvent, and the polymersomes are metastable kinetically trapped non-equilibrium structures.

During evaporation of the THF the composition changes within the interior of the polymersomes. To illustrate this, a small amount of the fluorescent dye rhodamine B was added to samples after the PBS and THF had been mixed, but before solvent evaporation. The polymersome membrane is impermeable to rhodamine B, as the interior of the polymersomes remains dark when observed by fluorescence spectroscopy (Figure 4a). However, after solvent evaporation for two minutes at 20 °C the interior of the polymersomes contains the fluorescent dye (Figure 4b). This means that the aggregates are permeable to rhodamine B during THF evaporation, and it is likely that they are also permeable to THF/PBS.

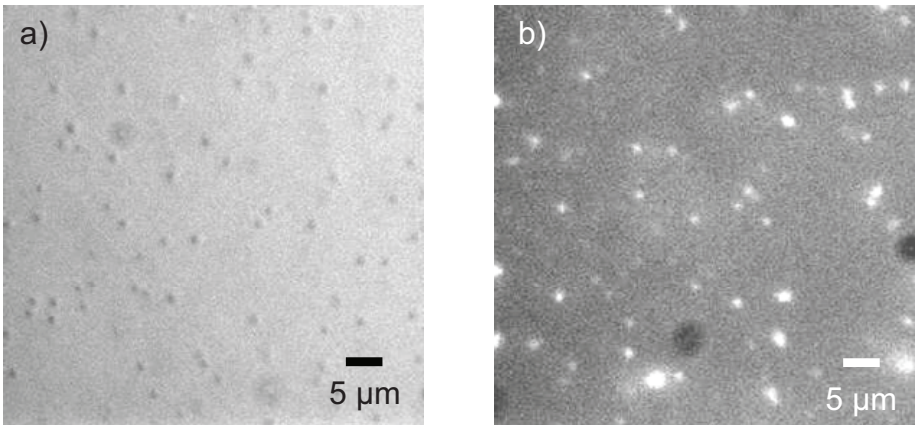


Figure 4. a) Fluorescence microscopy image of $PBLG_{50}$-K polymersomes in the THF/PBS mixture after the addition of rhodamine B. The rhodamine B is outside the polymersomes. b) Fluorescence microscopy image of $PBLG_{50}$-K polymersomes in PBS after THF evaporation, showing that the rhodamine B is inside the polymersomes. Scale bars = 5 µm.

The size of the polymersomes in PBS can be controlled by the time dependent particle size increase in the mixed solvent phase. Figure 5 shows the resultant sizes of the

polymersomes for which THF was evaporated at different times after addition of the aqueous phase. As the duration of the mixed solvent phase is extended and the particles increase in size, the polymersome diameters after THF removal also become larger. The sizes of the polymersomes in PBS are therefore dependent on the particle size in the mixed THF/PBS phase, which indicates that there is some degree of continuity between the particles pre- and post-THF evaporation, i.e. there is not complete disassembly and reassembly of the structures during the evaporation process. The largest polymersomes that could be formed from $PBLG_{50}$-K in this way at 20 ºC were ~ 2 μm. If the period of mixed solvent was extended further the polymersomes were not dispersed homogenously throughout the solution, but some formed a fine layer at the top of the PBS.

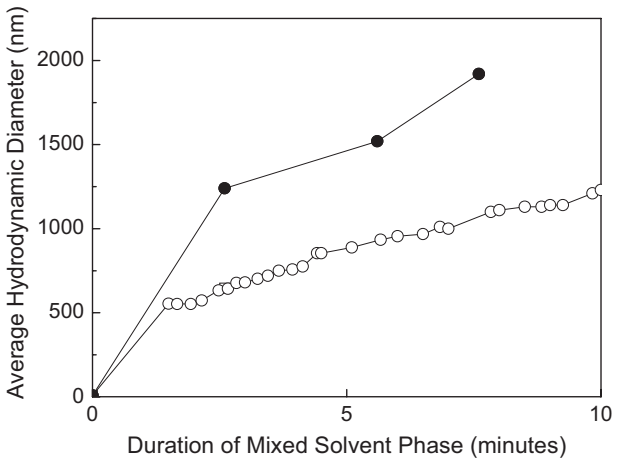


Figure 5. Average hydrodynamic diameter of the particles in 2:3 v/v THF:PBS (○), and in PBS after removal of the THF at 20 °C (●).

While the final sizes can be increased by allowing for growth of the particles before THF removal, a more dramatic change in polymersome size can be obtained by evaporating the THF at different temperatures. After one minute in the mixed solvent phase the THF was evaporated from the samples at 5 °C, 20 °C, 37 °C, and 70 °C. At each temperature evaporation was continued for 30 seconds after the boiling of THF subsided. The samples were analyzed with TEM and optical microscopy, confirming that polymersomes are the exclusive morphology at each temperature (Figure 6a). When the THF is evaporated from samples at 5 °C some of the polymersomes segregate to the top of the PBS, as was seen for extended time delays before evaporation. Removal of the THF at 20 °C yields polymersomes with an average D_h of ~ 1200 nm, as described above. Increasing the temperature to 37 °C and 70 °C led to decreased polymersome diameters of ~ 650 nm and 450 nm respectively (Figure 6b). Thus, using this rapid and simple method, polymersomes are formed upon addition of water, and these rearrange to stable polymersomes during the evaporation process with the final size able to be precisely controlled over the entire range from < 500 nm to > 2 μm by the temperature at which the THF is removed.[25]

Usually polymersome sizes increase when they are prepared at higher temperatures because the corona is more hydrated, hence the solvent-core interactions are greater and the vesicles reduce their curvature (i.e. grow) to minimize the core-solvent surface area.[26] In this case the trend is the opposite, probably because of the properties of the complex corona. The corona, peptide K, is a coiled-coil forming peptide that gradually changes conformation from α-helical to random coil as the temperature increases (Figure A2). This changing secondary structure increases the effective area per corona block, which may be the reason for the decrease in aggregation number.

When a period of particle growth in THF/PBS (at room temperature) was followed by THF evaporation at elevated temperatures, the growth in the mixed solvent phase again resulted in larger polymersomes in PBS, as was the case with evaporation at 20 ºC (Figure 6c). However, the polymersome sizes in PBS were predominantly determined by the temperature during THF evaporation rather than the particle size in THF/PBS. The samples prepared at 70 °C contain very few large polymersomes (Figure 6a), illustrating that the brief time of solvent evaporation at elevated temperature is sufficient for the molecular rearrangements that result in large scale structural changes.

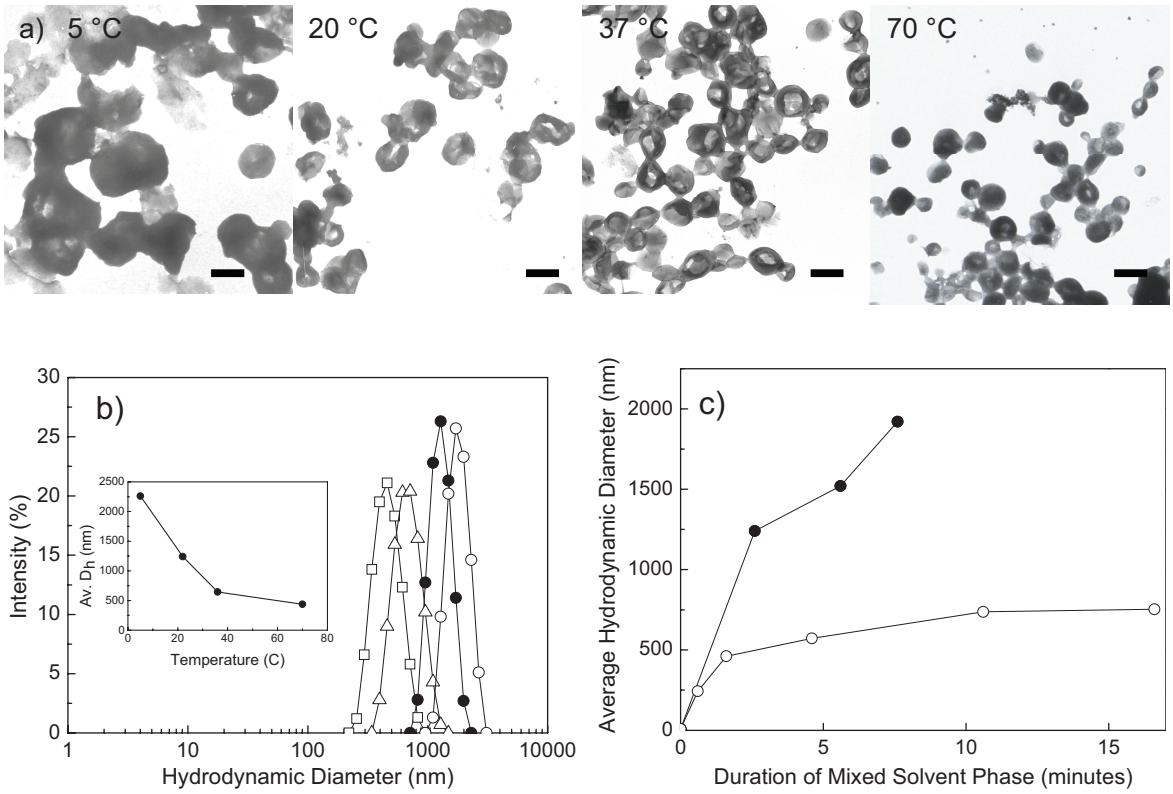


Figure 6. a) PTA stained TEM images of polymersomes prepared at different temperatures. Scale bars = 500 nm. b) The effect of the temperature at which the THF is evaporated on the D_h distributions of $PBLG_{50}$-K vesicles. Inset, average D_h as a function of temperature. c) The average D_h of $PBLG_{50}K$ as a function of the time between PBS addition and THF evaporation at 20 °C (●), and 70° C (○).

Osmolarity of aqueous phase

In all of the experiments described so far the aqueous phase was phosphate buffered saline of physiological ionic strength (50 mM phosphate, 100 mM KCl). At pH 7.0 the hydrophilic block of $PBLG_{50}$-K has a net charge of +3 (resulting from six positively charged lysine side chains and three negatively charged glutamic acid side chains), and the salt in the PBS is expected to affect the repulsion between charged head groups, and hence the self-assembly of the block copolymer. In order to investigate the sensitivity of polymersome size to salt content in the aqueous phase, polymersomes were prepared using aqueous solutions of a range of ionic strengths (Figure 7). In water the polymersome sizes were ~ $1/6^{th}$ the size of those prepared in physiological strength PBS. This is presumably because the absence of charge screening of the peptide K corona increases the repulsion between the charged peptides, resulting in a decrease of the aggregation number.[20] Above 0.5 mM buffer an abrupt increase in the polymersome size was observed, and at 5 mM buffer the particles had essentially the same size as with physiological ionic strength. To put this into perspective, at 5 mM buffer there is a (homogenous) charge density throughout the buffer of 0.03 charges/nm^3, in comparison to the charge density on peptide K of ~ 1 charge/nm^3, indicating a strong adsorption of counterions inside the corona layer.[27]

Without the charge screening the corona repulsion 'freezes' the structures at ~ 200nm: the larger polymersomes that were accessible in PBS by using low temperatures of THF evaporation, or by allowing for a period of growth prior to removing the THF are not accessible due to the strong charge repulsion between corona blocks. Also the conditions which reduce the polymersome size in PBS, such as using an elevated temperatures of THF evaporation or omitting the mixing step do not decrease the particle size in water because the repulsion within the corona overwhelms these effects. Hence the effect of salt on the polymersome sizes dominates the effect of temperature, which in turn dominates the duration of the mixed solvent phase.

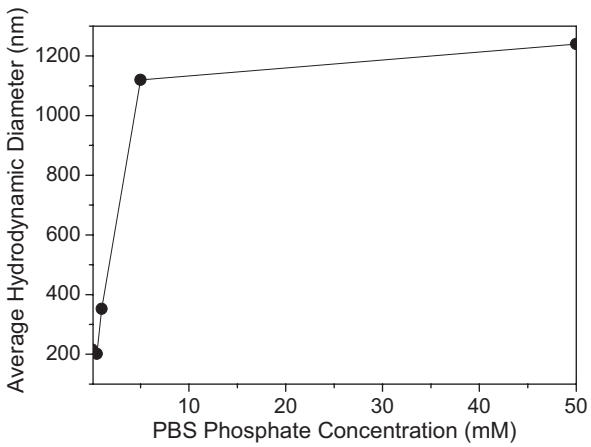


Figure 7. Average hydrodynamic diameter of $PBLG_{50}$-K vesicles as a function of ionic strength of the aqueous phase.

Regarding the salt content of the aqueous phase, this method to prepare polymersomes appears to be robust in comparison to the common slow water addition method followed by dialysis that was first published by Eisenberg and co-workers,[5] which for $PBLG_{50}$-K only worked when using water as the aqueous phase (Figure 8). When buffer was used (5 mM or 50 mM PBS), large undefined aggregates formed, presumably because the long period of stirring that this method required combined with the reduced electrostatic repulsion between sheets at higher ionic strength led to the collapse of hydrated structures.

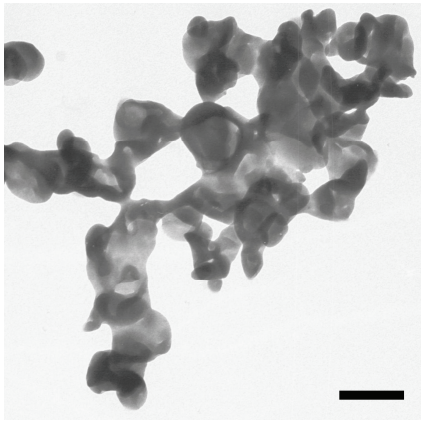


Figure 8. PTA stained TEM image of $PBLG_{50}$-K polymersomes prepared in water by the common slow water addition followed by dialysis method. Scale bar = 500 nm.

Mechanism of polymersome formation

The mechanism of polymersome formation using this method is likely to be similar to the gradual water injection method followed by dialysis, in which there is a structural evolution as water is added that is driven by changes in interfacial tension, core stretching, and repulsion between corona blocks. The most common route is structures of decreasing interfacial curvature, going from spherical micelles to rod-like micelles, lamellar sheets, which close to form polymersomes, and subsequent polymersome growth. Due to the rod-like blocks of $PBLG_{50}$-K the stability of planar interfaces is expected to be quite pronounced,[28] which may alter the route to polymersomes.[29] In the gradual water addition method water is injected very slowly to a solution of the block copolymer in an organic solvent, typically at a rate of ~ 0.2 wt% per minute, to allow for rearrangement of the polymer chains. The water content is increased in this way until the polymersomes are in frozen equilibrium (~ 10-50 wt%), and the organic solvent is then removed by dialysis.[6,16] In this water addition – solvent evaporation procedure the entire aqueous phase is added in less than 2 seconds, inducing rapid morphological reorganization. The structures are then adjusted and frozen by removing the organic solvent under reduced pressure. The reproducibility of the diameters and PDI of the polymersomes that this rapid water addition method yields, and the fact that polymersomes are the exclusive morphology, shows that the limited time available for large scale chain mobility is nevertheless sufficient for well-defined ordering of $PBLG_{50}$-K.

The properties of the polymersomes that form always depend on the characteristics of the block copolymer – and the range of possible block copolymers is what makes polymersomes so interesting. In general the sizes of polymersomes can be varied while the hydrophobic block is mobile. For $PBLG_{50}$-K the charged and structured corona block infers potential to regulate the polymersome sizes over a wide size range. The parameters that have been varied to precisely dictate the final polymersome size are the ratio of THF to PBS, the duration of the mixed solvent period, the temperature at which the THF is evaporated, and the salt content in the aqueous phase.

Different block copolymers

In order to test the scope of this simple technique it was also applied to range of different block copolymers, all of which yielded polymersomes. $PBLG_{35}$-K self-assembled into polymersomes of similar sizes and PDI to those composed of $PBLG_{50}$-K, but with less robust membranes, as seen by degree of collapse upon drying in TEM images (Figure 9a). The PBLG-K block copolymers were designed such that in aqueous solution the hydrophilic block, the designed peptide K, forms a noncovalent coiled-coil complex with peptide E, which has a complementary amino acid sequence.[30] E and K form a parallel dimer (denoted E/K), hence the binding of PBLG-K with E via coiled-coil folding results in a linear supramolecular diblock with the M_w of the corona twice that of PBLG-K.[31] In THF K and E do not fold into the coiled-coil conformation because the polarity is too low.[32] When the water-addition solvent-evaporation procedure was applied to an equimolar mixture of $PBLG_{35}$-K and E the resulting polymersomes were ~ 1/3rd the size of PBLG-K polymersomes (D_h ~ 400 nm, PDI 0.09, Figure 8b). The smaller polymersome diameters are expected because the larger area of the corona block in the polymeric complex increases the curvature of the corona-core interface.

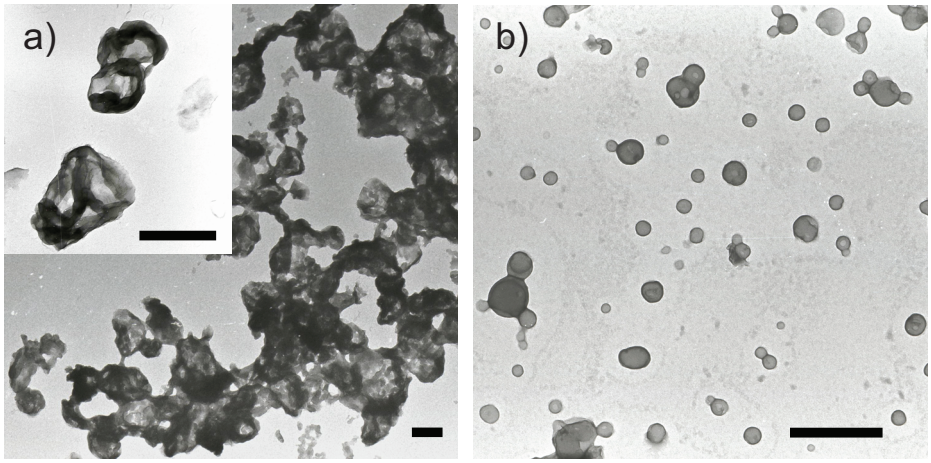


Figure 9. PTA stained TEM images of a) $PBLG_{35}$K polymersomes (inset showing extent of collapse), and b) polymersomes prepared with both $PBLG_{35}$K and E dissolved in the THF. Scale bars = 500 nm.

The method was also applied to a related series of block copolymers, $PBLG_n$-E. Whereas peptide K has a net charge of 3+, peptide E is negatively charged (3-) in PBS. Several $PBLG_n$-E block copolymers were used, with n varying from 37 to 100, and it was shown that all samples formed polymersomes (Figure 10). For $PBLG_{36}$-E the effect of each parameter on the final polymersome sizes was investigated in some detail, and all trends were the same as those observed for $PBLG_{50}$-K. The major difference between the self-assembly of the PBLG-K and PBLG-E block copolymers was that the sizes of the polymersomes formed from the PBLG-E series were significantly smaller than for the PBLG-K block copolymers (see Figure 11 for an example). The electrostatic interactions between corona chains therefore have a strong influence on which polymersome size is energetically favorable, as was described in detail for $PBLG_{50}$-K.

Thus far polymersomes have been prepared with negatively charged (E), positively charged (K), or neutral coronas (E/K). The ability of E and K to form a coiled coil during the solvent evaporation method allows the possibility of preparing polymersomes with different surface functionalities, tailored to particular applications.

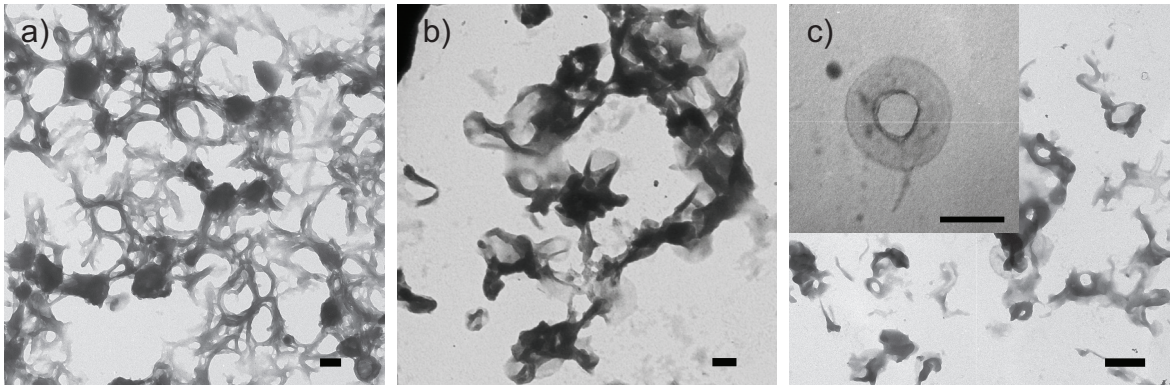


Figure 10. OsO4 stained TEM images of polymersomes prepared using a) $PBLG_{37}$-E, b) $PBLG_{80}$-E, and c) $PBLG_{100}$-E. OsO_4 stains hydrophobic substructures. Scale bars = 200 nm.

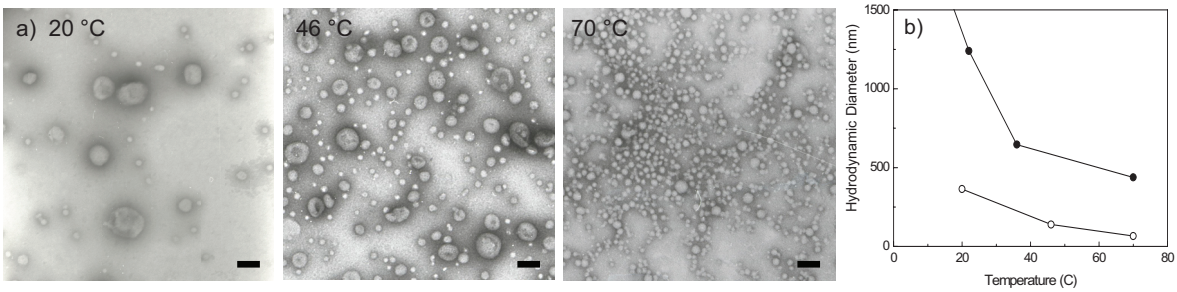


Figure 11. a) PTA stained TEM images of $PBLG_{37}$-E structures prepared at the temperatures indicated. Scale bars = 200 nm. b) The average D_h of $PBLG_{37}$-E structures (○) in comparison to $PBLG_{50}$-K polymersomes (●) as a function of the temperature at which the THF is evaporated.

The technique was additionally applied to traditional synthetic coil-coil block copolymers to further investigate its scope. PS_{106}-PAA_{17} is a polystyrene-*b*-poly(acrylic acid) with block proportions typical of those that have been demonstrated to pack into 'crew cut' polymersomes by the gradual water addition/dialysis method.[20] Using the water addition –

solvent evaporation technique PS_{106}-PAA_{17} formed well defined polymersomes with an average D_h of ~ 150 nm in water. In physiological strength PBS the polymersome sizes are larger, ~ 650 nm (Figure 12a, b), which is due to reduced repulsion between the ionic corona chains, as was also observed for the PBLG-K and PBLG-E series. The method was also employed with non-charged block copolymers that have been shown to form giant polymersomes by direct hydration. Two different poly(ethylene oxide)-*b*-polybutadiene block copolymers (PEO_{26}-PBD_{46} and PEO_{80}-PBD_{125}) formed polymersomes with average D_h values ranging from 180 nm to 350 nm in water and PBS (Figure 12c,d, Table 1), with the membrane thickness clearly depending on the M_n of the block copolymer.

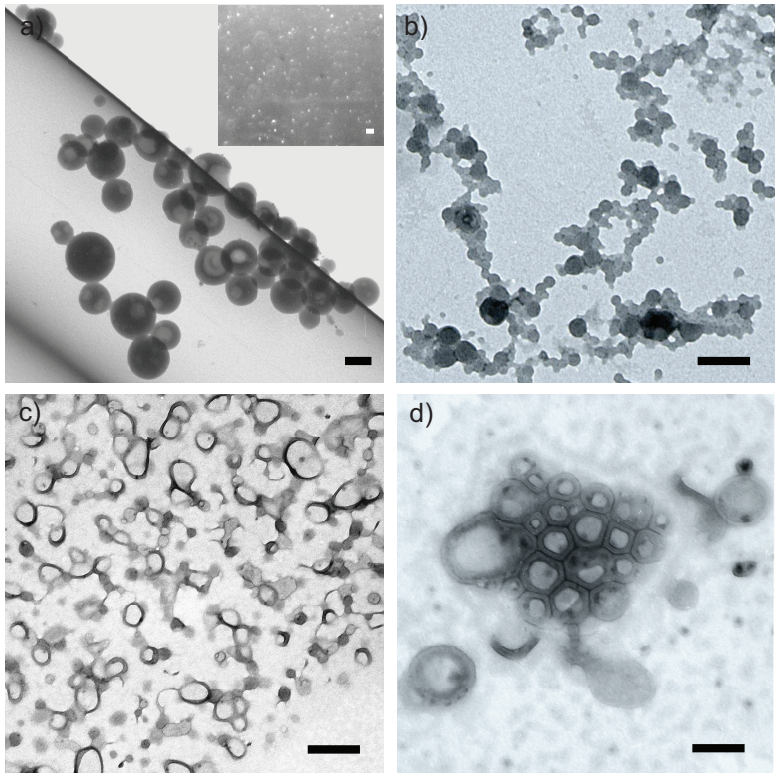


Figure 12. OsO4 stained TEM images of polymersomes prepared from a) PS_{106}-PAA_{17} in PBS (inset, optical microscope image), b) PS_{106}-PAA_{17} in H_2O, c) PEO_{26}-PBD_{46} in PBS, d) PEO_{80}-PBD_{125} in PBS. Scale bars = 200 nm.

Table 1. Different block copolymers to which the water addition – solvent evaporation (WA-SE) method was applied, together with the average hydrodynamic diameters of the polymersomes, and the average sizes using other polymersome preparation methods.

Sample	D_h using WA-SE method, nm		Other methods	D_h
	PBS[a]	Water[b]		
$PBLG_{50}$-K	1200	210	sonication[c]	undefined
$PBLG_{35}$-K	1173	165	sonication[c]	223 nm
$PBLG_{35}$-K/E	398		sonication[c]	152 nm
$PBLG_{37}$-E	192	168	sonication[c]	250 nm
$PBLG_{37}$-E/K	167		sonication[c]	170 nm
$PBLG_{37}$-E/K-PEG	130		sonication[c]	105 nm
$PBLG_{80}$-E	133	140	sonication[c]	385 nm
$PBLG_{100}$-E	149	132	sonication[c]	undefined
PS_{106}-PAA_{17}	600	150	-	-
PEO_{26}-PBD_{46}	200	350	Film hydration[33]	Microns
PEO_{80}-PBD_{125}	180	230	Film hydration[33]	Microns

[a] Conditions: 0.02 mg mL^{-1} block copolymer, 2 mL THF, 3 mL 50 mM PBS, pH 7.0, 20 °C THF evaporation.

[b] Conditions: 0.02 mg mL^{-1} block copolymer, 2 mL THF, 3 mL H_2O, 20 °C THF evaporation.

[c] In PBS, see Chapter 4.

CONCLUSIONS

In this Chapter a rapid, simple, robust, and tunable process for preparing polymersomes is demonstrated. Block copolymers that are molecularly dispersed in the organic solvent THF assemble into polymersomes upon quick addition of an aqueous phase. The fast addition of the aqueous phase does not negatively influence the final polymersome properties. The structures are frozen by evaporation of the THF under reduced pressure. The method itself is very robust, with the additional ability to adjust the polymersome sizes during water addition/solvent evaporation depending on the characteristics of the block copolymer in question. The potential of this method to tune the polymersome sizes is demonstrated with $PBLG_{50}$-K. Because $PBLG_{50}$-K has a charged and structured corona the temperature at which the THF is removed and the salt content of the aqueous phase determine the size of the polymersomes. By using different preparation parameters the same block copolymer assembles into polymersomes with the average size precisely specified within the 200 nm to 2 μm range. The approach is widely applicable as polymersomes were prepared from many types of block copolymers: peptide based rod-rod block copolymers having a range of hydrophobic block lengths, and with positively or negatively charged coronas, noncovalent polymer complexes, and synthetic charged and non-charged coil-coil polymers. The procedure is readily accessible as it requires only standard laboratory equipment, and takes less than five minutes, and a range of vesicle properties are readily accessible by varying the block copolymer/s used or simple procedural parameters.

EXPERIMENTAL SECTION

Materials

Peptides and peptide block copolymers were prepared and characterized as described in Chapter 4. The synthetic coil-coil block copolymers P697-StAA, P7252B-EOCL, P4753-BDEO, and P9055-BdEO were obtained from Polymer Source, Inc.. The molecular characteristics of the peptides and block copolymers are given in Table 1. Phosphate buffered saline, PBS: 30 mM $K_2HPO_4.3H_2O$, 19 mM KH_2PO_4, 100 mM KCl, pH 7.0. Rhodamine B was obtained from Fluka, and butylated hydroxytoluene stabilized tetrahydrofuran was from Biosolve.

Table 1. Molecular Characteristics of the Compounds used in this Study

Name	structure	M_n (g/mol)	PDI[3]
E	Ac-G(E I A A L E K)$_3$-NH_2	2380.6[1]	
$PBLG_{37}$-K	$PBLG_{37}$-G(K I A A L K E)$_3$-NH_2	10135[2,3]	1.3
$PBLG_{50}$-K	$PBLG_{50}$-G(K I A A L K E)$_3$-NH_2	13279[2,3]	1.5
$PBLG_{36}$-E	$PBLG_{36}$-G(E I A A L E K)$_3$-NH_2	10230[2,3]	1.1
$PBLG_{55}$-E	$PBLG_{55}$-G(E I A A L E K)$_3$-NH_2	14396[2,3]	1.3
$PBLG_{80}$-E	$PBLG_{80}$-G(E I A A L E K)$_3$-NH_2	19877[2,3]	1.4
$PBLG_{100}$-E	$PBLG_{100}$-G(E I A A L E K)$_3$-NH_2	24262[2,3]	1.4
$PBLG_{250}$-E	$PBLG_{250}$-G(E I A A L E K)$_3$-NH_2	57148[2,3]	1.7
PS_{106}-PAA_{17}		12240[4]	1.11[4]
PEO_{26}-PBD_{46}		3800[4]	1.04[4]
PEO_{80}-PBD_{125}		10400[4]	1.1[4]
PEO_{45}-PCL_{105}		15500[4]	1.4[4]

[1] Obtained from MALDI-TOF MS. [2] Based on a comparison of ^{1}H-NMR peaks. [3] GPC calibrated with polystyrene standards. [4] As specified by Polymer Source, Inc.. PBLG: poly(γ-benzyl L-glutamate), amino acids in the designed peptides are represented by their one letter codes, Ac: acetyl.

Preparation of polymersome suspensions

The majority of the polymersome suspensions were prepared as follows, with variations to this method described in the text. The block copolymer (0.02 μmol, or 0.01 μmol each of the PBLG-peptide block copolymer and the complementary peptide) was dissolved in 2 mL tetrahydrofuran (THF) in a 50 mL round bottomed flask. 3 mL of PBS was added in less than 2 seconds and vortexed for one minute at 200 rpm. The THF was evaporated using a rotary evaporator (40 rpm, water bath at 20 °C), yielding the polymersome suspensions. The final concentration of block copolymer was 6.7 μM.

For encapsulation experiments 2 μM rhodamine B in PBS was used. To test the permeability of the polymersomes 100 μL of 20 μM rhodamine B in PBS was added after vortexing.

For comparison with the current rapid preparation of polymersomes, samples were also prepared with the commonly used slow addition of the aqueous phase.[5,16] The block copolymer (0.02 μmol) was dissolved in 2 mL THF in a 50 mL round bottomed flask. 3 mL of PBS (5 mM and 50 mM) or water was added dropwise at a rate of 0.2 wt% (4 μL) per minute using a syringe pump (NE-300, just infusion, Prosense .B.V), while stirring at 700 rpm. The samples only contained well-defined aggregates (DLS) when there was no salt in the aqueous phase, and these were dialyzed against water at room temperature for at least 24 hours with at least 5 changes of buffer using dialysis tubing with a molecular weight cut-off of 1000 g/mol.

Characterization of polymersome suspensions

Circular Dichroism

Circular Dichroism spectra were obtained as detailed in the experimental section of Chapter 2, except that the temperature dependent spectra were measured in 5 °C intervals.

Dynamic Light Scattering

Dynamic light scattering was conducted as detailed in Chapter 3. To calculate the hydrodynamic diameter of objects in THF and mixtures of THF and water/PBS, viscosities and refractive indices of were used from reference 17.

Transmission Electron Microscopy

Transmission electron microscopy was conducted as detailed in the experimental section of Chapter 5.

Optical Microscopy

Differential interference contrast (DIC) and fluorescence optical micrographs were recorded with a Zeiss axiovert-200 inverted microscope equipped with a 63 x objective long-range working lens. The images were recorded with a black and white CCD camera (AxioCam MRm) connected to image-recording and -processing software (Axiovision 4.4).

Nuclear Magnetic Resonance

In order to quantify the amount of THF remaining in the PBS after the standard evaporation time ^{1}H-NMR spectra were recorded on a Bruker DPX300 spectrometer at room temperature. The proton resonance of water was used for calibration.

REFERENCES

1. Bangham, A. D.; Horne, R. W. *J. Mol. Biol.***1964,** 8, (5), 660-&.
2. Saunders, L.; Gammack, D.; Perrin, J. *J. Pharm. Pharmacol.* **1962,** 14, (9), 567-&.
3. Kita-Tokarczyk, K.; Grumelard, J.; Haefele, T.; Meier, W. *Polymer* **2005,** 46, (11), 3540-3563.
4. Nagayasu, A.; Uchiyama, K.; Kiwada, H. *Adv. Drug Deliv. Rev.* **1999,** 40, (1-2), 75-87.
5. Zhang, L. F.; Eisenberg, A. *Science* **1995,** 268, (5218), 1728-1731.
6. Chen, L.; Shen, H. W.; Eisenberg, A. *J. Phys. Chem. B* **1999,** 103, (44), 9488-9497.
7. Bellomo, E. G.; Wyrsta, M. D.; Pakstis, L.; Pochan, D. J.; Deming, T. J. *Nat. Mater.* **2004,** 3, (4), 244-248.
8. Yildiz, M. E.; Prud'homme, R. K.; Robb, I.; Adamson, D. H. *Polym. Advan. Technol.* **2007,** 18, (6), 427-432.
9. ONeil, C. P.; Suzuki, T.; Demurtas, D.; Finka, A.; Hubbell, J. A. *Langmuir* **2009,** 25, (16), 9025.
10. Discher, B. M.; Won, Y. Y.; Ege, D. S.; Lee, J. C. M.; Bates, F. S.; Discher, D. E.; Hammer, D. A. *Science* **1999,** 284, (5417), 1143-1146.
11. Lee, J. C. M.; Bermudez, H.; Discher, B. M.; Sheehan, M. A.; Won, Y. Y.; Bates, F. S.; Discher, D. E. *Biotechnol. Bioeng.* **2001,** 73, (2), 135-145.
12. Howse, J. R.; Jones, R. A. L.; Battaglia, G.; Ducker, R. E.; Leggett, G. J.; Ryan, A. J. *Nat. Mater.* **2009,** 8, (6), 507.
13. Shum, H. C.; Kim, J. W.; Weitz, D. A. *J. Am. Chem. Soc.* **2008,** 130, (29), 9543-9549.
14. Moscho, A.; Orwar, O.; Chiu, D. T.; Modi, B. P.; Zare, R. N. *Proc. Natl. Acad. Sci. U.S.A.* **1996,** 93, (21), 11443-11447.
15. Chapter 4, this thesis.
16. Shen, H. W.; Eisenberg, A. *J. Phys. Chem. B* **1999,** 103, (44), 9473-9487.
17. Saleh, M. A.; Akhtar, S.; Ahmed, M. S.; Uddin, M. H. *Phys. Chem. Liq.* **2001,** 39, (5), 551-563.
18. The method was tested with chloroform/methanol, DCM, and THF. Using $CHCl_3$/MeOH and DCM with 50 or 5 mM PBS or milli-Q water resulted in precipitation. With the water immiscible organic solvents monomodal size distributions with reasonably low PDI were observed in some instances with DLS, but macro aggregates were always visible.
19. $PBLG_{50}$-K is α-helical in THF, as determined by circular dichroism. The length of an average $PBLG_{50}$-K cylinder with complete α-helical secondary structure is 11 nm. The effective 'spherical' diameter of rods can be obtained by: L/ln(L/D), where L is the length of the rod, and D is the diameter. For PBLG50K this gives ~ 6.5 nm. For small objects the hydrodynamic diameter can be considerably larger than the actual object, hence a hydrodynamic diameter of 8 nm is in the expected range for an object with an effective diameter of 6.5 nm.
20. Soo, P. L.; Eisenberg, A. *J. Polym. Sci. Pol. Phys.* **2004,** 42, (6), 923-938.
21. Choucair, A. A.; Kycia, A. H.; Eisenberg, A. *Langmuir* **2003,** 19, (4), 1001-1008.
22. D. J. Adams, C. Kitchen, S. Adams, S. Furzeland, D. Atkins, P. Schuetz, C. M. Fernyhough, N. Tzokova, A. J. Ryan, M. F. Butler, *Soft Matter* **2009**, *5*, 3086.
23. Electron microscopy images of the intermediate structures, or of the particles prior to THF evaporation were not reliable due to evaporation of the THF during grid preparation, which could change the morphology of the structures.
24. Adding THF to decrease the H_2O:THF ratio decreases the hydrodynamic diameter.
25. Polymersomes form upon water addition to the THF solution, and their size is adjusted by the temperature at which the THF is evaporated. Note that when rhodamine B is added to polymersomes in the mixed solvent phase and then the THF evaporated at different temperatures all final polymersomes, be they larger or smaller than the polymersomes in the mixed solvent contain rhodamine B, hence during both size incease and size decrease processes the membrane in permeable.
26. Bryskhe, K.; Bulut, S.; Olsson, U. *J. Phys. Chem. B* **2005,** 109, (19), 9265.
27. Korobko, A. V.; Jesse, W.; Lapp, A.; Egelhaaf, S. U.; van der Maarel, J. R. C. *J. Chem. Phys.* **2005,** 122, (2).
28. Antonietti, M.; Forster, S. *Adv. Mater.* **2003,** 15, (16), 1323-1333.
29. He, X.; Schmid, F. *Macromolecules* **2006,** 39, (7), 2654.
30. Litowski, J. R.; Hodges, R. S. *J. Biol. Chem.* **2002,** 277, (40), 37272-37279.
31. Marsden, H. R.; Korobko, A. V.; van Leeuwen, E. N. M.; Pouget, E. M.; Veen, S. J.; Sommerdijk, N. A. J. M.; Kros, A. *J. Am. Chem. Soc.* **2008,** 130, (29), 9386-9393.
32. See Figure A1, Chapter 4.
33. Bermudez, H.; Hammer, D. A.; Discher, D. E. *Langmuir* **2004,** 20, (3), 540-543.
34. Ghoroghchian, P. P.; Li, G. Z.; Levine, D. H.; Davis, K. P.; Bates, F. S.; Hammer, D. A.; Therien, M. J. *Macromolecules* **2006,** 39, (5), 1673-1675.

APPENDICES

Addition of aqueous buffer

When PBS is added to the solution of $PBLG_{50}$-K in THF, polymersomes self-assemble, which are observed to increase in time with DLS and optical microscopy (Figure A1). This effect could be due to polymersome ripening, fusion, or aggregation, or a combination of the three. DLS is not well suited to distinguish between these phenomena. With optical microscopy the particles were sometimes observed in pairs as they diffused through the solution, although a fusion event was not observed. The large particles that are present after ~ 20 minutes do not appear to be clusters of smaller ones. However, the resolution of the particles is not great, therefore fusion and/or aggregation cannot be ruled out. For the predominant growth mechanism to be ripening or fusion, the PBLG blocks must be mobile under these solvent conditions (2:3 v/v THF:PBS), and the particles may slowly approach the thermodynamic particle size. The experiment was repeated with a lower ratio of THF to PBS (0.5:3 v/v THF:PBS). The particles were smaller (average D_h ~ 650 nm, PDI ~ 0.2) and there was no particle growth (Figure A1). These two differences could be because the PBLG chains are effectively immobile in the more polar mixture, and the particles are therefore unable to ripen or fuse, or alternatively this may be the equilibrium size in this solvent mixture. The equilibrium size of polymersomes depends in part on the effective size of the corona K, which is expected to be larger in more polar solvent mixtures as then the K-solvent interaction is greater (Yu, Y. S.; Zhang, L. F.; Eisenberg, A. *Macromolecules* **1998,** 31, (4), 1144-1154. Adams, D. J.; Kitchen, C.; Adams, S.; Furzeland, S.; Atkins, D.; Schuetz, P.; Fernyhough, C. M.; Tzokova, N.; Ryan, A. J.; Butler, M. F. *Soft Matter* **2009,** 5, (16), 3086-3096).

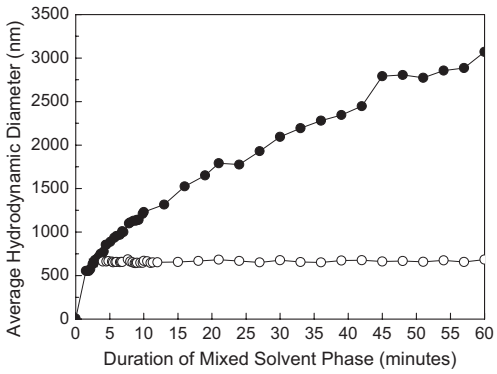


Figure A1. The change in average D_h of $PBLG_{50}K$ assemblies with time after addition of PBS (2:3 v/v THF:PBS (●), 0.5:3 v/v THF:PBS (○)).

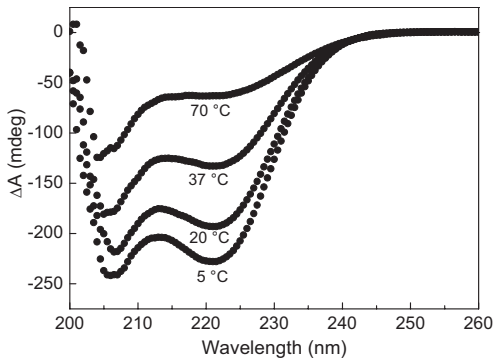


Figure A2. CD spectra of K at increasing temperatures. Conditions: [K] = 2 mg/mL, PB

A REDUCED SNARE MODEL FOR MEMBRANE FUSION

Let's get together: A minimal model system was developed to mimic the SNARE-protein-mediated fusion of biological membranes. Fusion between two populations of liposomes is controlled by a pair of complementary lipidated oligopeptides that form noncovalent coiled-coil complexes and thereby force the membranes into close proximity to promote fusion. The model system displays the key characteristics of in vivo fusion events.

INTRODUCTION

Membrane fusion is a key process in all living cells, as it facilitates the transport of molecules between and within cells. The process is triggered by the specific interaction of fusion proteins. This interaction brings two membranes into close proximity and is followed by local disruption of the lipids and merging of the membranes.[1] The required protein recognition for the fusion of transport vesicles with the neuronal membrane involves the coiled-coil interaction between three complementary SNARE proteins (SNARE=soluble NSF attachment protein receptor; NSF=N-ethylmaleimide-sensitive factor).[2] To induce intracellular transport, a four-helix coiled-coil bundle forms between two membrane-bound SNARE proteins and a cytoplasmic SNARE protein and forces the two membranes within a distance of 2–3 nm from one another (Figure 1c).[3] The exact mechanism and fundamental requirements of fusion are still unknown.[4] Reduced systems have therefore been studied to gain insight into the most important aspects of membrane fusion.[5]

In vivo membrane fusion is a highly controlled process. To mimic this process, model systems must include the following features: Specific molecular recognition must lead to the merging of lipid bilayers, liposome-content mixing must occur without leakage, i.e., with no rupture of the membranes, and there must be an increase in liposome size. Additionally, the fusion process must be inhibited by inverted cone lipids, as these lipids hinder the formation of the low-energy stalk intermediate,[6] and it should not be dependent on membrane curvature stress. However, none of the model systems so far have displayed all of the basic characteristics of native membrane fusion.[5] To date, the major unresolved question has been: What is the minimal machinery required for the controlled fusion of lipid membranes? This question is answered herein with a model system that contains simplified versions of SNARE proteins. These model proteins can cause liposome fusion with the key characteristics of native membrane fusion. In this novel approach, the operative features of SNARE proteins were used to create a simple and applicable membrane-fusion model.

RESULTS AND DISCUSSION

Two lipidated oligopeptide hybrids (LPE and LPK) were designed which possess all of the functional aspects of membrane-bound SNARE proteins (Figure 1). The protein-recognition domain of SNARE proteins is an eight-heptad repeat segment with a high propensity to form coiled coils.[7] This segment is connected through a flexible linker to a transmembrane domain that anchors the protein to the lipid membrane. In the design of the lipidated oligopeptides LPE and LPK, the recognition domain is mimicked by two three-heptad repeat coiled-coil-forming peptides (E and K, Figure 1a). These oligopeptides are the shortest known coiled-coil pair to assemble specifically into a stable heterodimer (Kd $\approx 10^{-7}$ M).[8] In this model system, the formation of the LPE/LPK complex is the driving force to bring two different liposomes close together. The role of the flexible spacer is fulfilled by a short poly(ethylene glycol) chain (PEG_{12}, Figure 1a). This spacer enables extension of the oligopeptide component from the surface of the liposomes. The lipidated oligopeptides are anchored spontaneously in the membrane by means of a phospholipid tail, 1,2-dioleoyl-sn-glycero-3-phosphatidylethanolamine (DOPE),[9] which mimics the function of the transmembrane domain of SNARE proteins (Figure 1a).

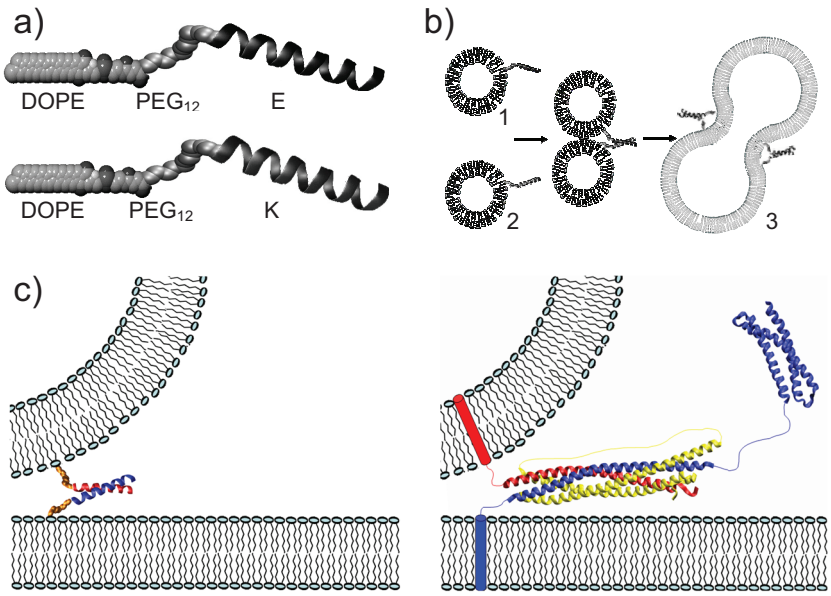


Figure 1. a) Space-filling model of the lipidated oligopeptides LPE and LPK, consisting of a DOPE tail linked through a PEG_{12} spacer to the coiled-coil-forming oligopeptides E and K. The amino acid sequence of E is $G(EIAALEK)_3$-NH_2, and that of K is $(KIAALKE)_3GW$-NH_2. b) The spontaneous incorporation of the DOPE tail in lipid bilayers results in liposomes decorated with either E or K peptides at the surface. When a liposome population carrying LPE (1) is mixed with a liposome population carrying LPK (2), coiled-coil formation (E/K) initiates liposome fusion (3). c) Comparison of the minimal model (left) with the SNARE-protein-based model (right).

Liposomes decorated with either LPE or LPK (3 mol%) were prepared with a nominal hydrodynamic diameter of 100 nm and a polydispersity index of approximately 0.2, as determined by dynamic light scattering (DLS).[10] The peptides were designed in such a way that heterodimers were stable, and homodimers would not form upon mixing.[8] However, as a result of the forced close proximity of the peptides anchored to the surface of the membrane, homocoils were present on these individual liposomes before mixing, as determined by circular dichroism (CD; Figure 2a). Nevertheless, like plain liposomes, LPE- or LPK-decorated liposomes did not show any self-fusion over time (as shown by DLS; Figure 2). Upon mixing of the decorated liposome populations, an immediate change in the peptide quaternary structure was observed by CD. The change in the CD spectrum was indicative of a transition from homocoiled LPE or LPK at the surface of the liposomes to aggregated heterocoils.[11] The observed change in peptide structure was accompanied by an increase in the hydrodynamic radius of the particles from approximately 100 nm to greater than 1 mm within 20 min (Figure 2).

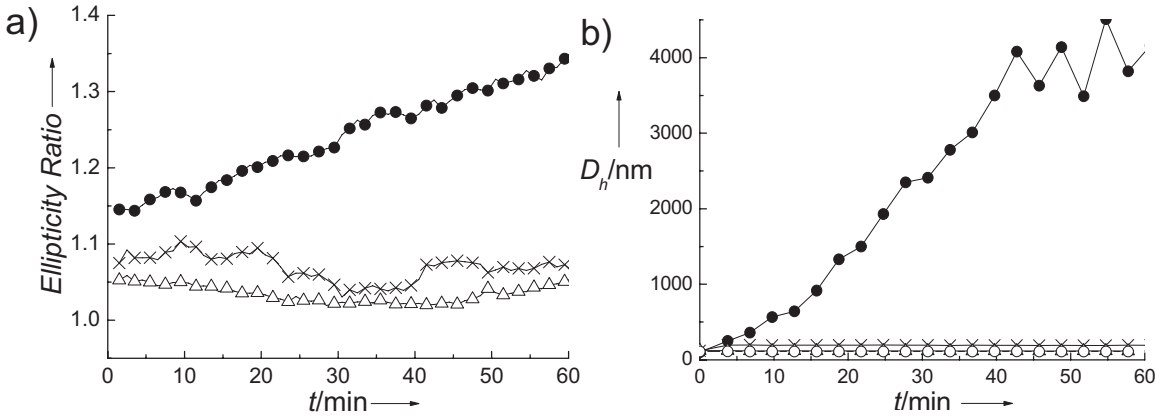


Figure 2. a) Ellipiticity ratios measured by CD of LPE- (Δ) and LPK-modified (×) liposomes. Upon mixing of these liposome batches, the aggregation of coiled coils was observed (●). b) The hydrodynamic diameter, D_h, measured by DLS, increased rapidly when the LPE- and LPK-decorated liposome populations were combined (●). In control experiments (with plain liposomes (○), plain liposomes mixed with LPE-decorated liposomes (Δ), and plain liposomes mixed with LPK-decorated liposomes (×)), no significant change in the hydrodynamic diameter was observed with time.

In the process of liposome fusion, three stages are distinguished, each of which requires energy input to overcome an energy barrier. In the first step, liposomes are brought into close proximity; merging of the outer lipid layers then occurs, followed by mixing of the inner lipid layers. From the initial fusion experiments, it was concluded that the energy gained by the formation of LPE/LPK coiled coils (ca. 14 kT per dimer; see Figure A1 in the Appendices) is sufficient to induce the aggregation of the two liposome populations. However, it is not sufficient to bring membranes into close proximity for membrane fusion to occur;[12] energy must also be provided for the second and third stages. Fluorescence experiments were conducted to determine whether the LPE/LPK interaction also transmits

enough force to the membranes to rearrange the lipids and hence promote lipid mixing followed by content mixing. The efficiency of lipid mixing was determined by using a fluorescence resonance energy transfer (FRET) assay. An LPK-decorated liposome batch was prepared with the donor dye nitrobenzofuran (NBD) and the acceptor dye lissamine rhodamine (LR) attached to the lipid-bilayer surface. A high FRET efficiency resulted from the short fluorophore distance. Upon mixing with a population of LPE-decorated liposomes, an increase in NBD emission was observed as a result of an increase in the distance between the membrane-bound donor and acceptor dyes (Figure 3a). This finding demonstrated that the formation of the LPE/LPK coiled-coil complex is sufficient to overcome the energy barrier that keeps undecorated liposomes apart and also results in at least hemifusion (i.e. lipid mixing of the outer lipid layers). As the fusion process can be halted at the hemifusion stage,[13] further experiments were conducted to ascertain whether the formation of the LPE/LPK complex also leads to mixing of the inner lipid layers. Therefore, the donor fluorophores on the outside of the LPK-decorated liposomes were deactivated to eliminate the FRET effect on the outer layer of the liposomes. Again, upon the addition of LPE-decorated liposomes, an increase in NBD fluorescence was observed. Thus, the merging of both the outer and the inner lipid layer, that is, complete fusion, does indeed occur (Figure 3a). Liposome fusion is used in biological systems to mix the contents of liposomes and hence to transmit chemical compounds and signals. There have been reports of lipid mixing in model systems without content mixing;[14] it was therefore investigated whether the lipid mixing in this system was accompanied by content mixing. The slightly fluorescent complex terbium citrate was encapsulated in LPK-modified liposomes, and the nonfluorescent ligand dipicolinic acid (DPA) was encapsulated in LPE-modified liposomes. When these two batches of liposomes were combined, an increase in fluorescence caused by the formation of the highly fluorescent terbium dipicolinic acid chelation complex[15] was observed (Figure 3b). From this result, it was concluded that membrane mixing resulted in content mixing. The input of too much energy can cause major destabilization of the lipid bilayers and lead to the occurrence of fusion not via the lowest-energy intermediate, but through the uncontrolled rupture of the liposomes accompanied by massive content leakage.[6] To determine whether this model was able to fuse liposomes without content leakage, ethylenediaminetetraacetic acid (EDTA) was added after a fusion experiment between LPK- and LPE-modified liposomes. If fusion proceeds without content leakage, the $Tb(DPA)_3^{3-}$complex should not be quenched by the strong chelator EDTA, which is unable to diffuse into the liposomes. Indeed, no decrease in fluorescence was observed (Figure 3b). These results show that the LPE/LPK-mediated liposome fusion proceeds in a controlled way, similar to the natural SNARE-mediated fusion process. Theoretical and experimental studies indicate that a key feature of all types of fusion between biological membranes is that they proceed through a stalk intermediate, which reduces the number of lipids involved in the fusion intermediates.[6,16] Phospholipids with a packing parameter of less than 0.5[17] have a spontaneous positive membrane curvature, which inhibits the stalk intermediate geometrically and reduces membrane

fusion.[18] To prove that the current model system mimics biological membrane-fusion events, oleoyl lysophosphatidylcholine (packing parameter ≈ 0.4) was added to the LPE- and LPK-bearing liposome populations. Upon mixing, fusion was inhibited, as concluded from the decrease in lipid mixing (Figure 3a). This result indicates that the stalk intermediate is also part of the fusion process in this model system.

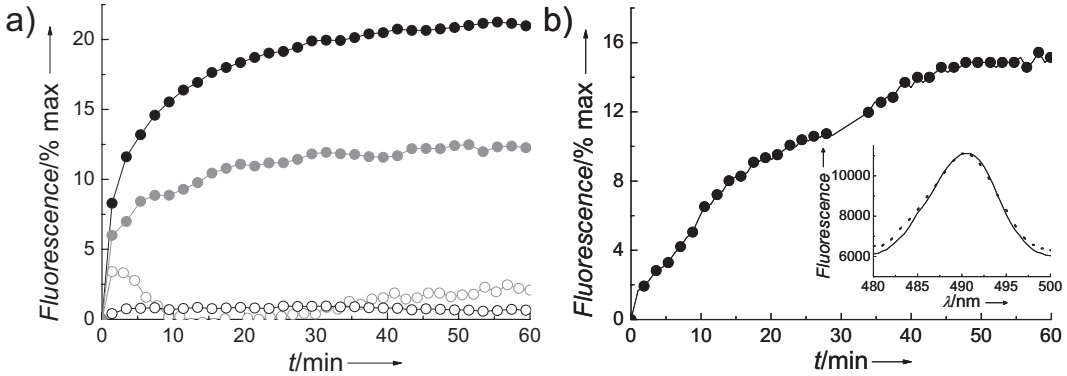


Figure 3. a) Lipid mixing between liposomes as indicated by an increase in NBD emission. Mixing of LPE- and LPK-decorated liposomes: ●; mixing of plain liposomes: ○; mixing of inner-layer lipids when LPE- and LPK-decorated liposomes were combined: ●. Lipid mixing was inhibited when LPE- and LPK-decorated liposomes containing oleoyl lysophosphatidylcholine (15 mol%) were mixed (○). b) Mixing of the aqueous compartments of decorated liposomes with encapsulated $Tb(citrate)_3^{3-}$ and DPA resulted in a fluorescence increase due to the formation of $Tb(DPA)_3^{3-}$. Inset: The content mixing proceeds without leakage, as the fluorescence intensity remains constant before (—) and after (····) the addition of the fluorescent quencher EDTA outside the fused liposomes.

For this system to be a true analogue of SNARE-mediated liposome fusion, it should be shown that curvature stress is not a driving force.[19] Cryo-TEM demonstrated that the fusion of LPE- and LPK-modified liposomes (Figure 4) resulted in the formation of larger liposomes in less than 1 min, a result indicative of fast docking and fusion events. The fused liposomes had complex, highly curved internal membrane morphologies. Thus, the fusion process is indeed not driven by a release of curvature strain in the membrane. The cryo-TEM data also support the observation that no leakage occurs during fusion. In the absence of leakage, the fusion of liposomes does not affect the total amount of lipid or the enclosed volume; therefore, fusion should result in liposomes with an excess of lipid. The observed folding of the bilayers to the interior of the liposomes, in combination with the terbium leakage assay, demonstrates that no or only limited exchange occurs between the interior aqueous phase of the liposomes and the surrounding medium.

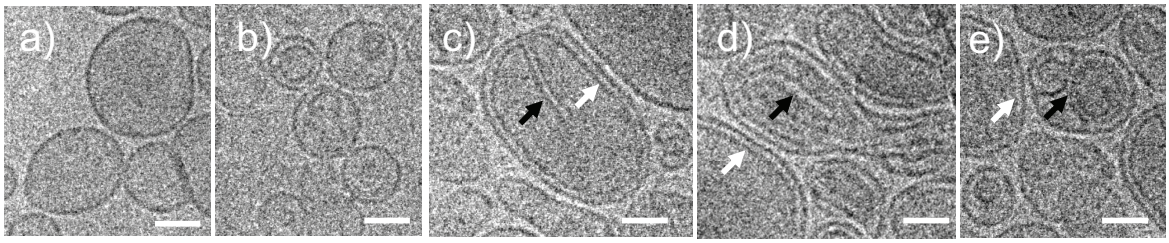


Figure 4. Cryo-TEM images showing fusion: a) LPE- and b) LPK-decorated liposomes; c–e) liposomes with complex membrane morphologies formed 30 s after the mixing of LPE- and LPK-modified vesicles. After fusion, the vesicles show double bilayers (white arrows) and invaginations (black arrows). Scale bars: 50 nm.

To further investigate the hypothesis that the fusion events are not affected by curvature stress, LPE- and LPK-modified liposome populations were prepared with a diameter of approximately 1 mm. These LPE- and LPK-modified liposomes did not change in size with time; however, fusion occurred upon mixing, and liposomes with diameters in the tens of microns were observed by optical microscopy[20] (Figure 5). Further analysis of the optical microscopy data showed that liposomes with a diameter of the order of 10 mm were also able to undergo fusion: a process reminiscent of cell–cell fusion[21] (Figure 5, inset). The specific fusion of liposomes of these dimensions proves that curvature stress is not the driving force for fusion in this model system.

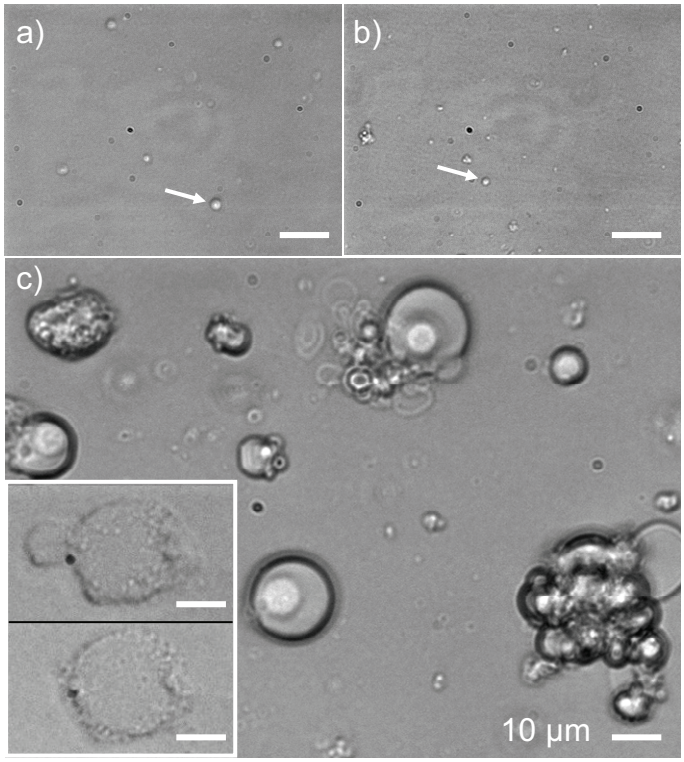


Figure 5. Optical microscopic images of large a) LPE- and b) LPK-functionalized liposomes before fusion. The liposomes are white; examples of liposomes are indicated by arrows. c) Upon mixing, giant liposomes were observed. Inset: Fusion of cell-sized liposomes. Scale bars: 10 mm.

There are two approaches to studying membrane fusion. One is to use known native fusogenic proteins, which can be expressed and studied in vitro or used in native fusogenic systems. Owing to the participation of multiple, often interacting, proteins prior to the actual membrane-fusion step in native systems, it is very difficult to isolate the effect of particular proteins.[22] The other, bottom-up approach enables the determination of the fundamental requirements, the scope, and the limitations of controlled lipid-membrane fusion; however, until now, the mode of recognition has been unrelated to that of natural SNARE-protein-based systems. Furthermore, to date none of the in vitro model systems that have been developed to mimic membrane fusion have met all the key requirements typical for in vivo membrane-fusion systems. The lipidated oligopeptides that were used bridge these two approaches. They are on the one hand analogues of SNARE proteins in the sense that membrane fusion occurs by the same recognition mechanism, and they display the same key characteristics. Therefore, the results are more directly applicable to native membrane fusion. On the other hand, as the shortest known hetero coiled coil is used in this model, they are the most reduced form of SNARE proteins possible, which makes them simple enough to enable ready synthesis and the use of a range of physical organic techniques to study their behavior. The reduced SNARE model presented herein has been shown to meet all of the characteristics of native membrane fusion, and this similarity combined with the ease of use makes the system a true minimal model for SNARE mediated membrane fusion. This fusion system extends the realm of synthetic biology and enables us to understand an aspect of nature—liposome fusion in eukaryotic cells— through mimicry. It may also lead to new functions, such as the directed delivery of encapsulated reagents to cells or liposomes.

EXPERIMENTAL SECTION

Materials and Methods

Materials

Fmoc-protected amino acids and Sieber Amide resin (0.62 mmol of NH_2 g^{-1} of resin) were purchased from Novabiochem. Fmoc-NH-PEG_{12}-COOH was purchased from IRIS Biotech. DOPC was purchased from Avanti Polar Lipids, DOPE was purchased from Phospholipid, and cholesterol was obtained from Fluka. DOPE-NBD and DOPE-LR were obtained from Avanti Polar Lipids. $TbCl_3 \cdot 6H_2O$ (99.9% pure) and sodium citrate, were purchased from Sigma-Aldrich. Dipicolinic acid (DPA, pyridine-2,6-dicarboxylic acid) (≥99.5%) and octaethylene glycol monododecyl ether were obtained from Fluka. All other reagents and solvents were obtained at the highest purity available from Sigma-Aldrich or BioSolve Ltd. and used without further purification. Milli-Q water with a resistance of more than 18.2 MΩ cm^{-1} was provided by a Millipore Milli-Q filtering system with filtration through a 0.22 μm Millipak filter. Phosphate buffered saline, PBS: 5 mM KH_2PO_4, 15 mM K_2HPO_4, 150 mM NaCl, pH 7.4.

General Methods

RP-HPLC was performed with a Shimadzu HPLC system with two LC-8A pumps, and an SPD-10AVP UV-VIS detector. Sample elution was monitored by UV detection at 214 nm and 256 nm. Samples were eluted with a linear gradient from A to B, A being 22.5% (v/v) H_2O, 0.1% (v/v) TFA in CH_3OH, and B 10% (v/v) CH_3OH, 0.1% (v/v) TFA in acetonitrile. Purification of the peptides and hybrids was performed on a Vydac C4 reversed phase column (214TP1022, 22 mm diameter, 250 mm length, 10.00 μm particle size) with a flow rate of 20 mL min^{-1}. For verification of sample purity a reversed phase Vydac C4 column (214TP54, 4.6 mm diameter, 250 mm length, 5.00 μm particle size) was used with a flow rate of 1 mL min^{-1} and a gradient of 10% – 100% B over 60 minutes. Sample elution was additionally monitored by an evaporative light scattering detector. MALDI-TOF mass spectra were acquired using an Applied Biosystems Voyager System 6069 MALDI-TOF spectrometer. Samples were dissolved in 1:1 (v/v) 0.1% TFA in water:acetonitrile (TA), at concentrations of ~0.3 mg mL^{-1} for K and E and ~3 mg mL^{-1} for LPE and LPK. Solutions for spots consisted of (v/v) 1:10 sample solution: 10 mg mL^{-1} ACH in TA. ^{1}H-NMR spectra were recorded on a Bruker DPX300 spectrometer using the residual proton resonance of deuterated methanol for calibration. FPLC was performed with an Äkta prime, Amarsham Pharmacia Biotech apparatus with a Pharmacia XK 26 column (135 mm x 25 mm) packed with Sephadex G50-fine. PBS was used as the eluent. The flow rate was 5 mL min^{-1}, UV sensitivity was set on 0.1 AU, 1%, the conductivity was set on 15-20 mS cm^{-1} and the wavelength for UV recording was 254 nm. Differential interference contrast (DIC) optical micrographs were recorded with a Zeiss axiovert-200 inverted microscope equipped with a 63 x objective long-range working lens. The images were recorded with a black and white CCD camera (AxioCam MRm) connected to an image-recording and –processing system (Axiovision 4.4).

Lipopeptide synthesis

The peptide components of LPE and LPK were prepared with standard solid-phase peptide synthesis protocols using Fmoc chemistry on an Applied Biosystems 431A automated peptide synthesizer, with a PL-Sieber Amide resin on a 0.25 mmol scale. The peptide coupling reagent was HCTU. The N-terminal Fmoc was removed with 20% (v/v) piperidine in NMP. After the peptide component was prepared, the resin was removed from the reaction vessel and Fmoc-NH-PEG_{12}-COOH was coupled to the immobilized peptides. The resin was swollen in NMP for 1 hour. 2.5 equivalents of Fmoc-NH-PEG_{12}-COOH and 2.5 equivalents of HCTU were dissolved in NMP (20 mL) and mixed with 5 equivalents of DIPEA. After pre-activation for 1 minute the mixture was added to the peptide-resin and shaken for 20 hours. The uncoupled amines were capped with 0.05 M acetic anhydride, 0.125 M DIPEA in NMP. The N-terminal Fmoc was removed with 20% (v/v) piperidine in NMP. The resin was washed thoroughly with 10 x 10 mL NMP, and 10 x 10 mL DCM. Next, succinic anhydride was coupled to the immobilized peptide-PEG. The resin was swollen in NMP. 5 equivalents of succinic anhydride were dissolved in NMP (20 mL) and mixed with 6 TEA. The mixture was added to the resin and shaken for 15 hours. The resin was washed thoroughly with 10 x 10 mL NMP, and 10 x 10 mL DCM. DOPE was coupled to the immobilized peptide-PEG_{12}-succinic acid in the same way, except that 3 equivalents of DOPE, 3 equivalents of HCTU, and 6 equivalents of DIPEA were used, and 1:1 (v/v) NMP:DCM was used to swell the resin and to couple the DOPE. After the peptide synthesis and after each subsequent coupling step the synthesis was tested by MALDI-TOF mass spectroscopy. Cleavage from the resin and deprotection was carried out by shaking 15 mg resin with 95:2.5:2.5 (v/v) TFA:water:TIS for one hour. The cleavage mixture and three subsequent rinses of the resin with the TFA mixture were added drop-wise to cold diethylether. The white precipitate was compacted with centrifugation and the supernatant removed. This was repeated three times with the addition of fresh diethylether. The pellets were dried in air or under reduced pressure. Bulk cleavage of the compounds was performed in the same way except using 47.5:47.5:2.5:2.5 (v/v) TFA:DCM:water:TIS for one hour.

The crude products of were purified by RP-HPLC, with gradient elution 30% to 80% B over 15 minutes for LPE, and 10% to 60% B over 15 minutes for LPK. After purification the compounds were lyophilized to give white powders. LPE had a yield of 7%, MALDI-TOF MS: M_n = 3768.9 g mol^{-1}. LPK had a yield of 22%, MALDI-TOF-MS: M_n = 3951.9 g mol^{-1}. The purity of the compounds was confirmed by means of RP-HPLC, MALDI-TOF MS, and ^{1}H-NMR. For each compound the purity was estimated from RP-HPLC to be greater than 95%.

Liposome Preparation

1mM lipid stock solutions were made in chloroform with the composition DOPC/DOPE/CH 50:25:25 mol%. For fluorescence studies a 1 mM lipid stock solution was made in chloroform with the composition DOPC/DOPE/CH/DOPE-LR/DOPE-NBD 49.5:24.75:24.75:0.5:0.5 mol%. To investigate the effect of lipids with positive curvature on lipid mixing 1 mM lipid stock solutions were made in chloroform with the composition DOPC/DOPE/CH/OLPC 42.5:21.25:21.25:15 mol% and DOPC/DOPE/CH/OLPC/DOPE-LR/DOPE-NBD 42.08:21.04:21.04:15:0.43:0.43 mol%. 1mM hybrid stock solutions were made in 1:1 (v/v) chloroform: methanol. Unless otherwise stated, liposome solutions are 1 mM in PBS. Three types of liposome solutions were prepared: plain liposomes, liposomes with 3 mol% LPE (97:3 (v/v) lipid stock solution: LPE stock solution), and liposomes with 3 mol% LPK (97:3 (v/v) lipid stock solution: LPK stock solution). To prepare small unilamellar vesicles the solvent was removed from the stock solution (2 mL) using a rotary evaporator to get a lipid film. Following this PBS (2 mL) was added to prepare a 1 mM liposome solution. The sample was vortexed for 1 minute and sonicated in a bath sonicator at 45 °C to 50 °C to get small unilamellar vesicles (this takes approximately 5 minutes and 2 minutes for plain and decorated liposomes respectively). The hydrodynamic diameter as determined by DLS was approximately 100 nm.

Liposome preparation for lipid mixing assay

The mixing of lipids between batches of liposomes was assayed according to (Struck, D Biochemistry 20, **1981**, 4093-4099). Fluorescence experiments were carried out with the Fluorescent Resonance Energy Transfer (FRET) pair DOPE-NBD (λ_{ex}= 460 nm λ_{em}= 534 nm) and DOPE-LR (λ_{ex}= 550 nm λ_{em}= 590 nm). Fluorescent LPK decorated liposomes were prepared (DOPC/DOPE/CH/DOPE-LR/DOPE-NBD 49.5:24.75:24.75:0.5:0.5 mol%). LPE decorated liposomes had no fluorescent labels.

Decorated liposome preparation for inner leaflet mixing assay

Reduction of DOPE-NBD/DOPE-LR containing vesicles with sodium dithionate ($Na_2S_2O_6$) resulted in liposomes with selectively eliminated fluorescence from the outer leaflet. For this assay, 2.5 mM fluorescent liposomes decorated with LPK were prepared. The fluorescence intensity of the sample was measured with a Varian UV-visible Spectrophotometer model Cary 3 Bio that excited the NBD (λ_{ex}= 460 nm) at 460 nm. Then, 10 vol% of the sample was replaced by a 20 mM solution of $Na_2S_2O_6$ in PBS. Hereafter, the fluorescence intensity was monitored with the UV Spectrophotometer and 2 minutes after equilibration, the $Na_2S_2O_6$ was removed by injecting the sample into an FPLC column. The liposome concentration was corrected for the column dilution, and the fluorescence intensity at 460 nm was measured by UV Spectroscopy and the CD intensity of the sample was measured. The final liposome concentration was typically 0.3 mM. The 10 vol% non-reduced liposome sample was diluted to the same final concentration. LPE decorated liposomes without the FRET pair as well as undecorated liposomes were made with the same final concentration for the mixing experiment.

Decorated liposome preparation for contents mixing assay

The mixing of aqueous contents between batches of liposomes was assayed according to (Wilshut, J Biochemistry **1980**, 26, 6011-6021). For this assay, 2.5 mM liposomes were prepared. LPK decorated liposomes were prepared in PBS containing 50 mM DPA, 20 mM NaCl and 100 mM NaOH (to prepare the sodium salt of DPA). LPE decorated liposomes were prepared in PBS containing 2.5 mM $TbCl_3$ and 150 mM sodium citrate. A sample of undecorated liposomes was prepared with the Tb solution. The Tb and DPA solutions had been filtered over a 200 nm filter. Liposomes were prepared from the films by first adding 500 μL of the Tb or DPA solutions in PBS and after 3 minutes of sonication 1.5 mL more was added. These solutions were added in two steps to promote a higher concentration of DPA or Tb encapsulation in the liposomes. Immediately after preparation, the unencapsulated solution was removed by passing the liposomes over the FPLC column that used a PBS buffer. Hereafter, the liposome concentration was corrected for the column dilution and the CD intensity of the sample was measured. The three different batches were taken to the same final concentration with PBS to allow 1:1 mixing for the experiments. The final concentration of the samples was typically 0.4 mM.

Preparation of large unilamellar vesicles/ large multilamellar vesicles (LUVs/LMVs). LUVs/LMVs were prepared according to a slight variation of the solvent evaporation method of (Moscho, A.; Orwar, O.; Chiu, D. T.; Modi, B. P.; Zare, R. N *Proc. Nat. Acad. Sci. U.S.A.* **1996**, 93, 11443-11447). In a 50 mL round bottom flask 1970 μL lipid stock solution (1 mM), 100 μL methanol, 30 μL hybrid stock solution (1 mM) were combined. 3 mL of 17 mM PBS was carefully added. The organic solvents were evaporated for 2 minutes using a rotary evaporator at 40 rpm and with the water bath at 40 °C. This yields 0.33 mM liposomes that are approximately 500 – 1000 nm in diameter.

Characterization of Liposomes

Circular Dichroism

CD spectra were obtained as detailed in the experimental section of Chapter 2. For CD time series measurements were started immediately after the solutions were mixed (1000 rpm for 30 seconds). 60 CD spectra were obtained at intervals of 1 minute. Each spectrum was one scan. All spectra were recorded in 20 mM phosphate buffer at pH 7.4. For analysis each spectrum had the appropriate background spectrum (buffer or liposomes in buffer) subtracted.

Dynamic Light Scattering

Dynamic light scattering was conducted as detailed in the experimental section of Chapter 3. For individual liposome batches the samples were allowed to equilibrate for 2 minutes. For DLS time series the solutions were mixed in the cuvette (1000 rpm for 30 seconds).

Measurements were started immediately after mixing and without 2 minutes of sample equilibration. 20 consecutive scans were measured in 1 hour.

Fluorescence Spectroscopy

Fluorescence measurements were performed using a FS920 fluorometer from Edinburgh Instruments with a DTMS-300X excitation monochromator and a peltier-controlled thermostatic cell. All spectra were obtained at 25 °C using a quartz cuvette with a 1 cm path length. The step size was 0.5 nm, with a sampling time of 0.5 s at each wavelength, and 1 scan was measured for each spectrum. For the lipid mixing assays excitation and emission slits were 1 nm. Emission spectra were measured from 490 nm to 700 nm at a fixed excitation wavelength of 460 nm. Fluorescence time series measurements were started immediately after mixing the solutions in the cuvette (30 seconds stirring at 1000 rpm). NBD fluorescence increase was measured in a continuous fashion for 1 hour (each scan was measured in 2 minutes). The NBD fluorescence was calibrated to enable calculation of the change in fluorescence percentage with time. The 0% fluorescence intensity was measured by diluting the fluorescent-labeled liposome batch 1:1 (v/v) with PBS to get the same overall fluorophore concentration as one would get after mixing the fluorescent-labeled liposomes 1:1 with unlabeled liposomes. After the one hour time series the 100% value was obtained. The liposomes were lysed by addition of 1% (w/v) Triton X-100 in PBS (10% (v/v) of 10% (w/w) Triton X-100 in PBS). The value that was obtained was multiplied by 1.55 to take into account the effect the Triton X-100 has on the NBD fluorescence. This value was obtained by preparing a 1 mM liposome solution that only contained the fluorophore NBD (DOPC/DOPE/CH/DOPE-NBD 49.75/24.875/24.875/ 0.5 mol%, 1mM). First, an emission spectrum was recorded for these liposomes to measure the NBD fluorescence intensity. Hereafter, the liposomes were lysed by adding 1% (w/v) Triton X-100 in PBS and an emission spectrum was recorded to determine the effect that Triton X-100 has on the NBD fluorescence. The value that was obtained was also multiplied by 1.1 to take into account the loss of 10 volume percent of sample that was replaced with Triton X-100. The percentage of fluorescence is calculated using equation 8, $F(\%) = (F(t) - F_0) / (F_{max} \times 1.55 \times 1.1 - F_0) \times 100$ (8) In this equation, F(t) is the fluorescence intensity measured at time t, F_0 is the 0% fluorescence and F_{max} is the 100 % fluorescence. The spectra were corrected by subtraction of buffer or liposome spectra. Content mixing is preferred as a technique to demonstrate the fusion event. The internal content mixing assay monitors the fusion of the aqueous compartments of the liposomes using molecules that are encapsulated into the liposomes. In this experiment, the molecules $Tb(citrate)_3^{3-}$ and dipicolinic acid (DPA), are used. Tb^{3+} ions are weakly fluorescent at λ_{ex} = 276 nm λ_{em} = 545 nm[3] and DPA does absorb but does not fluoresce at these wavelengths. Upon fusion (i.e. contents mixing), the highly fluorescent $Tb(DPA)_3^{3-}$ complex is formed that will show an increase in fluorescence intensity. For the content mixing assays excitation and emission slits were 5 nm. Emission spectra were measured from 480 nm to 520 nm at a fixed excitation wavelength of 276 nm. Fluorescence time

series measurements were started immediately after mixing the solutions in the cuvette (30 seconds stirring at 1000 rpm). The $Tb(DPA)_3^{3-}$ fluorescence increase was monitored for 1 hour (each scan was measured in 48 seconds). For calibration, the 0% fluorescence intensity was measured by diluting the Tb containing liposome batch 1:1 with PBS. After the one hour time series the 100% value was obtained. The liposomes were lysed by addition of 0.8 mM octaethylene monododecyl ether in a solution containing 20 μM free DPA (1% (v/v) 80 mM octaethylene monododecyl, 2 mM DPA in PBS). The percentage fluorescence is calculated according to equation 8. To see if there is any leakage of the contents, 1 mM ETDA can be added to the sample. The EDTA chelates to any Tb that has leaked, hereby disrupting the highly fluorescent $Tb(DPA)_3^{3-}$ that will be formed with any leaked DPA. In this way any increase in fluorescence signal is caused by pure content mixing. After the time series 1 mM EDTA (1% (v/v) 100 mM EDTA) was added to the mixture and the Tb fluorescence was recorded. Following this the liposomes were lysed with the addition of 0.8 mM octaethylene monododecyl ether, releasing the contents of the liposomes. All Tb fluorescence was quenched.

REFERENCES

1. L. V. Chernomordik, M. M. Kozlov, *Nat. Struct. Mol. Biol*. **2008**, 15, 675 – 683.
2. T. Weber, B. V. Zemelman, J. A. McNew, B. Westermann, M. Gmachl, F. Parlati, J. E. Rothman, *Cell* **1998**, 92, 759 – 772.
3. X. Chen, D. Araç, T. M. Wang, C. J. Gilpin, J. Zimmerberg, J. Rizo, *Biophys. J*. **2006**, 90, 2062 – 2074.
4. For recent reviews, see: a) J. Rizo, X. Chen, D. Araç, *Trends Cell Biol*. **2006**, 16, 339 – 350; b) R. Jahn, *Nat. Struct. Mol. Biol.* **2008**, 15, 655 – 657, and references therein.
5. a) Y. Gong, M. Ma, Y. Luo, D. Bong, *J. Am. Chem. Soc*. **2008**, 130, 6196 – 6205; b) G. Stengel, R. Zahn, F. Hook, *J. Am. Chem. Soc*. **2007**, 129, 9584 – 9585; c) Y. H. M. Chan, B. van Lengerich, S. G. Boxer, *Biointerphases* **2008**, 3, FA17 – FA21; d) Y. H. M. Chan, S. G. Boxer, *Curr. Opin. Chem. Biol.* **2007**, 11, 581 – 587;
   e) Y. Gong, J. Am. Chem. Soc. **2006**, 128, 14430 – 14431; f) T.-Y. Yoon, B. Okumus, F. Zhang, Y.-K. Shin, T. Ha, *Proc. Natl. Acad. Sci*. USA **2006**, 103, 19731 – 19736.
6. J. Zimmerberg, L. V. Chernomordik, *Adv. Drug Delivery Rev*. **1999**, 38, 197 – 205.
7. a) R. Jahn, T. Lang, T. C. Südhof, *Cell* **2003**, 112, 519 – 533; b) R. B. Sutton, D. Fasshauer, R. Jahn, A. T. Brunger, *Nature* **1998**, 395, 347 – 353; c) I. Fernandez, J. Ubach, I. Dulubova, X. Y. Zhang, T. C. Sudhof, J. Rizo, *Cell* **1998**, 94, 841 – 849.
8. a) J. R. Litowski, R. S. Hodges, *J. Biol. Chem*. **2002**, 277, 37272 – 37279; b) H. Robson Marsden, A. V. Korobko, E. N. M. van Leeuwen, E. M. Pouget, S. J. Veen, N. A. J. M. Sommerdijk, A. Kros, *J. Am. Chem. Soc.* **2008**, 130, 9386 – 9393; c) D. A. Lindhout, J. R. Litowski, P. Mercier, R. S. Hodges, B. D. Sykes, *Biopolymers* **2004**, 75, 367 – 375.
9. S. Cavalli, A. Kros, *Adv. Mater*. **2008**, 20, 627 – 631.
10. In the experiments discussed herein, there were approximately 1600 peptides on the outside of LPE- and LPK-decorated liposomes. However, fusion has also been observed with as few as 80 peptides on the outside of each set of liposomes: a number which approximates the amount of SNARE proteins on transport vesicles; see Reference 4.
11. a) M. M. Long, D.W. Urry, W. Stoeckenius, *Biochem. Biophys. Res. Commun.* **1977**, 75, 725 – 731; b) D.W. H. Frost, C. M. Yip, A. Chakrabartty, *Biopolymers* **2005**, 80, 26 – 33.
12. S. M. Dennison, M. E. Bowden, A. T. Brunger, B. R. Lentz, *Biophys. J*. **2006**, 90, 1661 – 1675.
13. F. S. Cohen, G. B. Melikyan, *J. Membr. Biol*. **2004**, 199, 1 – 14.
14. S. M. Dennison, M. E. Bowden, A. T. Brunger, B. R. Lentz, *Biophys. J.* **2006**, 90, 1661 – 1675.
15. J. Wilschut, N. D_zg_nes¸, R. Fraley, D. Papahadjopoulos, *Biochemistry* **1980**, 19, 6011 – 6021.
16. a) L. Yang, H.W. Huang, Science 2002, 297, 1877 – 1879; b) S. Wu, H. Guo, *J. Phys. Chem. B* **2008**, 113, 589 – 591.
17. V. V. Kumar, *Proc. Natl. Acad. Sci. USA* **1991**, 88, 444 – 448.
18. L. Chernomordik, *Chem. Phys. Lipids* **1996**, 81, 203 – 213.
19. R. Blumenthal, M. J. Clague, S. R. Durell, R. M. Epand, *Chem. Rev*. **2003**, 103, 53 – 69.
20. F. M. Menger, K. D. Garbielson, *Angew. Chem*. **1995**, 107, 2260 –2278; *Angew. Chem., Int. Ed. Engl.* **1995**, 34, 2091 – 2106.
21. C. Hu, M. Ahmed, T. J. Melia, T. H. Sollner, T. Mayer, J. E. Rothman, *Science* **2003**, 300, 1745 – 1749.
22. Y. A. Chen, R. H. Scheller, *Nat. Rev. Mol. Cell Biol.* **2001**, 2, 98–106.

APPENDICES

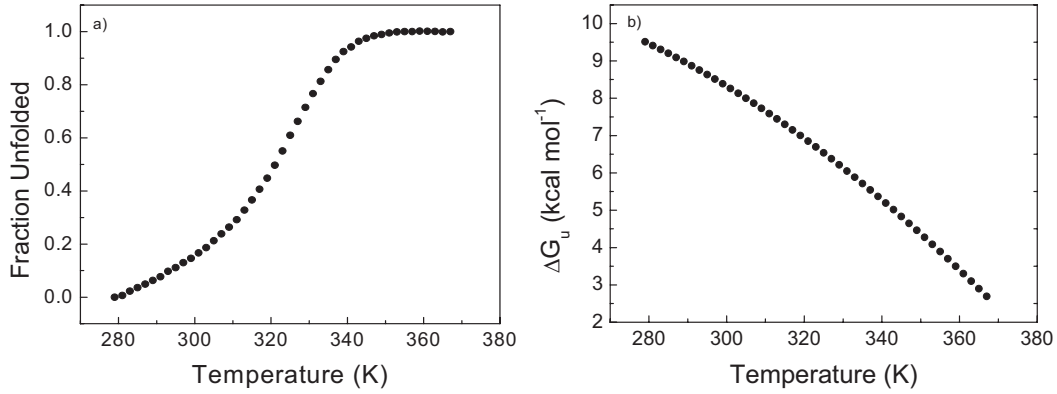


Figure A1.a) The thermal unfolding curve of E/K[i], derived from the temperature dependent ellipticity at 222 nm as followed by CD. (Heating and cooling rate 2 °C / min. [Total Peptide] = 40 μM, 50 mM phosphate, 100 mM KCl, pH 7.0 buffer). b) Free energy associated with the unfolding of E/K[i] as a function of temperature. At 25 °C the value of ΔG_u is 8.5 kcal mol^{-1}, or 14.4 kT. The dissociation constant at 25 °C calculated from this ΔG^{PBS} value is 5.6 x 10^{-7} M.

[i] The amino acid sequences of E and K are exactly the same as those of the peptide components of LPE and LPK except that for the temperature dependent data K does not have the C-terminal tryptophan residue.

Variations from the standard conditions

All of the results presented in Chapter 7 use 3 mol% lipopeptide incorporated into liposomes, and where possible 1 mM liposome concentrations are used. Each decorated liposome population is equimolar, and the experiments are conducted at 25 °C. The value of 3 mol% lipopeptide was chosen so that the CD signal would be large enough to be reliably interpreted. For the observed liposome sizes this corresponds to ~ 1600 peptides on the outside of the liposomes. After the characteristics of lipopeptide induced liposome fusion were established using these conditions, four variables were changed in order to investigate their effect on liposome aggregation and fusion, namely: liposome and lipidated peptide concentrations, ratios of LPK and LPE decorated liposomes, and the temperature at which the experiments were conducted. Initial information on the effects of these variables on liposome aggregation and fusion were obtained by DLS, and by using the total lipid mixing assay.

Liposome concentration

In the experiment in which the liposome concentrations were changed, 3% LPK modified fluorescent liposomes and 3% LPE modified liposomes were made with liposome concentrations of 0.2, 0.4, 0.6 and 0.8 mM. DLS time series were recorded to follow the change of liposome size with time caused by liposome aggregation or fusion (Figure A2a). All liposome concentrations result in particle size increases. For 0.2 mM decorated liposomes there is a linear increase in particle size with time, whereas for the more concentrated samples there is exponential size growth, with the more concentrated samples containing particles of many microns. As the number density of lipopeptide

modified liposomes in solution increases there is a corresponding increase in particle size because the liposomes encounter each other more often due to Brownian motion.
Fluorescence time series were also recorded to follow the total lipid mixing of these mixtures containing 0.2, 0.4, 0.6 and 0.8 mM liposomes (Figure A2b). The fluorescence increase reaches 17-22% for all these mixtures and is therefore comparable to the 20% obtained for mixing the 1 mM liposome solutions. There is a trend of increasing total lipid mixing with decreasing liposome concentration, although the absolute values were not fixed, as seen by the two values for 0.8 mM samples at one hour. These results suggest that the concentration of modified liposome does not dramatically affect the fusion event. Contrary to lipid mixing, liposome clustering is strongly dependent on the liposome concentration, therefore the liposome cluster size does not influence total lipid mixing to a large extent. These results also suggest that the larger size increase observed in Figure A2a for higher liposome concentrations is the result of aggregation of liposomes rather than fusion of liposomes.

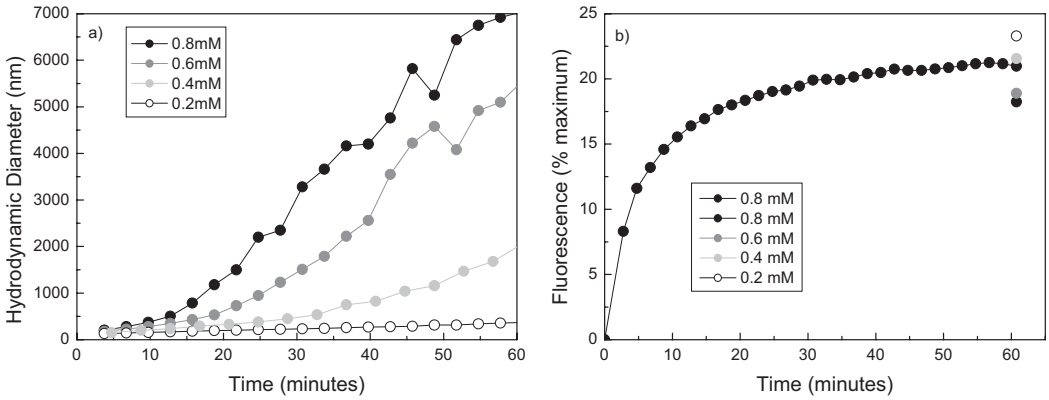


Figure A2. a) DLS time series recorded for mixtures of 3% LPK modified fluorescent liposomes and 3% LPE modified liposomes with liposome concentrations of 0.2, 0.4, 0.6 and 0.8 mM. b) Total lipid mixing as monitored by fluorescence spectroscopy for mixtures of 3% LPK modified fluorescent liposomes and 3% LPE modified liposomes with liposome concentrations of 0.2, 0.4, 0.6 and 0.8 mM.

Lipopeptide concentration

To evaluate the effect of lipopeptide concentration, samples were made with LPK modified fluorescent liposomes and LPE modified liposomes with 1, 0.5 and 0.1 mol% lipopeptide in place of the standard 3 mol%. The lipid concentration used was the standard 1 mM. A decrease in the peptide density on the membrane of the liposomes is expected to influence the bending and distortion of the membrane and the numbers of peptides bridging different liposomes, and hence the aggregation and fusion events.
For these samples, a DLS time series was recorded which showed a larger size increase and hence more aggregation or fusion with time for liposomes decorated with higher percentages of lipopeptide (Figure A3). The 4000 nm hydrodynamic diameter after 1 hour observed for 1 mol% hybrid is comparable with the size increase observed for the 3 mol% decorated liposomes. However, a significant decrease in size growth is observed for the

lower lipopeptide proportion of 0.5% and especially for 0.1%. There may be a hybrid density that leads to the largest clusters of liposomes determined by the balance of attractive forces originating from hetero coiled-coil formation and steric forces resulting from very high peptide densities. The threshold in the peptide density in order to induce aggregation and fusion appears to be close to 0.1 mol% hybrid in a 1 mM liposome sample.

The initial rate of decorated liposome aggregation and/or fusion is much faster when the liposomes are modified with 1 mol% lipopeptide rather than 3 mol% lipopeptide, but both reach the same order of initial liposomes fused after 1 hour. This difference may originate from the more accessible peptides that are not homocoiled on the liposome surface at densities of 1 mol%. The initial rate for the 0.5 mol% hybrid is more comparable in the first 20 minutes with the 1 mM liposome 3 mol% lipopeptide samples. As the peptide density was very low in these samples no information could be obtained using CD spectroscopy.

Total lipid mixing was monitored with time by fluorescence measurements as can be seen in Figure A3b. The samples with 1 mol% and 0.5 mol% hybrid sedimented, therefore the duration plotted is reduced. As the DLS sample for these mixtures did not show any precipitation, an explanation for this is probably the difference in stirring strength and further sample preparation. The 0.1% sample showed a 7% increase in fluorescence. This is significantly lower than the 20% increase in fluorescence observed when liposomes are decorated with 3 mol% lipopeptide, confirming that the lipid mixing depends on the hybrid concentration.

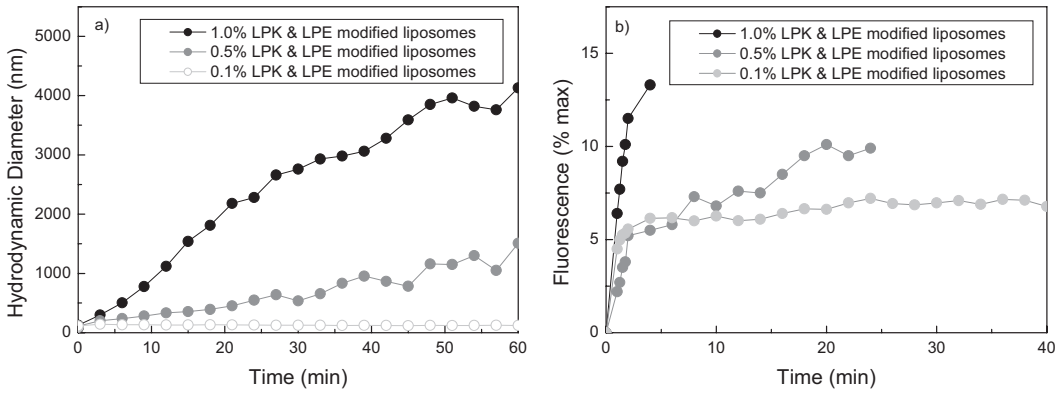


Figure A3. a) DLS time series for mixtures of LPK modified fluorescent liposomes and LPE modified liposomes with 1, 0.5 and 0.1 mol% lipopeptide. b) Total lipid mixing recorded by fluorescence spectroscopy for liposomes modified with 1, 0.5 and 0.1 mol% LPK and LPE.

Ratios of decorated liposome populations

Different ratios of LPK and LPE decorated liposomes were mixed together and the size increases were recorded with DLS, as seen in Figure A4. As the amount of one type of modified liposomes outstrips the other fewer liposomes cluster together. The size increase is comparable for LPK:LPE ratios of 2:1 and 1:2, so the peptide that is in the majority

does not influence the cluster size. As the amount of LPK-liposomes decreases and that of LPE-liposomes increases, the probability of finding a LPK decorated liposomes near a LPE decorated liposomes is reduced, and there are fewer aggregation possibilities. In the extreme situation, the LPK decorated liposomes may be surrounded by LPE decorated liposomes, and no more K is available or accessible to E for coiled-coil folding. The extent of lipid mixing is greater when LPE and LPK ratios of 1:2/4/8 are employed rather than 1:1, so although fewer liposomes cluster the number that proceed over the energy barrier is greater.

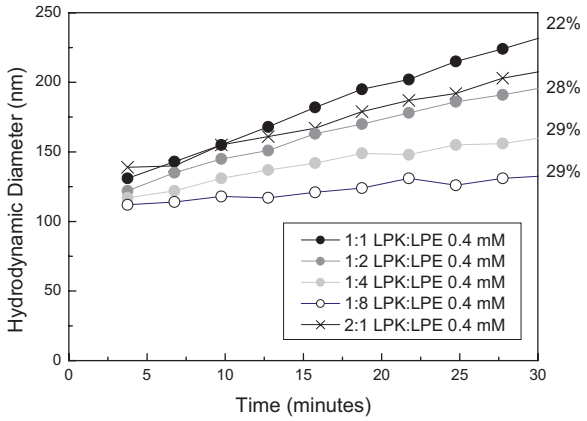


Figure A4. DLS time series for the assay in which 3 mol% LPK and LPE decorated liposomes (0.4 mM) were mixed in different ratios, i.e. 1:1, 1:2, 1:4, 1:8 and 2:1. Smaller LPK:LPE ratio resulted in smaller aggregates. The increase in fluorescence which accompanies lipid mixing is given at the right of the graph.

Temperature

The particle size and total lipid mixing experiments were repeated at 37 °C rather than at 25 °C. At 37 °C the modified liposomes cluster together very quickly in comparison to the increase observed under all conditions at 25 °C. The extent of lipid mixing was also greater, rapidly reaching a plateau of 30% fluorescence increase (Figure A5). This is the expected effect of increasing the temperature of the system to 37 °C because at this temperature E/K association still occurs (see Chapter 2), and the lipid membrane has greater fluidity, so the energy barrier to fusion is lowered.

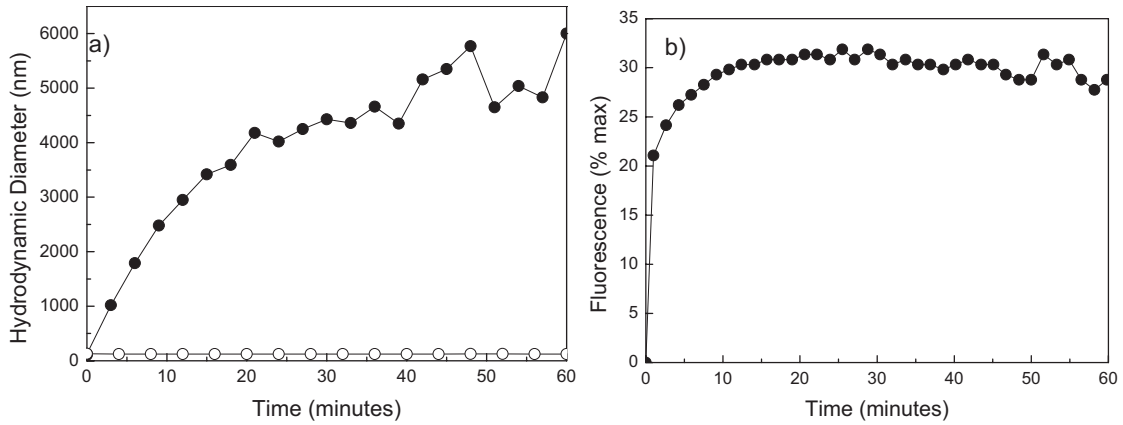


Figure A5. a) Change in particle size with time upon combining 3 mol% LPK decorated fluorescent liposomes with 3 mol% LPE decorated liposomes at 37 °C (●), and the equivalent without the lipopeptides (○), as monitored with DLS. b) Total lipid mixing upon combining 3 mol% LPK decorated liposomes with 3 mol% LPE decorated liposomes at 37 °C, as monitored by fluorescence spectroscopy.

Summary

LPK- and LPE-modified liposome clustering increases with increasing liposome concentration, with increasing lipopeptide concentration, when the two forms of modified liposomes are equimolar, and at 37 °C. That is, the greater the number of encounters between E and K the more decorated liposomes cluster together.

Large clusters of liposomes are not required for lipid mixing, and larger clusters of liposomes do not mean that the amount of lipid mixing is greater, therefore liposome aggregation is not the rate limiting step in the fusion process.

Lipid mixing still occurs with 80 rather than 1600 peptides anchored to the outer surface of the liposomes, analogous to the number of SNARE proteins on transport vesicles.

The rate and extent of lipid mixing is sharply increased by elevating the temperature to body temperature.

CHAPTER 8

POLYMER-PEPTIDE BLOCK COPOLYMERS – AN OVERVIEW AND ASSESSMENT OF SYNTHESIS METHODS

Incorporating peptide blocks into block copolymers opens up new realms of bioactive or smart materials. Because there are such a variety of peptides, polymers, and hybrid architectures that can be imagined, there are many different routes available for the synthesis of these chimera molecules. This Chapter summarizes the contemporary strategies in combining synthesis techniques to create well-defined peptide-polymer hybrids that retain the vital aspects of each disparate block. Living polymerization can be united with the molecular-level control afforded by peptide blocks to yield block copolymers that not only have precisely defined primary structures, but that also interact with other (bio)molecules in a well defined manner.

INTRODUCTION

Within the last five years the incorporation of peptide segments into block copolymers has been intensively investigated and can be classified into two groups: homopolypeptides, and designed sequences, both of which open up possibilities for novel materials with properties that are unavailable via purely synthetic polymers. One useful aspect of peptide blocks is their inherent ability to adopt stable conformations and self-assemble into precisely defined structures. Homopolypeptides are usually helical, i.e. fold into cylindrical rods, while designed peptides can have cylindrical or sheet-like morphology. These blocks have their shape and size defined to the sub-nanometer scale, which in itself allows unprecedented control over the material morphologies. In addition to spatially well-defined structures, another advantage of peptide blocks is that their structure is determined by noncovalent forces, and they can have reactive side-chains, both factors rendering the blocks ‘smart’, as they can switch conformations or properties upon changing external parameters such as pH, temperature, solvent, or ionic strength. Moreover, designed peptides can be constructed with exquisite control over the patterning of functionality. Based on a large amount of previous experimental research and theoretical modeling, peptide design is advanced enough that in many cases from the position of an amino acid in its primary sequence, its relative position in 3D space can be predicted with a high degree of certainty. This allows one to incorporate targeting, molecular recognition,

nucleation sites etc. into the blocks, creating further vistas of opportunities to polymer science.

As well as contributing to the final material properties, the functional groups of peptides (be they the N- or C-termini, or the side chains of natural or unnatural amino acids) can be used as 'handles', allowing a range of block copolymer synthesis techniques. Indeed one can even utilize the intermolecular interactions between peptides to couple polymer blocks. The advances in synthetic tools allow unprecedented control over structure, composition, and functionality of peptide hybrid materials.[1] Undoubtedly, these developments and future advances will allow the integration of biological design concepts of increasing utility in block copolymers, resulting in materials with properties unprecedented either in nature or synthetically.

This Chapter will review the diverse preparation routes of peptide-polymer block copolymers (Figure 1). The methods for synthesizing well-defined peptide-polymer conjugates are divided into seven strategies: 1 & 2) polypeptides initiated from solution phase polymers or from solid-supported polymers; 3 & 4) controlled radical polymerization initiated from solution phase peptides or from solid-supported peptides; 5) polymerization of macromonomers; 6) convergent synthesis of peptide-polymer hybrids; and lastly 7) noncovalent block copolymers. For each of these synthetic routes a brief overview is given of the types of blocks that it is suited to, along with the foremost advantages and limitations of the particular method. The first documented application of each approach is described, followed by other seminal contributions, and examples focusing on the activity pertaining to each route within the last five years, highlighting the current trends and pitfalls of each of the seven synthetic strategies.

The field of polymer bioconjugates is very broad due to the diversity of biological polymers and synthetic polymers that are available for conjugation. This leads to a wide array of physical, chemical, and biological properties, and hence potential applications. Bioconjugates are reviewed in a broad sense by Lutz and Börner[2] and Velonia,[3] where block copolymers incorporating amino acid, nucleobase, and saccharide based blocks are discussed. For more detailed information on the synthesis of polymer-peptide and polymer-protein block copolymers the reader is directed to reviews of Klok[4] and Nicolas.[5] Polymer-polypeptide block copolymers are concisely reviewed by Deming.[6] For reviews with an emphasis on the supramolecular structure formation of polymer-bioconjugates the reader is directed to Börner,[7,8], Kilbinger,[9] and Van Hest.[10]

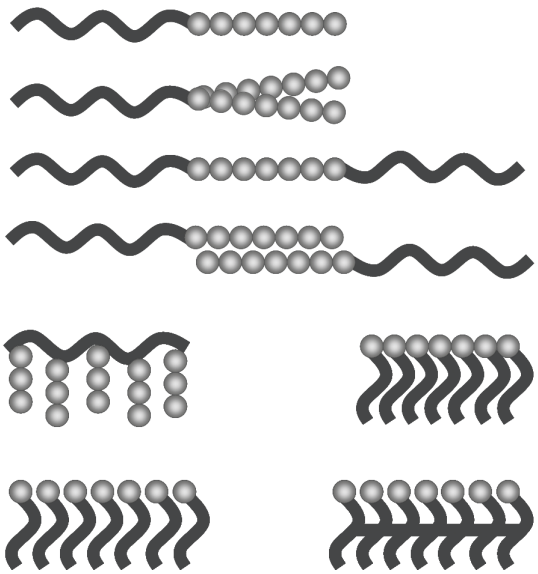


Figure 1. A selection of the many peptide-polymer hybrid architectures – linear/branched/pendant, diblock/multiblock, covalent/supramolecular – that are accessible by judicious combinations of synthesis techniques. Examples of methodologies that can be combined are ring-opening polymerization, solid-phase peptide synthesis, dual initiators, reversible addition-fragmentation chain transfer radical polymerization, atom transfer radical polymerization, nitroxide-mediated polymerization, coupling pre-synthesized blocks together, and noncovalent bonds. The balls represent amino acids, the lines represent polymers.

1. Polypeptides Initiated from Solution Phase Polymers

In solution polymers principally act as initiators of homopolypeptides. The most common homopolypeptides are based upon glutamic acid and lysine, as these are known to be the best controlled, but many other monomers can be used.[11] These homopolypeptides, which fold into rods, are predominantly chosen for their well-defined structural organization. Functionality is obtained through the response of the structure to environmental conditions, and by utilizing reactive side-chains.

The most frequently used synthetic methodology for the preparation of homopolypeptide blocks is the ring-opening polymerization (ROP) of protected α-amino acid-N-carboxyanhydrides (α-NCAs) initiated by a primary amino end-functionalized polymer.[11] Indeed this was one of the first routes to be explored in the preparation of polymer-peptide block copolymers, with Gallot and coworkers investigating anionic polymerization followed by ROP of NCAs in the 1970s.[12] This technique allows multi-gram scale synthesis, but has the disadvantage of being beleaguered by chain-breaking transfer and termination reactions, homopolymer contamination, precipitation of the growing polypeptide chain at a certain molecular weight, and the formation of secondary structure, all of which make it difficult to prepare polypeptides with predictable molecular weights and low polydispersity indices (PDI often > 1.2).[6, 13] Increased control over chain length and PDI can be obtained using ammonium initiators,[14] transition metal complexes as

macroinitiators,[15] hexamethlydisilazane,[16] or high vacuum techniques, [17] all of which reduce chain transfer and termination, and have allowed living NCA polymerizations.

Parallel to efforts to improve control over chain growth are investigations into non-linear hybrids. Whether AB_2 mikto-arm block copolymers behave differently to AB linear type block copolymers based on polystyrene and poly(glutamic acid) in the solid-phase has recently been investigated.[18] Styrene was polymerized using standard atom transfer radical polymerization (ATRP) conditions and the end-terminus was subsequently modified by an amine- or bifunctional amine group allowing the polymerization of benzyl-L-glutamate (BLG), resulting in linear or branched rod-coil block copolymers with differing organization in the solid-phase.

A greater number of peptides per molecule, and different molecular properties can be obtained by grafting many polypeptides from polymers, either from multiple positions on a linear polymer,[19] or from the branches of dendrimers. For example, polyphenylene dendrimer endgroups were converted from alkynes to amines, which initiated the ROP of up to 16 polylysine chains per polymer dendrimer. Similar polylysine chain lengths were achieved for different degrees of grafting, although the PDI increased from ~ 1.15 to ~ 1.40 as the number of peptide chains increased from 4 to 16.[20]

Both aspects of molecular architecture – control of chain growth, and pattern of chain growth – were addressed by Kim *et al*. They utilized a trifunctional initiator (1,3,5-tris(2-hydroxyethyl)cynuric acid) for the sequential polymerization of polystyrene (PS) and BLG.[21] After the formation of the three PS-arms, a nickel(0) catalyst was prepared at the termini for the living polymerization of the carboxyanhydrides (Figure 2).

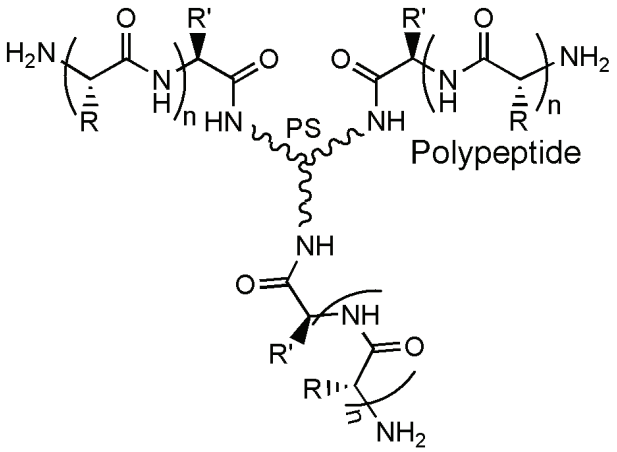


Figure 2. The living ROP of BLG-NCA was achieved using amido–amidate nickelacycle initiators. Styrene was polymerized from a trifunctional initiator using ATRP, followed by ROP, resulting in triarm polymer–peptide block copolymers.[21]

Also addressing control over chain growth and chain architecture, Hadjichristidis and coworkers have made applied high vacuum techniques for the living ROP of NCAs initiated from amino-functionalized polystyrene (Figure 3). Using this method large

peptide-polymer hybrids can be produced with low PDIs (e.g. 88000 g/mol, PDI 1.11), and with 100 % yields. Linear and miktoarm peptide-polymer hybrids have been demonstrated using this technique, with the PDI increasing slightly to 1.2 for four arm stars due to steric restrictions on the growing peptide chains.[17]

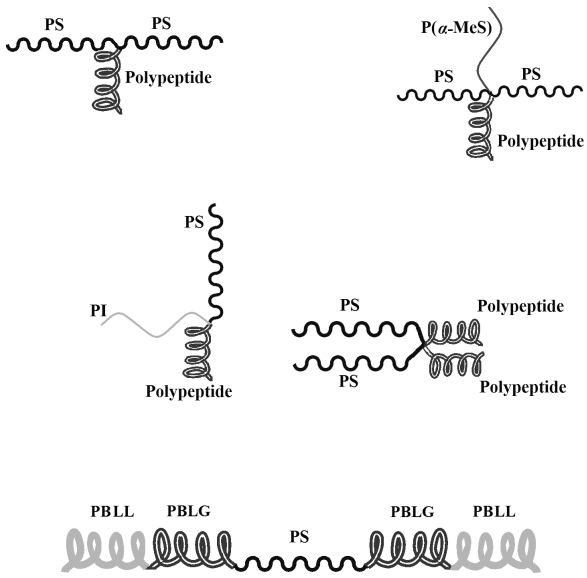


Figure 3. Living ROP of BLG-NCA and benzyl-L-lysine-NCA initiated from amino functionalized polystyrene was made possible by using high vacuum techniques. The polystyrene blocks were prepared by living anionic polymerization, also using high vacuum. A range of structures were available by placing the amine functionality either at the PS termini or within the chain.[17]

Regardless of the synthetic advances in preparing homopolypeptides, amino functionalized polymers remain the most commonly used initiators, as they were 30 years ago,[22] as the synthesis is very straight forward. This is illustrated in the work of Zhang *et al* who documented different approaches to the synthesis of double-hydrophilic block copolymers composed of poly(L-glutamate) and poly(N-isopropylacrylamide) (PLG-PNIPAM). A new double-initiator was synthesized bearing a reversible addition-fragmentation chain transfer (RAFT) agent for the poly(N-isopropylacrylamide) synthesis and an amine group for the peptide polymerization.[23] This allows flexibility in the block copolymer synthesis, as either the synthetic or peptide block can be polymerized first, with the NCA polymerization initiated from an amine or ammonium. Of these different methods the traditional route, RAFT polymerization followed by primary amine initiated NCA polymerization gave the best molecular characteristics, with reasonable yields and PDIs (1.2-1.5) for a range of block lengths (n = 27–600, m = 228–360) and block ratios. More recently, a stimuli-responsive zwitterionic hybrid block copolymer was studied.[24] Using the more successful RAFT followed by ROP route a poly(N-isopropylacrylamide)-block-poly(glutamic acid-co-lysine) ($PNIPAM_n(PLG_x$-*co*-$PLL_y)_m$) was synthesized. It was shown that the conformation of the polypeptide block could be controlled as a function of

pH, as at low pH the block copolymer is positively charged due to protonation of the lysine side chain, and at high pH it is negatively charged due to deprotonation of the glutamic acid side chain. In addition the NIPAM block is temperature sensitive resulting in reversible aggregation (Figure 4).

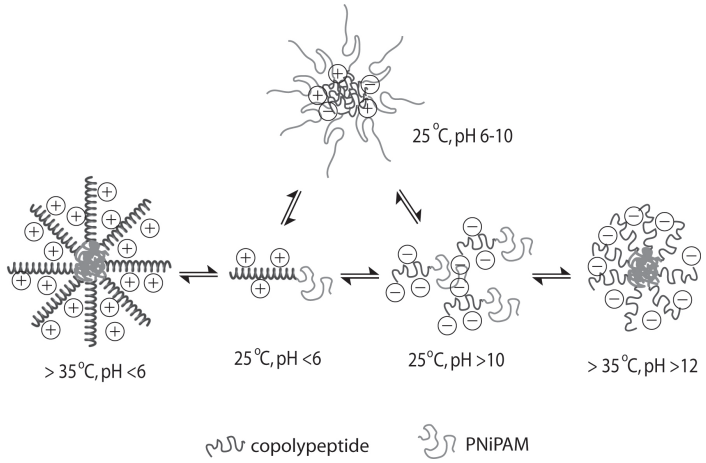


Figure 4. Amino terminated PNIPAM was prepared by RAFT polymerization and subsequently used to initiate the ROP of a mixture of benzyl-L-glutamate and benzyl-L-lysine NCAs, resulting in the zwitterionic PNIPAM$_n$(PLG$_x$-*co*-PLL$_y$)$_m$, whose self-assembly was influenced by pH and temperature.[24]

2. Solid-Phase Peptide Synthesis from Solid-Supported Polymers

The majority of advances in peptide-polymer hybrids make use of designed peptides as they have a greater range of efficacies than homopolypeptides. It is not practical to synthesize larger designed peptides in solution; therefore synthesis on a solid support using peptide synthesizers is commonplace. The advantage of this method is the exact control over the amino acid sequence and the improved ease of purification.

In the early 1980s a simple method of using solid-phase peptide synthesis (SPPS) to access peptide-polymer block copolymers was developed by the groups of Mutter and Bayer.[25-27] PS beads that were regularly used for SPPS were loaded with amino-terminated poly(ethylene glycol) (PEG) via an acid labile benzyl-ether linker. SPPS could be conducted from the PEG with high efficiencies, and cleavage at the ether linker liberates the peptide-PEG block copolymer. This was commercialized as PAP resin (Rapp polymere), which has been used by several groups to synthesize peptide-PEG conjugates.[28-33]

A recent example of the use of these pre-loaded resins is the preparation of an amphiphilic block peptide in which a β-sheet forming peptide ($L_4K_8L_4$) was conjugated with the hydrophilic PEG through an short enzyme-cleavable peptide sequence (VPRGS).[34] This is representative of the increasing complexity in the design of the peptide block. These amphiphiles were shown to dissolve into aqueous solutions, with the peptide having α-helical secondary structure. Upon addition of the enzyme thrombin the peptide was

cleaved from the PEG, triggering the propensity of the peptide to fold into β-sheets, and the assembly of long fibers (Figure 5).

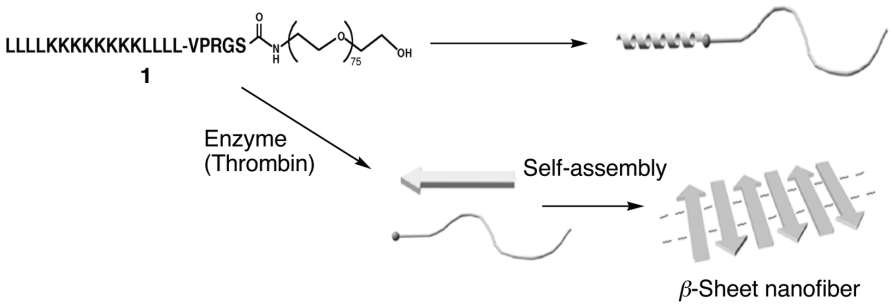


Figure 5. SPPS on resin preloaded with PEG afforded peptide-PEG hybrids. Through careful design of the peptide block, the hybrid could be cleaved by an enzyme, leading to the peptide changing secondary structure from an α-helix to a β-sheet, which subsequently aggregated into fibres.[34]

Unfortunately, only resins pre-loaded with PEG are commercially available, and the range of molecular weights available is limited. To access a greater range of hybrids, a polymer can also be attached to the resin followed by SPPS. Polystyrene was attached to a commercially available resin, followed by SPPS of an octapeptide from the base and the N-terminus of the polymer, resulting in di- and triblock copolymers (Figure 6). Typical difficulties in peptide-polymer hybrid synthesis were encountered during the synthesis: even with a long coupling time of 24 hours the first amino acid coupled poorly; additionally, isolation of the hybrid was complicated by the amphiphilic nature of the block copolymer. To reduce this longer PS blocks were used for subsequent investigations.[35]

A drawback to SPPS is that this technique is not suited to the synthesis of many homopolypeptides. This is because using automated peptide synthesis even short homopolypeptides tend to aggregate, resulting in low yields; additionally, peptide synthesizers can only be used to construct peptides up to approximately 40 residues in length before the yield becomes prohibitively poor. It would be possible to produce homopolypeptides by ROP of NCAs from a polymer functionalized solid support, but this has not yet been explored.

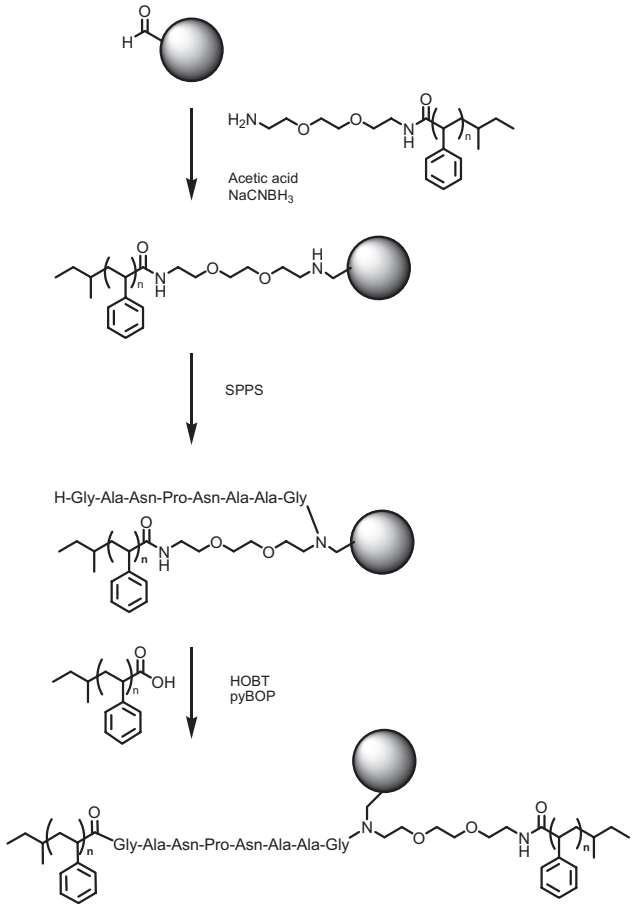


Figure 6. PS was attached to a resin via a secondary amine, which was used for SPPS. After the peptide was synthesized the hybrid could be cleaved or carboxylated PS coupled to the N-terminus of the peptide, resulting in a triblock hybrid. Adapted from [35].

3. Controlled Radical Polymerization Initiated from Solution Phase Peptides

A versatile route to well-defined peptide-polymer bioconjugates is to first construct the peptide block, which is then used to initiate the polymerization of the synthetic block in solution. In this way homopolypeptides or designed peptide blocks can be used, and the polymer can be attached at the N- or C-terminus, from an internal amino acid, or from multiple amino acids. A popular route to the synthesis of peptide-polymers is based on the following steps: 1) synthesis of the (oligo)peptide and introduction of the initiating group using solid-phase peptide synthesis; 2) Cleavage from the resin resulting in (de)protected peptide; 3) controlled radical polymerization (ATRP, RAFT, nitroxide-mediated polymerization (NMP)) in solution resulting in the hybrid peptide-polymer.

This frequently used pathway to polymer-peptide block copolymers is quite recent, being first demonstrated by Börner and co-workers in 2004, whereby a pentapeptide was synthesized by SPPS, which was then used in solution as a macroinitiator for the ATRP of *n*-butyl acrylate. The resulting block copolymer exhibited a low PDI of 1.19, and a controllable Mn.[36] More recently, Börner *et al* presented a convenient approach for the synthesis of bioactive peptide-polymer conjugates using RAFT polymerization rather than

ATRP.[37] The N-terminus of a small oligopeptide was modified with a chain-transfer agent based on trithiocarbonates. Polymerization of *n*-butylacrylate yielded polymers with narrow polydispersity (~1.1) and good control over the molecular weight.

The properties of peptide blocks that open up a new range of materials can also be a hindrance during the synthesis of the peptide-polymer hybrids. Recently poly(*n*-butyl acrylate) blocks were synthesized from a $(TV)_5$ peptide segment which has the propensity to form amyloid type aggregates.[38] This is symptomatic of many amphiphilic block copolymers, which are difficult to work with due to an inherent tendency to unwanted large scale organization. Nevertheless, the multiple configurations available to peptide blocks offer opportunities to circumvent this. To prevent the formation of undesirable β-sheet aggregates during the RAFT polymerization of *n*-butyl acrylate, which could hinder the polymerization, reversible pseudoproline defects were introduced. After polymerization the native undisturbed peptide segment was reestablished by changing the pH, which resulted in the aggregation of the polymer-peptide hybrid into large beta-sheet domains and a fibril superstructure (Figure 7).

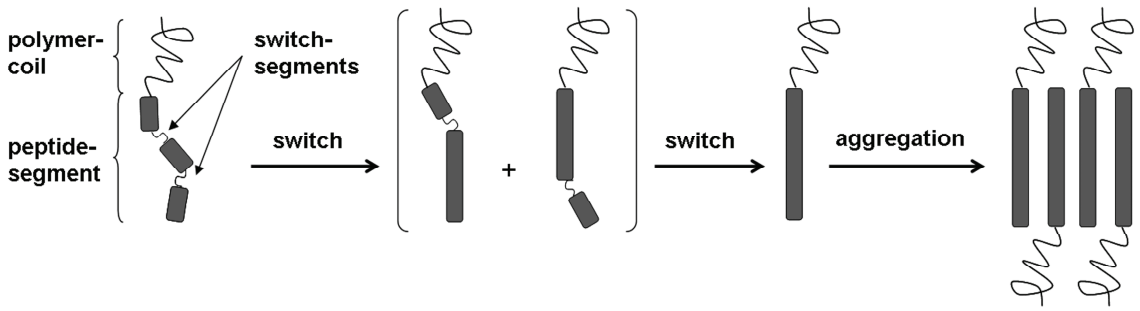


Figure 7. Aggregation during peptide initiated RAFT polymerization was prevented by incorporating pH-controlled defects into the peptide secondary structure.[38]

The polymers in all of the examples in this section have been initiated from the modified N-termini of peptides cleaved after SPPS. Maynard and co-workers recently chose to use a different approach by placing the initiating group at one of the amino acids in the peptide sequence.[39] Two types of ATRP-initiators were introduced in the side chain of tyrosine and serine respectively. These modified amino acids could be treated as per ordinary amino acids in SPPS protocols using Fmoc-chemistry. The Fmoc protected serine derivative bearing a 2-bromoisobutyrate moiety was investigated for the controlled polymerization of poly(hydroxyethyl methacrylate) HEMA and an N-acetylglucosamine-modified HEMA (Figure 8). In both cases well defined peptide-polymer hybrids were obtained (PDI < 1.3).

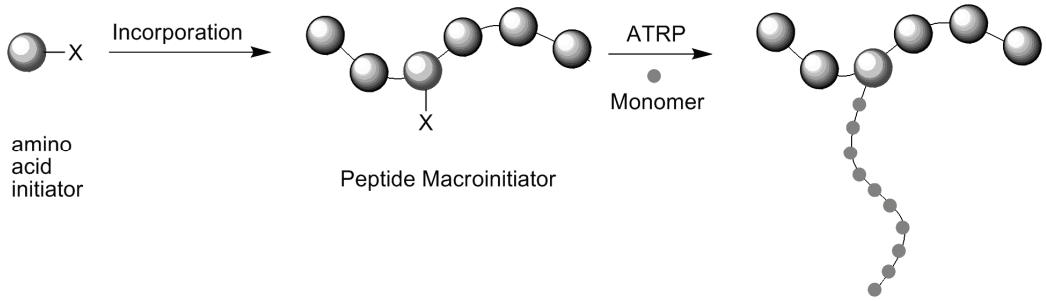


Figure 8. The range of polymer-peptide architectures is extended by initiating the polymerization from the middle of the peptide block.[39]

Another approach for non-N-terminal polymer attachment involved a peptide sequence able to form β-hairpin motifs that was modified with two ATRP initiating groups.[40] The peptide sequence contained two serine residues, one at the C- and one at the N-terminus. While still resin bound, these hydroxyl functions were modified with 2-bromoisobutyric acid. After cleavage from the resin, methyl methacrylate was polymerized resulting in an ABA triblock copolymer hybrid. Unfortunately, the peptide was no longer able to adopt its desired β-hairpin motif, showing that the polymer blocks have to be chosen with care in order to not prevent the peptides from assembling in the designed controlled manner.

The number of non-terminal polymer blocks synthesized from each peptide is further increased in the following example in which the side chains of three lysine residues in a cyclic octapeptide were modified to initiate ATRP. Cyclic oligopeptides composed of an alternating sequence of D- and L-amino acids have been shown to assemble in solution to form nanotubes with a well-defined diameter, which are held together by a large number of hydrogen bonds between the individual peptides.[41] This noncovalent stacking is analogous to the polymerization of monomers to form a linear synthetic polymer. Biesalski *et al* described the synthesis of peptide-polymer hybrid nanotubes by modifying a cyclic octapeptide with three initiation sites for the controlled radical polymerization by the ATRP technique, resulting in cyclic peptides with up to three pendant polymer chains (Figure 9).[42] The initial grafts were PNIPAM, polymerized in water,[42] but due to fast reactions, control over the molecular characteristics (e.g., graft density and molar mass of peptide-attached PNIPAM) was not trivial in these studies. Better control was achieved when conducting the ATRP in 2-propanol and adding a sacrificial initiator to the polymerizations, which favorably interfered with the ATRP equilibrium and that produced ‘‘free’’ polymer that could be analyzed with respect to the evolution of molar mass and molar mass distribution (up to ~ 4500 g/mol, PDI 1.2-1.4).[43] Larger degrees of polymerization were obtained for poly(*n*-butyl acrylate), synthesized in dimethyl sulfoxide (up to ~ 30000 g/mol, PDI 1.2-1.4). In this solvent the cyclicpeptides were not preassembled[44] It is not clear if this factor lead to the longer polymers however, as with PS it was shown that the degree of polymerization was similar when initiated from the nanotubes (in acetone) or from free initiator in solution. The PS was close to the theoretically expected molar mass (Mn up to ~ 6000 g/mol), with low PDIs of 1.05–1.10.[45]

With all three polymer-peptides an increase in the length of the grafted polymer lead to a consecutive reduction in the length of the supramolecular nanotubes.[45]

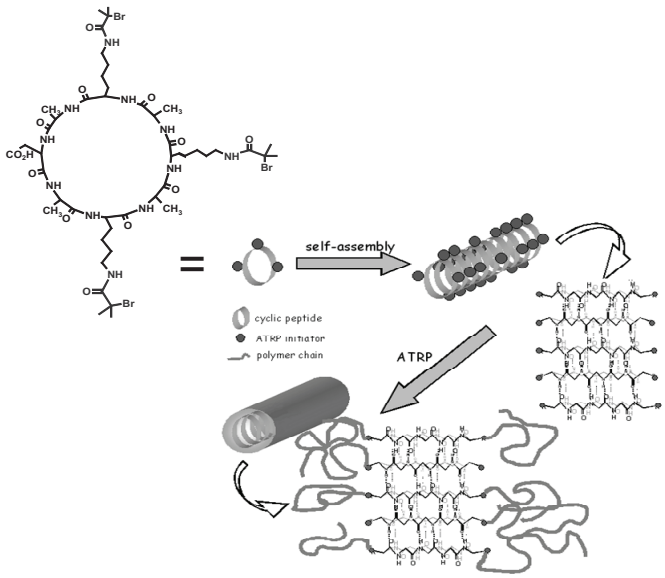


Figure 9. Cyclic peptides with pendant polymers stack into noncovalent 'polypeptides'. The length of the stacks decreases upon increasing the molar mass of the polymer chains. The polymer can be synthesized from aggregated or monomeric cyclic peptides.[45]

All of the examples in this section have employed designed, monodisperse peptides. In order to further control the hybrid properties it is therefore desirable to improve the synthesis of the polymer. In an interesting study the influence of the initiator was investigated as it has been shown in the past that the choice of initiator is critical in ATRP.[46] In many cases, the N-terminus of a peptide is modified with 2-bromoisobutyryl bromide to yield an amide-based initiator. However, polymerization of methacrylate monomers resulted in polymers with molecular weights higher than expected and higher polydispersity compared to ester-based initiators (Figure 10). It was suggested that not all peptides successfully initiate polymerization or that significant termination took place. Therefore initiators coupled to a peptide via an ester linkage should be studied in more detail.

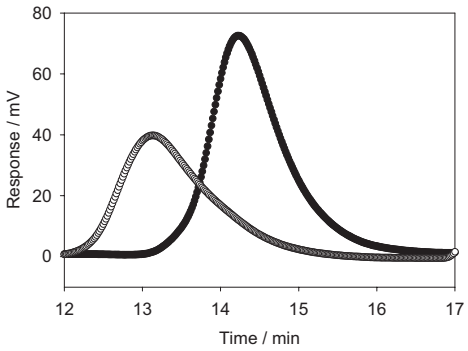


Figure 10. The ATRP of methacrylic monomers using ester-based initiators was more controlled than when using standard amide-based peptide initiators.[46]

Recently, several groups have started to explore the use of dual initiators to construct polypeptide-polymer hybrids in solution. Menzel, Heise and coworkers designed a bifunctional initiator for the sequential nickel mediated polymerization of amino acid NCAs and ATRP of methyl methacrylates (Figure 11).[47] Polymerization of benzyl-L-glutamate using the nickel initiator resulted in a controlled polymerization, although the experimental molecular weights were higher compared to the theoretical expected molecular weight. This was explained by the presence of a small amount of inactive impurities, which has also been reported by Deming for similar catalysts.[48] The obtained poly(γ-benzyl L-glutamate) (PBLG) macroinitiator was subsequently applied in the ATRP of methyl methacrylate. Initial studies were done in dimethyl sulfoxide, however better results were obtained in dimethyl formamide with a linear increase in molecular weight as a function of time.[47] Removal of metals after polymerization can be important in some biomedical applications.[49] More recently the group switched back to using amines as the initiator for NCAs combined with a nitroxide group in a bifunctional initiator for the controlled radical polymerization of styrenes.[50] The polymerization of BLG was studied in several solvents and at different temperatures. Previously it was shown that NCAs could be polymerized in a living fashion as long as the temperature was kept at 0 °C.[51] Also in this case the best results were obtained at low temperature resulting in defined polymers with low PDIs (1.1).

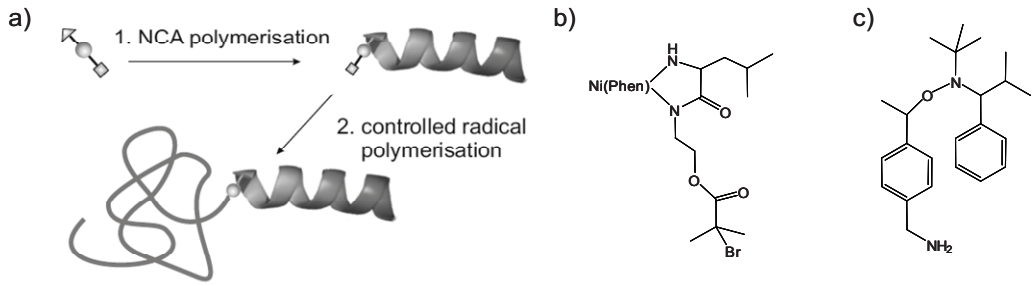


Figure 11 a) Synthesis of rod–coil polypeptide block copolymers starting from the bifunctional initiator b)[47] or c).[50]

4. Controlled Radical Polymerization Initiated from Solid-Supported Peptides

The possibility of combining solid-phase peptide protocols with controlled radical polymerizations while the peptide is still anchored to a resin has also only recently been investigated. In these studies an amino acid sequence is synthesized bearing a polymerization initiator at the N-terminus, which is used to grow the second block on the resin. A clear advantage of these methods is that side products such as homopolymers and unreacted monomers can simply be removed by washing steps.

This path to peptide-polymer block copolymer was first demonstrated by Wooley *et al* in 2003.[52] The protein transduction domain of the HIV-1 TAT protein, which is a 15-mer oligopeptide, was synthesized from which NMP was conducted starting from the N-

terminus, to yield the synthetic polyacrylate segments in the polymer-peptide hybrid. Using an extension of the NMP procedure it was shown that large amphiphilic triblock copolymers could also be obtained in good yields (Figure 12).[52] Washburn and co-workers used the same methodology to prepare GRGDS-poly(2-hydroxyethyl methacrylate) by ATRP protocols. After cleavage of the polymer-peptide from the resin using a trifluoroacetic acid wash, a clean product was obtained.[53] Previous studies have shown that the ester moieties in (meth)acrylates are not affected under these conditions.[54] In a subsequent investigation of Wooley and coworkers amphiphilic polymer-peptides were prepared via NMP and ATRP composed of an antimicrobial peptide headgroup (tritrpticin) and a poly(acrylic acid) block (tritrpticin-b-PAA), and a polystyrene block (tritrpticin-b-PAA-b-PS).[55] Dispersion into aqueous buffer yielded micellar assemblies with peptides exposed at its surface, which were shown to possess antimicrobial activity.

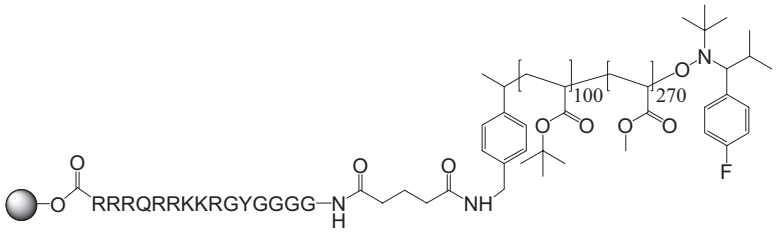


Figure 12. Polymers initiated from the N-terminus of the peptides that are anchored to the resin can still achieve high molecular weights, and impurities can be readily washed away.[52]

5. Polymerization of Macromonomers

In many cases peptides are desired in block copolymers for their bioactive properties. The incorporation of peptide sequences as side chains of polymers has the advantage over main chain peptide-polymer block copolymers that it is possible to introduce a much higher concentration of peptide sequences, and therefore bioactive moieties, in the polymer. Side chain peptide polymers can be synthesized via polymerization of macromonomers which include peptides or by attaching the desired sequence to a pre-formed polymer backbone. An advantage of polymerization of macromonomers is that each unit is identical, resulting in well defined hybrid molecules. The disadvantage is that it is necessary to synthesize a complex monomer. To date it has not been possible with either method to synthesize long polymers with larger peptides, most likely due to steric hindrance. In the past, it has been shown that side-chain peptide-polymer hybrids could be prepared via conventional free-radical polymerization.[56-58] However, the very nature of this polymerization method does not allow for the synthesis of well-defined polymeric architectures. Therefore a different approach was explored by van Hest and coworkers who studied the possibility of the controlled polymerization of methacrylates with oligopeptides in the side chain. Inspired by elastin, a VPGVG derivative of methacrylate was polymerized using a difunctional PEG macroinitiator and ATRP protocols.[59,60] This led to polymers with lower critical solution temperature behavior due to the elastin-based

peptide sequence. However, the degree of polymerization was rather low (DPn < 10). To obtain higher molecular weight polymers, elastin-based side-chain polymers were prepared using RAFT polymerization starting from a methacrylate derivative of VPGVG.[59,61] Well-defined homopolymers were obtained with Mn varying between 25000 and 62000 g/mol and low PDIs (1.03-1.23). However, the experimental values for Mn deviated significantly from theoretical values, which was attributed to the complex architecture of the monomer. RAFT polymerization allows for the easy introduction of functional groups at the termini, and as an example, the thioester group was modified using a previously described method[62] which involves the treatment of the polymer with an excess of initiator (4-cyanopentanoic acid dithiobenzoate) resulting in two carboxylate endgroups. To investigate the scope of peptide complexity that can be used, a cyclic decameric peptide (gramicidin-S) modified with a methacrylate group was polymerized (Figure 13).[63] This peptide is known for its antibiotic properties and typically adopts a β-sheet conformation, with both intra- and intermolecular hydrogen bonding. Using ATRP conditions a well-defined polymer was obtained after 15.5 hours with low a PDI (1.09), however the degree of polymerization was rather low (average DPn 13). This shows that this method of preparing polymers with peptides in the side chain is only accessible for small oligopeptides as larger peptides (>10 amino acids) hinder an efficient polymerization.

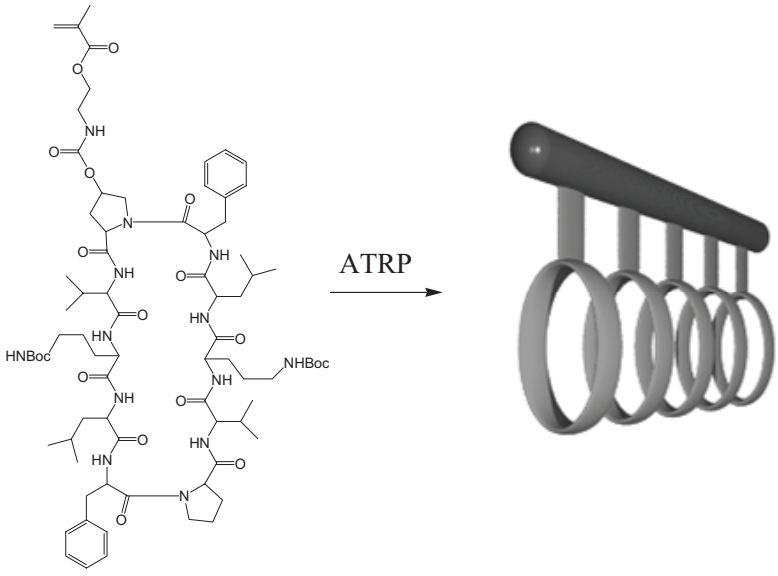


Figure 13. The cyclic decapeptide gramicidin S was modified with a methacrylate handle and polymerized by ATRP resulting in polymethacrylate with pendant gramicidin S. The secondary structure of the peptide moiety was retained within the resulting polymer.[63]

Frauenrath and coworkers produced a complex monomer with four elements: a tetrapeptide that forms β-sheets to noncovalently organize the monomers, a diacetylene moiety that can be polymerized once the monomers are organized, a short aliphatic coil segment to prevent global order, and different endgroups which modify the peptide-driven assembly. The peptide induced aggregation lead to supramolecular polymers that were

microns long, and this structure was retained when the diacetylene groups were cross-linked by UV irradiation, leading to a backbone polymer with pendant peptides (Figure 14).[64-69]

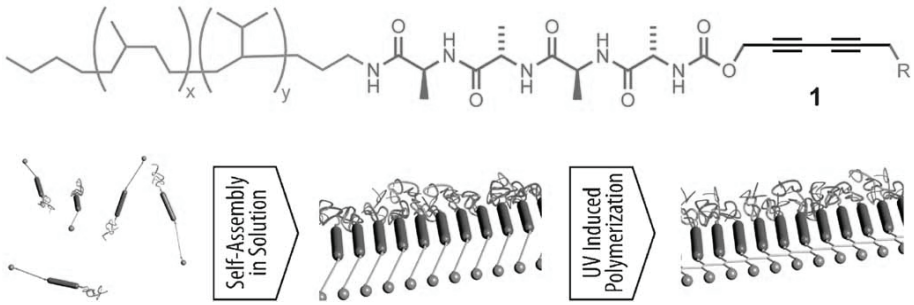


Figure 14. Monomers with four functional units assembled into noncovalent nanorods via peptide interactions, and were then covalently linked by UV polymerization of the diacetylene groups.[64]

6. Convergent Synthesis of Peptide-Polymer Hybrids

The direct coupling of a pre-formed peptide/polymer block to another has been used since 1955,[70] initially covalently linking polymers to proteins,[70-72] and later to prepare peptide–polymer conjugates.[73] In general the difficulty of this approach lies in the reduced accessibility of functional groups on macromolecules relative to small molecules, which can limit reaction conversion, and also in the isolation of the desired conjugate from a reaction mixture containing macromolecular starting materials and/or by-products.[4] Coupling strategies are consequently most suitable for the synthesis of polymer-peptide hybrids with low to moderate molecular weights.[37] In contrast the polymerization from a peptide approach allows for the preparation of high molecular weight conjugates (Mn > 30000 g/mol).[38,55]

A 'tidy' method of conjugating peptide and polymer blocks is via an amide bond in the same manner that the peptide was built up. This has usually been achieved by coupling a carboxylated polymer to the N-terminus of the peptide. This is a very straight forward method as it does not require any modification of the peptide, and any amino acid can be used. Kros *et al* synthesized peptide-PS hybrids by coupling acid terminated-PS (Mn = 2000 g/mol) to the N-terminus of the resin-bound peptide using standard amino acid coupling conditions.[31] The weight of the coupled PS chains was ~ 1000 g/mol showing that the shorter chains coupled more efficiently, exemplifying the inherent limitations of coupling blocks together when one block is attached to a resin. In contrast Cornelissen *et al* were able to couple PS_{35}-COOH to the N-terminus of a resin-bound peptide and obtained a Mn higher than theoretically expected. In this case it was observed that the reaction was slow and incomplete.[35] A reason for these conflicting reports could be the fact that different resins were used which have different porosities and degrees of functionalization. The same conjugation procedure was demonstrated recently with a single length polymer, resulting in monodisperse PEG-peptide hybrids. Fmoc-PEG-COOH was synthesized with 17 or 29 ethylene glycol monomers and coupled to a resin-bound

peptide. This approach results in well defined bioconjugates that may have different biological properties from their polydisperse counterparts. However, as with the previous two examples, the coupling was not quantitative as only 60% of the peptide blocks were conjugated with PEG after a coupling time of three days.[74]

In solution the quantitative coupling of a polymer block to a peptide was achieved with amino acid coupling conditions, albeit the polymer chain was also relatively short (Mn = 2100 g/mol, PDI = 1.10).[75] Interestingly the polymer, carboxylated poly(*n*-butyl acrylate), was coupled not to the N-terminus of a linear peptide, but to the primary amines of lysine side chains in a cyclic octapeptide. Also in solution, the concept of convergent synthesis using amino acid coupling conditions was extended to polymerization. Amide bonds were formed between dicarboxy PEG and amino terminated oligoalanine-PEG_5-oligoalanine, resulting in mulitblock copolymers that were inspired by spider silk.[76]

Again making use of amide bond formation, preformed oligopeptide blocks have been coupled to solid-supported polymers. In an interesting approach polymethacrylate brushes were formed on glass slides by ATRP polymerization, and then the end groups were converted to an activated ester using *p*-nitrophenyl chloroformate.[77] Similarly to SPPS, this application has the advantage that side products and reagents can be washed away. Amino acid coupling conditions were then used to couple bioactive hepta- and octapeptides to the polymer brushes via their N-terminal amine groups.[78]

Another method of coupling preformed blocks is the Michael addition of the thiols from cysteine side chains of peptides onto activated alkenes on polymers (for example PEG diacrylate[79,80] PEG acrylate bound to macroparticles,[80] or maleimide moieties on the surface of polyphenylene dendrimers[20]). The advantage of this coupling technique is that the reaction is very selective, can occur in quickly in physiological conditions, and does not require the use of metallic catalysts. PEG diacrylate and peptides containing thiols were copolymerized by photo illumination to form hydrogels linked by polyacrylate and having peptide pendants, bound via Michael addition to the PEG diacrylate. The coupling rate depends on the amino acid sequence, but was always complete within 1 minute.[81] This method is promising but has not been widely used to create peptide-polymer hybrids.

The [3+2] cycloaddition[82-84] between azides and strained[85] or terminal[86] alkynes has recently emerged as a chemical handle for conjugation in a non copper-mediated[87-89] and copper(I)-catalyzed[90,91] manner, also known as the “click” reaction. This is potentially a very useful coupling handle for peptide-polymers: both azides and alkynes are unreactive towards functional groups present in biomolecules, the cycloaddition product is highly thermally and hydrolytically stable, the copper(I) catalyzed “click” reaction can occur efficiently at room temperature, and metal-free azide-alkyne cycloaddition is possible, as reviewed by Lutz,[92] which is important because in some applications the presence of copper salts negatively influences the properties of peptides/proteins. This approach is

suitable for a wide range of biomolecular applications. For example proteins,[93] enzymes, [94] virus particles[95] and cells,[96] have been selectively modified using this method.
In 2005 Cornelissen *et al* were the first to apply click chemistry to the convergent synthesis of peptide-polymer block copolymers. Azide-terminated polystyrene was conjugated to small oligopeptides, and to proteins resulting in giant amphiphiles.[97] In order to induce spontaneous [3+2] cycloaddition it was envisaged that strained and electron-deficient alkyne derivatives (Figure 15a) should be activated enough for the click reaction to proceed at room temperature.[98] In a step towards this, poly(ethylene glycol) was modified with such an activated alkyne and reacted with azide-bearing oligopeptides resulting in a 80% yield after 36 hours at 37 °C (Figure 15b).

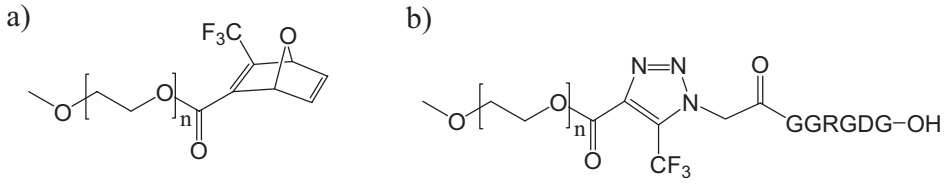


Figure 15. a) By using strained and electron deficient oxa-bridged bicyclic systems the use of copper catalysts is circumvented in the coupling of a peptide-polymer hybrid via the "click" reaction b).[98]

Pegylation, the bioconjugation of poly(ethylene glycol) with biomolecules, is one of the most studied and applied biomedical fields to date.[73] Recent studies have shown that brush-like PEG macromolecules are as biocompatible as their linear counterparts. Therefore Lutz *et al* studied the functionalization of the bromine chain-ends of poly(oligo(ethylene glycol) acrylate) prepared by ATRP.[99] The polymerization was stopped at low monomer conversion in order to obtain a polymer with a high degree of end-functionalization (~90%). At higher monomer conversions increasing amounts polymers are formed without a functional endgroup, making separation between these polymers necessary.[100] The bromine group was substituted for an azide group which was subsequently used to "click" an alkyne-modified peptide resulting in a polymer-peptide hybrid. Yields were typically in the order of 75%.[99]
Since its introduction in polymer science, [3+2] cycloaddition has already been exploited for the synthesis of a wide variety of synthetic polymer architectures including end-functionalized polymers, block copolymers, cyclic polymers, graft copolymers, star-shaped copolymers, dendrimers and crosslinked materials, as recently reviewed by Lutz,[101] Binder,[102] and Schubert,[103] and it is envisaged that this techniques will be increasingly applied in the creation of peptide-polymer conjugates.

7. Noncovalent Peptide-Polymer Hybrids

The degree of control over the organization of peptide-polymer block copolymers can be increased not only by using the single molecule properties of peptides (well-defined shape and functionality), but also by utilizing their supramolecular interactions. This was demonstrated in 2008 whereby two block copolymers containing coiled-coil forming peptides, PS-G(EIAALEK)$_3$ (PS-E) and (KIAALKE)$_3$G-PEG (K-PEG) were connected via the specific coiled-coil complex to form a noncovalent tri-block copolymer (Figure 16). The assembly of these block copolymers into rod-like micelles in solution involved both coiled-coil formation and polystyrene aggregation.[31] All peptide-polymer hybrids self-assemble to some degree, whether it be the polymer wrapping around the peptide, or aggregation driven by the polymer, the peptide, or both blocks. An emerging area is to control when peptide-polymer amphiphiles aggregate by utilizing designed peptide blocks. This possibility will likely be further explored in the coming years.

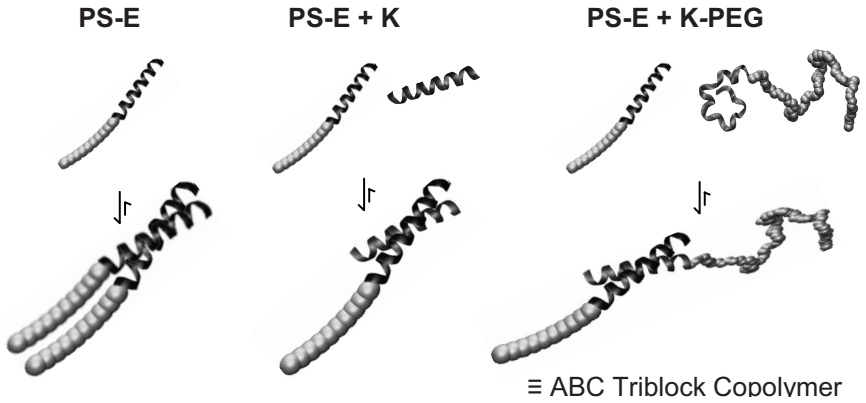


Figure 16. The blocks, and hence self-assembling properties, of peptide-polymer block copolymers can readily and reversibly be changed via the noncovalent coiled-coil interaction of the peptide block.[31] Schematic representation of the hierarchical self-assembly of the hybrids PS-E and K-PEG containing complementary peptide blocks.

CONCLUSIONS

Recent developments in peptide-polymer block copolymer synthesis are two-pronged: one focus is on increasing the molecular level control of the hybrids – control over the block length and polydispersity of synthetic polymers and homopolypeptides on the one hand, and control over the intra- and intermolecular interactions of designed peptide blocks on the other; and the other focus is on broadening the available architectures of peptide-polymer block copolymers. Just as there are many polymers and peptides with widely differing properties available to make up these chimera molecules, there are likewise many different synthesis methods available to create the hybrids. Each synthesis method has its own particular advantages and disadvantages with regards to the conjugation of these different blocks. To summarize the field to date: polymerization in solution, either of synthetic polymers or homopolypeptides can yield large polymers; solid-phase synthesis has been investigated for shorter designed peptides; coupling of preformed blocks is best suited to short blocks; the more elaborate architectures have all been demonstrated with either short peptides or short polymers - grafting of long polymers or peptides is difficult; and only short polymers have been attached noncovalently. In fact many of the hybrids discussed in this review have less than 10 monomers in a block, pushing the definition of ‘polymer’. That is not to say that increasing the size as well as the architectural complexity is not possible, it remains a challenge. This challenge exemplifies the development of this field of research – to increase the fecundity of the hybrids by further exploring peptide-polymer space. With such an increasing wealth of procedures at hand, multifaceted blocks will be able to be combined at will such that the hybrids resonate with new characteristics with contemporary and unforeseen relevance.

REFERENCES

1. Langer, R.; Tirrell, D. A. *Nature* **2004,** 428, (6982), 487-492.
2. Lutz, J. F.; Borner, H. G. *Prog. Polym. Sci.* **2008,** 33, (1), 1-39.
3. Le Drournaguet, B.; Velonia, K. *Macromol. Rapid Commun.* **2008,** 29, (12-13), 1073-1089.
4. Gauthier, M. A.; Klok, H. A. *Chem. Commun.* **2008**, (23), 2591-2611.
5. Nicolas, J.; Mantovani, G.; Haddleton, D. M. *Macromol. Rapid Commun.* **2007,** 28, (10), 1083-1111.
6. Deming, T. J., Polypeptide and polypeptide hybrid copolymer synthesis via NCA polymerization. In *Peptide Hybrid Polymers*, Springer-Verlag Berlin: Berlin, 2006; Vol. 202, pp 1-18.
7. Borner, H. G. *Macromolecular Chemistry And Physics* **2007,** 208, (2), 124-130.
8. Borner, H. G.; Schlaad, H. *Soft Matter* **2007,** 3, (4), 394-408.
9. Konig, H. M.; Kilbinger, A. F. M. *Angew. Chem.-Int. Edit.* **2007,** 46, (44), 8334-8340.
10. Van Hest, J. C. M. *Polymer Reviews* **2007,** 47, (1), 63-92.
11. Smeenk, J. M.; Lowik, D.; van Hest, J. C. M. *Curr. Org. Chem.* **2005,** 9, (12), 1115-1125.
12. Billot, J. P.; Douy, A.; Gallot, B. *Makromol. Chem.* **1977,** 178, (6), 1641-1650.
13. Kricheldorf, H. R. *Angew. Chem.-Int. Edit.* **2006,** 45, (35), 5752-5784.
14. Dimitrov, I.; Schlaad, H. *Chem. Commun.* **2003**, (23), 2944-2945.
15. Deming, T. J. *Nature* **1997,** 390, (6658), 386-389.
16. Lu, H.; Cheng, J. J. *J. Am. Chem. Soc.* **2008,** 130, (38), 12562-12563.
17. Karatzas, A.; Iatrou, H.; Hadjichristidis, N.; Inoue, K.; Sugiyama, K.; Hirao, A. *Biomacromolecules* **2008,** 9, (7), 2072-2080.
18. Babin, J.; Taton, D.; Brinkmann, M.; Lecommandoux, S. *Macromolecules* **2008,** 41, (4), 1384-1392.
19. Yu, H. J.; Chen, X. S.; Lu, T. C.; Sun, J.; Tian, H. Y.; Hu, J.; Wang, Y.; Zhang, P. B.; Jing, X. B. *Biomacromolecules* **2007,** 8, (5), 1425-1435.
20. Mihov, G.; Grebel-Koehler, D.; Lubbert, A.; Vandermeulen, G. W. M.; Herrmann, A.; Klok, H. A.; Mullen, K. *Bioconjugate Chem.* **2005,** 16, (2), 283-293.
21. Abraham, S.; Ha, C. S.; Kim, I. *J. Polym. Sci. Pol. Chem.* **2006,** 44, (9), 2774-2783.
22. Gallot, B. *Prog. Polym. Sci.* **1996,** 21, (6), 1035-1088.
23. Zhang, X. Q.; Li, J. G.; Li, W.; Zhang, A. *Biomacromolecules* **2007,** 8, (11), 3557-3567.
24. Li, J. G.; Wang, T.; Wu, D. L.; Zhang, X. Q.; Yan, J. T.; Du, S.; Guo, Y. F.; Wang, J. T.; Zhang, A. *Biomacromolecules* **2008,** 9, (10), 2670-2676.
25. Becker, H.; Lucas, H. W.; Maul, J.; Pillai, V. N. R.; Anzinger, H.; Mutter, M. *Makromo. Chem. Rapid* **1982,** 3, (4), 217-223.
26. Bayer, E.; Dengler, M.; Hemmasi, B. *Int. J. Pept. Protein Res.* **1985,** 25, (2), 178-186.
27. Bayer, E. H., B.; Albert, K.; Rapp, W.; Dengler, M. In *Peptides, Structure and Function.*, Proceedings of the 8th American PeptideSymposium, Pierce Chemical Company: Rockford, IL, 1983; Hruby, V. J., Rich, D. H., Ed. Pierce Chemical Company: Rockford, IL, 1983; p 87–90.
28. Burkoth, T. S.; Benzinger, T. L. S.; Jones, D. N. M.; Hallenga, K.; Meredith, S. C.; Lynn, D. G. *J. Am. Chem. Soc.* **1998,** 120, (30), 7655-7656.
29. Rosler, A.; Klok, H.-A.; Hamley, I. W.; Castelletto, V.; Mykhaylyk, O. O. *Biomacromolecules* **2003,** 4, (4), 859-863.
30. Hamley, I. W.; Krysmann, M. J. *Langmuir* **2008,** 24, (15), 8210-8214.
31. Marsden, H. R.; Korobko, A. V.; van Leeuwen, E. N. M.; Pouget, E. M.; Veen, S. J.; Sommerdijk, N. A. J. M.; Kros, A. *J. Am. Chem. Soc.* **2008,** 130, (29), 9386-9393.
32. Eckhardt, D.; Groenewolt, M.; Krause, E.; Borner, H. G. *Chem. Commun.* **2005**, (22), 2814-2816.
33. Rosler, A.; Klok, H. A.; Hamley, I. W.; Castelletto, V.; Mykhaylyk, O. O. *Biomacromolecules* **2003,** 4, (4), 859-863.
34. Koga, T.; Kitamura, K.; Higashi, N. *Chem. Commun.* **2006**, (47), 4897-4899.
35. Reynhout, I. C.; Lowik, D.; van Hest, J. C. M.; Cornelissen, J.; Nolte, R. J. M. *Chem. Commun.* **2005**, (5), 602-604.
36. Rettig, H.; Krause, E.; Borner, H. G. *Macromol. Rapid Commun.* **2004,** 25, (13), 1251-1256.
37. Hentschel, J.; Bleek, K.; Ernst, O.; Lutz, J. F.; Borner, H. G. *Macromolecules* **2008,** 41, (4), 1073-1075.
38. Hentschel, J.; ten Cate, M. G. J.; Borner, H. G. *Macromolecules* **2007,** 40, (26), 9224-9232.
39. Broyer, R. M.; Quaker, G. M.; Maynard, H. D. *J. Am. Chem. Soc.* **2008,** 130, (3), 1041-1047.

40. Ayres, L.; Hans, P.; Adams, J.; Lowik, D.; van Hest, J. C. M. *J. Polym. Sci. Pol. Chem.* **2005,** 43, (24), 6355-6366.
41. Ghadiri, M. R.; Granja, J. R.; Milligan, R. A.; McRee, D. E.; Khazanovich, N. *Nature* **1993,** 366, (6453), 324-327.
42. Couet, J.; Jeyaprakash, J. D.; Samuel, S.; Kopyshev, A.; Santer, S.; Biesalski, M. *Angew. Chem.-Int. Edit.* **2005,** 44, (21), 3297-3301.
43. Couet, J.; Biesalski, M. *Macromolecules* **2006,** 39, (21), 7258-7268.
44. Loschonsky, S.; Couet, J.; Biesalski, M. *Macromol. Rapid Commun.* **2008,** 29, (4), 309-315.
45. Couet, J.; Biesalski, M. *Small* **2008,** 4, (7), 1008-1016.
46. Adams, D. J.; Young, I. *J. Polym. Sci. Pol. Chem.* **2008,** 46, (18), 6082-6090.
47. Steig, S.; Cornelius, F.; Witte, P.; Staal, B. B. P.; Koning, C. E.; Heise, A.; Menzel, H. *Chem. Commun.* **2005**, (43), 5420-5422.
48. Deming, T. J.; Curtin, S. A. *J. Am. Chem. Soc.* **2000,** 122, (24), 5710-5717.
49. Gil, E. S.; Hudson, S. A. *Prog. Polym. Sci.* **2004,** 29, (12), 1173-1222.
50. Knoop, R. J. I.; Habraken, G. J. M.; Gogibus, N.; Steig, S.; Menzel, H.; Koning, C. E.; Heise, A. *J. Polym. Sci. Pol. Chem.* **2008,** 46, (9), 3068-3077.
51. Vayaboury, W.; Giani, O.; Cottet, H.; Deratani, A.; Schue, F. *Macromol. Rapid Commun.* **2004,** 25, (13), 1221-1224.
52. Becker, M. L.; Liu, J. Q.; Wooley, K. L. *Chem. Commun.* **2003**, (2), 180-181.
53. Mei, Y.; Beers, K. L.; Byrd, H. C. M.; Vanderhart, D. L.; Washburn, N. R. *J. Am. Chem. Soc.* **2004,** 126, (11), 3472-3476.
54. Angot, S.; Ayres, N.; Bon, S. A. F.; Haddleton, D. M. *Macromolecules* **2001,** 34, (4), 768-774.
55. Becker, M. L.; Liu, J. Q.; Wooley, K. L. *Biomacromolecules* **2005,** 6, (1), 220-228.
56. Murata, H.; Sanda, F.; Endo, T. *Macromolecules* **1996,** 29, (17), 5535-5538.
57. Murata, H.; Sanda, F.; Endo, T. *Macromolecules* **1997,** 30, (10), 2902-2906.
58. Lubbert, A.; Nguyen, T. Q.; Sun, F.; Sheiko, S. S.; Klok, H. A. *Macromolecules* **2005,** 38, (6), 2064-2071.
59. Ayres, L.; Vos, M. R. J.; Adams, P.; Shklyarevskiy, I. O.; van Hest, J. C. M. *Macromolecules* **2003,** 36, (16), 5967-5973.
60. Ayres, L.; Koch, K.; Adams, P.; van Hest, J. C. M. *Macromolecules* **2005,** 38, (5), 1699-1704.
61. Fernandez-Trillo, F.; Dureault, A.; Bayley, J. P. M.; van Hest, J. C. M.; Thies, J. C.; Michon, T.; Weberskirch, R.; Cameron, N. R. *Macromolecules* **2007,** 40, (17), 6094-6099.
62. Perrier, S.; Takolpuckdee, P.; Mars, C. A. *Macromolecules* **2005,** 38, (6), 2033-2036.
63. Ayres, L.; Grotenbreg, G. M.; van der Marel, G. A.; Overkleeft, H. S.; Overhand, M.; van Hest, J. C. M. *Macromol. Rapid Commun.* **2005,** 26, (16), 1336-1340.
64. Jahnke, E.; Millerioux, A. S.; Severin, N.; Rabe, J. P.; Frauenrath, H. *Macromol Biosci* **2007,** 7, (2), 136-143.
65. Jahnke, E.; Lieberwirth, I.; Severin, N.; Rabe, J. P.; Frauenrath, H. *Angew. Chem.-Int. Edit.* **2006,** 45, (32), 5383-5386.
66. Weiss, J.; Jahnke, E.; Frauenrath, H. *Macromol. Rapid Commun.* **2008,** 29, (4), 330-339.
67. Jahnke, E.; Severin, N.; Kreutzkamp, P.; Rabe, J. P.; Frauenrath, H. *Adv. Mater.* **2008,** 20, (3), 409-414.
68. Jahnke, E.; Weiss, J.; Neuhaus, S.; Hoheisel, T. N.; Frauenrath, H. *Chem.-Eur. J.* **2009,** 15, (2), 388-404.
69. Weiss, J.; Jahnke, E.; Severin, N.; Rabe, J. P.; Frauenrath, H. *Nano Lett.* **2008,** 8, (6), 1660-1666.
70. Jatzkewitz, H. *Z. Naturforsch. Pt. B* **1955,** 10, (1), 27-31.
71. Mitz, M. A.; Summaria, L. J. *Nature* **1961,** 189, (476), 576-&.
72. Abuchowski, A.; Vanes, T.; Palczuk, N. C.; Davis, F. F. *Journal Of Biological Chemistry* **1977,** 252, (11), 3578-3581.
73. Duncan, R. *Nat. Rev. Drug Discov.* **2003,** 2, (5), 347-360.
74. Niculescu-Duvaz, D.; Getaz, J.; Springer, C. J. *Bioconjugate Chem.* **2008,** 19, (4), 973-981.
75. ten Cate, M. G. J.; Severin, N.; Borner, H. G. *Macromolecules* **2006,** 39, (23), 7831-7838.
76. Rathore, O.; Sogah, D. Y. *J. Am. Chem. Soc.* **2001,** 123, (22), 5231-5239.
77. Tugulu, S.; Arnold, A.; Sielaff, I.; Johnsson, K.; Klok, H. A. *Biomacromolecules* **2005,** 6, (3), 1602-1607.
78. Tugulu, S.; Silacci, P.; Stergiopulos, N.; Klok, H. A. *Biomaterials* **2007,** 28, (16), 2536-2546.
79. Lutolf, M. P.; Tirelli, N.; Cerritelli, S.; Cavalli, L.; Hubbell, J. A. *Bioconjugate Chem.* **2001,** 12, (6), 1051-1056.

80. Heggli, M.; Tirelli, N.; Zisch, A.; Hubbell, J. A. *Bioconjugate Chem.* **2003,** 14, (5), 967-973.
81. Salinas, C. N.; Anseth, K. S. *Macromolecules* **2008,** 41, (16), 6019-6026.
82. Huisgen, R. *Pure Appl. Chem.* **1989,** 61, (4), 613-628.
83. Huisgen, R., *1,3-Dipolr Cycloaddition Chemistry*. Wiley: New York, 1984; Vol. 1, p 1-176.
84. Meldal, M.; Tornoe, C. W. *Chem. Rev.* **2008,** 108, (8), 2952-3015.
85. Agard, N. J.; Prescher, J. A.; Bertozzi, C. R. *J. Am. Chem. Soc.* **2004,** 126, (46), 15046-15047.
86. Rostovtsev, V. V.; Green, L. G.; Fokin, V. V.; Sharpless, K. B. *Angew. Chem., Int. Edit.* **2002,** 41, (14), 2596-2599.
87. Mock, W. L.; Irra, T. A.; Wepsiec, J. P.; Manimaran, T. L. *J. Org. Chem.* **1983,** 48, (20), 3619-3620.
88. Mock, W. L.; Irra, T. A.; Wepsiec, J. P.; Adhya, M. *J. Org. Chem.* **1989,** 54, (22), 5302-5308.
89. Lewis, W. G.; Green, L. G.; Grynszpan, F.; Radic, Z.; Carlier, P. R.; Taylor, P.; Finn, M. G.; Sharpless, K. B. *Angew. Chem.-Int. Edit.* **2002,** 41, (6), 1053-1057.
90. Feng, T.; Tsao, M. L.; Schultz, P. G. *J. Am. Chem. Soc.* **2004,** 126, (49), 15962-15963.
91. Cavalli, S.; Tipton, A. R.; Overhand, M.; Kros, A. *Chem. Commun.* **2006**, (30), 3193-3195.
92. Lutz, J. F. *Angew. Chem.-Int. Edit.* **2008,** 47, (12), 2182-2184.
93. Deiters, A.; Cropp, T. A.; Summerer, D.; Mukherji, M.; Schultz, P. G. *Bioorg. Med. Chem. Let.* **2004,** 14, (23), 5743-5745.
94. Speers, A. E.; Cravatt, B. F. *Chem. Biol.* **2004,** 11, (4), 535-546.
95. Wang, Q.; Chan, T. R.; Hilgraf, R.; Fokin, V. V.; Sharpless, K. B.; Finn, M. G. *J. Am. Chem. Soc.* **2003,** 125, (11), 3192-3193.
96. Link, A. J.; Vink, M. K. S.; Tirrell, D. A. *J. Am. Chem. Soc.* **2004,** 126, (34), 10598-10602.
97. Dirks, A. J. T.; van Berkel, S. S.; Hatzakis, N. S.; Opsteen, J. A.; van Delft, F. L.; Cornelissen, J.; Rowan, A. E.; van Hest, J. C. M.; Rutjes, F.; Nolte, R. J. M. *Chem. Commun.* **2005**, (33), 4172-4174.
98. van Berkel, S. S.; Dirks, A. T. J.; Debets, M. F.; van Delft, F. L.; Cornelissen, J.; Nolte, R. J. M.; Rutjes, F. *ChemBioChem* **2007,** 8, (13), 1504-1508.
99. Lutz, J. F.; Borner, H. G.; Weichenhan, K. *Macromolecules* **2006,** 39, (19), 6376-6383.
100. Hong, S. C.; Lutz, J. F.; Inoue, Y.; Strissel, C.; Nuyken, O.; Matyjaszewski, K. *Macromolecules* **2003,** 36, (4), 1075-1082.
101. Lutz, J. F. *Angew. Chem.-Int. Edit.* **2007,** 46, (7), 1018-1025.
102. Binder, W. H.; Sachsenhofer, R. *Macromol. Rapid Commun.* **2007,** 28, (1), 15-54.
103. Fournier, D.; Hoogenboom, R.; Schubert, U. S. *Chem. Soc. Rev.* **2007,** 36, (8), 1369-1380.

SUMMARY

Of the various biomolecular building blocks in use in nature, coiled-coil forming peptides are amongst those with the most potential as building blocks for the synthetic bottom-up self-assembly of nanostructures. There are many reasons for this: they have well defined size and surface functionality, the amino acid sequence can be designed to direct not just intra, but also highly specific intermolecular interactions, the binding energy of coiled coils is compatible with other self-assembly processes, and they can readily be conjugated with other molecular building blocks. The ease of working with and getting information about coiled coils has meant that they have been one of the most highly studied protein motifs. Coiled coils have been studied in isolation that form discrete coiled-coil complexes, and also that pack into larger assemblies. They have additionally been studied connected to water soluble blocks such that assemblies are constructed because of coiled-coil formation. However, one of the largest areas of potential has barely been delved into: native coiled coils are cogs from a great machine, and they clearly have the ability to function in and influence complex systems composed of multiple building blocks. The true potential of coiled-coil building blocks for synthetic chemists is only apparent when they are connected to other components, with each component contributing a function. Ideally a balance is struck between the different units such that all can play their role and novel functions emerge from their interactions. This thesis represents efforts at piecing together coiled coils with one or two other self-assembling components.

In Chapter 2 the coiled-coil unit that is to be used in the subsequent hybrids is investigated. The peptides, denoted E and K, are composed of three heptad repeats and form a parallel heterodimer in aqueous solution. The binding properties are determined using experimental and computational techniques, with the results from the two approaches supporting one another. The binding energy of the coiled-coil dimer was found to be ~ -11 kcal mol^{-1}. Using computational methods, details of binding are readily estimated. In the simulations the packing together of hydrophobic amino acid side chains in the coiled-coil core provided almost the entirety of the binding energy. On the contentious issue of whether salt-bridges exist and add to the binding energy, the simulations suggest that salt-bridges are not common, and that the charged side chains detract from the binding energy, but are necessary to impart specificity to the binding.

In Chapter 3 the first hybrid is constructed by coupling peptide E with a short polystyrene chain. The conjugation of E to the hydrophobic polystyrene provides a method to study orthogonal self-assembly. The self-assembly of PS_9-E is investigated on its own and together with peptide K and a hydrophilic hybrid K-PEG_{77}. Because E is water soluble it functions as the corona in the PS_9-E block copolymer, and tempers PS induced aggregation such that spherical micelles form. It is found that coiled-coil folding between E and K still occurs to a large extent when the peptides are conjugated with PS and/or

PEG, resulting in linear noncovalent di- and triblock copolymers. PS-E/K also forms spherical micelles, whereas PS-E/K-PEG undergoes hierarchical self-assembly into rod-like micelles. The coiled-coil linker in PS-E/K-PEG can be dissociated by raising the temperature. This reduction in the corona size causes a morphological change from rod-like to spherical micelles with a frozen core such that upon refolding of the coiled coil the micelles remain spherical. Thus, the coiled-coil forming block is utilized in three ways: one is for its hydrophilic character, it can act as a corona to control aggregation induced by the hydrophobic block; secondly, by forming a coiled coil the surface characteristics of the particles are modified and the range of hybrids that form organized aggregates can be extended; and finally the reversible nature of the coiled-coil connection infers additional environmental response to the nanostructures.

While Chapter 3 focused on the effect of the hydrophilic coiled-coil block on amphiphilic self-assembly, Chapter 4 extends the self-assembly of coiled-coil hybrids by varying the hydrophobic block. In order to create larger self-assembled structures, and to probe the limit of the hydrophobic block size, a series of poly(γ-benzyl L-glutamate)-E (PBLG-E) block copolymers were synthesized, and the self-assembly of the series in aqueous solution was investigated. PBLG was polymerized from E with average block length ranges from 36 monomers to 250 monomers. This approach lends itself to modular self-assembly, as both the hydrophobic block and the hydrophilic block/s can be varied. Up until 80 BLG monomers, peptide E was sufficient to induce well defined assembly of the amphiphile, while with longer PBLG blocks complexation of E with K or K-PEG was required for well-defined structural formation. Taking just 4 molecules from this small library – $PBLG_{36}$-E, $PBLG_{100}$-E, K, and K-PEG, polymersomes with a range of sizes, membrane thicknesses (ranging from 18 nm to at least 60 nm), and surface properties were accessible, as well as disk-like micelles.

The PBLG-E series represents the first of a new class of peptide: polypeptide-*b*-peptides, in which the flexibility of chain length of polypeptides is united with the flexibility of functionality of designed peptides. Peptide E was synthesized on solid support, and then PBLG was polymerized by ring-opening polymerization from the N-terminus of E while still on solid-support. The technique offers the advantage of very easy purification, as homopolymer, which is a scourge of NCA polymerizations, can be readily removed by washing the resin. Additionally, by using a relatively gentle cleavage mixture larger block copolymers are cleaved from the resin first, followed by those with shorter PBLG blocks, and finally peptide fragments, such that no further purification is necessary.

Many methods are required to produce polymer vesicles because for each method there is a limited range of vesicle properties that can be produced; not all block copolymers form vesicles with all methods; and additionally, in many instances some methods are not suitable due to the practical issue of availability of time or equipment, or requirements of the block copolymer itself or material to be incorporated. Chapters 5 and 6 investigate two new methods for producing vesicles from block copolymers. They take two methods that have been used for many decades to produce liposomes and that have particular advantages, and adapt them to make them suitable for block copolymers, which have different assembly characteristics than lipids. The detergent aided polymersome

preparation utilizes detergent molecules to molecularly disperse the block copolymer in aqueous solution, a role that is usually taken by organic solvents. The shielding effect of the detergent on the block copolymer is then reduced such that the intrinsic morphology of the block copolymer, i.e. polymersomes, emerges. This method has the advantage of not requiring organic solvent or a high energy input (e.g. sonication), hence will be of great utility when sensitive biomolecules are to be encapsulated in the polymersomes. The block copolymer used to demonstrate the technique, $PBLG_{36}$-E, has a much larger self-assembling energy than lipids do, and the method is explained with an emphasis on the adaptations necessary due to the properties specific to block copolymers. The other technique is termed water-addition solvent-evaporation, and is very rapid and simple. The block copolymer is dissolved in THF, the aqueous phase is added quickly, and the THF is evaporated. The parameters that drive aggregation and determine the sizes of the structures are very easily and quickly controlled: the solvent quality for the hydrophobic block is reduced to the desired level in less than two seconds, leading to microphase separation and structure formation; control of the interactions within the corona, which leads to precise tuning of the polymersome sizes, is also very straight forward, depending on the salt content in the water or the temperature at which the organic solvent is evaporated. Therefore, within a couple of minutes the polymersomes are formed, tuned, and stabilized, and retain their integrity for months. The same block copolymer, $PBLG_{50}$-K, could be made to assemble into polymersomes with a narrow size distribution, with the average size precisely adjusted between 200 nm and 2000 nm. The technique was demonstrated with charged peptidic block copolymers, non-covalent block copolymers, and traditional coil-coil block copolymers. This technique appears to be very practical in terms of time, equipment, the range of block copolymers for which it can be used, and the ability to tune the polymersome properties. Both techniques will open up possibilities in block copolymer vesicle research and applications.

Chapter 7 turns to a different type of hydrophobic block – lipids. The conjugation of coiled-coil peptides to lipids opens up new possibilities as the hybrids can be anchored into an orthogonal self-assembled assembly – lipid bilayers such as synthetic liposomes or cell membranes. The peptides E and K are utilized to create a minimal model for SNARE protein mediated membrane fusion. Hybrids are synthesized which mimic SNARE proteins – they contain the active, force producing coiled coils, a short flexible spacer, and a lipid tail to attach the hybrids onto liposomes. Not only do the hybrids mimic the structural components of SNARE proteins, but importantly they mimic the membrane fusion properties. Populations of liposomes are decorated with one each of the lipidated peptides and coiled-coil folding holds different liposomes in close proximity and induces the liposomes to fuse with lipid and content mixing and no leakage of the aqueous content. The fusion is not driven by membrane tension, and lipids with negative curvature restrict the fusion process. This is the first SNARE protein mediated membrane fusion model that meets all the key characteristics on native fusion, and is therefore a suitable analogue to study liposome fusion in vivo.

As the rest of this thesis hinted, the possible components, architectures, and properties of peptide-polymer block copolymers are multifarious. The conjugation of such disparate

blocks is not trivial; however the latest polymer-peptide hybrids exhibit excellent control over composition, structure, and functionality of the molecules. This is achieved through the careful combination of synthesis methods, tailored for particular classes of hybrids, as reviewed in Chapter 8.

PERSPECTIVES

Prior to using the coiled-coil dimer E/K to influence the self-assembly of coiled-coil hybrids, their properties as a unit were investigated. The experimental findings were backed up and elaborated upon by a molecular dynamics simulation. The next step to take would be to use the computational results to help design a coiled-coil unit that better suited a particular synthetic biology goal. At three heptad repeats the E/K unit is amongst the shortest heterodimeric coiled-coil unit that has been synthesized. Of course coiled-coil binding units of different lengths would have different effects on the systems into which they were incorporated. The design of peptides with three or more heptad repeats is routine, but heading in the other direction, at two heptad repeats only homodimers have been successfully designed and tested. Because the computational simulations give access to the binding contributions of each amino acid in a peptide it was reasoned that this may be able to be used as a tool to design a short heterodimeric coiled coil. In the simulations some residues were very destabilizing to the E/K dimer, particularly the negatively charged glutamic acid residues. These were exchanged for non-charged but polar amino acids. In this way a two heptad repeat peptide was produced that forms homo coiled coils, but as of yet the balance of destabilization of self-binding and heterodimer stability has not been achieved, and is an area of continuing research.

This thesis asked simple questions: can coiled coils function when covalently attached to large hydrophobic blocks? How large can the hydrophobic blocks be? Can coiled coils function when incorporated noncovalently with a supramolecular assembly? In answering these curiosities of fundamental science, coiled-coil hybrids were synthesized and their self-assembly investigated. As is often the case when new ground is explored, there were unexpected consequences, and some of the work from this thesis is already being developed for applications. PBLG-E and PBLG-K vesicles have a high potential as drug delivery devices as compounds can be loaded in the aqueous interior or in the hydrophobic membrane, and the nanocapsules themselves are very modular, with a large variation in membrane thickness and surface chemistry to choose from. These vesicles are currently being developed to deliver the influenza vaccine. The liposome fusion system is being adapted as a general drug delivery system, and is also being investigated for the delivery of fluorescent DNA markers to cells, to convey calcium carbonate to monolayers, to test *in situ* video atomic force microscopy, and to add a further orthogonal dimension by fusing liposomes which contain fiber-forming coiled-coil peptides.

This thesis uses one coiled-coil building block and a handful of other blocks to extend the self-assembly of coiled-coil units, assemblies, and systems; but naturally there are almost unlimited possibilities for functional systems involving coiled coils.

SAMENVATTING

Een coiled-coil motief is opgebouwd uit meerdere peptiden die een helix structuur bezitten. De binding van deze peptiden is zeer specifiek en is gebaseerd op de interactie tussen repeterende complementaire aminozuur sequenties. Van de vele biomoleculaire bouwstenen die gebruikt worden in de natuur horen coiled-coil vormende peptiden bij diegenen met de meeste potentie als bouwstenen voor de synthetische zelf-assemblage van nanostructuren (bottom-up approach). Coiled-coil peptiden hebben een goed gedefinieerde grootte en oppervlakte functionaliteit, de aminozuur volgorde kan worden ontworpen voor specifieke intra- en intermoleculaire interacties, de bindingsenergie is verenigbaar met andere zelf-assemblage processen en ze kunnen eenvoudig gecombineerd worden met andere synthetische bouwstenen. Het gemak van het werken met en het vergaren van informatie over coiled-coil structuren heeft ertoe geleid dat ze een van de meest bestudeerde eiwitstructuren zijn. Zowel geïsoleerde coiled-coils, die discrete complexen vormen, als coiled-coils die assembleren in grotere aggregaten zijn bestudeerd. Tevens zijn coiled-coil structuren gekoppeld aan hydrofiele blokken die het mogelijk maakten aggregaten te vormen met behulp van coiled-coil formatie. Echter, één van de gebieden met de meeste potentie is nog nauwelijks bestudeerd: natuurlijk voorkomende coiled-coil complexen als radertjes in een grote machine die de mogelijkheid hebben te functioneren in complexe systemen opgebouwd uit meerdere bouwstenen en die deze systemen zelfs kunnen beïnvloeden. Het ware potentieel van coiled-coil bouwstenen wordt voor synthetisch chemici pas duidelijk wanneer ze gekoppeld worden aan andere componenten, waarbij iedere component zijn eigen functie heeft. Idealiter wordt er een balans gevonden tussen de afzonderlijke componenten, waardoor nieuwe functies verkregen worden uit de interacties tussen de componenten. Dit proefschrift beschrijft verschillende manieren om coiled-coil structuren te combineren met één of meerdere (niet)-peptide componenten.

In hoofdstuk 2 wordt de coiled coil eenheid, die later wordt gebruikt in de volgende hoofdstukken voor het vormen van hybride moleculen onderzocht. Het peptiden paar genaamd E en K, bestaan elk uit drie repeterende sequenties van zeven aminozuren die ontworpen zijn om een parallelle heterodimeer te vormen in waterig milieu. De bindingseigenschappen worden bepaald door gebruik te maken van experimentele en theoretische technieken, waarbij de resultaten van deze twee strategieën elkaar ondersteunen. De bindingsenergie van een E/K coiled-coil dimeer werd experimenteel bepaald (~ 11 kcal mol^{-1}). Uit computersimulaties bleek dat de belangrijkste bijdrage aan de bindingsenergie geleverd werd door het samenpakken van de zijketens van de hydrofobe aminozuren in de coiled-coil kern. In de controversiële kwestie of zoutbruggen ook bijdragen aan de binding, suggereren de simulaties dat deze niet veel voorkomen en

dat geladen zijketens de bindingsenergie zelfs verlagen maar nodig zijn om de vereiste specificiteit voor de E/K peptidenbinding te verkrijgen.
In hoofdstuk 3 is een polymeer-peptide hybride beschreven. De conjugatie van peptide E met polystyreen resulteert in een polymeer amfifiel (PS_9-E). De zelf-assemblage van PS_9-E is onderzocht evenals PS_9-E/K en PS_9-E/K-PEG_{77} mengsels. Omdat peptide E oplosbaar is in water fungeert het als de corona in het PS_9-E block copolymeer, terwijl het hydrofobe PS de zelf-assemblage induceert waarbij sferische micellen ontstaan. De coiled-coil complexatie tussen de peptiden E en K vindt nog steeds plaats wanneer de peptides geconjugeerd zijn met PS en/of PEG, wat resulteert in lineaire, niet covalente di- en triblock copolymeren. PS-E/K vormt ook sferische micellen, terwijl PS-E/K-PEG mengsels leidde tot de vorming van cylindrische micellen. De coiled-coil binding in PS-E/K-PEG kan worden verbroken door de temperatuur te verhogen. Deze reductie in de grootte van de corona veroorzaakt een verandering in de morfologie van het systeem van cylindrische naar sferische micellen met een rigide kern van polystyreen zodat ook na het opnieuw vormen van de coiled-coil binding sferische micellen waar te nemen zijn. Samenvattend, het coiled-coil vormende E/K motief wordt op drie manieren gebruikt: ten eerste zorgt het hydrofiele karakter ervoor dat de corona van de micellen uit coiled coils bestaan en zo wordt de aggregatie van de micellen gecontroleerd; ten tweede worden door het vormen van het coiled coil complex de eigenschappen van het oppervlak gemodificeerd. Ten derde, het reversibele karakter van de coiled-coil binding zorgt ervoor dat de nanostructuren kunnen reageren op externe omgevingsfactoren.
Terwijl hoofdstuk 3 is gericht op het onderzoek naar het effect van het coiled-coil motief op de zelf-assemblage van amfifielen, wordt in hoofdstuk 4 de zelf-assemblage van coiled-coil hybrides uitgebreidt door variatie aan te brengen in het hydrofobe blok. Een reeks van poly(γ-benzyl L-glutamaat)-E blokcopolymeren (PBLG-E) met verschillende molecuulgewichten voor het PBLG blok werden gesynthetiseerd en de zelf-assemblage in waterige milieu onderzocht, met als doel het vormen van grotere geordende structuren. Peptide E werd gesynthetiseerd op een vaste drager gevolgd door de PBLG synthese, waarbij de polymerisatiegraad gevarieerd werd tussen 36 en 250 monomeren BLG. Deze aanpak is geschikt voor modulaire zelf-assemblage, doordat zowel het hydrofobe blok als het hydrofiele blok gevarieerd kunnen worden. $PBLG_n$-E met $n < 80$ bleken goede amfifielen te zijn en in staat om goed gedefinieerde aggregaten te vormen. Wanneer een langer PBLG blok werd gebruikt was complexatie met K (PBLG-E/K) of K-PEG (PBLG-E/K-PEG) nodig voor de vorming van geordende aggregaten. Door gebruikmaking van slechts 4 moleculen uit deze klasse van verbindingen- $PBLG_{36}$-E, $PBLG_{100}$-E, K en K-PEG-K konden polymeersomen (vesicles die bestaan uit polymeren) met verscheidene groottes, membraandiktes en oppervlakte eigenschappen gesynthetiseerd worden, evenals schijfvormige micellen.
De $PBLG_n$-E moleculen vormen een nieuwe klasse van peptides: polypeptide-*blok*-peptiden, waarin de flexibiliteit van de lengte van de keten van de polypeptiden is verenigd met de flexibiliteit van de functionaliteit van ontworpen peptiden. Peptide E werd gesynthetiseerd op een vaste drager, waarna PBLG werd gevormd door middel van

een ring-opening polymerisatie vanuit de N-terminus van peptide E, terwijl deze nog verbonden was aan de vaste drager. Deze techniek heeft als voordeel dat de zuivering erg eenvoudig is, omdat nevenproducten (bv. PBLG) gemakkelijk van de resin gescheiden worden.

In de literatuur zijn veel verschillende methoden beschreven om vesicles te maken van polymeren, omdat in veel gevallen de methoden niet geschikt zijn voor alle amfifiele polymeren of vanwege practische bezwaren zoals de tijd benodigde, de benodigde instrumenten en de vereisten die gesteld worden aan de intrinsieke eigenschappen van het blokcopolymeer of het materiaal wat geïncorporeerd moet worden in de vesicles. In de hoofdstukken 5 en 6 worden twee nieuwe methoden beschreven voor het maken van vesicles uit blokcopolymeren gebaseerd op methoden die al tientallen jaren gebruikt worden om liposomen te maken. In de eerste methode wordt een detergent gebruikt om de blokcopolymeer moleculen op homogene wijze op te lossen in waterige oplossingen, iets waar normaal gesproken organische oplosmiddelen voor gebruikt worden. Vervolgens werd het detergent langzaam verwijdert door middel van verdunning gevolgd door dialyse waarna vesicles verkregen werden. Deze methode heeft als voordeel dat er geen organische oplosmiddelen worden gebruikt en tevens dat er geen hoge energie-input bronnen (bv. sonicatie) vereist zijn, waardoor deze methode toegepast kan worden om gevoelige biomoleculen (bv eiwitten) te encapsuleren in deze polymeersomen. Het blokcopolymeer dat werd gebruikt om deze techniek te demonstreren bestond uit $PBLG_{36}$-E moleculen. Dit molecuul heeft een veel hogere zelf-assemblage energie dan lipiden en de methode wordt uitgelegd met de nadruk op de aanpassingen die nodig zijn vanwege de specifieke eigenschappen van blokcopolymeren. In de tweede methode werd het blokcopolymeer opgelost in THF, waarna de waterige fase snel werd toegevoegd en de THF verwijdert werd. De parameters die het aggregatiegedrag bepalen zijn eenvoudig en snel te controleren: de kwaliteit van het oplosmiddel voor het hydrofobe PBLG-blok kan worden gereduceerd tot het gewenste niveau in twee seconden, wat leidt tot microfase scheiding en de vorming van de structuur; het controleren van de interacties binnen de corona, wat ervoor zorgt dat de grootte van de polymeersomen nauwkeurig bepaald kan worden, is ook erg eenvoudig. Deze hangt af van de zoutconcentratie en de temperatuur waarbij het organische oplosmiddel verdampt wordt. Op deze wijze kunnen binnen een paar minuten polymeersomen gevormd worden, waarbij de diameter nauwkeurig gestuurd kan worden. Bovendien zijn de verkregen polymeersomen zeer stabiel en blijft de structurele integriteit tenminste enkele maanden behouden. Met $PBLG_{50}$-E werden polymeersomen gemaakt met een goed gedefinieerde diameter die gevarieerd kon worden tussen 200 en 2000 nm. De algemene toepasbaarheid van deze techniek werd verder gedemonstreerd met geladen, peptide bevattende blokcopolymeren, niet-covalente blokcopolymeren en traditionele coiled-coil blokcopolymeren. Deze techniek blijkt erg praktisch en snel te zijn waarbij geen speciale apparatuur nodig is, en toepasbaar is voor veel verschillende blokcopolymeren.

In hoofdstuk 7 werden de peptiden E en K geconjugeerd aan een fosfolipide, waardoor deze hybride moleculen (LPE en LPK) verankerd konden worden in lipide bilagen zoals

synthetische liposomen of celmembranen. Deze moleculen werden ontwikkeld om een minimaal model te maken voor mebraanfusie geïnspireerd op het natuurlijke SNARE eiwit complex. Experimenteel werd aangetoond dat dit modelsysteem dezelfde karakteristieken heeft als de SNARE eiwit complexen. LPE en LPK bootsen niet alleen de structurele eigenschappen van de SNARE eiwitten na maar ook de eigenschappen die fusie drijven. Wanneer twee populaties liposomen, gedecoreerd met LPE of LPK, gemengd werden, werd een snelle fusie waargenomen, waarbij de lipiden van de liposomen zich vermengen, evenals de inhoud zonder dat lekken plaatsvindt. De fusie wordt niet gedreven door membraan spanning en lipiden met een negatieve kromming hinderen het fusieproces. Dit is het eerste model voor membraanfusie met behulp van SNARE eiwitten die alle belangrijke eigenschappen in zich heeft zoals ze ook voorkomen in de cel en is daarom geschikt voor onderzoek aan de fusie van liposomen in vivo.
Zoals dit proefschrift al impliciet aangaf, zijn de mogelijke componenten, architecturen en eigenschappen van peptide-polymeer blokcopolymeren zeer divers. De conjugatie van zulke zeer verschillende blokken is echter niet triviaal. In hoofdstuk 8 wordt een overzicht gegeven van de meest recente synthetische methoden die gebruikt worden voor de synthese van deze hybride moleculen.

PERSPECTIEVEN

De zelf-assemblage van de peptiden E en K en de coiled-coil vorming zijn in detail bestudeerd. De experimentele bevindingen werden ondersteund en uitgebreid door moleculaire dynamische (MD) simulaties. De volgende stap die genomen zou moeten worden is het gebruik van computer simulaties die bijdragen aan het ontwerp van een coiled-coil eenheid die een bepaald synthetisch biologisch doel dient. Met drie repeterende heptameren is het bestudeerde E/K complex één van de kortste heterodimerische coiled-coil vormende eenheden die gesynthetiseerd zijn. Uiteraard heeft de lengte van de coiled-coil invloed op de systemen waarop ze toegepast wordt. Het ontwerp van peptiden met drie of meer repeterende heptameren is goed beschreven in de literatuur, maar coiled-coil complexen gebaseerd op peptiden met slechts twee repeterende heptameren leidt alleen tot de vorming van stabiele homodimeren, Omdat computer simulaties toegang bieden tot de bepaling van de bijdrage aan de bindingsenergie van elk aminozuur, zou het mogelijk moeten zijn om met deze simulaties peptiden te ontwerpen die in staat zijn om heterodimerische coiled-coils te vormen. Uit de simulaties bleek dat sommige aminozuren een zeer destabilizerende rol spelen bij de vorming van het E/K coiled-coil complex, met name het negatief geladen glutaminezuur (Glu). Deze werden vervangen door neutraal polaire aminozuren. Op deze manier werd er een peptide gesynthetiseerd met twee repeterende heptameren dat een homodimeer coiled-coil complex vormt, maar tot dusver is het niet mogelijk gebleken een stabiel heterodimeer complex te vormen. Er is dus op dit gebied meer onderzoek noodzakelijk.

In dit proefschrift werd de eenvoudige vraag gesteld of het mogelijk is om een coiled-coil complex te functionaliseren met hydrofobe eenheden waardoor nieuwe functies verkregen konden worden. Kunnen de coiled-coil peptiden nog steeds functioneren wanneer ze verankerd worden in een supramoleculair aggregaat? Voor het beantwoorden van deze fundamentele vragen werden coiled-coil hybride moleculen gesynthetiseerd en hun zelf-assemblage gedrag onderzocht. Zoals vaak het geval is wanneer een nieuw en onbekend terrein verkend wordt bleken er onverwachte consequenties te zijn en delen van het beschreven werk uit dit proefschrift wordt op dit moment verder ontwikkeld voor mogelijke toepassingen. PBLG-E en PBLG-K vesicles hebben veel potentie als drug delivery systemen waarbij moleculen geëncapsuleerd kunnen worden in het water bevattende interieur van de vesicles of in het hydrofobe membraan. Tevens zijn de nanocapsules eenvoudig te modificeren, met een grote variatie in de dikte van het membraan en oppervlakte chemie waaruit gekozen kan worden. De vesicles worden ontwikkeld om te kunnen dienen als leverancier van het influenza vaccin. Gebaseerd op het minimale model voor fusie wordt momenteel een generieke methode ontwikkeld om medicijnen in de cel te brengen. Verder zijn er nog meer toepassingen mogelijk voor het membraanfusie model: het leveren van fluorescente DNA markers aan cellen, het overbrengen van calcium carbonaat aan monolagen, het testen van *in situ* atomic force microscopie en het toevoegen van nog een orthogonale dimensie door het fuseren van liposomen die fiber vormende coiled coils bevatten.

In dit proefschrift werd een coiled-coil motief gebruikt in combinatie met andere bouwstenen waarmee de zelfassemblage van de coiled-coil eenheden gecontroleerd kon worden en waarbij er bijna ongelimiteerde mogelijkheden zijn voor het ontwerpen van functionele systemen die gebruik maken van een coiled coil motief.

ABBREVIATIONS

A	alanine
Ac	acetyl
ACH	α-cyano-4-hydroxycinnamic acid
ATRP	atom transfer radical polymerization
BLG	γ-benzyl L-glutamate
BOC	tertiary-butoxycarbonyl
bZIP	basic region leucine zipper
CD	circular dichroism
C_p	heat capacity
CH	cholesterol
D	aspartic acid
D_2O	deuterated water
DCM	dichloromethane
D_h	hydrodynamic diameter
DIPEA	N,N-diisopropylethylamine
DLS	dynamic light scattering
DMF	N,N-dimethylformamide
DNA	deoxyribonucleic acid
DOPC	1,2-dioleoyl-sn-glycero-3-phosphatidylcholine
DOPE	1,2-dioleoyl-sn-glycero-3-phosphatidylethanolamine
DOPE-LR	1,2- dioleoyl-sn-glycero-3-phosphatidylethanolamine-lissamine-rhodamine B
DOPE-NBD	1,2-dioleoyl-sn-glycero- 3-phosphoethanolamine-N-(7-nitro-2-1,3-benzoxadiazol-4-yl) (ammonium salt)
DPA	dipicolinic acid
E	glutamic acid
EM	electron microscopy
EDTA	ethylenediaminetetraacetic acid
Fmoc	fluorenylmethoxycarbonyl
FPLC	fast protein liquid chromatography
FRET	fluorescence resonance energy transfer
FT-IR	fourier transform infrared
G	glycine
ΔG_u	Gibbs free energy of unfolding
GdnHCl	guanidinium hydrochloride
GEF	guanine nucleotide exchange factor
GPC	gel permeation chromatography
HIV	Human immunodeficiency virus
HCTU	1H-benzotriazolium 1-[bis(dimethylamino)methylene]-5-chloro-hexafluorophosphate (1-),3-oxide
HEMA	poly(hydroxymethyl methacrylate)
ΔH_u	enthalpy of unfolding
I	isoleucine
K	lysine
K_u	dimer dissociation constant
L	leucine

MALDI-TOF	matrix-assisted laser desorption-ionization time-of-flight
MD	molecular dynamics
M_n	number average molecular weight
MS	mass spectroscopy
NBD	nitrobenzofuran
NCA	*N*-carboxyanhydrides
NMP	nitroxide-mediated polymerization
NMP	N-methyl-2-pyrrolidone
NMR	nuclear magnetic resonance
NSF	N-ethylmaleimide-sensitive factor
OLPC	oleoyl lysophosphatidylcholine
P	proline
PAA	poly(acrylic acid)
PBD	polybutadiene
PBLG	poly(γ-benzyl L-glutamate)
PBS	phosphate buffered saline
PCL	polycaprolactone
PDI	polydispersity index
PEG	poly(ethylene glycol)
PLL	poly-L-lysine
PNIPAM	poly(N-isopropylacrylamide)
PTA	phosphotungstic acid
PS	polystyrene
PSCOOH	monocarboxy terminated polystyrene
PYBOP	(1H-benzotriazol-1-yloxy)tripyrrolidinophosphonium hexafluorophosphate
R	arginine
RAFT	reversible addition-fragmentation chain transfer
RNA	ribonucleic acid
ROP	ring-opening polymerization
RP-HPLC	reversed-phase high-pressure liquid chromatography
S	serine
SEM	scanning electron microscopy
SNARE	soluble NSF attachment protein receptor
SPPS	solid-phase peptide synthesis
TEA	triethanolamine
TEM	transmission electron microscopy
TFA	trifluoroacetic acid
TFE	trifluoroethanol
tBu	tertiary butyl
T	threonine
T_g	glass transition temperature
T_m	melting temperature
THF	tetrahydrofuran
TIS	triisopropylsilane
TMSBr	bromotrimethylsilane
UV	ultraviolet
V	valine
VdW	van der Waals
VIS	visible
W	tryptophan
Y	tyrosine

CURRICULUM VITAE

Hana Robson Marsden was born on the second of January 1980 in Wellington, New Zealand. In 1998 she started studying a range of science and mathematics subjects at Victoria University of Wellington. She conducted research projects on the development of functionalized self-assembled monolayers on quartz crystal microbalances for use as chemical sensors, and the synthesis of titanium precursors for the production of piezoelectric ceramic films. She assisted in chemistry and technology practical courses. During her undergraduate degree she was awarded the Curtis-Gordon research scholarship in chemistry, an Industrial Research Ltd. scholarship, and a scholarship from the Foundation for Science Research and Technology. In 2002 she obtained her Bachelor of Science and Technology, with first class honors in materials science. She then received a Summer Research Scholarship from the Australian National University, and worked on the use of proteins to template mineral growth in the group of John White. Following this she worked on developing high temperature superconductors in the Materials Technologies group at Industrial Research Limited. In 2003 she left New Zealand and worked on thin film solar cells in the Physics of New Materials group at Rostock University, Germany.

In May 2004 Hana began her PhD research in the Soft Matter Chemistry group at Leiden University. Her research, conducted under the supervision of copromotor Alexander Kros, concerned the orthogonal self-assembly of hybrid molecules containing coiled-coil forming peptides. A selection of the results of this research are presented in this thesis. During her PhD studies Hana attended the 2004 Physical Chemistry Han-sur-les winter school and presented her work at the 2005 Macroscopic Physical Chemistry Schiermonnikoog meeting, from 2004 to 2009 at the Dutch Polymer Days and Dutch Synthesis days, and at the Materials Research Society 2007 fall meeting in Boston. Throughout her PhD she supervised 2 bachelor students and 4 masters students in their research internships, some results of which are part of Chapters 4 – 7.

Hana is currently working as a post-doc in the Soft Matter Chemistry group, extending the membrane fusion system developed in this thesis to living cells.

PUBLICATIONS

Kemmitt, T.; Gainsford, G. J.; Robson-Marsden, H. Multiple bridging modes in a novel trinuclear titanium 1,3-dioxypropane compound, Ti_3(methyliminodiethanolate)$_2$(1,3-propanediolate)$_4$ *Acta Crystallographica Section C - Crystal Structure Communications* **2002,** 58, m310-m312.

Kemmitt, T.; Gainsford, G. J.; Al-Salim, N. I.; Robson-Marsden, H.; Sevast'yanov, D. V. Influence of ligand architecture on bridging bond strength in dimeric titanium aminoalkoxy-diolates *Australian Journal Of Chemistry* **2003,** 56, (11), 1147-1152.

Henderson, M. J.; Perriman, A. W.; Robson-Marsden, H.; White, J. W. Protein-poly(silicic) acid interactions at the air/solution interface *Journal Of Physical Chemistry B* **2005,** 109, (44), 20878-20886.

Marsden, H. R.; Korobko, A. V.; van Leeuwen, E. N. M.; Pouget, E. M.; Veen, S. J.; Sommerdijk, N. A. J. M.; Kros, A. Noncovalent triblock copolymers based on a coiled-coil peptide motif *Journal Of The American Chemical Society* **2008,** 130, (29), 9386-9393.

Marsden, H. R.; Elbers, N. A.; Bomans, P. H. H.; Sommerdijk, N. A. J. M.; Kros, A. A Reduced SNARE Model for Membrane Fusion *Angewandte Chemie-International Edition* **2009,** 48, (13), 2330-2333.

Marsden, H. R. and Kros, A. Polymer-Peptide Block Copolymers - An Overview and Assessment of Synthesis Methods, *Macromolecular Bioscience*, **2009**, 9, 939-951.

Marsden, H. R. and Kros, A. Coiled-coil self-assembly in synthetic biology: inspiration and progress, accepted *Angewandte Chemie-International Edition*.

Marsden, H. R.; Handgraaf, J.-W.; Kros, A. Quantifying the Binding of a Heterodimeric Coiled-coil Motif. A Combined Experimental and Computational Study, manuscript in preparation.

Marsden, H. R.; Handgraaf, J.-W.; Sommerdijk, N. A. J. M.; Kros, A. Uniting Polypeptides with Sequence-Designed Peptides: Synthesis and Self-Assembly of Poly(γ-benzyl L-glutamate)-block-Coiled-Coil Peptide Copolymers, submitted.

Marsden, H. R.; Barnier Quer, C. Sanchez, E. Y.; Gabrielli, L.; Jiskoot, W.; Kros, A. Detergent Aided Polymersome Preparation, manuscript in preparation.

Marsden, H. R.; Gabrielli, L.; Kros, A. Rapid Preparation of Polymersomes by a Water Addition – Solvent Evaporation Method, manuscript in preparation.

ACKNOWLEDGEMENTS

> *By thinking of life as process, we must think of the organism actively and continuously engaged with its ecology at a complex hierarchy of levels—that is, we must think of the functioning of a system, not of life as the property of the organism alone.*
> *Louis Sander, Psychoanalytic Dialogues 12(1):11-42, 2002.*

This thesis, a collection of my research efforts of the last five years, is actually a front, or will soon come to be a front, for my life in the Netherlands. Behind the thesis, the five Dutch years have been woven from the personalities, the land, the work, the visitors, the language, the trips. These threads have been constantly fabricating something new and shifting, and I would like to hold up some strands that are particularly bright.

At the beginning there was the convent, the orchard, the lake, thunder and lightning, evenings at the kitchen table in the attic, Silvia with her intense ways, Rene who made me take breaks, Rene with morning sickness, hordes of New Zealanders. Cycling to the dunes and the straight muted coast. Wim tirelessly showing us the ropes and knowing everything, Dutch courses, and milk.
Then there was Ahmed on a quest, light scatting at night, swords, flat water, smooth rocks and never-ending Scandinavian days. There was capoeira, Valeska off-the-wall, Anna activated. There was Nathan and his princess, El 4 eva, and later on Flixie-pie. There was dialysis, and mass spec at the hospital, and microscopy and Gerda and Fons and Nico and Hans, keeping it all together. There were buildings from the 1600s and the secret garden; windmills with ancient Kauri beams, lubricated with lard, and plenty of bicycles. There was Sasha and his integral of e^x from the east, and disaster and new life.
Then there were the seventh floor years, with Nina the diligent, Luca at the perfect time, being me in the lab, and Christophe keeping on. There were the soaring poplars shifting outside the window, and drizzle, and mist, and mould, and 2 pm sunsets. There was Chun on the logic-train, and pragmatic Frank locking and loading. Joris the bold, Ke the acster, Ho Sze, Costas Agrios, Eduardo, Fabiola, Cecilia, and Valeria. Esther with her energy-spring, and Marsida my little sister. There was the beat and curving water in Amsterdam. There was moksi, residence permits, and chips in cones. There were Germans and Bulgaria and home.
There were walls of windows, and windowsills with sunshine and radiators. There was Finn and Esther and Joe and Amy on a limb, and a red bicycle and a ladybird. There was alpha-Alex the reader and clarifier, Agur, Hans, and chortling Edgar. There was Joanna, Jan-Willem, and silver-toothed Jacques. There was perseverance and curiosity. There was

Yoshiko and Kristo K. M. Kulju of the succulaciae, and tomatoes and frogs and reeds and stinging nettle and elderflower and mushrooms and dusk and the couch.
There was a glance on a bicycle, and a bump and a fright at the same time, and then there was delight and Otto, and a great rush of feelings and events. There was the hospital in a whole new light, and nurses and doctors and grandparents and heart gripping situations and the grind of repetition, and help materialising, and work understanding. There was Elena. There was the world to discover. There was the forest and time to see it changing. There were rabbits and peacocks. There were mothers and kids on the lawn. There were the Slovaks, and Rene and Margarita and Osha and Lily and Andrea. There was Robert and Sylvia and Tristanoček and another to discover everything together with.

In an instant there could be Tossy and Mum and Dad and Finn and Esther and Osha and Amy and Ben and Nuku and Joe and Carey and Campbell and David and Hilly and Hester and Joop and Bridget and Rachel and Sue and Lisa and David and Simon and Nastassja and Christian and Amber.

There was always Christian, the constant gardener, over the edge, and turning it into gold.

So thanks everyone. Either you were involved with the projects presented in this book, or we've been hanging out, or I've had you in mind, but the point is that you've been part of making me me, you've fleshed out the Dutch years. Also, I've had the feeling that you've all wished the best for me, and same back at ya. Especially thank you to Mum and Dad and Tossy and Finn and the whanau, you've made me me forever, and to Christian and Otto, we'll make ourselves as we ride on ride on.